

**The Modulation of Retinol and Lipid Binding Proteins to enhance cell
death in Ewing's Sarcoma Family of Tumours**

Dr Shireen Niala Gopaul Arasu

Submitted in accordance with the requirements for the degree of
Doctor of Philosophy

The University of Leeds
Leeds Institute of Molecular Medicine
School of Medicine

November 2017

The candidate confirms that the work submitted is her own and that appropriate credit has been given where reference has been made to the work of others.

This copy has been supplied on the understanding that it is copyright material and that no quotation from the thesis may be published without proper acknowledgement.

Acknowledgements

I would like to thank all the members of the Candlelighters Children's Cancer Research Group (Lab 4) for their support, as I made the transition from clinician to research student. In particular, I am grateful to Dr Helen Payne and Andrea Berry for their help and advice.

I would like to thank my supervisors, Professor Sue Burchill, Professor Colin Fishwick and Dr Martin Elliott for their guidance through the past several years. Their continued understanding, patience and encouragement were essential to the completion of this work.

My thanks to the Tony Bramall Charitable Trust in partnership with Cancer Research UK for the Bramall Clinical Fellowship, without which this research project would not have been possible.

To my parents for helping me to survive the stress of these last few years and not letting me give up. I am forever indebted to you for making those countless trips across the seas to support me. Your maddening attention to punctuation has driven me to finally learn to punctuate prose!!

Finally, I wish to thank my husband, Arasu, and my two wonderful children, Maya and Rohan, who provided unending inspiration and entertainment when I'd rather be doing anything other than drafting my thesis.

Abstract

There have been few advances in treatment for patients with tumours belonging to the Ewing's Sarcoma Family of Tumours (ESFT) in the past three decades. Currently just 1 in 5 young people with metastatic disease survive to 5 years, and 1 in 10 who appear to do well initially, face the grim prospect of late relapse up to 20 years after so-called cure. Combined with significant treatment related morbidity these figures emphasise the need for more effective treatments with minimal toxicity. Fenretinide is a chemotherapeutic that has cytotoxic effects in several cancers, making it an attractive potential therapeutic. However, its use in clinical practice has been limited by poor solubility and bioavailability. I have hypothesised that this may be overcome by modulating extra- and intra-cellular binding proteins including Retinol Binding Protein 4 (RBP4) and the intra-lipid binding proteins (iLBPs) to increase the amount of fenretinide delivered to the cell. In this thesis, I have investigated the binding relationships between candidate carrier proteins and fenretinide or fenretinide-like molecules using *in silico* modelling and surface plasmon resonance.

Using this approach, I have confirmed that RBP4 binds to fenretinide consistent with its role as a chaperone protein for this interesting compound. Cellular Retinol Binding Proteins (I and IV) do not bind fenretinide and therefore are not candidate intracellular transporters of retinamides. Interestingly CRBP-IV may predict poor outcome in some patients. Cellular Retinoic Acid Binding Protein 2 and Fatty Acid Binding Protein 5 remain interesting candidate chaperone proteins for fenretinide and its derivatives. CRBPs (II and III) were not detected in ESFT. *In silico* consensus modelling alone was of limited value to predict protein-binding partners for fenretinide and its analogues. However, the combination of *in silico* modelling using the permissive eHiTS programme followed by surface plasmon resonance may be a useful preclinical tool to identify potential carrier proteins of retinamides including fenretinide.

Table of Contents

Acknowledgements	iii
Abstract	iv
Table of Contents	v
List of Tables	ix
List of Figures	
List of Abbreviations	xvi
Introduction	1
1.1 Cancer.....	1
1.1.1 The history of cancer.....	1
1.1.2 Epidemiology of Cancer	2
1.1.3 Biology of Cancer	2
1.2 Ewing's Sarcoma Family of Tumours	5
1.2.1 Epidemiology of ESFTs.....	5
1.2.2 Biology of ESFTs	5
1.2.3 Genetics and epigenetics of ESFTs	6
1.2.4 Prognosis of ESFTs	8
1.2.5 Treatment of ESFTs.....	9
1.3 Vitamin A and retinol	13
1.3.1 Retinamides	15
1.4 Proteins involved in retinoid/retinamide transport.....	19
1.4.1 Retinol Binding Protein 4.....	19
1.4.2 Transthyretin	21
1.4.3 Stimulated by Retinoic Acid 6 receptor.....	21
1.4.4 The Cellular Retinol Binding Proteins.....	22
1.4.5 Binding interactions	30
1.5 The Nomenclature of retinoid binding transport proteins.....	28
1.6 Hypothesis	33
Chapter 2	36
Retinol Binding Protein 4 - The extra-cellular compartment	36
2.1 Introduction	36
2.2 Methods	38
2.2.1 Cell Culture	38
2.2.2 Viable Cell Number	41

2.2.3 RNA expression examined by Reverse Transcriptase – quantitative polymerase chain (RTqPCR)	42
2.2.4 Protein Expression	46
2.2.5 Statistical Analysis.....	55
2.3 Results	56
2.3.1 Doubling times for ESFT Cell lines.....	56
2.3.2 Expression of Retinol Binding Protein 4 in ESFT Cell Lines	57
2.3.4 RBP4 ELISA Method Optimisation	61
2.4 Discussion	69
2.5 Future work	73
Chapter 3 Intracellular Lipid Binding Proteins	75
3.1 Introduction	75
3.1.1 Cellular Retinol Binding Proteins.....	75
3.2 Methods	77
3.2.1 Sub cellular Fractionation.....	77
3.2.3 Immunohistochemistry	79
3.2.7 Scoring and Statistical analysis.....	87
3.3 Results	89
3.3.1. CRBP-I.....	90
3.3.2 CRBP-II	94
3.3.3 CRBP-III.....	98
3.3.4 CRBP-IV.....	100
3.3.5 CRABP2.....	102
3.3.6 FABP5.....	105
3.3.7 Immunohistochemistry	108
3.3.8 Summary of Results.....	131
3.4 Discussion.....	132
3.4.1 The value of prognostic markers in ESFT at diagnosis	132
3.4.2 Expression of intra-cellular lipid binding proteins in cell lines.....	135
3.4.3 CRABP2.....	138
3.4.4 Methodological considerations	140
3.4.5 Future Work	141
Chapter 4 Protein Interactions with retinamide and retinamide like compounds- in silico Modelling.....	143
4.1 Introduction	143

Material and methods.....	145
4.2.1 The Protein Structures	145
4.2.2 The Ligands	145
4.2.3 The computational tools	146
4.2.4 eHiTS method	147
4.2.5 Assessing the eHiTS docking	148
4.2.6 AUTODOCK method.....	150
4.2.7 Glide method.....	150
4.2.8. Appraising the scoring function	151
4.2.9 Consensus docking approach	152
4.3 Results	153
4.3.1 The Retinol Binding Proteins.....	153
4.3.2 Chemical Ligands and Energy Minimisation.....	157
4.3.3 Docking Solutions of Retinol Binding Protein 4 and retinamide ligands	158
4.3.4 Docking Solutions of Cellular Retinol Binding Protein 1 and retinamide ligands	164
4.3.5 Docking Solutions of Cellular Retinol Binding Protein 4 and retinamide ligands	170
4.3.6 Docking Solutions of Cellular Retinoic Acid Binding Protein 2 and retinamide ligands.....	177
4.3.7 Docking Solutions of Fatty Acid Binding Protein 5 and retinamide ligands	183
4.3.8 Summary of Results.....	187
4.4 Discussion.....	189
Chapter 5.....	199
5.1 Introduction	199
5.2 Material and Methods.....	201
5.2.1 Knock down experiments	201
5.2.2 Target gene activation with 5 aza-2'-deoxycytidine	204
5.2.3 Surface Plasmon Resonance (SPR)	204
5.3 Results	216
5.3.1 Protein Modulation experiments.....	216
5.3.3 CRBP-IV.....	225
5.3.4 Demethylation of CRBPs.....	233
5.3.2 Surface Plasmon Resonance Preparation of a CM5 chip	236

5.3.5. Optimisation of Ligand regeneration conditions	240
5.4 Discussion	251
5.4.1 Knock in and knock out experiments.....	251
5.4.2 Modulation of the CRBPs in ESFT cells by treatment with fenretinide	253
5.4.5 Biacore	254
5.4.6 Limitations and future work	259
6 Discussion	263
6.1 Intracellular Lipid Binding Proteins	263
6.2 Retinol Binding protein 4	267
6.3 Binding Interactions.....	268
6.4 Comparing the methodologies used in assessing binding interactions.....	272
6.5 Modulation of fenretinide and the retinamides.....	274
6.6 The future of cancer and ESFT therapeutics.....	277
6.7 Future Work	280
6.8 Final Conclusions	281

List of Tables

Table 1.1. The frequency of the chromosomal rearrangements in ESFTs.....	7
Table 1.2 Euro Ewing’s 2012 treatment protocol for Ewing sarcoma.	12
Table 1.3 The nomenclature of the Retinol Binding Proteins.	29
Table 2.1 Details of ESFT and positive control cell lines.....	39
Table 2.2 Details of primers and probe sequence used in RTqPCR.	45
Table 2.3 Details of primary, secondary and control antibodies.....	49
Table 2.4 The doubling times for the 6 ESFT cell lines.....	56
Table 2.5. The intra- assay variability of the RBP4 ELISA.	65
Table 2.6. The inter- assay variability of the RBP4 ELISA.	66
Table 2.7 RBP4 concentration in the six ESFT cell lines.....	68
Table 2.8. Summary of studies for the relationship between mRNA and protein concentration in mammalian cells.	71
Table 3.1 Details of antibodies used as subcellular fraction markers.....	79
Table 3.2 Clinical details of patient tumour samples.	80
Table 3.3 Details of the optimisation of IHC antibodies.....	85
Table 3.4 Negative and positive tissues used as controls in IHC of iLBPs.....	86
Table 3.5 Protocol for Mayer’s haematoxylin staining of frozen sections for IHC.....	87
Table 3.6 Details of the positive control RNA and protein lysate used in detecting iLBP targets.	89
Table 3.7 The FABP5: CRABP2 mRNA ratio in the 6 ESFT cell lines.	108
Table 3.8 Summary of the iLBP expressions in the ESFTs.....	130
Table 4.1 The chemical name, structure and assigned molecule number of the retinamide ligands.....	146
Table 4.2 The search strategy for defining each protein used.....	153
Table 4.3 Comparison of structural differences between Retinol Binding Proteins.....	156
Table 4.4 Energy minimisation values of the proteins.....	157
Table 4.5 Energy minimisation values of the chemical ligands.....	156
Table 4.6 Summary od computational binding predictions between retinol binding proteins.....	Error! Bookmark not defined.
Table 5.1 Details of siRNA used in RNAi experiments.....	202

Table 5.2 Recipe for the production of retinoid, retinamide and other ligand stock solutions.	209
Table 5.3. The level of protein captured on the CM5 chips.	241
Table 5.4: Summary of binding predictions between retinol binding proteins and retinoids or retinamides using Surface Plasmon Resonance.	250
Table 5.5 A comparison of the equilibrium dissociation constants (K_d) between RBP4, TTR and small molecules.	257
Table 5.6. A comparison of the equilibrium dissociation constants (K_d) for CRBP-I and small molecules by SPR and FRET studies.	258

List of Figures

Figure 1.1 Summary of Retinoid metabolism	14
Figure 1.2 The chemical structure of a retinoid molecule	14
Figure 1.3 The chemical structure of a retinamide molecule (fenretinide).....	16
Figure 1.4 The interactions of RBP4, TTR and STRA6 proteins.....	22
Figure 1.5 A Phylogenetic tree for the intra-cellular Lipid Binding Proteins.....	23
Figure 1.6 The three dimensional structure of an intracellular Lipid Binding Protein molecule.	24
Figure 1.7 The structure of the CM5 chip used at the SPR interface.	32
Figure 1.8 The principle of operation of SPR affinity biosensors.....	33
Figure 1.9 Summary of my project hypothesis.....	35
Figure 2.1 The structure of a lipocalin molecule.....	36
Figure 2.2 The flow diagram of RBP4 sandwich ELISA.....	54
Figure 2.3 ESFT growth curve.....	57
Figure 2.4 RBP4 mRNA in ESFT cells.....	58
Figure 2.5 Expression of RBP4 protein in ESFT cells	59
Figure 2.6 Expression of RBP4 protein in fenretinide resistant cell lines.....	60
Figure 2.7 RBP4 protein expression in non ESFT cancer cell lines.....	61
Figure 2.8 The absorbance of light by RBP4 protein.....	62
Figure 2.9 Volume comparison of RBP4 standard curve.....	63
Figure 2.10 The correlation co-efficients of the log RBP4 standard curves..	65
Figure 2.11 The stability of RBP4 coated ELISA plates.....	67
Figure 2.12 Post transcriptional factors affecting protein formation from mRNA.....	72
Figure 3.1 Summary of the subcellular fractionation method.....	78
Figure 3.2 CRBP-I mRNA expression in ESFTs.....	89
Figure 3.3 CRBP-I protein expression in ESFT.....	90

Figure 3.4 Sub-cellular CRBP-I protein localisation.....	91
Figure 3.5 CRBP-I protein expression in non ESFT cancer cell lines.....	92
Figure 3.6 CRBP-I protein expression in non ESFT cancer cell	94
Figure 3.7 The expression of CRBP-II mRNA in ESFTs	94
Figure 3.8 CRBP-II protein expression in ESFT cells.....	96
Figure 3.9 CRBP-II protein expression in ESFT and non -ESFT cancer cell lines	97
Figure 3.10 The expression of CRBP-III mRNA	98
Figure 3.11 CRBP-III protein expression in ESFT cells	99
Figure 3.12 The expression of CRBP-IV protein expression in ESFT cell line	102
Figure 3.13 CRBP-IV mRNA expression in ESFT cells	102
Figure 3.14 CRABP2 mRNA expression in ESFT cell lines	101
Figure 3.15 CRABP2 protein expression in ESFT cell lines.....	102
Figure 3.16 CRABP2 protein expression in non ESFT cancer cell lines..	103
Figure 3.17 FABP5 mRNA expression in ESFT cell lines.....	104
Figure 3.18 FABP5 protein expression in ESFT cell lines.....	105
Figure 3.19 FABP5 protein expression in non ESFT cancer cell lines.....	106
Figure 3.20 CRBP-I protein in ESFT by Envision.....	108
Figure 3.21 CRBP-I protein in ESFTs by Novo-Link.....	109
Figure 3.22 Optimisation of CRABP2, CRBP-IV and FABP5 by IHC.....	111
Figure 3.23 The expression of CRABP2, CRBP-IV and FABP5 proteins in a panel of ESFT.....	112
Figure 3.24 The relationship between the three target proteins.....	113
Figure 3.25 Relative expression of CRABP2 in the ESFT panel.....	114
Figure 3.26 The IHC staining of CRABP2 in an ESFT panel.....	115
Figure 3.27 Sub-cellular localization of CRABP2 protein.....	116
Figure 3.28 The CRABP2 protein expression in the ESFTs when stratified for recognized clinical prognostic factors.	120
Figure 3.29 Relative expression of FABP5 protein in the ESFT panel.....	120
Figure 3.30. Immunohistochemistry staining for FABP5 in a panel of ESFTs	122
Figure 3.31. Sub-cellular localization of FABP5 protein expression	123

Figure 3.32. The FABP5 protein expression in the ESFTs when stratified for recognized clinical prognostic factors.....	125
Figure 3.33 Relative expression of CRBP-IV protein in the ESFT panel.....	125
Figure 3.34 Expression of CRBP-IV protein in panel of ESFTs.....	127
Figure 3.35. The CRBP-IV protein expression (H-scores) in the ESFTs when stratified for recognized clinical prognostic factors.....	130
Figure 4.1 RBP4 protein with a representative molecular surface.....	152
Figure 4.2 This computational modelling demonstrating the superimposition of the retinol binding proteins.	155
Figure 4.3 An Autodock graph showing the top docking conformations of RBP4-retinol.....	162
Figure 4.4 A computational modelling schematic of retinol in the RBP4 binding pocket.....	163
Figure 4.5 A computational eHiTS modelling schematic with top RBP4-retinol poses.....	164
Figure 4.6 An Autodock graph showing the top docking conformations for CRBP-I and retinol.....	169
Figure 4.7 A computational modelling schematic of retinol in the CRBP-I binding pocket.....	170
Figure 4.8 A computational eHiTS modelling schematic for CRBP-I and retinol.....	170
Figure 4.9 An Autodock graph showing top docking conformations for CRBP-IV and retinol.....	175
Figure 4.10 A computational modelling schematic of retinol in the CRBP-IV binding pocket.....	176
Figure 4.11 A computational eHiTS modelling schematic for CRBP-IV-retinol.....	177
Figure 4.12 An Autodock graph showing the top docking conformations in CRABP2-retinoic acid.....	182
Figure 4.13 A computational modelling schematic of retinoic acid in the CRABP2- binding pocket.....	182
Figure 4.14 A computational eHiTS modelling schematic for CRABP2-retinoic acid.....	183
Figure 4.15 An Autodock graph showing the top docking conformations of palmitic acid and FABP5 protein.....	187

Figure 4.16 A computational modelling schematic of palmitic acid and FABP5.....	188
Figure 4.17 A representation of docking results in the Autodock software.....	195
Figure 5.1. Effect of fenretinide on the viable cell number.....	217
Figure 5.2 CRBP-I mRNA knock down using siRNA.....	222
Figure 5.3 CRBP-I protein expression in modulated cells.....	223
Figure 5.4 CRBP-I protein knock down in SK-N-MC.....	218
Figure 5.5 Expression of complementary CRBPs in cells in which CRBP-I has been modulated.....	219
Figure 5.6 Effect of fenretinide on ESFT cells in which CRBP-I has been knocked down.....	220
Figure 5.7 CRBP-I protein expression in ESFT cells that have been treated with fenretinide.....	222
Figure 5.8 Sub-cellular localisation of CRBP-I in ESFT cells that have been treated with CRBP-I siRNA.....	223
Figure 5.9 CRBP-IV mRNA knock down using siRNA.....	224
Figure 5.10 CRBP-IV protein expression in modulated cells.....	225
Figure 5.11 Expression of complementary CRBPs in cells in which CRBP-IV has been modulated.....	227
Figure 5.12 Effect of fenretinide on ESFT cells in which CRBP-IV has been knocked down.....	229
Figure 5.13 CRBP-IV protein expression in ESFT cells that have been treated with fenretinide.....	231
Figure 5.14 Growth curve of ESFT cells treated with 5 aza-2'-deoxycytidine.....	232
Figure 5.15 Binding profile of RBP4 protein onto a CM5 chip	234
Figure 5.16 Binding profile of CRBP-I protein onto a CM5 chip.....	236
Figure 5.17 Binding profile of CRBP-IV protein onto a CM5 chip.....	237
Figure 5.18 The interactions between RBP4 and small molecules	241

Figure 5.19 The effect of TTR on the interactions of the RBP4 protein.....	249
Figure 5.20 The interactions between CRBP-I and small molecules.....	245
Figure 5.21 The interactions between CRBP-IV and small molecules.....	247
Figure 6.1 Candidate intra-cellular Lipid Binding Protein transporters for fenretinide.....	265

List of Abbreviations

- 2D** - two-dimensional
3D - three-dimensional
4-HPR - fenretinide, N-(4-hydroxyphenyl)retinamide
4-oxo 4-HPR - 4-oxo-fenretinide
4 – MPR - 4- methoxy fenretinide
A375 - Melanoma cell line
A673 - ESFT cell line
AML - Acute Myeloid Leukemia
APML - Acute Pro-Myelocytic Leukemia
ANOVA - Analysis of variance
Autodock - automated docking ware
ATCC - American Type Culture Collection
ATRA - all trans retinoic acid
B2M - beta-2-Microglobulin
Boc1- β -carotene dioxygenase.
BRCA1 - Breast cancer 1 gene
BRCA2 - Breast cancer 2 gene
BSA - bovine serum albumin
C - cyclophosphamide
CD99 - Cluster of differentiation 99
CD133 - Cluster of differentiation 133
CDK - Cyclin-dependent kinase
CDKN2A - CDK inhibitor 2A
cDNA - complementary DNA
cm - centimetre
CMV - cytomegalovirus
COG - Children's Oncology Group
C_t - cycle threshold
CO₂ - carbon dioxide
CRABP2 - cellular retinoic acid binding protein 2
CRBPs- cellular retinol binding proteins
CRBP-I - cellular retinol binding protein I

CRBP-II - cellular retinol binding protein II
CRBP-III - cellular retinol binding protein III
CRBP-IV - cellular retinol binding protein IV
CRISPR - Clustered Regularly Interspaced Short Palindromic Repeats,
CYPs - cytochrome P450
D - doxorubicin
DES1 - dihydroceramide desaturase 1
dH₂O - distilled water
DMEM - Dulbecco's Modified Eagle Medium
DMEM/F12 - DMEM nutrient mixture F-12
DMSO - dimethyl sulphoxide
DNA - deoxyribonucleic acid
Dox - doxycycline
DTT - dithiothreitol
EGF - epidermal growth factor
eHiTS - exhaustive flexible docking method
E1AF - Early region 1A enhancer binding protein
ECM - extracellular matrix
EDTA - ethylene-diamine-tetra-acetic acid
ELISA - enzyme- linked immunosorbent assay
ERK - extracellular signalling-regulated kinases
ESFT - Ewing's sarcoma family of tumours
Euro-EWING-99 - European Ewing Tumour Working Initiative of National Groups 1999
EVAIA - etoposide-vincristine-doxorubicin-ifosfamide-actinomycin
EWS - Ewing sarcoma breakpoint region 1
EWS-ETS - ESFT translocation with Erythroblastoid virus transforming sequence
EWS-ERG - ESFT translocation with ETS related gene
EWS-ETV1 - ESFT translocation with ETS translocation variant 1
EWS-FEV - ESFT translocation with Fifth Ewing variant
ExpASy - Expert Protein Analysis System
ELISPOT - enzyme-linked immunospot assay
EZ-PCR - Mycoplasma detection kit
FABP5 - Fatty Acid Binding Protein 5
FCS - foetal calf serum
FISH - fluorescence *in situ* hybridisation

FLCN - folliculin
FLI-1 - Friend leukaemia integration 1
FRET - fluorescence resonance energy transfer
g - gram
GLIDE - computational modelling software
GST - Glutathione S-transferases
h - hour
HEP G2 - hepatocellular adenocarcinoma cells
H₂O - water
H₂O₂ - hydrogen peroxide
HDAC - Histone deacetylases
HCl - hydrochloride
HMB2 - human melanoma cell line
hTERT - human telomerase reverse transcriptase
HT-29 - human colon adenocarcinoma
HuR - human antigen R
iLBPs - intra lipid binding proteins
IE - ifosfamide-etoposide
IGF1 - Insulin-like growth factor 1
IGF1R - Insulin-like growth factor receptor
IGF2 - Insulin-like growth factor 2
IHC - immunohistochemistry
IMR-32 - neuroblastoma cell lines
kb - kilobase
kDa - kilodalton
LIMM - Leeds Institute of Molecular Medicine
L - litre
LCFA - long-chain fatty acids
LRAT - lecithin:retinol acyltransferase
M - molar
MCF-7 - breast cancer cell line
MEN1 - Multiple endocrine neoplasia type 1
MEN2a - Multiple endocrine neoplasia type 2a
MEN2b - Multiple endocrine neoplasia type 2b
ml - millilitre
mg - milligram

Mg - magnesium
MgCl₂ - magnesium chloride
min - minute
mm - millimetre
mM - millimolar
ml - milliliter
mRNA - messenger RNA
ms - millisecond
MSC - mesenchymal stem cell
MSH2 - DNA mismatch repair protein 2
MSH6 - DNA mismatch repair protein 6
MW - molecular weight
MYC - Myelocytomatosis
N/A - not applicable
NEAA - non-essential amino acids
ng - nanogram
NHU - normal human urothelial cells
NOS - sodium orthovanadate
nm - nanometre
nM - nanomolar
O₂ - oxygen
°C - degrees Celsius
OPD - *o*-phenylenediamine
p16 - protein 16
p53 - protein 53
PAGE - polyacrylamide gel electrophoresis
PARP - Poly (ADP-ribose) polymerase
PPARs- peroxisome proliferator-activated receptors
PBS - phosphate buffered saline
PBST - phosphate buffered saline with 1% tween
PCR - polymerase chain reaction
PFA - paraformaldehyde
pH - potential of hydrogen
pI - isoelectric point
PMS2 - Mismatch repair endonuclease
PMSF - phenylmethylsulfonyl
pPNET - peripheral primitive neuroectodermal tumour

PPIA - Peptidylprolyl isomerase A
PTEN - Phosphatase and tensin homolog
pRb - retinoblastoma protein
qPCR - quantitative PCR
RA - retinoic acid
RAR (α, β and γ) - retinoic acid receptor α , β and γ
RBP4 - retinol binding protein 4
RXR (α, β and γ) - retinoid X receptor α , β and γ
RAS - oncogene family
RET - receptor tyrosine kinase
RB1 - retinoblastoma protein
RDES - ESFT cell line
RG108 - inhibitor of DNA methyltransferase
RIPA - Radio-Immunoprecipitation Assay
RNA - ribonucleic acid
RNAi - RNA interference
RNase - ribonuclease
ROS - reactive oxygen species
rpm - revolutions per minute
RPMI - Roswell Park Memorial Institute
RT - reverse transcriptase
RT –ve - reverse transcriptase negative
RT4 - Human bladder cancer cell line
RT112 - Human bladder transitional cell carcinoma
RTqPCR - Reverse transcription polymerase chain reaction
s - second
S - DNA synthesis
SCID - severe combined immunodeficient
SCD1 - Stearoyl-CoA desaturase
SDS - sodium dodecyl sulphate
SEM - standard error of the mean
siRNA - small interfering RNA
SKES-1 - Ewing's sarcoma family of tumour cell line
SK-N-MC - Ewing's sarcoma family of tumour cell line
SK-N-SH - Ewing's sarcoma family of tumour cell line
SH-SY-5Y - neuroblastoma cell line
SHEP-1 - neuroblastoma cell line

SMAD4 - tumour suppressor gene
SPR - surface plasmon resonance
STAG2 - stromal antigen 2
STK11 - liver kinase
STRA6 - stimulated by retinoic acid 6 receptor
T24 - human urinary bladder cancer
TEMED - tetra-methyl-ethylenediamine
TBP - TATA binding protein
TBS - TRIS buffer solution
TC-32 - Ewing's sarcoma family of tumours cell line
TEMED - Tetramethylethylenediamine
Tert - telomerase reverse transcriptase
THY1 - Thymus cell antigen 1
TP53 - tumour antigen p53
TRK - tyrosine kinase
TSC1 - tuberous sclerosis 1
TSC2 - tuberous sclerosis 2
TSG - tumour suppressor gene
TTC-466 - ESFT cell line
TTR - transthyretin
T98G - Human glioblastoma multiforme
U - unit
µg - microgram
UK - United Kingdom
UKCCSG - UK Children's Cancer Study Group
µl - microlitre
µm - micrometre
µM - micromolar
UV - ultraviolet
V - volt
V - vincristine
v/v - volume/volume
VAC - vincristine-actinomycin-cyclophosphamide
VACA - vincristine-doxorubicin-cyclophosphamide-actinomycin
VAI - vincristine-actinomycin-ifosfamide
VAIA - vincristine-doxorubicin-ifosfamide-actinomycin

VC - vincristine-cyclophosphamide

VEGF-A - Vascular endothelial growth factor A

VIDE - etoposide-vincristine-doxorubicin-ifosfamide

w/v - weight/volume

WHO - World Health Organisation

WNT - proto-oncogene

Yr - year

YK-279 - an inhibitor of the fusion product ES-FLI1

Introduction

1.1 Cancer

1.1.1 The history of cancer

Evidence of cancer cells have been found in dinosaur fossils from 70 – 80 million years ago (Rothschild, Witzke et al. 1999). However, the ancient Egyptians were the first to record cancer as a disease, and this dates back to 2500 BC (Sudhakar 2009). This civilization was able to differentiate benign tumours from malignancies and engineered treatment regimens around pharmacological, surgical and magical principles. Throughout the middle ages, the Greeks (Hippocrates) and the Romans (Galen) regarded cancer as a disease caused by an excess of black bile (which though generally fatal), that was thought to be curable only in its earliest stages (Gallucci 1985, Diamandopoulos 1996). In fact, it is Hippocrates who is credited with coining the term "cancer" because a tumour looked like a "crab" in that there was a central tumour body and the tumour metastases which were similar to the legs of the "crab". It was during this time, that cancer was accepted as a biological process and treatment became based upon observation and experience. During the 17th century, Gaspare Aselli discovered the vessels of the lymphatic system and suggested abnormalities of the lymph as the primary cause of cancer. In the 18th century, observations about environmental cancers were made and this link was investigated. The medical discipline of oncology was born with the first systematic experiments in cancer. With the advent of improved technology (microscopes) in the late 19th century, the study of cancer revealed that these cells were markedly different in appearance from that of the normal cells. In the early 20th century, cancer research in cell culture, chemical carcinogens, diagnostic techniques and chemotherapy firmly established oncology as a science. Cancer has now been recognised as a genetic disease, which, together with exposure to environmental factors (viruses,

chemical and physical carcinogens), leads to its development and progression. Advances in molecular biology and genetics have allowed translational researchers to make great strides in the understanding, diagnosis, treatment, prevention and potentially finding a cure for this disease. The challenges towards achieving this include: the nature of the disease (metastatic disease, late relapses, second cancers and rare cancer types); hindrances to research (funding among others) and the lack of education (preventative strategies).

1.1.2 Epidemiology of Cancer

Cancer is the leading cause of death in many developed countries, and is the second leading cause of death globally. It was responsible for 8.8 million deaths in 2015. Globally this accounts for approximately 16% or one in six deaths (Bray, Jemal et al. 2012, Soerjomataram, Lortet-Tieulent et al. 2012, Ferlay, Soerjomataram et al. 2015). In 2012, there was an estimated 14.1 million new cases of cancer worldwide and 8.2 million people died from the disease (Ferlay, Soerjomataram et al. 2015). By the year 2025, it is expected that there will be an estimated 19.3 million new cancer cases and 11.4 million deaths. Worldwide, the burden of cancer has doubled between 1975 and 2000 (www.WHO.int/factsheet February 2017) and it is predicted that it will double again by 2020 and triple by 2030 (Plummer, de Martel et al. 2016). An estimated 169.3 million years of healthy life were lost globally because of cancer in 2008 (McGuire 2016). The economic impact of cancer is extremely significant and has been increasing exponentially. The total annual economic cost of cancer in 2010 was estimated at approximately 0.85 trillion pounds (McGuire 2016).

1.1.3 Biology of Cancer

Cancer is a disease that arise because of uncontrolled growth and spread of abnormal cells, which, if remains unchecked, can lead to death. There are more than 100 different types of cancer that can affect humans and can be

classified histologically into six groups (carcinoma, sarcoma, myeloma, leukaemia, lymphoma and mixed types). Alternatively, it can be categorised by the anatomical location from where it had first developed. The biological profile of cancer behaviour is dependent upon its cell of origin. From a clinical and scientific viewpoint, this disease presents a remarkably diverse and complex challenge to treatment. Despite variations in the development and progression of different cancer types, it has been recognised that all cancers possess common biological capabilities. This has provided a rationale for common approaches to treatment. Six hallmarks were first described by Hanahan and Weinberg (2000) and this included sustained proliferative signalling. Cancer cells, unlike normal cells, do not require external signals (growth factors, hormones) to promote cell division and multiplication. There are multiple ways in which cancer cells can do this: producing these signals themselves (autocrine signalling); permanently activating the signalling pathways that respond to these signals; or by destroying 'off switches' that prevents excessive growth from these signals. In addition, cancer cells appear resistant to growth preventing signals from within them and from their neighbouring cells. Tumour suppressor genes have been 'turned off', and contact inhibition has been lost in these cells. Cancer cells have acquired the ability to invade surrounding tissue and metastasise to distant sites. Another principle is the ability to evade cell death. Cancer cells, though abnormal, are able to evade the apoptotic mechanism. Another hallmark of cancer is the induction of angiogenesis. Cancer cells acquire the ability to orchestrate production of new vasculature by activating the 'angiogenic switch', thus ensuring the receipt a continual supply of oxygen and other nutrients. Finally, cancer cells demonstrate limitless replicative potential by altering telomere length.

More recent studies have also suggested that avoiding immune destruction, promoting inflammation, deregulating cellular pathways and demonstrating genome instability and mutation are other important features in cancer progression (Hanahan and Weinberg 2011).

Normal cells can become cancerous through a multi-stage process, which can be due to inherited (genetic) or acquired (physical, chemical or biological carcinogens) mutations in the deoxyribonucleic acid (DNA). It is clear that

most cancers develop because of mutations in two types of genes: tumour suppressor genes (TSG) and oncogenes. Tumour suppressor genes code for proteins that keep cell proliferation in check. These proteins include DNA repair enzymes and the inactivation of these genes lead to tumour development. Usually both alleles that code for the protein must be functionally altered before cells produce a malignant phenotype –“ two-hit hypothesis” (Knudson 1978). Proto-oncogenes promote cellular growth, proliferation and inhibition of apoptosis. Upon activation, a proto-oncogene proliferates or up-regulates and becomes a tumour-inducing agent, an oncogene (Todd and Wong 1999). Examples of proto-oncogenes include: RAS (Bos 1989), WNT (Zhang, Pan et al. 2017), MYC (Felsher and Bishop 1999) , ERK (Holmes, Roberts et al. 2007) and TRK (Kaplan, Hempstead et al. 1991).

Unlike normal cells, cancer cells ignore signals to arrest division, differentiate, or to undergo apoptosis. They have defects in normal cellular processes, that allow cells to divide, invade the surrounding tissue, and spread by way of vascular and/or lymphatic systems. Rapid cell division results in increased acquisition of genetic mutations and encourages further cell dysregulation (faster growth, metastasis and resistance to treatment). These cells can override the apoptotic signals and manifest itself in drug resistance.

Cancer is a genetic disease, which is now thought to be influenced by, or associated with multiple factors. Abnormal genes can be inherited and passed on from generation to generation. Advancing age, exposure to carcinogens (www.cancer.gov/carcinogens), and infections (www.cancer.gov/about-cancer/causes-prevention/risk) have all been linked to risk factors for adult cancers.

Paediatric malignancies are a spectrum of biologically diverse cancers that are different from those seen in adults. They are at least partly the result of developmental pathways dysregulation with paediatric tumours harbouring few mutations in genes that code for relatively druggable targets. These are in general genomically quiet tumours. Indeed newer facets of research are investigating gene regulation and epigenetics in the paediatric cohort. There is an increasing realisation that in some tumours epigenetic events are the

major drivers for their formation. Paediatric cancer represents an interface for clinical translation, where genetic and molecular markers are being incorporated into clinical algorithms (tumour classification and disease surveillance). The use of genomic expression, epigenetic profiling technology and experimental tumour model systems is advancing our understanding of this disease. Further comprehensive characterisation of aggressive, chemo-resistant paediatric cancers (e.g. Ewing's Sarcoma Family of tumours) may result in improved therapeutic strategies and better outcomes for these patients.

1.2 Ewing's Sarcoma Family of Tumours

1.2.1 Epidemiology of ESFTs

Paediatric cancer is rare and occurs in 0.5% of the population (Parkin, Stiller et al. 1988). The Ewing's sarcoma family of tumours (ESFT) is made up of neoplasms that arise primarily in children and young people (10-24 year olds) and comprise 3.1% of all paediatric malignancies (Ayadi, Chaari et al. 2010). It is the second most common primary bone tumour with a peak incidence in 10 to 24 year olds (Rodriguez-Galindo, Billups et al. 2002). It represents 40 to 45% of paediatric malignant bone tumours (Ayadi, Chaari et al. 2010). There is a slightly higher predisposition to the disease in males when compared to females (ratio 1.4: 1) (McNally, Blakey et al. 2012).

1.2.2 Biology of ESFTs

This type of cancer was first described in 1918 (by Aurthur P Stoui) and then again in 1921 by James Ewing. Initially, Ewing's sarcoma, Askin's tumour (malignant small cell tumour of thoraco-pulmonary region) and peripheral primitive neuro-ectodermal tumour were described as separate entities based on the histological appearance and the site of the tumour. Following the identification of the EWS-ETS gene rearrangement (pathognomonic of Ewing's Sarcoma- ESFT), it became evident that these diseases were part

of the same family of tumours - the Ewing's Sarcoma family of Tumours (Delattre, Zucman et al. 1992, Grier 1997).

Most Ewing's sarcomas are diagnosed in bone, commonly the pelvis, diaphyseal regions of the long bones (like the femur) and the bones of the chest wall. However, up to 15% of these tumours can be extra-osseous including deep paravertebral, thoracic, proximal limb soft tissue, kidney, bladder, lung, prostate and the meninges.

ESFTs appear as a featureless sheet of small, round cells which are thought to arise from the mesenchymal stem cells (Riggi, Suva et al. 2010). They are histologically indistinguishable from other small round cell tumours of childhood, including neuroblastoma, lymphoma and rhabdomyosarcoma. ESFTs are poorly differentiated, with scant cytoplasm and a large nucleus but little mitotic activity. It has, however, been recognised that 90% of this family of tumours express the cell surface glycoprotein CD99 which is used to diagnose ESFTs (by immunohistochemistry) along with clinical features (age of patient, site of tumour) and the presence of the EWS-ETS fusion gene.

1.2.3 Genetics and epigenetics of ESFTs

ESFTs are characterised by a unique non-random chromosomal rearrangement between the *EWS* gene on chromosome 22q12 to a member of the *ETS* transcription gene family, most commonly to *FLI-1* on 11q24 (Delattre, Zucman et al. 1992). Identification of several breakpoints for both *EWS* and *FLI-1* showed that the *EWS-FLI-1* fusion genes are heterogeneous: the breakpoints of type 1 occur at exon 7 of *EWS* and exon 6 of *FLI-1*, while type 2 breakpoints are at exon 7 of *EWS* and exon 5 of *FLI-1*. This rearrangement occurs in 85% of ESFTs. Other *EWS-ETS* rearrangements have been described in the remaining 15% of cases. These include *EWS-ERG*, *EWS-ETV1* and *EWS-FEV* (Burchill 2008) (Table 1.1).

Table 1.1. The frequency of the chromosomal rearrangements in ESFTs. EWS= Ewing Sarcoma Breakpoint Region 1; FLI1= Friend leukaemia integration 1 transcription factor; ERG= ETS related gene; ETV1= ETS translocation variant 1; E1AF= Early region 1A enhancer binding protein; FEV=Fifth Ewing variant.

Fusion Transcript	Chromosomal translocation	Frequency
EWS-FLI1 Type I	t(11;22)(q24;q12)	60%
EWS-FLI1 type II	t(11;22)(q24;q12)	25%
EWS-ERG	t(21;22)(q22;q12)	10%
EWS-ETV1	t(7;22)(q22;q12)	rare (<1%)
EWS-E1AF	t(17;22)(q12;q12)	rare (<1%)
EWS-FEV	t(2;22)(q33;q12)	rare (<1%)

The sequencing of ESFTs has revealed that there are few recurrent somatic mutations reported in Ewing's sarcoma. Studies have highlighted that gain in copy numbers of chromosome 8 in nearly 50% tumours (Shukla, Schiffman et al. 2013). In addition, there were mutations in TP53 (5-20% tumours) and STAG2 (20%) (Kovar, Auinger et al. 1993, Huang, Illei et al. 2005, Solomon, Kim et al. 2011) (two genes known to be cancer associated). TP53 is a tumour suppressor gene while STAG2 is a member of the cohesion multimeric complex that regulates sister chromatid exchange during mitosis and meiosis.

Paediatric cancers and ESFTs in particular, are considered to possess a 'quiet' genome, which shows one of the lowest mutation rates among all cancers (0.15 mutation per mega base) (Brohl, Solomon et al. 2014) (Crompton, Stewart et al. 2014). The EWS-FLI1 fusion protein along with epigenetic modifications are the main drivers for Ewing's sarcoma oncogenesis. Surprisingly even though EWS-FLI1 has been identified as a prime vulnerable candidate in this chain of events, attempts at eliminating or inactivating this fusion protein has been largely unsuccessful. This

oncogenic transcription factor has not been found to be druggable as it lacks intrinsic enzymatic activity as well as being disordered (unable to form a rigid three dimensional structure under physiological conditions) (Ng, Potikyan et al. 2007) (Uren, Tcherkasskaya et al. 2004) with low hydrophobicity. Within recent times, changes in the primary focus of therapeutics towards epigenetic modifications has resulted in promising developments. Some epigenetic changes like silencing is potentially reversible and so epigenetically acting drugs may be used as supplements to conventional chemotherapy. Since epigenetic modifications can be used as cancer targets, drugs like zebularine (demethylation agent) (Zhou, Cheng et al. 2002) and RG108 (histone deacetylase inhibitors) (Rondelet, Fleury et al. 2017) can be employed to specifically target these changes.

1.2.4 Prognosis of ESFTs

At the time of diagnosis, approximately 20-25% of patients present with clinically detectable metastatic disease (Cotterill, Ahrens et al. 2000). Of these patients, 10% present with metastases of the lungs and an equal percentage present with bony infiltrates. A further 5% of patients have disease in multiple distant sites (Gettys, Anderson et al. 2014). Patients presenting with localised disease have up to a 75% chance of 5 year survival (Paulussen, Ahrens et al. 1998, Linabery and Ross 2008). The presence of metastatic disease is the most important adverse prognostic factor (Paulussen, Ahrens et al. 1998, Cotterill, Ahrens et al. 2000), those patients with disseminated bony disease having a 5 year survival of less than 20 %; while those with lung metastases having a 5 year survival of 30-40% (Cotterill, Ahrens et al. 2000, Miser, Goldsby et al. 2007). The prognosis of refractory or recurrent Ewing's sarcoma remains dismal, with only about 4-8 % being event free at 5 years (Rodriguez-Galindo, Navid et al. 2008). The persistence of EWS-ETS specific mRNA (minimal residual disease) in the bone marrow after treatment, poor response to initial therapy, being older (>15years), having a larger tumour (>200mls) and the site of the tumour at diagnosis (pelvis vs distal extremities) are all unfavourable prognostic markers (Paulussen, Ahrens et al. 1998, Cotterill, Ahrens et al.

2000, Grier, Krailo et al. 2003). In addition, other genetic factors such as p16 and p53 mutations also contribute to a poorer outcome (Paulussen, Ahrens et al. 1998).

Over the last few decades, there has been significant improvement in survival outcomes in many types of cancer (Kersey 1997); patients have benefited from significant improvements in surgery, chemotherapy and radiotherapy. Genomic sequencing have identified cancers with gene alterations, rearrangements and mutations, while the introduction of targeted therapy (immunotherapy, biotherapy and gene therapy) have dramatically improved survival outcomes in the last decade (Morales-Espinosa, Garcia-Roman et al. 2015). Cancers with identified alterations like Acute Promyelocytic Leukaemia (APML) and leukaemia's are virtually curable with a survival outcome of 95-98% (Rice and de The 2014). Unfortunately this has not been the case in ESFTs where little progress has been made in the last 40 years, especially in the treatment of metastatic disease (Biswas and Bakhshi 2016). Even though this paediatric cancer has a well-recognised genetic alteration, survival outcomes have not improved and there are still tough clinical challenges that need to be overcome. These include: anticancer drug resistance/non druggable fusion gene, inevitable late recurrences, cancer progression and metastasis and the fact that this is a rare disease, so engagement or investment into orphan drugs are minimal. As a result, there is an urgent need for new, more effective treatment in this disease.

1.2.5 Treatment of ESFTs

ESFT is an aggressive sarcoma, with treatment relying upon a multidisciplinary approach that combines chemotherapy and local therapy including surgery, radiotherapy or both.

James Ewing recognized that this sarcoma was radio- sensitive (Ewing 1972). Initially, the approach to treating localized disease involved single modality radiotherapy (Gaspar, Hawkins et al. 2015). This was, however, associated with a high rate of local recurrence (30-35%) and an increased

risk of late effects (growth impairments, secondary malignancies). Gradually, surgery was introduced as an alternative treatment for local disease. Its indication have included removal of expendable bones and bone replacement, (endoprostheses, allografts and vascularized autografts). Surgery is not without its complications of endo-prosthetic infection, replacement of endoprostheses in growing children and bone healing difficulties. Currently, surgery is most effective when a tumour is resectable with wide surgical margins, appearing superior to definitive radiotherapy for local control (Jenkin 1966, Craft, Cotterill et al. 1997, Donaldson, Torrey et al. 1998, Schuck, Rube et al. 2002, Schuck, Ahrens et al. 2003, Bacci, Forni et al. 2004, Krasin, Rodriguez-Galindo et al. 2004, Granowetter, Womer et al. 2009, DuBois, Krailo et al. 2015). Definitive radiotherapy is now only advised for inoperable lesions (e.g. large tumours or those located in unfavourable positions like the vertebra).

Prior to the advent of cytotoxic chemotherapy, the survival rate for patients with localised ESFT was about 10% (Jenkin 1966, Balamuth and Womer 2010). The need for systemic treatment was obvious as patients usually died from metastases. With the advent of chemotherapy combined with surgery and radiotherapy, 5 year survival rates in patients with localized disease has improved to 70-80% (Balamuth and Womer 2010).

Chemotherapy was first used in the treatment of ESFT in 1962 and since then there has been a host of single and multi-agent chemotherapies. Their success depended upon their ability to halt cell division by damaging DNA or RNA. The rate of cells division, cell type and the phase of the cell cycle affect the effectiveness of chemotherapy. Drugs commonly used in chemotherapy regimens against ESFT include: cyclophosphamide, actinomycin, doxorubicin, vincristine and etoposide. Cyclophosphamide is an alkylating agent that is cell cycle non-specific. It produces irreversible DNA cross links in cells with low levels of ALDH and this leads to apoptosis (Davidoff and Mendelow 1993). Other agents are cell cycle specific. Actinomycin inhibits transcription by binding DNA at the transcription initiation complex and so preventing RNA chain elongation. It acts through multiple cell cycle phases including $G_1/S/G_2$ (Kim, Kong et al. 2005). Doxorubicin inhibits transcription by inhibiting topoisomerase II enzyme,

thereby preventing RNA chain re-sealing. This is found throughout G_2 but there is some effect in G_1/S (Barlogie, Drewinko et al. 1976). Vincristine binds the tubulin protein, preventing chromosome separation during metaphase (G_1) (Kothari, Hittelman et al. 2016). Finally etoposide complexes with DNA and the topoisomerase II enzyme, preventing re-ligation and this results in DNA strand breakage in G_1/S (Smith, Soues et al. 1994). Ewing's sarcoma family of tumours are a relatively drug-resistant cancer with no new and effective agents identified in the last 40 years and the treatment effect of single-drug chemotherapy has been sub-optimal (Pishas and Lessnick 2016). Thus, multi-drug regimens are necessary to control tumour cells at various stages of the cell cycle, eliminate local or distant micro metastases, and reduce the emergence of drug-resistant cells

At present, in Europe, VIDE (vincristine, ifosfamide, doxorubicin and etoposide) is considered the standard induction chemotherapy, whilst in North America, the compressed VDC-IE (vincristine-doxorubicin-cyclophosphamide followed by ifosfamide-etoposide) is standard. Unfortunately, the former regimen is associated with significant toxicity while the latter has reported much fewer side effects. The current Euro Ewing 2012 trial is comparing both of these induction regimens (Table 1.2). The VAC (vincristine, actinomycin D and cyclophosphamide) is used for consolidation of standard risk patients (Euro-EWING 99 trial outcome) and VAI (vincristine, actinomycin D and ifosfamide) for the high risk/metastatic patients. In North America, consolidation included 5 alternate cycles of VC (vincristine, cyclophosphamide) and IE (ifosfamide and etoposide). The Euro Ewing's 2012 trial is also evaluating treatment both with and without Zoledronic acid (Table 1.2). This compound belongs to the class of drugs known as bisphosphonates and have been used to treat bone metastases in breast (Powles, McCroskey et al. 2006) and prostate cancer (Berry, Waldron et al. 2006). Zoledronic acid, which is known to prevent fractures in patients with cancer, (Sunyecz 2010) reduces bone re-absorption, inhibits growth of ESFT cell lines both *in vitro* and in mouse models (Odri, Dumoucel et al. 2010). It has also been shown to exhibit a synergistic effect in combination with ifosfamide. This may be particularly attractive as a therapy for ESFT, as

it modulates the bone microenvironment, which is known to be important in ESFT (Redini and Heymann 2015).

Table 1.2 Euro Ewing's 2012 treatment protocol for Ewing sarcoma. VDE= vincristine, ifosfamide, dactinomycin and etoposide; VAC= vincristine, dactinomycin and cyclophosphamide; VDC= vincristine, doxorubicin and cyclophosphamide; IE= ifosfamide and etoposide; VC= vincristine and cyclophosphamide.

Trial	Eligible Patients	Protocol
Euro Ewing 2012	All patients with ESFT	<div style="display: flex; flex-direction: column; align-items: flex-start;"> <div style="margin-bottom: 20px;"> <p>6 VIDE cycles</p> <ul style="list-style-type: none"> → 8 VAC → 8 VAC + zoledronate </div> <div> <p>5 VDC + 4 IE cycles</p> <ul style="list-style-type: none"> → 3VC + 4 IE → 3 VDC + 4 IE + zoledronate </div> </div>

It is clear that the survival of patients with detectable metastatic disease is greatly reduced when compared to patients with non-metastatic disease. In addition, approximately 20% of these patients with localised disease have disseminated tumour cells in bone marrow and blood at diagnosis (Vermeulen, Ballet et al. 2006). Their clinical course and prognosis is similar to those with metastatic disease.

Furthermore, chemotherapy is ineffective in 25% of patients with non-metastatic disease and in 75% of those with metastatic Ewing's sarcoma. Patients with early relapse or recurrence have an extremely poor five year event free survival (Rodriguez-Galindo, Billups et al. 2002). This data demonstrates the urgent need for novel, alternative approaches to treat this disease. New strategies have targeted tumour vasculature (Scharovsky, Mainetti et al. 2009), the inhibition of the EWS-FLI1 oncogene product (Toretsky, Connell et al. 1997), disruption of EWS-FLI1 binding with RNA helicase A (the complex promotes oncogenic transformation), production of

antibodies to insulin-like growth factor -1 receptor (blockade of this receptor inhibits Ewing's sarcoma cell growth and metastases) and inhibitors of tyrosine kinase (decreases proliferation of ES cells). Other avenues of research include the use of the antibody, rapamycin, to inhibit the proliferation of ESFT through cell cycle arrest and down-regulation of the EWS-FLI1 protein (Mateo-Lozano, Tirado et al. 2003) and small molecules to restore the function of tumour suppressor genes (like p53). Many of these approaches are in the infancy stages of research and are associated with significant toxicities, non-specific side effects, poor selectivity and clinical effectiveness. However, there is another targeted therapy that appears promising in respect to this rare disease; the synthetic vitamin A derivative, fenretinide, which produces apoptotic cell death in ESFTs (Qian, Zhang et al. 2009).

1.3 Vitamin A and retinol

Vitamin A is an organic compound required by biological systems. It plays an important role in vision, bone growth, reproduction, cell division and differentiation as well as regulation of the immune system (Gerster 1997). Retinol cannot be synthesized in biological systems but is acquired through diet as β -carotene, retinol or retinyl esters. β -carotene is stored in the liver and can be converted to retinal. Retinol (80-90%) is stored as retinyl esters in the hepatocytes while the remaining 10-20% of the body's retinoid content enters circulation, bound to Retinol Binding Protein 4 (RBP4). It can also be oxidized to yield retinal and retinoic acid with these endogenous retinoids binding to various down-stream retinoic acid receptors (RAR α , β and γ) and retinoid X receptors (RXR α , β and γ). Binding of the retinoid ligands to these nuclear hormone receptors initiates cell signalling pathways thereby regulating cellular proliferation, differentiation and apoptosis. These important cellular processes have essential physiological roles which include the maintenance of immunity, barrier integrity, reproduction and embryonic development (Gudas 1994, Gudas 2012). Retinol can be esterified to retinyl esters (for storage) by lecithin: retinol acyltransferase (LRAT) (Figure 1.1).

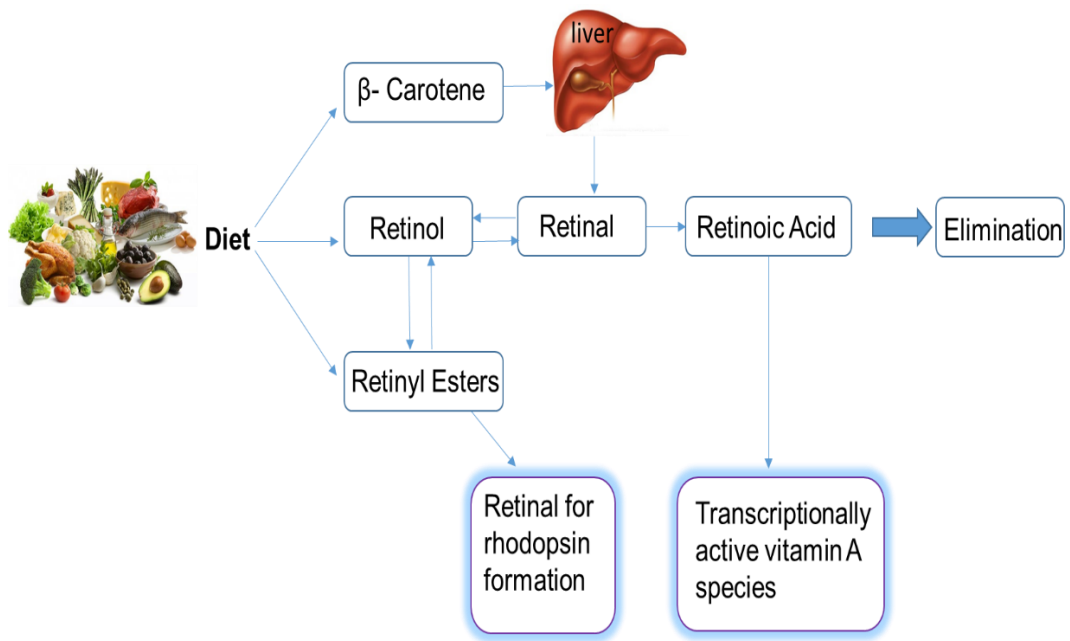


Figure 1.1 Summary of Retinoid metabolism. The diet provides biological systems with vitamin A in the form of β -carotene, retinol and retinyl esters. Vitamin A is stored in cells as β -carotene and retinyl esters. However, these retinoids can be oxidised to retinal and retinoic acid and also converted to retinol, as required.

Retinol belongs to a class of chemicals called retinoids, of which there are more than 4000 natural and synthetic compounds. They consist of a bulky hydrophobic cyclic region (β -ionone ring), an isoprenoid backbone and a polar end group (Figure 1.2).

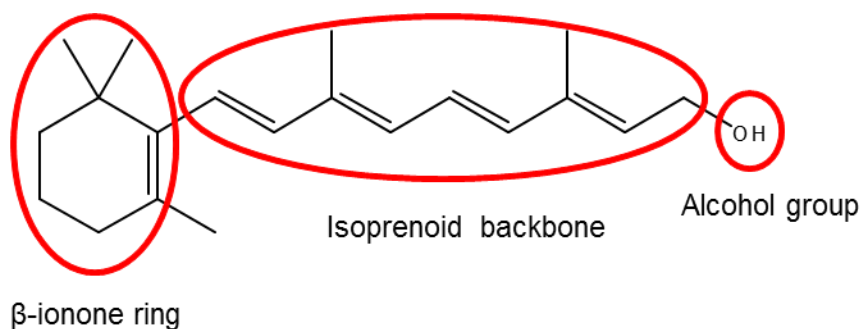


Figure 1.2 The chemical structure of a retinoid molecule (retinol). It contains a β -ionone ring (cyclical group), an isoprenoid backbone (a polyene side chain) and a polar end group.

The activation of RXR receptors by retinoids (like retinoic acid) which activates transcription and cell proliferation play important roles in development, cell differentiation, metabolism, and cell death. Therefore it is not surprising that retinoids such as all trans retinoic acid (ATRA) have proven effective in cancer treatment including APLM (Fang, Chen et al. 2002, Mistry, Pedersen et al. 2003), neuroblastoma (Matthay, Villablanca et al. 1999), head and neck, lung and liver cancers (Harnish, Jiang et al. 1992, Dragnev, Rigas et al. 2000, Breccia, Latagliata et al. 2008). Although retinoids have activity in some cancers, their value is limited due to unacceptable toxicity. The toxic effects (hypervitaminosis) in humans include nausea, headache, and fatigue, loss of appetite, dizziness, dry skin, desquamation, lipid alterations, connective tissue toxicity and cerebral edema. Additionally, long term toxicity include scaling, anorexia, headache, psychiatric changes, bone and joint pain, osteopenia, osteoporosis and fractures. Severe toxicity can lead to eye damage, high levels of calcium, and liver damage, severe congenital malformations and teratogenic effects. (Penniston and Tanumihardjo 2006). In addition, retinoids have not shown any therapeutic efficacy in the treatment of ESFTs. (Burchill, Berry et al. 1998, Malone, Perloff et al. 2003).

1.3.1 Retinamides

Another group of synthetic compounds, which are biochemically related to retinoids, are the retinamides. They are structurally very similar to retinoic acid, containing a β -ionone ring and an isoprenoid back bone but with an amide end group (Figure 1.3). Retinamides have an improved toxicity profile compared to that of the retinoids (Formelli, Clerici et al. 1993, Garaventa, Luksch et al. 2003). The identification of selective retinoic acid derivatives, which are capable of inducing apoptosis and displaying synergy with other anticancer therapies, therefore promises to be a more effective and a less toxic strategy for treatment.

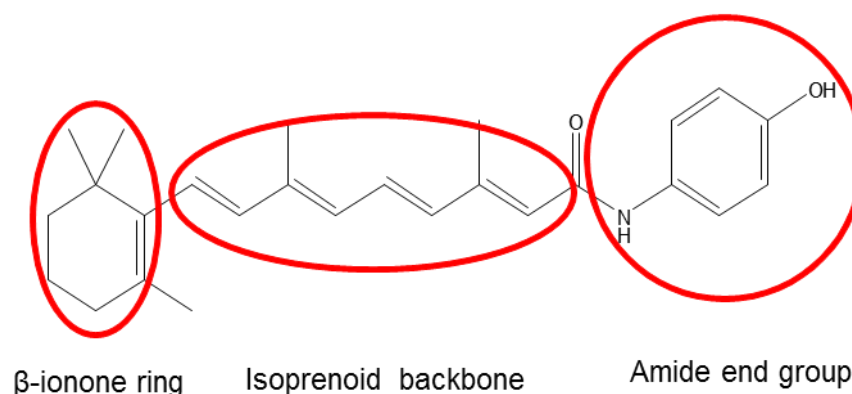


Figure 1.3 The chemical structure of a retinamide molecule (fenretinide). It contains a β -ionone ring (cyclical group), an isoprenoid backbone (a polyene side chain) and an amide end group.

Fenretinide (N-(4-Hydroxyphenyl) retinamide/ 4-HPR) (Figure 1.3) is one such retinamide that appears promising for cancer treatment. It was produced since the late 1960s and has well recognized chemo-preventive (Moon 1989), apoptotic and antitumor activity (Pollard and Luckert 1991, Formelli and Cleris 1993, Goto, Takahashi et al. 2003). It has also been shown to have some clinical activity in breast cancers, (Abou-Issa, Moeschberger et al. 1995, Kazmi, Plante et al. 1996), head and neck (Oridate, Lotan et al. 1995), prostate, bladder and skin cancers (Moon and McCormick 1982, McCormick and Moon 1986, Moon, Pritchard et al. 1989, Pollard, Luckert et al. 1991, Hsieh, Ng et al. 1995, Bushue and Wan 2010), colo-rectal (Ziv, Gupta et al. 1994), small cell and non-small cell lung cancer (Kalemkerian, Slusher et al. 1995, Ohlmann, Jung et al. 2002, Villablanca, London et al. 2011), neuroblastoma (Di Vinci, Geido et al. 1994, Mariotti, Marcora et al. 1994, Reynolds, Wang et al. 2000) leukemia, (Ozpolat, Tari et al. 2004) (Delia, Aiello et al. 1993) and ovarian cancers (De Palo, Veronesi et al. 1995). Most importantly, ESFT cell lines have been shown to be sensitive to fenretinide *in vitro* (Lovat, Ranalli et al. 2000, Myatt and Burchill 2008) and *in vivo* (Ponthan, Lindskog et al. 2003) (Myatt, Redfern et al. 2005) (Maurer, Kalous et al. 2007).

Fenretinide is known to initiate the cell death cascade (apoptosis) in transformed, pre-malignant and malignant cells, but not in normal cells (Ulukaya, Kurt et al. 2001, Navarro-Zorraquino, Guemes et al. 2002, Boya, Morales et al. 2003). Although the exact mechanism by which this occurs is not fully understood, it is thought that the retinamide induces apoptosis in tumour cells by interacting with diverse signaling molecules. Reactive Oxygen species (ROS) (Darwiche, Hatoum et al. 2004) (Maurer, Metelitsa et al. 1999), ceramide (sphingolipid second messenger) and glycosphingolipid GD3 (Lovat, Corazzari et al. 2004), MAPk's, JNK, p38 RAR dependent pathways, stress kinases, ER stress, autophagy have all been implicated (Mody and McIlroy 2014). These mechanisms of action suggest that fenretinide is effective against cancer because it is directed against two of the well-defined hallmarks of cancer: enabling of replicative immortality and resisting cell death.

The metabolism of fenretinide produces an active metabolite, 4'-oxo fenretinide (4'-oxo 4-HPR), which is able to act synergistically with 4-HPR which is also active against some 4-HPR-resistant cell lines (Villani, Appierto et al. 2006). More recently, a second polar metabolite of fenretinide (4'-OH 4-HPR) has been elucidated *in vitro* (Mehta, Hawthorne et al. 1998, Illingworth, Boddy et al. 2011). In addition, an inactive metabolite 4-methoxy fenretinide (4-MPR) (Mehta, Hawthorne et al. 1998) has also been identified (Villani, Appierto et al. 2006) (Children's Oncology, Villablanca et al. 2006, Formelli, Cavadini et al. 2008).

The substitution of the amide-linked 4-hydroxyphenyl group for the carboxylic group of ATRA (to form fenretinide) has markedly reduced side effects and toxicities. It rarely induces dermatologic (skin dryness and rashes) or metabolic toxicity, but does cause reversible changes in dark adaptation and impaired night vision (nyctalopia) in 23% of patients. (Formelli, Cavadini et al. 2010).

Fenretinide is one of the few retinamides that have been approved for pharmacokinetic assessment in cancer therapy clinical trials. Phase I trials have included assessing the pharmacokinetics of fenretinide in children with neuroblastoma (Garaventa, Luksch et al. 2003, Kummar, Gutierrez et al. 2011); the administration of a new oral formulation of the drug (Kummar,

Gutierrez et al. 2011) and the intravenous delivery of fenretinide to patients with refractory or relapsed haematological emergencies (Mohrbacher, Yang et al. 2017). Currently, there is an ongoing Phase I trial evaluating the administration of an intravenous fenretinide emulsion along with safinol, a stereo chemical-variant dihydroceramide precursor (ClinicalTrials.gov Identifier: NCT01553071).

There has been multiple phase II clinical trials evaluating the efficacy of fenretinide in recurrent malignant gliomas (Puduvalli, Yung et al. 2004), oral pre-malignant lesions (Williams, Somasekar et al. 2009), recurrent small cell lung cancer (Schneider, Worden et al. 2009) and advanced renal carcinoma (Vaishampayan, Heilbrun et al. 2005). Interestingly, an oral, capsular fenretinide preparation has been assessed for efficacy in a paediatric cohort with refractory /recurrent neuroblastomas (Garaventa, Luksch et al. 2003). This retinamide has also been involved in Phase III trials which evaluated efficacy and toxicity of fenretinide in preventing tumour recurrence in patients with transitional cell carcinoma of the bladder (Sabichi, Lerner et al. 2008) as well as the prevention of a second breast cancer (Veronesi, Mariani et al. 2006).

Despite the substantial cytotoxic activity of fenretinide in transformed (but not normal) cells and its improved toxicity profile, the response rates of patients in clinical trials have been less than anticipated. This is likely attributable to the low bioavailability of the oral formulation (corn oil capsule); after a single dose of 10mg/kg, the bioavailability was approximately 16% in beagle dogs (Liu, Chen et al. 2007). A second formulation using a lipid matrix, Lym-X-Sorb (LXS) to envelope the hydrophobic, poorly soluble fenretinide was evaluated by Kummar et al 2011. Although the latter achieved a marginally higher plasma level, this formulation was poorly tolerated due to increased gastro-intestinal complaints, and there was wider interpatient variability of plasma levels (Poondru, Zhou et al. 2001). Its poor water solubility (0.00119 mg/mL) resulted in a large number of capsules needing to be ingested in order to achieve dosing between 300- 2500mg/m², and this directly affected patients' compliance (Garaventa, Luksch et al. 2003) (Children's Oncology, Villablanca et al. 2006). More recent trials have employed an intravenous fenretinide emulsion preparation that has obtained

plasma drug levels that were 5 to 7 times that of the capsule formulation (Villablanca, London et al. 2011). While this data demonstrates that the intravenous delivery may resolve some of the previous problems associated with limited fenretinide plasma levels, modest toxicities suggests that further development of alternative formulations of the drug needs to be assessed. The chemical modulation of its structure, as well as the use of analogues or mimetics and inhibitors to proteins involved in the transport and metabolic pathway may provide solutions to the pharmacokinetic challenges described above. A better understanding of cancer cell biology of this drug may provide the basis for a different novel anticancer therapy.

1.4 Proteins involved in retinoid/retinamide transport

1.4.1 Retinol Binding Protein 4

Retinol Binding Protein 4 (RBP4) is a 21kDa protein that was first isolated in 1968 (Kanai, Raz et al. 1968). It functions as a transporter for vitamin A / retinol in the serum, shuttling retinol (among other poorly soluble biological compounds) from the liver and adipocytes to the peripheral tissues (Kameko, Ota et al. 1992). This protein is mainly synthesized in the liver, but 15 - 20% is produced by adipocytes (Makover, Soprano et al. 1989). RBP4 requires the availability of retinol for it to be released from hepatocytes. The protein binds to retinol rendering it soluble in an aqueous medium (Newcomer, Jones et al. 1984). RBP4 (98%) is bound to retinol which results in the maintaining a low level of free retinol in the plasma. This has the effect of protecting cells from hydrophobic toxicity (Blaner 1989) (Newcomer and Ong 2000) (Raghu and Sivakumar 2004).

Fenretinide binds well to *apo* RBP4 and the crystal structure of fenretinide-RBP4 complexes compares well with retinol-RBP4 (Berni and Formelli 1992) (Zanotti, Marcello et al. 1994). Retinol and fenretinide positions within the binding pocket of RBP4 are superimposed almost perfectly. The binding pocket is fairly rigid and so may not allow different modes of binding of the retinoids. However, the bulky end group of fenretinide is located in the flexible loop region surrounding the opening of the β barrel. As we attempt to

modulate the effects of fenretinide, it would be important to observe what happens to the interactions between the retinamides and their binding proteins. These modulations may serve to increase efficacy of both fenretinide and fenretinide-like molecules.

The RBP4 gene is located on chromosome 10, near to the region that has been linked to type 2 diabetes (Weijnen, Rich et al. 2002). Therefore, it is not surprising that elevated levels have been observed in obesity, insulin resistance and type 2 diabetes (Lewandowski, Stojanovic et al. 2008). Despite established links between obesity and cancer, very few studies have investigated RBP4 levels and its role in cancer.

Higher circulating levels of RBP4 are associated with prostate cancer (Uehara, Takahashi et al. 2013), colon adenoma (Abola, Thompson et al. 2015), ovarian cancer (Cheng, Liu et al. 2014), oral squamous cell cancer (Parris, Aziz et al. 2014) and pancreatic cancer (El-Mesallamy, Hamdy et al. 2013). High serum RBP4 levels correlate with a poorer prognosis in patients with hepatocellular carcinoma (Jia, Wei et al. 2011). In sharp contrast, a decreased level of RBP4 was detected in epithelial ovarian cancer patients (Lorkova, Pospisilova et al. 2012).

Variations in RBP4 levels are also reported in several non-malignant disease states. Patients with chronic renal failure have markedly increased levels of RBP4 as compared to healthy controls (Lespine, Periquet et al. 1996). Other chronic conditions like preterm labour, intra-amniotic infection/inflammation and pre-eclampsia are associated with higher levels of RBP4 (Johansen, Redman et al. 1999, Zusterzeel, Peters et al. 2007, Chaiworapongsa, Romero et al. 2010, Mazaki-Tovi, Vaisbuch et al. 2010).

Acute stressful conditions like sepsis, elective surgery, burns and critical illness of pulmonary origin are associated with lower levels of RBP4 (Moody 1982, Langouche, Vander Perre et al. 2009). Decreased levels of RBP4 are also seen in variety of infections : bronchitis, upper respiratory tract infections, tonsillitis, diarrhoea, stomatitis, urinary tract infections, shigellosis and gastrointestinal upset (Arroyave and Calcano 1979), liver disease (Bluher, Tonjes et al. 2008) (Tacke, Weiskirchen et al. 2008), hyperthyroidism (el-Shahawy, Tucker et al. 1971) and sickle cell disease (Warrier, Kuvibidila et al. 1994).

1.4.2 Transthyretin

Transthyretin (TTR) was first crystallized in 1966 (Haupt and Heide 1966) and the native structure was described in 1978 (Blake, Geisow et al. 1978). The TTR gene is located on chromosome 18 and encodes for TTR protein, a tetrameric carrier protein with a molecular weight of 55 kDa. It is primarily produced in the liver and excreted into plasma and cerebro-spinal fluid. This protein has also been found in retinal pigment epithelium, choroid plexus pineal gland (Izumoto, Younger et al. 1992), pancreas (Kameko, Ichikawa et al. 1986) and gastrointestinal mucosa (Gray, Gray et al. 1985). Not only does TTR bind and transport thyroxine (Hagen and Elliott 1973), it also plays a role in the transport of retinol (vitamin A axis) to target cells.

When retinol is bound to RBP4, a conformational change occurs in the loop extending from residue 34 to 37, and this produces an increased affinity for TTR (Figure 1.4). The apo form does not complex with transthyretin. *Holo*-RBP4 binds to TTR and this increases the affinity of RBP4 for retinol which in turns reduces the non-specific release of retinol from the complex to acceptors other than the membranes of target cells (Heller and Horwitz 1973, van Jaarsveld, Edelhoch et al. 1973). This *holo*-RBP4-TTR complex (75kDa) is much larger than RBP4 alone (21kDa), preventing its glomeruli filtration from circulation (Zanotti, Marcello et al. 1994), thereby leading to an increase in circulating RBP4 levels. It would be interesting to determine whether this relationship holds true for interactions between RBP4 and fenretinide or fenretinide-like molecules (Section 1.6)

1.4.3 Stimulated by Retinoic Acid 6 receptor

RBP4 binds to the cell membrane receptor Stimulated by Retinoic Acid 6 receptor (STRA6), which is encoded by the STRA6 gene on chromosome 15. STRA6 removes retinol from the *holo*-RBP4-TTR complex (Figure 1.4), and transports it across the membrane to be metabolised (Kawaguchi, Yu et al. 2011). It has a molecular weight of 99 kDa, and is a large hydrophilic membrane bound protein with extracellular, transmembrane and intracellular

domains. It is widely expressed in the choroid plexus as well as the brain, eye, testis, spleen, kidney and the female reproductive tract, (Blaner 2007) where it plays an important role in cellular homeostasis.

STRA6 independently promotes cell proliferation and is found to be up regulated early in some breast and colon cancers (Berry, Levi et al. 2014), Wilms's tumours, melanomas, ovarian and endometrial cancers (Szeto, Jiang et al. 2001). In cancer, STRA6 and RBP4 up regulation and activation progressively triggers JAK2/STAT3 signaling which results in the induction of multiple STAT target genes. The STATs are proto-oncogenes associated with inflammation, oncogenic transformation (proliferation, invasion and angiogenesis) and usually confer a survival advantage (Koptyra, Gupta et al. 2011) (Ferbeyre and Moriggl 2011) (Quesnelle, Boehm et al. 2007).

Within the normal internal milieu, TTR and STRA6 compete for *holo* RBP4 (Figure 1.4) which provides a mechanism to protect tissues from hyper-activation of STRA6 and oncogenic transformation (Berry, Croniger et al. 2012). More recently, some studies have suggested that STRA6 is not the only means by which retinol enters cells (Berry, O'Byrne et al. 2012). These alternatives are important to evaluate when investigating the transport of vitamin A and its derivatives intra-cellularly.

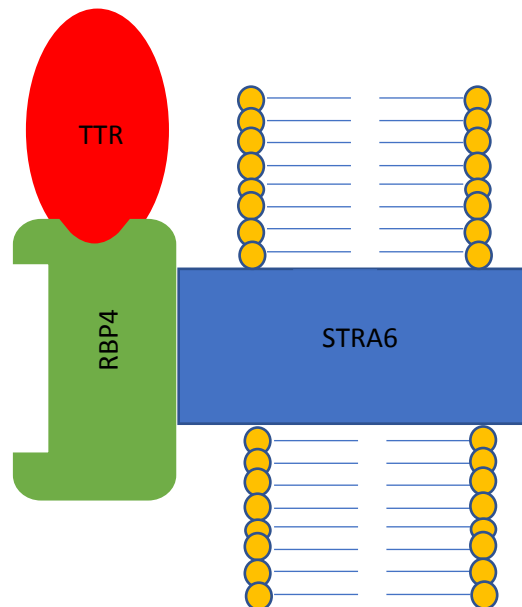


Figure 1.4 The interactions of RBP4, TTR and STRA6 proteins. TTR is a plasma protein which is capable of binding to a RBP4 protein loop. This complex is retained in circulation (due to increased size) and has increased affinity for retinol. Retinol is transported to the cell surface membrane via the TTR-RBP4 complex. It is then incorporated into cells after passing through the cell membrane protein STRA6.

1.4.4 The Cellular Retinol Binding Proteins

The Cellular Retinol Binding Proteins belong to the intracellular Lipid Binding Protein superfamily and they include: cellular retinol binding protein-I (CRBP-I), cellular retinol binding protein-II (CRBP-II), cellular retinol binding protein-III (CRBP-III), cellular retinol binding protein-IV (CRBP-IV), cellular retinoic acid binding protein 2 (CRABP2) and fatty acid binding protein 5 (FABP5). They are phylogenetically related, with CRBP-I being more closely related to CRBP-III; and CRBP-II to CRBP-IV (Figure 1.5). There is variable expression of the CRBPs in different tissues (Kuppumbatti, Rexer et al. 2001) Even though these proteins share a high degree of homology (Folli, Calderone et al. 2002), there are significant differences in the side chains. These CRBPs are a group of small cytosolic proteins with a molecular weight of 15kDa. These proteins are structurally similar to each other, containing 10 β strands arranged into 2 anti-parallel β pleated sheets. They take the form a β -barrel within which a hydrophobic ligand is sandwiched. The entrance to the barrel is closed by a loop between the first and second β strands. This loop consists of a single α helix followed by a turn and then another helix (Figure 1.6).

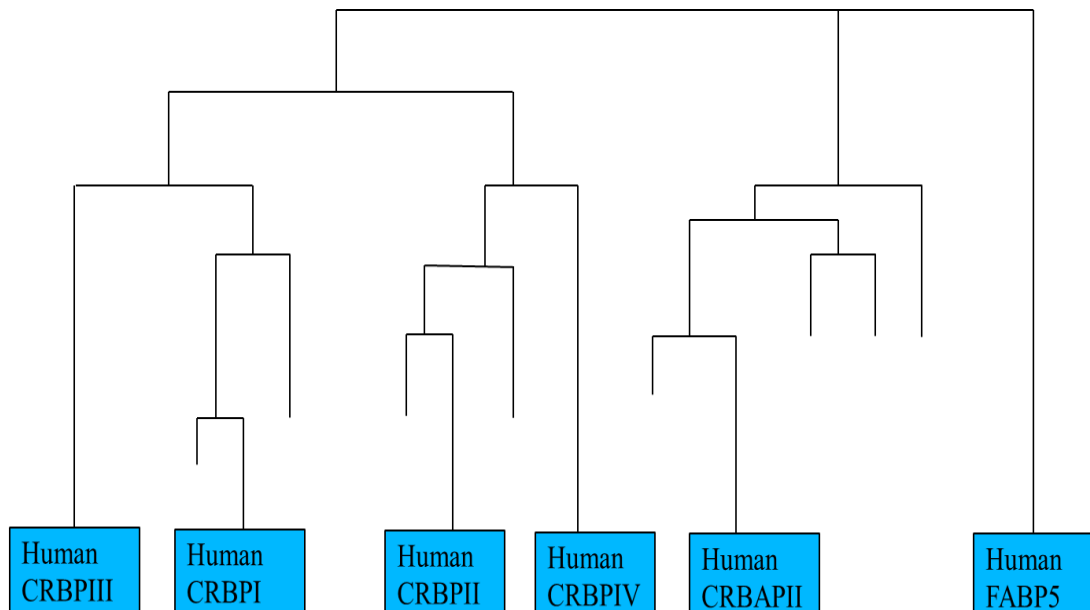


Figure 1.5 A Phylogenetic tree for the intra-cellular Lipid Binding Proteins. The neighbour-joining method has been used for phylogenetic tree construction and the bootstrap scores are based on 1000 replicates. Protein amino acid sequences was obtained from GenBank™ or SwissProt : human CRBP-I (PO9455); human CRBP-II (P50120); human CRBP-III (P82980); human CRBP-IV (Q96R05); human CRABP2 (P29373); and human FABP5 (1714345A). This

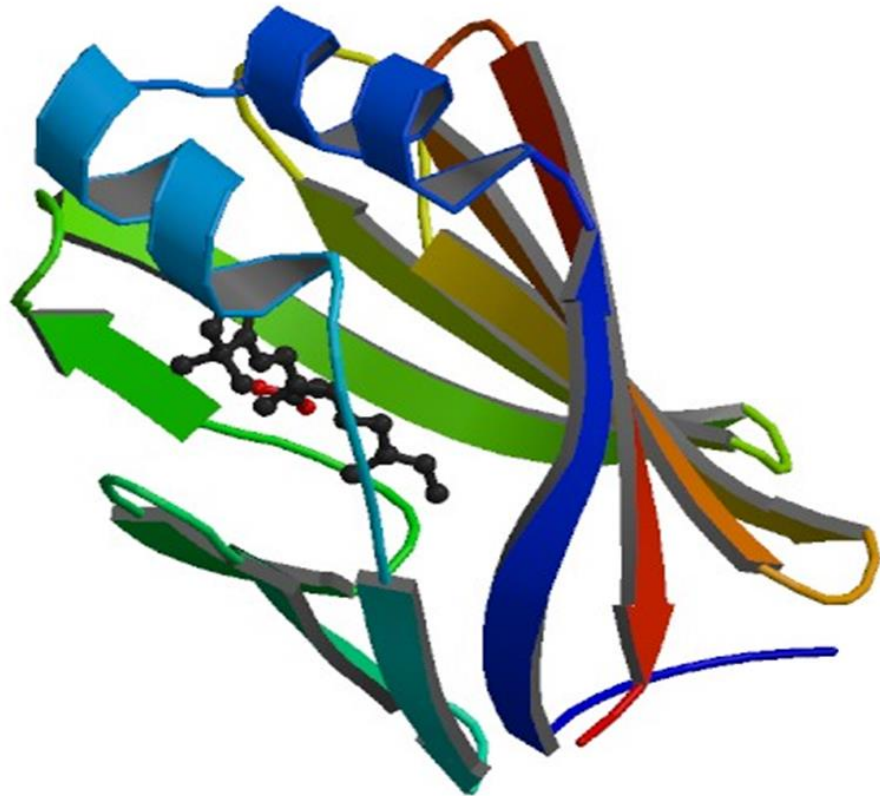


Figure 1.6 The three dimensional structure of an intracellular Lipid Binding Protein molecule. It contains a ten stranded, antiparallel, symmetrical β -barrel fold, (beta sheet) with two α -helices. The β barrel contains the binding pocket for the molecule. This protein contains retinal bound deep within the binding pocket.

1.4.4.1 CRBP-I

CRBP-I has 3 isoforms: isoform A containing 135 amino acids (MW= 15kDa); isoform B containing 153 amino acids (MW= 17kDa); isoform C consists of 95 amino acids (MW= 11kDa). The gene that codes for this protein is found on chromosome 3. This protein is ubiquitous but has a high level of expression in adult ovary, pancreas, liver, pituitary and adrenal gland (Folli, Calderone et al. 2001). It is ,however, not, found in skin fibroblasts and intestinal epithelium (Doldo, Costanza et al. 2015). This protein is capable of binding to retinol , retinal and the trimethylmethoxy phenyl derivatives of retinol (Wang, Kane et al. 2011). CRBP-I binds to retinoids that are oriented

in the opposite direction to retinoids that are bound to RBP4. The retinol is accepted with its hydroxyl group buried deep within the structure. The majority of CRBP-I is expressed in the cytosolic pool (Bashor, Toft et al. 1973) and more recently so, in lipid droplets within the cytoplasm (Kuppumbatti, rexa,2001), where it binds to retinol that enters cells via the process of diffusion. The lecithin: retinol acyltransferase (LRAT) then converts it to retinyl esters (Batten, Imanishi et al. 2004). An alternative pathway also exists, in which CRBP-I is coupled to the intra-cellular portion of STRA6 protein. Here retinol is accepted from the membrane protein which in time is then shuttled to interact with the JAK-STAT complex where it continues to activate further down-stream receptors (Murray 2007).

1.4.4.2 CRBP-II

CRBP-II is a protein which consists of 134 amino acids. The gene responsible for its production is found on chromosome 3. There are 2 isoforms (A and B) with the identical amino acid sequence except that the B form is acetylated (Schaefer, Kakkad et al. 1989). It is found primarily in adult small intestine, where it is highly expressed. CRBP-II plays several roles in the trafficking of retinol. It is involved in the intestinal absorption of vitamin A where it can bind to specific transporters on the brush border membrane, thereby facilitating diffusion. It can also act as a reservoir to keep the concentrations of free retinoids very low within the cell. In addition, retinol bound to CRBP-II is oxidised at a 50th of the rate of retinol alone, suggesting that CRBP-II serves to sequester retinol from oxidation within the intestinal epithelium. It is speculated that CRBP-II may direct retinol to a specific esterifying enzyme, resulting in the production of fatty acyl esters of retinol that are incorporated into chylomicrons for release to the lymph (Demmer, Birkenmeier et al. 1987, Ong and Page 1987). The localization of CRBP-II is restricted to the cytoplasm of the villus associated columnar absorptive cells of the proximal intestinal epithelium. It represents approximately 1% of the entire cytosolic protein in the small bowel. CRBP-II binds to retinol, retinal and the trimethylmethoxy phenyl derivatives of retinol (Kane, Bright et al. 2011).

1.4.4.3 CRBP-III

CRBP-III is another of the family of cellular retinol binding proteins. It contains 135 amino acids and is encoded by a gene found on chromosome 12. There are 3 naturally occurring variants. It is highly expressed in the kidney and liver but to a lesser extent in heart, muscle spleen, adipose, mammary tissue, adult lymph nodes and the appendix. CRBP-III binds retinol and the active metabolite retinoic acid. It plays a role in lipid and energy metabolism and may be important in the incorporation of retinol into breast milk (Piantedosi, Ghyselinck et al. 2005). In studies with CRBP-I deficient mice, the CRBP-III protein levels were elevated in tissues that normally express CRBP-III. There was a suggestion that CRBP-I and CRBP-III share some physiologic actions within tissues and that each can compensate for the absence of the other, helping to maintain normal retinoid homeostasis (Piantedosi, Ghyselinck et al. 2005).

1.4.4.4 CRBP-IV

CRBP-IV is another member of this family of proteins containing 134 amino acids. It is the protein product of a gene found on chromosome 1. It is expressed primarily in kidney, heart and transverse colon. It has also been detected in the lymph node, appendix, ascending colon, heart and spleen (Folli, Calderone et al. 2002). CRBP-IV will bind to retinol, but prefers retinoic acid (RA) as its substrate. The retinol-CRBP-IV complex is unstable, possibly due to an incompatible side chain that makes orientation of the β -ionone ring within the binding cavity difficult. Potentially CRBP-IV protein has a distinct mode of binding retinol, as evidenced by its atypical absorption spectrum when compared to the other 3 proteins in this group (Folli, Calderone et al. 2002). It has also shown a low affinity for retinol.

1.4.4.5 CRABP2

The CRABP2 protein belongs to this family of cellular retinol binding proteins. It consists of 136 amino acids and has a molecular weight of 15 kDa. It is encoded for by a gene on chromosome 1 (Donovan, Olofsson et al.

1995), and while being predominantly expressed in the skin, it has also been detected in the male and female reproductive tracts, kidney, bladder and the gastrointestinal tract (Ruberte, Friederich et al. 1992). Its main substrate is retinoic acid. It is involved in the shuttling of RA from the cytosol to the nucleus where it interacts with the nuclear receptor RAR to promote transcriptional activity. Apo CRABP2 binds to Human antigen R protein (HuR). This increases the RNA binding affinity thereby enhancing stabilisation and upregulation of HuR transcript targets. In the presence of retinoic acid, this protein complex dissociates and CRABP2 continues shuttling retinoic acid to the nucleus (Zhang, Vreeland et al. 2016).

1.4.4.6 FABP5

The FABP5 protein belongs to the group of proteins known as the intracellular lipid binding proteins. It is a product of the gene found on chromosome 8. FABP5 consists of 135 amino acids, has a molecular weight of 15 kDa. It is primarily expressed in the epidermis but can also be found in the female reproductive tract, gastrointestinal tract, kidney, bladder, lungs, bone marrow, gall bladder and liver (Hertzel and Bernlohr 2000, Furuhashi and Hotamisligil 2008). This protein is capable of binding to hydrophobic ligands like long-chain fatty acids (LCFAs), eicosanoids, other lipids and retinoic acid. It is associated with in the cellular uptake of lipids, their transport and regulation of metabolic pathways including: gene expression, cell proliferation, differentiation, lipid oxidation and storage within the cytoplasm (Hertzel and Bernlohr 2000, Furuhashi, Fucho et al. 2008, Storch and Corsico 2008, Furuhashi, Ishimura et al. 2011, Smathers and Petersen 2011). Recent studies have determined that FABP5 is capable of inducing metastasis by promoting up-regulation of vascular-endothelial growth factor (VEGF) (Jing, Beesley et al. 2000, Jing, Beesley et al. 2001). In addition, FABP5 is known to interact with peroxisome proliferator-activated receptors (PPARs) (Berger, Ralph et al. 2012). FABP5 has been shown to be a strong and independent prognostic factor of poor outcome in breast cancer (Liu, Graham et al. 2011).

In vitro and *in vivo* studies has suggested that the relative level of FABP5 to CRABP2 may be a critically important determinant of cellular proliferation

and survival (Liu, Graham et al. 2011). Both of these proteins bind to retinoic acid but the binding affinity of CRABP2 for RA exceeds that of FABP5 by 100 fold (Dong, Ruuska et al. 1999). When the cell expresses both proteins, the CRABP2 /RAR pathway predominates, leading to cell cycle arrest or apoptosis (Schug, Berry et al. 2007). Conversely, when the FABP5/CRABP2 is high, the FABP5/PPAR pathway is induced leading to cell proliferation. The relationships of these proteins to each other have been evaluated in astrocytic gliomas (Campos, Centner et al. 2011), glioblastomas (Barbus, Tews et al. 2011) and breast cancer (Liu, Graham et al. 2011), and have been presented as interesting prognostic factor. It would be illuminating to evaluate whether this relationship holds true for Ewing's sarcoma.

1.4.4.7 The Nomenclature of retinoid binding transport proteins

With increasing improvements in technology, the proteomic communities continue to make novel and interesting discoveries. New proteins are regularly uncovered, characterised and catalogued based upon existing data-banks ([www.http://scop.mrc-lmb.cam.ac.uk](http://scop.mrc-lmb.cam.ac.uk)). As more information became available about the structure and function, new candidates were added to existing classifications, and nomenclature of existing proteins were changed. The seven proteins of interest in this thesis were discovered at different time points, and each has had a variety of names and abbreviations attached to it. The preferred abbreviation that is used throughout this thesis is included in bold in Table 1.3.

All the target proteins belong to the Calycin superfamily (share a similar β -barrel structure). The RBP4 protein belongs to the lipocalin family of proteins (extracellular proteins that are involved in ligand binding, receptor binding and macromolecular complexes formation) while CRBP-I, CRBP-II, CRBP-III, CRBP-IV, CRABP2 and FABP5 are members of intra Lipid Binding Protein/ cytosolic Fatty Acid Binding Protein family.

Table 1.3 The nomenclature of the Retinol Binding Proteins. This includes RBP4, iLBPs and the associated genes. * = the preferred abbreviation used throughout this thesis.

Gene	Synonyms of Protein product	Abbreviations
RBP4	Retinol binding protein 4 Plasma retinol binding protein	RBP4* PRBP RBP
RBP1	Retinol-binding protein 1 Cellular retinol-binding protein Cellular retinol-binding protein 1	RBP1 CRBP CRBPI, CRBP-I* , CRBP1, CRBP-1
RBP2 CRBP2	Retinol-binding protein 2 Cellular retinol-binding protein II	CRBP-II*
RBP5	Retinol-binding protein 5 Cellular retinol-binding protein III	CRBP-III*
RBP7	Retinol-binding protein 7 Cellular retinol-binding protein IV Cellular retinoic acid-binding protein IV Cellular retinoic acid-binding protein 4	CRBP-IV* CRBP4 CRABP4
CRABP2	Cellular retinoic acid-binding protein 2 Cellular retinoic acid-binding protein II	CRABP2* CRABP-II
FABP5	Fatty acid-binding protein, epidermal Epidermal-type fatty acid-binding protein Fatty acid-binding protein 5 Psoriasis-associated fatty acid-binding protein homolog	E-FABP FABP5* PA-FABP

1.4.5 Binding interactions

One or more of the members of the intracellular Lipid Binding Protein family are potentially the intra-cellular carriers for fenretinide and fenretinide-like molecules. Therefore it is central to this thesis that there be a robust and accurate method of evaluating binding interactions between the target proteins and small molecules. The rapidly increasing availability of chemical libraries has made high throughput screening of compounds, an attractive starting point for assessing these interactions.

Experimental determination of the structure of biomolecular interactions can, however, be a laborious, time-consuming and costly endeavour. Computational modelling, by contrast, has the potential to deliver (high-resolution) models of protein–protein-small molecule interactions. Since its inception in the late 1960s, this field has made significant advancements in both software and hardware (Schlick, Collepardo-Guevara et al. 2011). This process utilises molecular docking, which is defined as a prediction of the structure of a molecular complex starting from the individual structures of its participants.

The various docking algorithms rely upon the availability of the three dimensional model of the proteins and small molecules, the ability to perform sampling (exploring the conformational landscape of the interaction) and generating and assessing the likelihood of the generated structural models (scoring). Sampling and scoring remain two very difficult problems given the natural properties of biomolecules (in particular flexibility and thermodynamics). Docking programs implement scoring schemes based on simpler molecular mechanics, empirical observations, evolution/homology or a combination of these (Moal, Moretti et al. 2013). The scoring functions tend to be adapted to the particular sampling schemes with those algorithms that generate a very large number of models tending to use simple but fast-to-compute scoring functions. Attempts have been made to include electrostatic interactions, atomic repulsion produced by steric clashes and desolvation energies in these scoring functions. In addition, more complex scoring functions assume that the ideal interaction complex possesses the

lowest energy well and has therefore applied clustering algorithms to molecular simulations (Shortle, Simons et al. 1998).

Biological systems (protein–protein-ligand complexes) sometimes refuse to behave under the experimental conditions required to obtain structural data. In such cases, bioinformatics prediction methods may provide hints or help direct the next steps in gathering experimental information about protein small molecule interactions. A valid approach to this could be the use of surface plasmon resonance (SPR).

SPR was developed in the 1970s and has since been used to facilitate research in a wide variety of fields including biology, biochemistry and medicine. SPR biosensors have been used for measuring: physical qualities (humidity, temperature); chemical sensing (measured variations in adsorption or chemical reactions which allow calibration of hydrocarbon concentrations); and real time bio-sensing (measures change in refractive index because of a binding reaction) (Homola, Yee et al. 1999). It has become an integral part of many current analytical methods.

Most widely used SPR sensors consists of three main subsystems : an optical reader (a prism coupler, grating coupler or optical waveguide-based SPR system), a bio-recognition element (measures the analyte) and a sample delivery system (Homola 2003). The bio-sensor used in my work (BIAcore) relied upon an optical prism transducer system. Samples and buffers are delivered to the CM5 chip (a glass slide coated with a thin gold film) by a microfluidic system. A dextran matrix covers the surface and acts as a substrate to which the molecules can attach. One binding partner (ligand) is attached to the sensor surface via the dextran matrix, while the other (analyte) is injected in a continuous flow of solution (Figure 1.7).

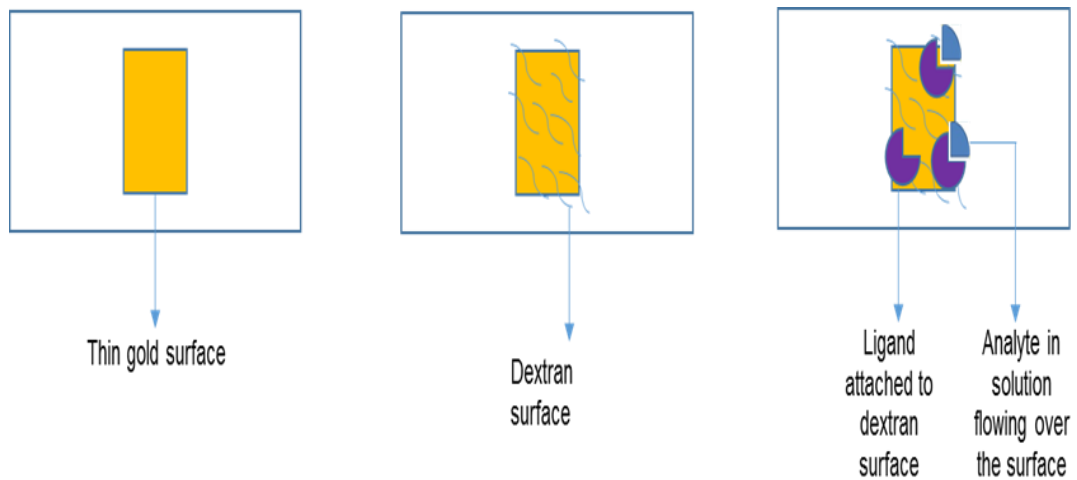


Figure 1.7 The structure of the CM5 chip used at the SPR interface. A thin gold layer (50nm) is placed on a glass slide and acts as the metal binding surface. Then a dextran matrix is attached to the gold surface and ligands are coupled to the chip. The analyte is presented to the ligand in solution and binding affinities are measured.

SPR is used to detect bio molecular interactions as they happen in real time (Homola, Yee et al. 1999, Singh 2016). It works on the principle that the analyte of interest is detected by measuring the change of the refractive index in the target solution (Guo 2012). Surface plasmons are coherent electron oscillations that exist at the interface between two surfaces, typically on a metal-dielectric interface (50nm gold coating on CM5 chip- Dextran coating). These are in essence, light waves that are trapped at the interface because of their interactions with the free electrons of the metal (Guo). SPR causes either a reduction in the intensity of light reflected or the angle of incidence from the glass slide of the sensor surface, as molecules bind. The refractive index close to the surface changes and this is proportional to the mass of the material bound (Figure 1.8). Complex analysis of results can provide information about binding affinities, specificity, kinetics and concentrations.

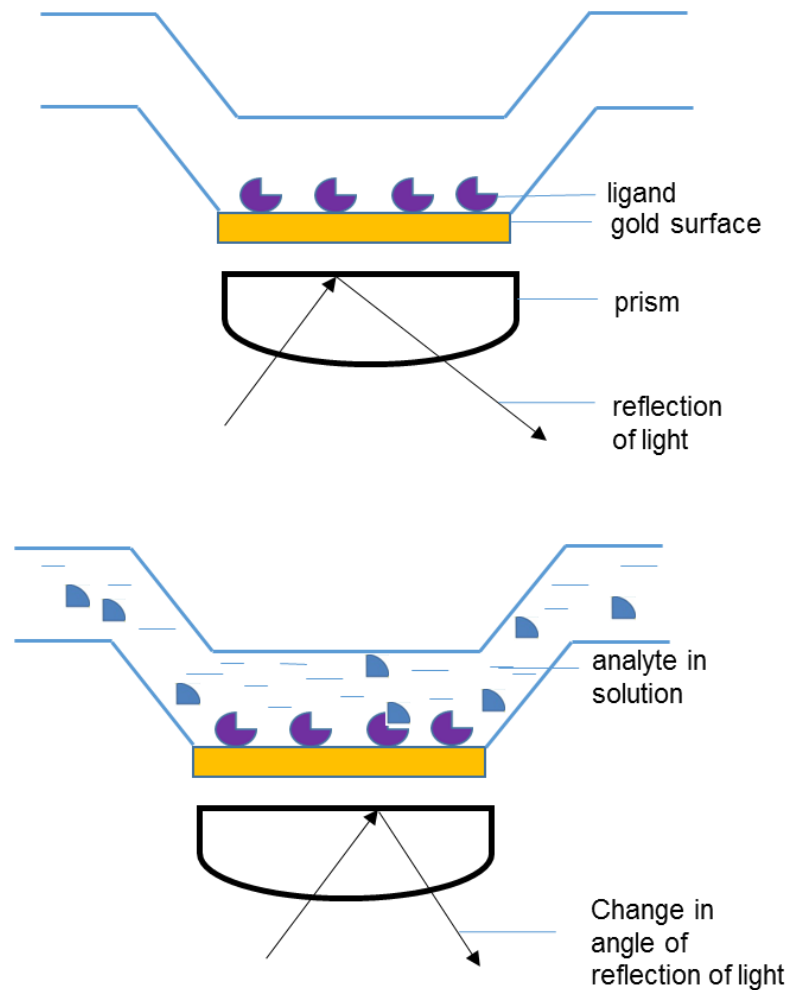


Figure 1.8 The principle of operation of SPR affinity biosensors. A change in the refractive index at the metal surface is produced when the analyte in solution, is passed over the chip. Binding reactions occur between the analyte and ligand resulting in a change in the intensity of reflected light or angle of incident light.

1.6 Hypothesis

Fenretinide is a promising anti-cancer agent that has shown some activity in preclinical studies of ESFTs. The mechanism by which this drug induces apoptosis in malignant cells is not fully elucidated, but it appears to be different to the classical retinoids. RBP4 protein is able to bind both retinol and fenretinide in a similar manner and transports them to their target cells. While in circulation, RBP4-retinol complexes with TTR to prevent elimination by kidney filtration. It would therefore not be unreasonable to assume that RBP4-fenretinide would couple to the TTR protein, providing a similar

stabilisation benefit. To investigate this hypothesis, I will examine the effect that RBP4 (alone or in combination with TTR) has on the activity of fenretinide, to establish whether this interaction may provide a novel mechanism to enhance the therapeutic effect of fenretinide.

Thus far, the clinical usage of fenretinide has been limited by its poor solubility and bioavailability. As part of this study, the binding relationships and biological effects of RBP4 with novel fenretinide-like molecules will be investigated, to test whether these might serve as carriers of fenretinide. Intra-cellularly, retinoid activity is mediated by specific binding proteins and their nuclear receptors. Therefore it is possible that fenretinide and fenretinide-like molecules will bind to one or more of the intra-Lipid Binding Proteins: CRBP-I, CRBP-II, CRBP-III, CRVP-IV, CRABP2 or FABP5 and one or more of them might be involved in the initiation of cell death by retinamides. These interactions will be investigated in this thesis (Figure 1.9).

These studies may identify new targets for the development of more effective treatments by the modulation of the retinamides and their bioavailability. In addition, new biomarkers to select patients for more personalised treatment may be revealed.

The main objectives of my research have therefore been to:

1. Examine the expression profile of RBP4 protein in ESFTs and conditioned media from ESFTs (Chapter 2).
2. Characterise the intra-cellular Lipid Binding Proteins in ESFT cell lines and tumours (Chapter 3).
3. Utilise computational modelling as a high throughput screen for measuring binding affinity and kinetics between retinoids/ retinamides with RBP4, TTR and the intra-cellular Lipid Binding Proteins (Chapter 4).
4. Investigate the potential role of the intra-cellular Lipid Binding Proteins (selected from Chapter 3) in the induction of cell death by retinamides (Chapter 5).

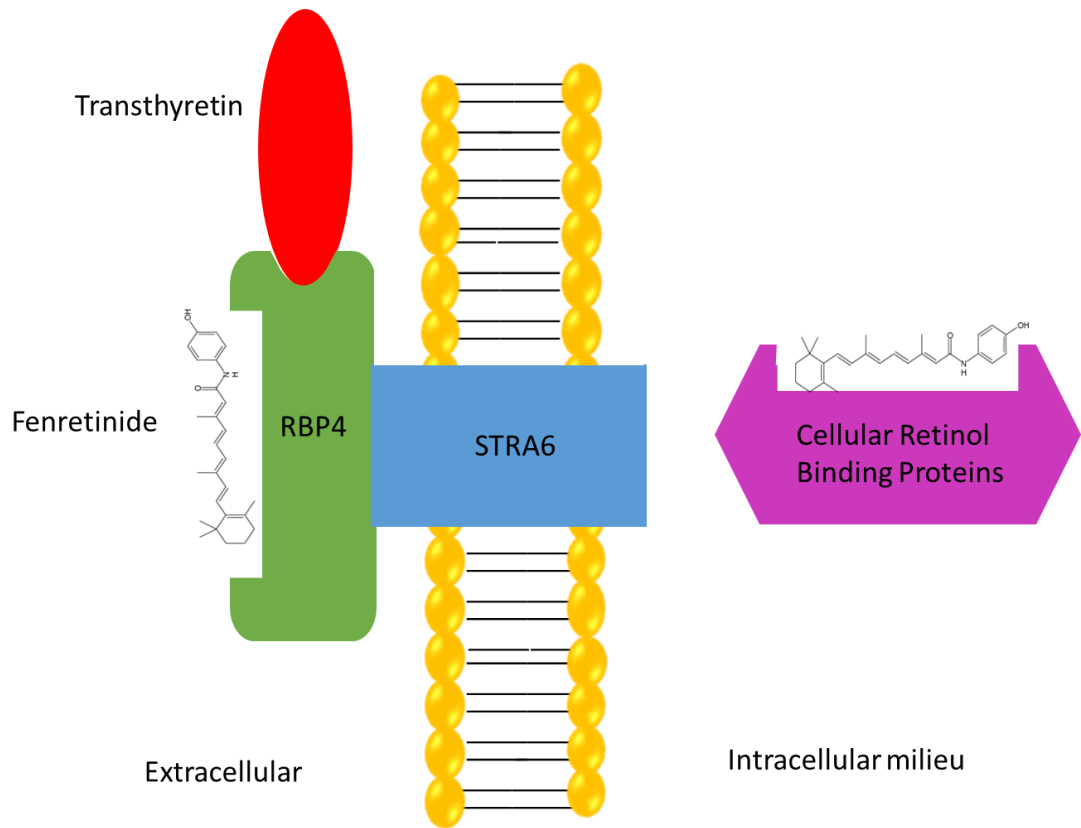


Figure 1.9 Summary of my Project Hypothesis. Fenretinide is transported to the cell surface membrane bound to RBP4 and TTR. It passes through the cell membrane protein, STRA6, and is internalised. Intra-cellular lipid binding proteins transport fenretinide to its target organelles. The cell then proceeds to cell death or survival dependent upon cell type (malignant, normal) and which receptors are stimulated.

Chapter 2

Retinol Binding Protein 4 - The extra-cellular compartment

2.1 Introduction

Lipocalins are a family of ten small molecular weight proteins that transport small hydrophobic molecules such as steroids, bilins, retinoids and lipids (Flower, North et al. 2000). They possess an eight-stranded, antiparallel, symmetrical β -barrel fold, which is in essence a beta sheet that has been rolled into a cylindrical shape. Inside this barrel is located a ligand binding site which plays an important role in lipocalin-dependent transport (Grzyb, Latowski et al. 2006)(Figure 2.1).

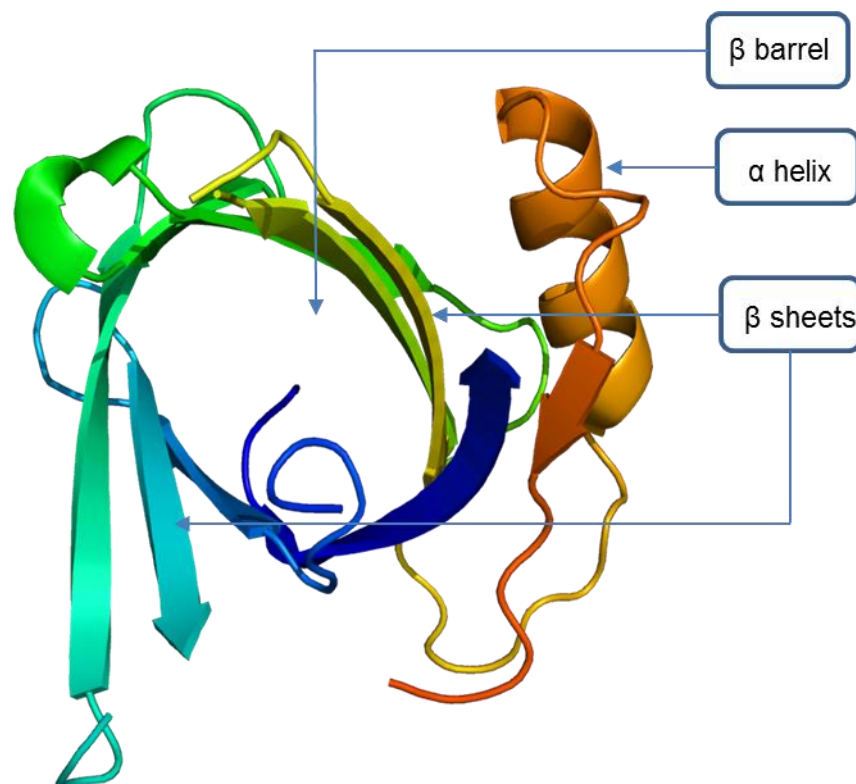


Figure 2.1 The three dimensional structure of a lipocalin molecule. It contains an eight-stranded, antiparallel, symmetrical β -barrel fold, (beta sheet) which has been rolled into a cylindrical shape and a single α -helix. The β barrel contains the binding pocket for the molecule.

The structural stability of lipocalins makes them ideal candidates for biomedical applications (Hosse, Rothe et al. 2006). Various members of this family act as scavengers or mediators of inflammation, scaffolds for artificial protein design (anticalins), antidotes, antagonistic therapeutics and targeted therapy (Flower 1996). RBP4 belongs to the lipocalin family of proteins and performs several functions including the transport of vitamin A as well as functioning as a novel adipokine (Balagopal, Graham et al. 2007, Sell and Eckel 2007, Yao-Borengasser, Varma et al. 2007, Langouche, Vander Perre et al. 2009, Broch, Ramirez et al. 2010).

Normal human RBP4 serum levels range between 40-60 µg/ml (Kanai, Raz et al. 1968). In healthy humans, RBP4 levels are highly regulated and remain relatively constant (Blaner 1989). This homeostatic balance is disrupted in the diseased state (Mills, Furr et al. 2008, Williams, Edvardsson et al. 2008). Serum RBP4 levels are decreased with infection (Arroyave and Calcano 1979), liver disease (Alkhoury, Lopez et al. 2009, Kwon, Park et al. 2009), hyperthyroidism (Smith, Goodman et al. 1971) and sickle cell disease (Warrier, Kuvibidila et al. 1994). Interestingly, serum RBP4 levels are also decreased in various types of cancer including colon and ovarian cancer (Basu, Chan et al. 1985, Gericke, Raila et al. 2005). Conversely, increased RBP4 levels are detected in insulin resistance and diabetes.

This difference in circulating RBP4 levels in various pathologies has been exploited for clinical benefit, with the hope of improving the delivery of therapy (Wu, Li et al. 2009). For instance, manipulation of RBP4 levels has been suggested as a rationale for anti-diabetic therapies (Yang, Graham et al. 2005).

It may be possible to augment the fenretinide induced cell death effect seen in ESFTs (Myatt and Burchill 2008), by modulating the interaction with RBP4. Expression of RBP4 in ESFTs and the possibility of regulating this, in order to modify the cellular response of fenretinide, has not previously been investigated.

The aim of this chapter is to characterise Retinol Binding Protein 4 in normal cells, ESFT and non ESFT cancer cell lines studied.

2.2 Methods

2.2.1 Cell Culture

Cell lines were passaged in a sterile microbiological safety cabinet (BioMat2 Class II Microbiological Safety Cabinets, Medical Air Technology Ltd, Oldham, UK). The hoods were cleaned with Trigene Advance Hospital Blue (Trigene 10%, v/v in dH₂O; Scientific Laboratory Supplies, Nottingham, UK) followed by ethanol (ethanol absolute 70 %, v/v in dH₂O) before initial use. A single cell line was in use in the hoods at any one time, in order to prevent cell line cross contamination. The cells were maintained in a humidified incubator (Sanyo CO₂ incubator, MCO-20AIC; Leicestershire, UK) with 5% CO₂ in air at a temperature of 37°C.

Six ESFT cell lines were studied: A673, RDES, SKES-1, SK-N-MC, TC-32 and TTC-466. These possessed the definitive EWS-FLI fusion transcript of which type 1 was most abundant. In addition, they contained a variety of p16 and p53 status (tumour suppressor genes), which are known to have an impact on ESFT prognosis. These cells are representative of ESFTs.

This is known to Hep G2, NHU, MSC, SK-N-SH, SH-SY-5Y, SHEP-1 and MCF-7 cells were also used in these studies as positive controls for various experiments. The origins, cytogenetics and media required for the culture of different cell lines are described in Table 2.1. All cell specific tissue culture media above were purchased from Invitrogen Life Technologies (Paisley, Scotland) and supplemented with 2 mM glutamine (L-Glutamine solution, Sigma- Aldrich, Dorset, UK) and Foetal Calf Serum (FCS: Biosera Ltd, East Sussex, UK) at the percent specified in Table 2.1.

Table 2.1 Details of ESFT and positive control cell lines. The cell line origin, source and culture media are stated. The EWS-ETS fusion type for ESFT are recorded. All cells are of human origin. PPNET= peripheral primitive neuro-ectodermal tumour, N/A= Not applicable, NB=neuroblastoma. * Conditioned media is media that has been previously incubated with cells for 48 h and so contains secreted proteins like enzymes, hormones, growth factors and cytokines. (P16- or P53- = protein not expressed; P16+ or P53+ = protein expressed). All cell lines were substrate adherent culture.

CELL LINE	ORIGIN	Genetics- Fusion transcript	MEDIA Required
ESFT cell Lines			
A673	15 yr. old female, pPNET Source: American Type Culture Collection (ATCC)	EWS- FLI-1 type 1 P16- P53-	Dulbecco's Modified Eagle Medium (DMEM) + 2mM glutamine + 10% FCS
RDES	19 yr. old male, Primary Ewing's Sarcoma of the humerus Source : ATCC	EWS-FLI-1 type 2 p16+/- p53-	RPMI 1640 + 2mM glutamine +10% FCS
SKES-1	18 yr. old male, Ewing's Sarcoma Source : ATCC	EWS-FLI-1 Type 2 P16+/- P53-	Mc Coy's 5A + 2mM glutamine + 15% FCS
SK-N-MC	14 yr. old female, pPNET Source : ATCC	EWS-FLI-1 type 1 p16+/- p53-	DMEM + 2 mM glutamine + 10%FCS
TC-32	17 yr. old female, pelvic pPNET Source : Dr J. Toretsky	EWS-FLI-1 Type 1 P16- P53-	RPMI 1640 + 2mM glutamine + 10% FCS
TTC-466	5 yr. old female, pPNET from metastatic site in	EWS-ERG	RPMI 1640 + 2mM glutamine + 10%

	the lung Source : Dr P. Sorenson	P16+/ P53-	FCS + 10% Conditioned Media*
Positive Control Cell Lines			
HEP G2	15 yr. old male Caucasian, with hepatocellular carcinoma Source : Prof Julia Newton-Bishop	N/A	RPMI 1640 + 2mM glutamine + 10% FCS
NHU	Source : ATCC CSC-C1578	N/A	Keratinocyte medium + EGF + BPE + cholera toxin
MSC	Source :Dr E Jones	N/A	Non – haematopoietic stem cell media (Miltenyi Biotech, Bisley, UK)
SK-N-SH	4 yr. old female, NB Source : ATCC	N/A	50% DMEM + 50%Modified Eagle Medium + 2mM glutamine + 10%FCS
SH-SY5Y	4 yr. old female, NB Source: Dr R. A Ross(SM), CA Redfern	Sub clone of SK-N-SH	DMEM + 2mM glutamine +10%FCS
SHEP-1	4 yr. old female,NB	Sub clone of SK-N-SH	DMEM + 2mM glutamine + 10%FCS
MCF-7	69 yr. old female Caucasian, breast cancer Source : ECACC	N/A	DMEM + 2mM glutamine + 10% FCS

The ESFT cell lines studied reflect the different tumour sites, EWS-ETS fusion type (confirmed by fluorescence in situ hybridization and RTqPCR), p53 and p16 heterogeneity of primary ESFT. All ESFT lines express CD99 at the cell surface (confirmed by immunohistochemistry and flow cytometry) and are yeast, bacterial and mycoplasma-free (determined every four months using the EZ-PCR mycoplasma test kit, Geneflow, Staffordshire,

UK). Cytogenetic testing (G-banding) is performed annually by Mr P Roberts (The Leeds Genetics Laboratory, St James University Hospital, Leeds).

The ESFT cell lines (substrate adherent cells) were maintained on 75 cm² Falcon Primaria Tissue Culture Flasks (BD Biosciences, Oxford, UK). The cells were passaged twice weekly and utilized for experiments when they reached an optimal confluence of 80-90%. Cells were harvested by washing with 5 ml of Phosphate Buffered Saline (Oxoid Limited, Hampshire, UK). PBS was aspirated and then cells were incubated for 2 minutes (min) with 5 ml of ethylene diaminetetraacetate acid (EDTA; 0.1% in PBS w/v; AnalaR Nomapur; VWR International Limited, Leicestershire, UK). The EDTA was aspirated and the cells were incubated for 2-5 min with 5ml of trypsin solution (0.25% porcine trypsin w/v in 0.9% sodium chloride: Sigma-Aldrich, Company Ltd) until they detached from the plate. Flasks were gently tapped to encourage the cells to dislodge from the plastic and this was checked with a light microscope (Nikon Eclipse TS100 Inverted Microscope). Once cells had detached from the flask, the trypsin was neutralized by adding an equal volume of media containing 10%FCS. The cell suspension was centrifuged in an Eppendorf Centrifuge (Eppendorf UK Limited, Stevenage, UK) at 402 g for 5 min and the supernatant removed by aspiration. The cell pellet was then retained for extraction of protein and RNA.

In all cell culture experiments, unless otherwise stated, cells were seeded at 1×10^6 cells/10 cm³ tissue culture dishes (Primaria; BD Biosciences,) 2×10^5 cells per well of a 6 well plate and 5×10^4 cells per well of a 24 well plates. Cells were seeded and left to adhere to the plastic, for 24 h prior to any treatment (Section 2.2.1).

2.2.2 Viable Cell Number

In order to seed cells at a fixed density, viable cell numbers were counted using the Neubauer haemocytometer (Assistant, Sondheim/Rhon, Germany, supplied by VWR). Cell suspension (10 µl) was added to 10 µl of trypan blue solution (0.4%, Sigma-Aldrich Company Ltd) and 20 µl placed on the haemocytometer. Viable cells that did not take up the blue dye were counted within the grids of the haemocytometer. This method was most reliable when

counting between 50-150 cells per grid. The mean number of cells within the 4 areas of the haemocytometer was calculated and was equivalent to the cell concentration $\times 10^4$ cells/ml.

In high through put experiments, the viable cell number was counted using the automated Vi-Cell XR Cell Viability Analyser (Beckman Coulter Ltd, Buckinghamshire, UK). This machine uses the principle of the trypan blue exclusion assay

2.2.3 RNA expression examined by Reverse Transcriptase – quantitative polymerase chain (RTqPCR)

2.2.3.1 Extraction of RNA from cell lines

The six ESFT cell lines were cultured on BD Primaria 75 cm² flask in appropriate media. The media was removed by aspiration and the cells were washed in ice cold PBS. RNA was extracted from cells at 80% confluence (Section 2.2.1). Qiagen RNeasy RNA Mini kit (Qiagen Ltd, West Sussex, UK) was used to extract RNA: B buffers (homogenising buffer) were company proprietary. The cell pellet was disrupted by adding 350 μ l Buffer RLT (lysis buffer : guanidine thiocyanate) and pipetting gently before vortexing for 1min (Fisons WhirliMixer). The lysate was placed directly into a QIA shredder column (PSC Paxgene Shredder Column) with a collection tube at the bottom of the column. The column was centrifuged at 16800 g for 2 min. An equal volume (350 μ l) of 70% ethanol (absolute ethanol diluted v/v in dH₂O, Sigma-Aldrich) was added to the homogenised lysate and mixed well by pipetting. The sample (700 μ l) was then transferred to an RNeasy spin column (Qiagen Ltd) and centrifuged for 15 seconds(s) at 8000 g and the flow through was discarded. A 700 μ l aliquot of Buffer RW1 (contains guanidine thiocyanate salt) was added to each of the columns which were then centrifuged for 15 s at 8000 g and again all flow through was discarded. Buffer RPE (500 μ l) was then placed in the RNeasy column which was centrifuged for 15 s at 8000 g. It was then centrifuged (8000 g) for a further 2 min to ensure that no ethanol was carried over during RNA elution. The RNeasy column was placed in a new collection tube and centrifuged at

16800 g for 1 min. The flow through was discarded and the column was then placed in a new 1.5 ml eppendorf. RNase free water(50 µl) (Qiagen RNeasy mini kit, Qiagen Ltd) was added directly to the spin column just above the membrane and centrifuged for 1 min at 8000 g. The eluate (30 µl) was replaced in the spin column and the centrifugation step repeated. This was carried out to maximise the yield of RNA. The samples were aliquoted (20 µl volumes) into eppendorfs and stored at -80 °C, until use.

2.2.3.2 Spectrophotometric measurement of nucleic acid

RNA concentration was quantified using a Nanodrop ND 1000 (Labtech International Ltd, East Sussex, UK). The absorbance of nucleic acids at 260 and 280 nm was measured and the RNA concentration of the samples calculated by assuming that 40 µg/ml RNA solution has an absorbance of 1 at 260 nm. The purity of RNA was assessed by the absorbance ratio at 260/280 nm. A sample was considered as being free from contaminating proteins and chemicals if the ratio was within the range of 1.8 – 2.0.

2.2.3.3 Synthesis of cDNA

Within the ESFT cells, the analysis of RBP4 gene expression required the use of 500 ng of RNA per PCR reaction. The RNA extracted from the ESFT cells was diluted in RNase free water (Qiagen Ltd) to a stock concentration 400 ng/µl. RNA was then placed in reverse transcriptase (RT) containing tubes (10 µl) as well as in the RT negative tubes (5 µl), in which reverse transcriptase was absent. Samples were heated to 95 °C for 5 min before immediately cooling on ice. RT positive mix (30 µl) containing a final concentration of 1 x First Strand buffer(Life Technologies Ltd, Paisley, UK), deoxynucleotide triphosphates (dNTPs:1mM,GE Healthcare Life Sciences, Buckinghamshire), magnesium chloride (MgCl₂: 8 mM, Amersham Biosciences) ,random hexamer primers(0.3 µg; (Life Technologies Ltd), RNasin Plus RNase Inhibitor(16 units; Promega UK, Hampshire, UK), DTT (0.1 M, (Life Technologies Ltd), Superscript III Reverse Transcriptase(200 Units; (Life Technologies Ltd) was added to the RT positive tubes, to give a final volume of 40 µl. RT negative mix (15 µl) was added to the RT negative

tubes giving a final volume of 20 μ l. The RT negative mix was the RT positive mix minus the reverse transcriptase enzyme. Each sample was then incubated in Techne TC5000 gradient thermal cycler (Keison Products, Essex, UK), heating the samples to 25 $^{\circ}$ C for 5 min and then increasing to 50 $^{\circ}$ C for 60 min. The reaction was inactivated by heating to 70 $^{\circ}$ C for 15 min. The cDNA was used in the polymerase chain reaction (PCR).

2.2.3.4 Polymerase Chain Reaction

The RT positive samples were divided to generate a 20 μ l sample for target mRNA analysis and a 20 μ l sample to confirm amplification of cDNA for a housekeeping RNA (β 2-micro-globulin: β 2M). The target gene PCR mix (80 μ l) containing 1X Taqman Universal PCR mix, sequence specific reverse and forward primers and probes (Assay on demand: Applied Biosystems) (Table 2.2), DNase free water (Sigma Aldrich Company Ltd) was added to both RT positive and RT negative tubes. β 2M PCR (10 nM) mix (80 μ l) containing specific reverse and forward sequences was added to the RT positive β 2M tubes. Samples were then transferred to a MicroAmpTM Optical 96 well reaction plate and covered with MicroAmpTM Optical Adhesive Film (Applied Biosystems). The optical plate was then placed on the ABO PRISM 7700 Sequence Detector (Applied Biosystems) and held for 2 min at 50 $^{\circ}$ C, followed by one cycle of 95 $^{\circ}$ C for 10 min. Following this, samples were amplified using 40 cycles of denaturing at 95 $^{\circ}$ C for 15 s and an annealing phase at 60 $^{\circ}$ C for 1 min. Cycle threshold values (C_t) were calculated and results analysed using the 7500 system software (Applied Biosystems). Samples were analysed in triplicate, apart from the RT negatives, which were done in duplicate. The housekeeping gene, β 2M, was used to control for amplification efficiency and RNA quality. The fold change in target gene mRNA expression was determined using the comparative C_t method (Schmittgen and Livak 2008) normalising for both β 2M and the positive control sample, using the following formula:

$$2^{-\Delta\Delta C_t}$$

Where $\Delta C_t \text{ RBP4} = C_t \text{ RBP4} - C_t \beta 2M$

$CT = \Delta C_t \text{ test sample} - \Delta C_t \text{ reference sample (HEPG2)}$

Hep G2 was chosen as the positive control for RBP4, because amplification of RNA produced good, reproducible C_t values above the limit of detection.

Table 2.2 Details of primers and probe sequence used in RTqPCR. The target genes were RBP4, CRBPI-IV, CRABP2 and FABP5 and the housekeeping gene was β 2M. The sequence of the B2M housekeeping gene probe, the forward primer and reverse primer are detailed below.

Target RNA	Taqman® Assay ID	Amplicon length	Probe spans exon
RBP4	HS00198830_m1	90	4-5
CRBP-I	HS01011512_g1	77	1-2
CRBP-II	HS00188160_m1	111	2-3
CRBP-III	HS00230385_m1	76	2-3
CRBP-IV	HS00364812_m1	62	3-4
CRABP2	HS00275636_m1	113	1-2 2-3
FABP5	HS02339437_g1	149	1-2
Housekeeping gene RNA	Sequence (5'-3')		Probe spans exon
B2M probe	CCTCCATGATGCTGCTTACATGTC TC		3
B2M forward primer	GAGTATGCCTGCCGTGTG		2
B2M reverse primer	AATCCAAATGCGGCATCT		4

2.2.4 Protein Expression

2.2.4.1 Protein Extraction from cells

Media was aspirated from cells cultured in 75 cm² Falcon Primaria Tissue Culture Flasks (80% confluence). The cells were rinsed with 5 ml of ice-cold PBS which was then transferred to a 15 ml tube (Corning® centrifuge tubes: Sigma- Aldrich Company Ltd). Two mls of fresh PBS was added to the flask and cells removed from the flask bottom using a cell scraper (Sigma Aldrich Company Ltd) and transferred to a 15 ml centrifuge tube. The flask was washed with an additional 2 ml of PBS to collect any remaining cells and this was then added to the 15 ml Corning tube. The cell suspension was centrifuged at 402 g for 5 min at room temperature. The supernatant was aspirated and discarded. The cell pellet was re-suspended in 200µl of Radio immunoprecipitation assay buffer (RIPA) (PBS containing 1% Nonidet P-40, 0.5% sodium deoxycholate, 0.1% SDS) with protease inhibitors: phenylmethylsulfonyl fluoride (PMSF, 100 µl/ml), sodium orthovanadate (NOS) (10 µl/ml), leupeptin (1 µl/ml) and aprotinin (30 µl/ml) (Sigma-Aldrich Company Ltd). The cell suspension was incubated on ice for 30 min and then centrifuged (Sigma 1-14 Microfuge: Scientific Laboratories Supplies, Yorkshire, UK) at 12470 g for 10 min at 4 °C. The supernatant was collected and 5 µl of it was added to 45 µl of dH₂O to determine the protein concentration using the Bradford Assay (Section 2.2.4.2). The remaining supernatant was added to an equal volume of sodium dodecyl sulphate (SDS) loading buffer (100 mM Tris-HCL, (pH 8.3), 4% SDS, 0.2% Bromophenol Blue, 20% Glycerol, 200 mM DDT) (Sigma-Aldrich Company Ltd), aliquoted and stored at -20 °C.

2.2.4.2 Quantification of protein concentration by Bradford Assay

Protein concentration of the samples was measured using the Bio-Rad DC Protein Assay (Bio-Rad Laboratories, Inc., Hemel Hempstead, Hertfordshire, UK), which is based on the Lowery Assay (Lowery and Holt 1951). All reagents in the kit were proprietary. Standards were prepared using Bovine Serum Albumin (Sigma-Aldrich Company Ltd (0-2 mg/ml) in 10% RIPA buffer. Samples (5 µl) were analysed in triplicate on a 96 well plate (Nunc-

Immuno™ Plates: Thermo Scientific Ltd, Leicestershire, UK). Reagent SA was prepared by adding 20 µl of reagent S (Bio-Rad Laboratories Inc.) to 1 ml of reagent A (Bio-Rad Laboratories Inc.) and then 25 µl of it was then added to each well. Reagent B (200 µl) (Bio-Rad Laboratories Inc.) was pipetted onto each well and the plate gently shaken for 10 s on the Heidolph Unimax orbital platform shaker (Scientific Laboratory Supplies Ltd, Nottingham, UK). The 96 well plate was then incubated at room temperature for 15 min before measuring the absorbance at 490 nm on a Thermo Scientific Multiskan EX Microplate Photometer (Thermo Scientific Ltd, Leicestershire, UK). The protein concentration was calculated by reading the sample absorbance on the BSA standard curve.

2.2.4.3 SDS-PAGE and Western blotting

The Bio-Rad Mini-Protean II Electrophoresis Cell Apparatus (Bio-Rad, Hertfordshire, UK) was used to separate proteins by SDS-polyacrylamide gel electrophoresis (SDS-PAGE). The percentage of acrylamide in the resolving gel was dependent upon the size of the protein of interest. For most proteins, a 15% resolving gel was used (15% acrylamide mix: Severn Biotechnology Ltd, Worcestershire, UK), (0.375M Tris (MP Biomedicals Inc.), 0.1% SDS(w/v), 0.1% ammonium-persulfate (w/v) (Sigma Aldrich Company Ltd), 0.004% N,N, N', N'-Tetramethylethylenediamine (TEMED: Sigma-Aldrich Company Ltd) The gel was allowed to polymerise for 45 min after being overlaid with 200 µl of 2-methyl-2-butanol (Sigma-Aldrich Company Ltd) to prevent the gel surface drying and to improve its polymerisation. After removal of the 2-methyl-2-butanol, 5 ml of stacking gel (5% acrylamide mix, 0.126 M Tris-HCl (pH 6.8), 0.1%SDS(w/v), 0.1%ammonium persulphate (w/v), 0.01%TEMED(w/v)) was added to the polymerised resolving gel and a comb inserted, ensuring that no bubbles were trapped between the comb and gel. The comb was removed once the stacking gel had polymerised and the wells rinsed three times with dH₂O in order to remove any non-polymerised acrylamide. The gel was transferred to the electrophoresis tank containing 2 x SDS running buffer (25 mM Tris-HCl, (ICN Biomedicals Inc., Hampshire, UK), 250 mM Glycine (Sigma-Aldrich Company Ltd) and 0.1% SDS(w/v). Protein extracts

(50 µg) and LI-COR molecular weight markers (5 µl; LI-COR Biosciences, Cambridgeshire, UK) containing SDS loading dye, made to a fixed volume, were loaded into the wells and the gel electrophoresed at 80 Volts(V) initially, and then increased to 100 V, at room temperature. The dye front was monitored carefully to ensure sufficient separation of proteins and that the proteins did not run off the gel as shown by the position of the bromophenol dye front.

Following electrophoresis, the stacking gel was removed and the resolving gel washed in transfer buffer (Gershoni's buffer: 25 mM Tris-HCl pH 8.3(MP Biomedicals Inc.), 192 mM Glycine (Sigma-Aldrich Company Ltd), 20% methanol(v/v) and 0.1% SDS(w/v) for 30 min. The Bio- Rad transfer kit was assembled with the gel placed on Amersham Hybond™-C Extra

Nitrocellulose membrane (GE Healthcare, Amersham, Buckinghamshire, UK) and then sandwiched between two sheets of 3 mm filter paper (Whatmann , Brentford, Middlesex, UK) and foam pads. A magnetic flea was added to the transfer tank which was placed on a magnetic stirrer in order to circulate the buffer during protein transfer. An ice block was also inserted in the tank to keep the buffer cool during the transfer process. The proteins were transferred to the nitrocellulose membrane at 100 V for 120 min at 4 °C. After transfer, the nitrocellulose membrane was placed in 5 ml of Odyssey Blocking Buffer (LI-COR Biosciences) and agitated for 1h at room temperature.

The membrane was incubated, by shaking with primary anti-body at a previously determined optimal dilution in PBS containing 0.1% Tween ®20(PBS-T) and Odyssey Blocking Buffer (50:50 v/v) and left overnight at 4 °C. The membrane was then washed three times in PBS. An appropriate secondary antibody (Alexa Fluor 680: Molecular Probes, supplied by Cambridge Biosciences) was applied at optimised concentrations (Table 2.3) and incubated for 1 h in the dark. Finally, the membrane was washed in the dark, 3 times (5 mins each) in PBS-T and then once for 5 min in PBS in order to remove the Tween-20 from the membrane. An Odyssey Infrared Imaging Scanner (LI-COR Ltd) was then used to visualise the membrane and identify proteins to which the antibodies had bound.

The intensity of the band visualized was quantified by densitometry using LICOR Odyssey infra-red imaging software. Protein expression determined by SDS-PAGE and western blotting was expressed as a ratio of densitometry value of the target protein relative to that of the loading control protein. The loading protein controls are proteins that are expressed constitutively within the cells of interest. As a result, they can be used as a control to confirm equal loading of protein in each well.

Table 2.3 Details of primary, secondary and control antibodies used in Western blots, at their optimised concentrations.

Primary Antibody	Antibody ID and Supplier	Species	Optimised Concentration
RBP4	Ab 73022: Abcam Plc.	Rabbit polyclonal	1.4µg/ml
CRBP-I	Sc-30106: Santa Cruz Biotechnology Inc.	Rabbit polyclonal	0.4µg/ml
CRBP-II	Ab 76631: Abcam Plc	Mouse monoclonal	1.0µg/ml
CRBP-III	Sc-98897: Santa Cruz Biotechnology Inc.	Rabbit polyclonal	1.0µg/ml
CRBP-IV	Sigma - HPA034749 Sigma-Aldrich Ltd	Rabbit polyclonal	0.2mg/ml
CRABP2	10225-1-AP Proteintech	Rabbit polyclonal	0.2µg/ml
FABP5	Ab 37267, Abcam Plc	Rabbit polyclonal	0.4µg/ml
α – Tubulin	Sc-5286: Santa Cruz Biotechnology Inc.	Mouse monoclonal	0.4µg/ml
β – Actin	Ab 8227: Abcam Plc	Rabbit polyclonal	0.2µg/ml
Sodium potassium ATPase	Ab7671: Abcam Plc	Mouse monoclonal	0.4µg/ml
Anti-TATA binding	1TBP18:	Mouse monoclonal	1.3µg/ml

protein TBP antibody	Abcam Plc		
Secondary Antibodies	Supplier	Species	Concentration
Goat anti rabbit	A21076 : Alexa Fluor 680 Molecular probes, Invitrogen, Paisley, UK	N/A	0.4µg/ml
Rabbit anti mouse	A21065 : Alexa Fluor 680 Molecular probes, Invitrogen, Paisley, UK	N/A	0.4µg/ml

2.2.4.4 Development and optimisation of Enzyme Linked Immunosorbent Assay (ELISA) for RBP4

A sandwich Enzyme Linked Immunosorbent Assay (ELISA) for human RBP4 was adapted from a protocol used by Vallet et al (Vallet 1994). Sheep RBP4 coating antibody (5.5 µl : AbD Serotec Ltd, Oxfordshire, UK) was pipetted into 11 ml of coating antibody buffer (50mM NaCO₃, pH 9.6) and mixed well by vortexing (Fisherbrand Whirlimixer Cyclone Vortex Mixer).

The capture antibody (100 µl) was instilled into each well of a 96 well plate (Nunc-Immuno™ Plates: Thermo Scientific Ltd, Leicestershire, UK). The plate was covered with a plate sealer (Biological Instrumentation Supplies) and shaken vigorously on a Heidolph Unimax 1010 plate shaker (Scientific Laboratory Supplies, Nottingham, UK) at 500 rpm for 1 h and then stored at 4 °C overnight. The following day the plate was removed from the cold room and gently warmed by agitating on a platform at room temperature.

Initially, the ELISA was established using Liquichek Immunoassay Plus Control level 3 (Bio-Rad, Hertfordshire, UK) as the standard. This is a liquid produced from human serum that contains 40 common serum analytes, including RBP4. The various components had been quantified for use as a

standard. However, during the establishment of the ELISA, the manufacturers discontinued the quantification of the concentration of RBP4 protein and so an alternative was generated to produce specific RBP4 standard curves: purified recombinant Human RBP4 lyophilized (Millipore, Hertfordshire, UK). RBP4 lyophilised powder was reconstituted in 500 μ l of Buffer B (2.5 mM $\text{NaH}_2\text{PO}_4 \cdot \text{H}_2\text{O}$, 7.5 mM $\text{Na}_2\text{HPO}_4 \cdot 2\text{H}_2\text{O}$, 500 mM NaCl, 0.002% Tween 20) to make a stock RBP4 solution (100 ng/ml). A standard curve of 2 to 15 ng/ml of RBP4 was prepared for each assay.

The plate sealer was removed and the contents discarded by inverting the plate and blotting onto absorbent paper. Buffer B (200 μ l) was used to wash each of the wells and the plate was blotted onto absorbent paper. This step was repeated 3 times to give a total of 4 washes.

The original protocol was optimised in a volume of 100 μ l (the standards and samples). To reduce reagent costs and increase sensitivity for dilute samples, the assay was optimised in a 25 μ l final volume. Buffer B (25 μ l) was pipetted in triplicate into wells A1-3 of the 96 well plate. (Thermo Scientific Ltd). RBP4 standards and unknown samples (25 μ l) were then pipetted onto the plate in triplicate. The plate was sealed and then shaken vigorously at 500 rpm for 1 h, at room temperature.

The primary antibody was prepared fifteen minutes prior to the end of the sample incubation. Rabbit RBP4 Antibody, (11 μ l: Dako UK Ltd, Cambridgeshire, UK) was diluted in 11 ml Buffer B and mixed by pipetting. The plate was removed from the shaker after 1 h and washed four times with buffer B (200 μ l). The rabbit RBP4 antibody (100 μ l) was pipetted into each well and the plate sealed and shaken at 500 rpm for 1 h at room temperature.

The secondary antibody was also prepared fifteen minutes prior to the completion of incubation with the primary antibody. Rabbit conjugated HRP conjugated antibody (11 μ l: Dako UK Ltd) was pipetted into 11 ml of Buffer B and shaken. After 1 h, the plate was washed and blotted four times with buffer B (200 μ l) before adding 100 μ l of the secondary antibody to each well. The 96 well plate was sealed and shaken at 500 rpm for 1 h at room temperature.

Ten minutes before the end of the incubation with the secondary antibody, 4 tablets of 1,2-phenylenediamine dihydrochloride (OPD: Dako UK Ltd, Cambridgeshire, UK) were dissolved in 12 ml Buffer C (Citric Acid Phosphate Buffer, pH 5.0; 34.7 mM $C_6H_8O_7$, 66.7 mM $Na_2HPO_4 \cdot 2H_2O$). After 1 h of shaking, the plate was washed 4 times with buffer B (200 μ l). Thirty percent hydrogen peroxide (5 μ l: H_2O_2 ; Sigma- Aldrich) was then added to activate the OPD and mixed by inverting the tube carefully. The oxidation product of o-phenylenediamine produced by activation is 2, 3-diaminophenazine. This soluble end product is orange-brown in colour and can be quantified spectrophotometrically. The activated OPD (100 μ l) was placed on each well and the plate sealed and shaken at 500 rpm at room temperature. The reaction (colour development) was measured after 15 min by pipetting 100 μ l of the Stop Solution (1.5 M H_2SO_4 : AnalaR Nomapur; VWR International Limited, Leicestershire, UK) into each well. The plate was gently agitated manually for 10 s.

The optical density of the samples was read on the Berthold Mithras LB 940 (Berthold Technologies (U.K.) Ltd, Hertfordshire, UK) plate reader at 490nm. Optimisation experiments demonstrated that the OPD substrate was not excited at 690 nm on Thermo Scientific Multiskan EX Microplate Photometer (Thermo Scientific Ltd, Leicestershire, UK) and this step was included in the ELISA to correct for background contributions (Figure 2.2).

The RBP4 standard curve was produced by plotting the log RBP4 concentration (x-axis) against log absorbance (A) of standard (y-axis).

Where $\log A = \log (A_{490nm} - A_{690nm})$

The RBP4 concentration of unknown samples was calculated by reading the log absorbance from the standard log curve.

2.2.4.5 Preparation of samples for ELISA

ESFT and HEPG2 cells were seeded into 75 cm² Falcon Primaria tissue culture flasks at a density of 2×10^5 /ml. The cells were then placed in an incubator in 5% CO₂ in air at 37 °C. After 72 h, the media was aspirated and retained. Cells were harvested and the viable cell number counted using the Vi-cell (Section 2.2.2). Protein was extracted from the cells as described in Section 2.2.4 and the protein aliquots were stored at -20 °C.

2.2.4.6 Concentrating the Media

Media (1 ml) was aliquoted (50 µl) for non-concentrated samples. The remaining media (14 ml) was concentrated using Centricon Plus-70 centrifugal filter units (Millipore UK Ltd). The centricon unit was pre-rinsed by centrifuging with dH₂O (70 ml) for 5 min at 3500 g (room temperature) in order to remove excess glycerine. The centricon cap and concentrate collection cup were washed with 70% ethanol (w/v: Sigma Aldrich Ltd). Media (14 ml) was pipetted in the filter cup, sealed with the cap and then placed in the filtrate collection cup. The centricon unit was placed in a swing bucket centrifuge (Eppendorf Swing Bucket Centrifuge, Cole-Parmer UK, London, UK), and centrifuged at 3500 g for 15 min at room temperature. After completion of the concentrating step, the centricon-plus 70 device was removed and the sample filter cup separated from the filtrate collection cup. The concentrate cup was inverted and placed on top of the sample filter unit. The entire unit was inverted and placed in a centrifuge and centrifuged for 2 min at 1000 g at room temperature. The concentrate cup was removed from the sample filter cup, ensuring that the filter cup remained inverted during the process. The concentrated sample was then pipetted into a 500 µl eppendorf.

Comparison of the ELISA standards and samples prepared in Buffer B, media and RIPA buffer determined that it was acceptable to produce the ELISA standards for the ESFT protein samples in RIPA buffer and the standards for the conditioned cell media samples in media.

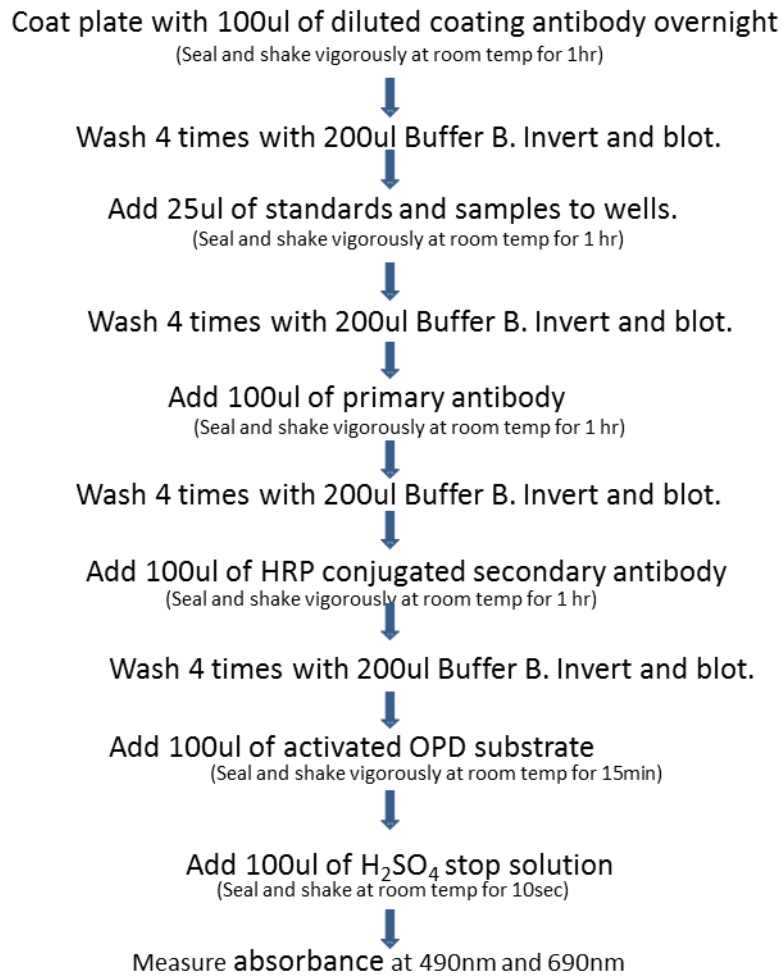


Figure 2.2. Flow Diagram of RBP4 sandwich ELISA. The standard curve for analysis of protein cell extracts was prepared in RIPA buffer whereas for analysis of media, the standard curve was prepared in media. The optical density was measured at 490nm (maximal excitation) and 690nm (background) on Thermo Scientific Multiskan EX Micro plate Photometer, (51118170: Thermo Scientific Ltd, Leicestershire, UK)

2.2.5 Statistical Analysis

Analyses were undertaken using the GraphPad prism 6 software. RBP4 mRNA expression detected by RTqPCR was analysed by two-way analysis of variance (ANOVA) when comparing 3 or more cell lines. Variation between cell lines were compared using Bonferroni's post hoc multiple comparison test and differences were considered statistically significant when $p < 0.05$.

2.3 Results

2.3.1 Doubling times for ESFT Cell lines

The doubling times for the 6 ESFT cell lines used in this project were calculated from growth curves experiments performed (Table 2.4). Sample growth curves (A673, SK-N-MC and TC-32 cell lines) used to perform these calculations are presented in Figure 2.3.

Table 2.4 The doubling times for the 6 ESFT cell lines; results are shown as mean doubling time (h) (n=3).

Cell Lines	Mean Doubling Time
A673	21 hours
RDES	29 hours
SKES-1	23 hours
SK-N-MC	17 hours
TC-32	17 hours
TTC-466	23 hours

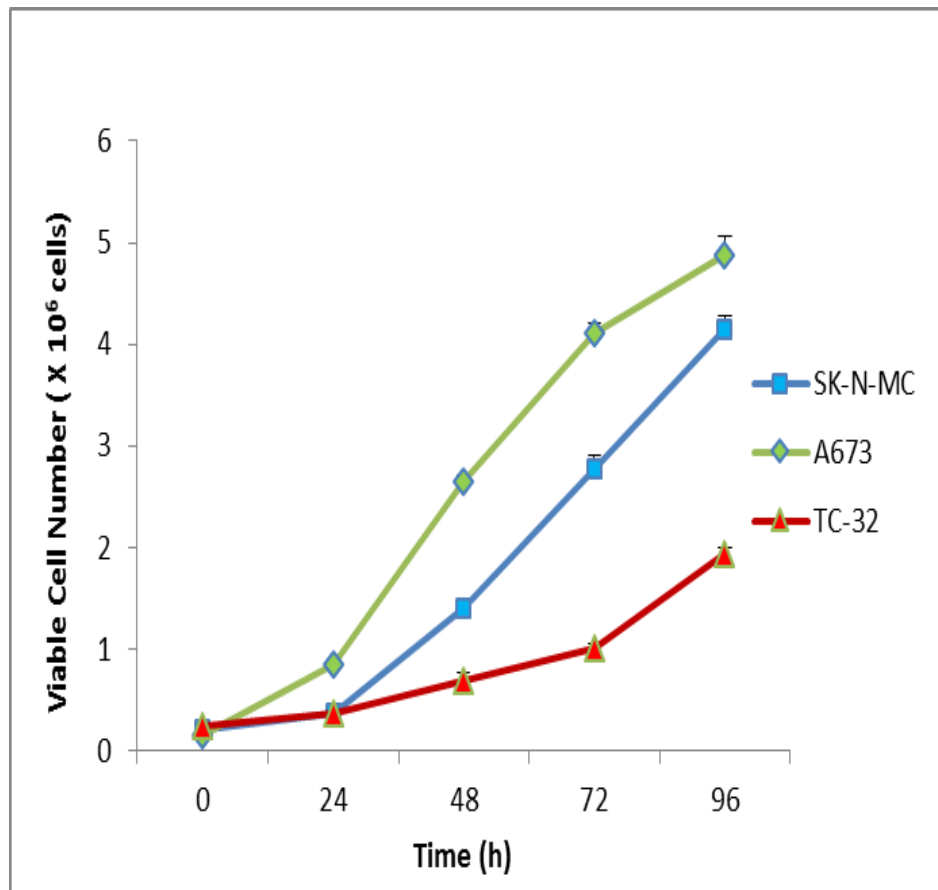


Figure 2.3. Viable Cell Number of the ESFT cell lines with time (96h)

2.3.2 Expression of Retinol Binding Protein 4 in ESFT Cell Lines

There was heterogeneous expression of RBP4 mRNA in ESFT cell lines detected by RTqPCR (Figure 2.4). The RDES ($\Delta\Delta C_t = -3.92$) and SK-N-MC cell lines ($\Delta\Delta C_t = -3.89$) had the highest levels of mRNA and SKES-1 ($\Delta\Delta C_t = -6.01$) had the lowest level, of all the ESFT cell lines examined. RDES and SK-N-MC cell lines had significantly higher levels of RBP4 mRNA than A673, SKES-1, TC-32 and TTC-466 ($p = 0.0001$). All 6 ESFT cell lines showed significantly lower levels of expression of RBP4 mRNA when compared to the positive control cell line, HEP G2. ($p = 0.0009$)

The 6 ESFT cell lines and HEP G2 were amplified for the housekeeping gene, $\beta 2M$. The $\beta 2M$ mRNA was detected in all the cell lines, ($\Delta\Delta C_t = 16.09-18.75$). The HEP G2 cell line was used as a positive control and RNase free water as the negative control. There was no detection of amplified mRNA in samples in the absence of reverse transcriptase or in samples in which RNA

was replaced with RNase free dH₂O. This was consistent with efficient and specific cDNA formation and amplification.

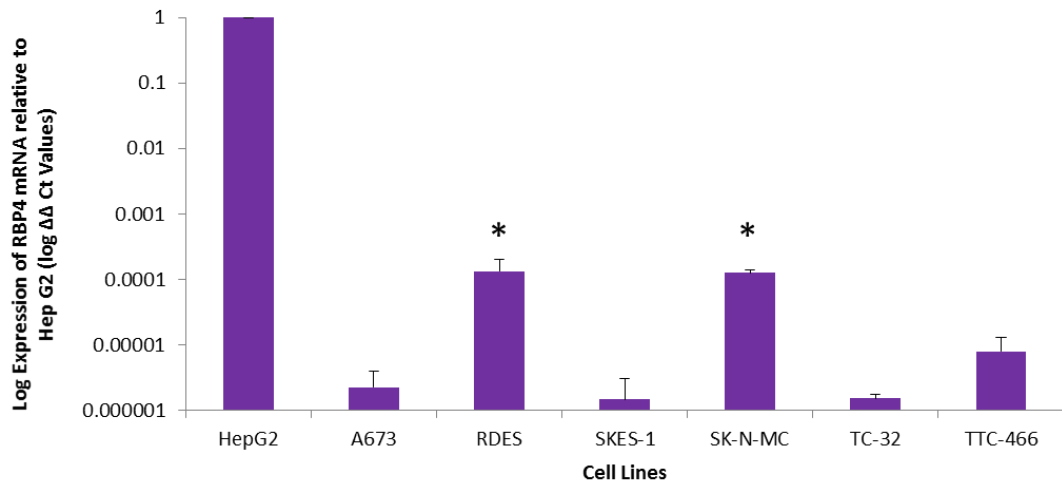


Figure 2.4 The expression of RBP4 mRNA in ESFT cell lines examined using the RTqPCR and the $\Delta\Delta$ Ct method. B2M was used as the control mRNA and HEP G2 cell line as the standard for reporting. Each reaction contained 400ng/ μ l RNA. (n=9) The difference in expression of RBP4 mRNA between the positive control and the ESFT cell lines were statistically significant using ANOVA post hoc ,Bonferroni procedure ($p=0.0009$)

2.3.3 Protein expression of RBP4 in ESFT, other cancer and normal cell lines

RBP4 protein (21 kDa) was not detected in the cell extracts of the 6 ESFT cell lines, but was in the recombinant RBP4 protein extract (R&D Systems, Inc. Minneapolis, USA) and the positive control cell line, HEP G2 (Figure 2.5). Equal protein loading was confirmed by probing the immune-blot for α -Tubulin (50 kDa). However, α -tubulin was not detected in the HEPG2 cell extracts. Since β - Actin (42 kDa) was detected, it was used all the cell extracts studied.

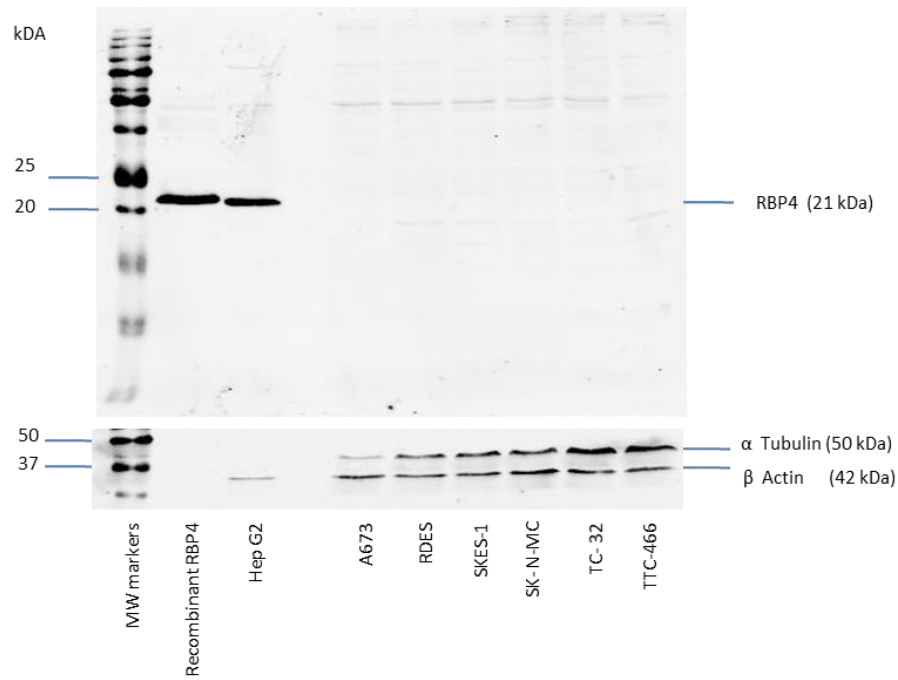


Figure 2.5. Expression of RBP4 protein in ESFT cell extracts, by western blot. Recombinant RBP4 and HEP G2 extracts were used as positive controls. MW= molecular weight; kDa= kilo daltons

Extracts from cancer cell lines that were known to be resistant to fenretinide (Myatt and Burchill 2008) including SK-N-SH, SHEP-1 and SH-SY-5Y did not express RBP4 protein; β -Actin showed uniform protein loading apart from mesenchymal stem cell line (MSC), which was under-loaded. RBP4 expression was not detected in the normal human urothelial cells (NHU: immortalised by overexpression of the telomerase gene, known as h-TERT) and Mesenchymal Stem Cells (MSC) (Figure 2.6). HEP G2 cells were used as the positive control and β - Actin as the loading control.

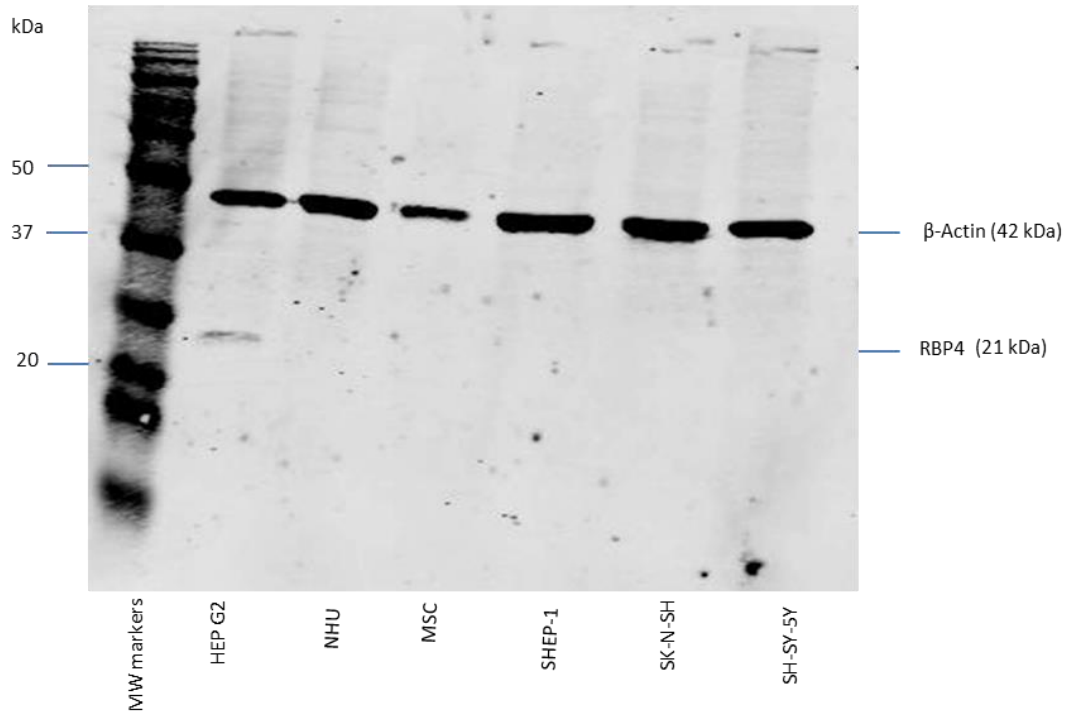


Fig 2.6. Western Blot analysis for RBP4 protein in fenretinide resistant cell lines, using HEP G2 as the positive control and β -Actin as the loading control. MW= molecular weight; NHU= Normal human urothelial cells; MSC= Mesenchymal stem cells; SHEP-1 , SK-N-SH and SH-SY-5Y = neuroblastoma cell lines.

Non ESFT cancer cell line protein extracts were also analysed by Western blot for RBP4 protein. The cell lines studied were HT-29 (colorectal adenocarcinoma), HMB2 (melanoma), A375 (melanoma), T98G (glioblastoma), IMR-32 (neuroblastoma), RT-4 (bladder cancer), RT-112 (bladder cancer), T-24 (bladder carcinoma), and MCF-7 (breast cancer). These cell lines did not produce detectable RBP4 protein. HEP G2 was the positive control cell line and β -Actin was the loading control (Figure 2.7).

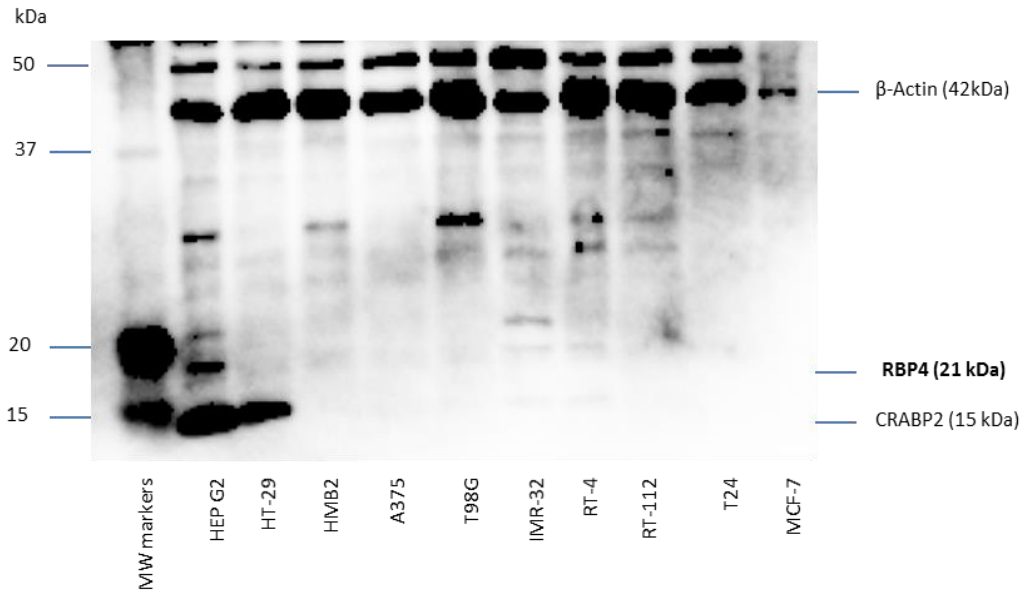


Fig 2.7. Western blot analysis for RBP4 protein in non ESFT cancer cell lines protein extract, using HEP G2 as the positive control and β -Actin was the loading control. The cell lines used included HEP G2, HT-29, HMB2, A375, T98G, IMR-32, RT-4, RT-112, T-24 and MCF-7. MW= molecular weight.

2.3.4 RBP4 ELISA Method Optimisation

2.3.4.1 Absorbance

Experiments were performed using the human RBP4 standard (E8018-K: Millipore) to determine the optimal optical density of absorbance of the substrate (OPD). The ELISA was scanned at several wavelengths including 405 nm, 450 nm, 490 nm, 550 nm, 620 nm and 690 nm. Maximal energy absorbance occurred at 490nm with none at 690nm (Figure 2.8). According to Beer Lambert's Law, analyte concentration is directly related to the absorbance of light through the analyte, as stated in the equation below:

$$A = ebc$$

Where A = absorbance

e = molar absorptivity

b = path length of analyte

c = concentration of the analyte

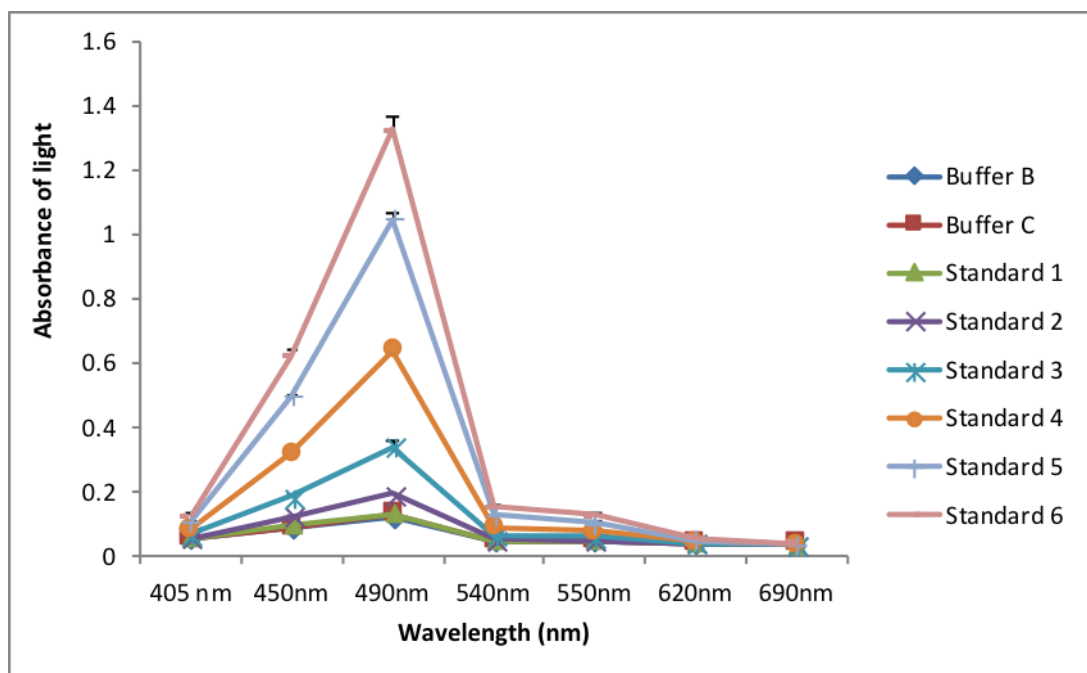


Figure 2.8 The absorbance of light by RBP4 protein. The absorbance of buffers B, C, and standards 1 - 6 were measured at various wavelengths (405nm, 450nm, 490nm, 540nm, 550nm, 620nm, 690nm) in order to determine the optimal wavelength for excitation. These buffers and standards are used in the RBP4 ELISA . Buffer B = diluting buffer; Buffer C = citric acid buffer, standard 1 = 0.1ng/ml RBP4; standard 2 = 0.4ng/ml RBP4 ; standard 3 =1.2ng/ml RBP4 , standard 4 = 3.7ng /ml RBP4 ; standard 5 = 11.1ng/ml RBP4 and standard 6 = 33.3ng/ml RBP4

2.3.4.2 ELISA Volume Optimisation

The original ELISA protocol was designed for a reaction volume of 100 μ l. Experiments comparing the use of identical concentrations of the RBP4 standards in 25 μ l and 100 μ l aliquots on the same reaction plate were carried out and shown to give comparable results (Figure 2.9). This was performed in an attempt to rationalise reagent cost as well to make efficient use of patient samples received. The absorbance of light for the RBP4 samples demonstrated saturation with increasing concentration. The curves were then mathematically transformed by plotting the log RBP4 concentration (x-axis) against the log absorbance of light (y-axis) for 25 μ l (red) vs 100 μ l (blue) aliquots of sample. The linear regression lines

demonstrated accurately fitted the data ($R^2 = 0.97, 0.98$) and the absorbance were approximately equal even though there was a four- fold increase in sample volumes. Future experiments were therefore carried out using reduced reaction volumes (25 μ l).

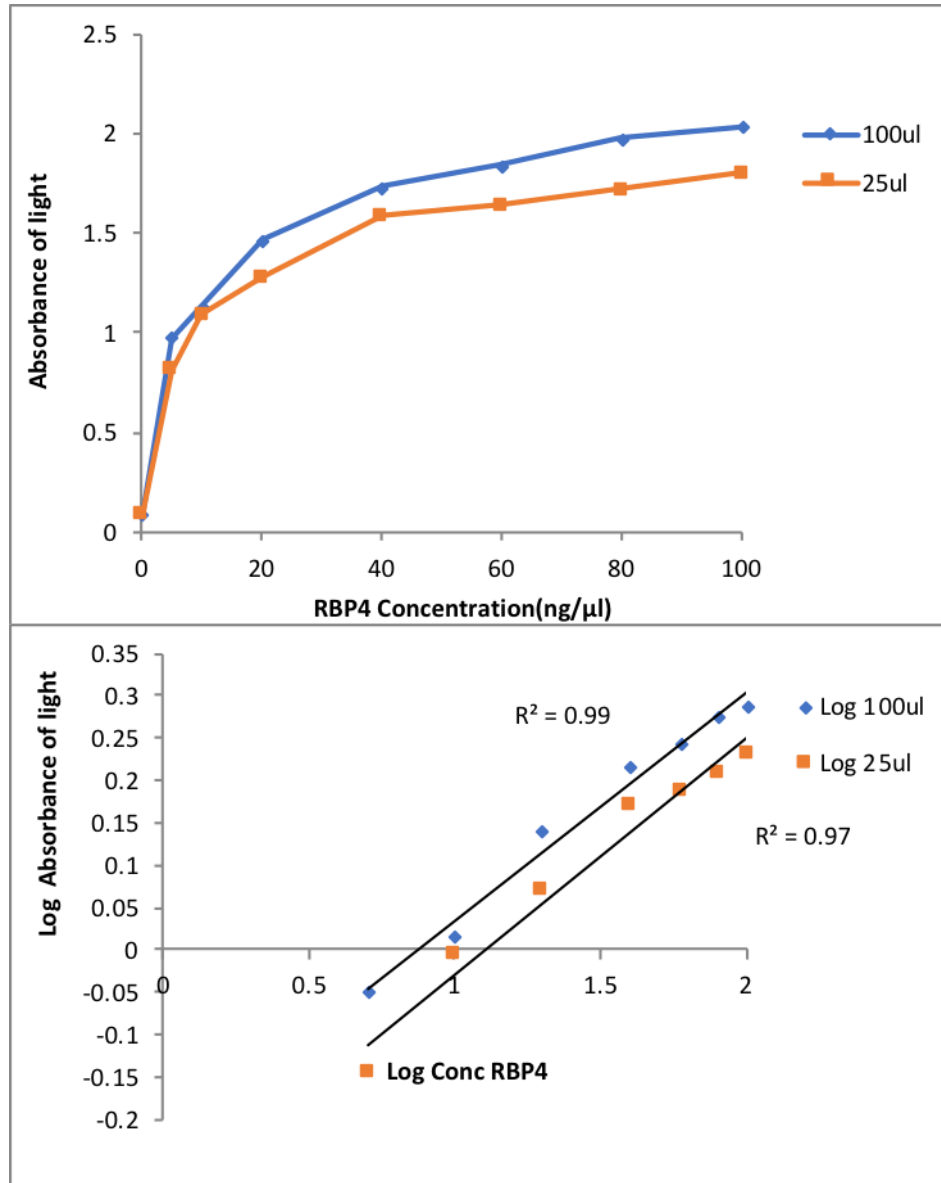


Figure 2.9 Volume comparison of RBP4 standard curve prepared in 25 μ l and 100 μ l volumes. **a)** The x axis shows increasing concentration of RBP4 standards (ng/ml) and the corresponding absorbance of light plotted on the y axis. The red curve shows the absorbance when standards were prepared in 25 μ l aliquots and the blue curve shows comparable standards in 100 μ l volumes. **b)** The \log_{10} plot of RBP4 ELISA volume optimisation demonstrating the correlation of fit of the data. The RBP4 standard curves prepared in 25 μ l and 100 μ l volumes showed good co-relation with R^2 values of 0.97 and 0.99 respectively. There was no significant difference in the optical density observed ($p=0.61$) by Mann-Whitney U test.

2.3.4.3. Limits of the Standard Curve

The Millipore RBP4 standard was provided at a stock concentration of 100ng/ml. Initial experiments investigated the relationship between optical density and RBP4 concentration over the ranges of 0-100 ng/ml. The relationship appeared to be that of a kinetic curve tending towards saturation (Figure 2.9). The graph appeared linear between 2-20 ng/ml RBP4. When a 'best fit' regression line was plotted for these concentrations, the correlation was poor with an $R^2=0.74$. As a result, the data was transformed by plotting the log RBP4 concentration (x-axis) against the log absorbance of light (y-axis). When a regression line was applied to this data, the correlation was better for the concentration range 2-15 ng/ml ($R^2=0.99$). This data between this range was reproducible and reliable (Figure 2.10).

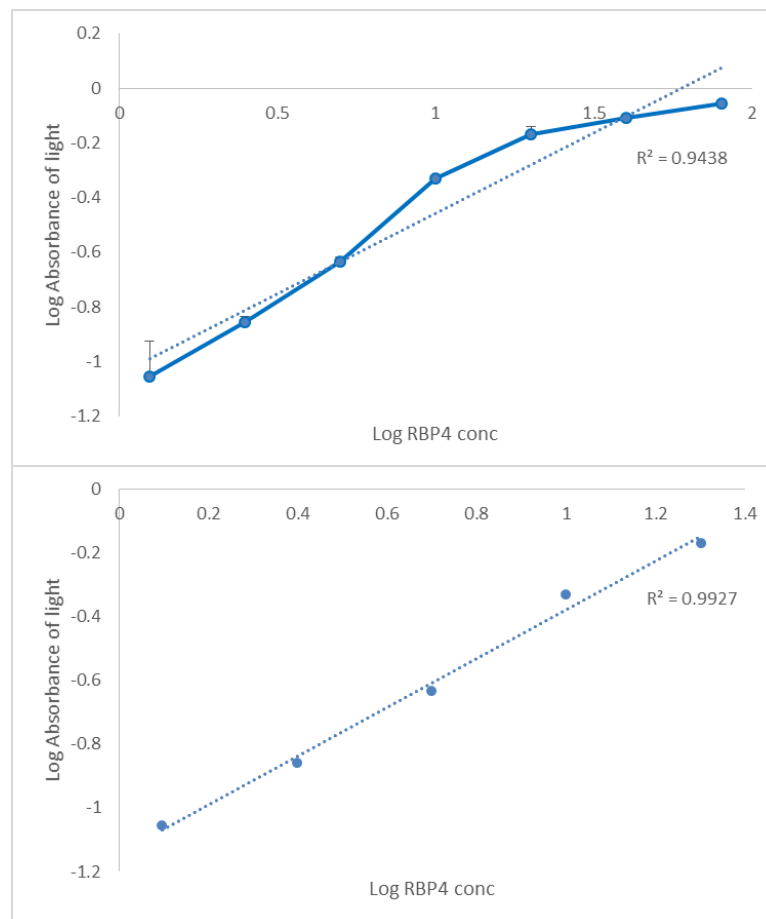


Figure 2.10 The correlation coefficients for the log RBP4 Standard Curves. **a)** The log RBP4 concentration (0-80ng/ml) against the log of absorbance. **b)** The \log_{10} plot of the data set in **(a)** but restricted to RBP4 concentrations 0-20ng/ml. The R^2 values are closer to 1 in the latter RBP4 concentration range, consistent with the conclusion that the assay was more accurate when the concentration of RBP4 standards were 0-20ng/ml.

2.3.4.4. Assay Variability

2.3.4.4.1. Intra- assay variability

RBP4 standard curves were produced on the same day using the ELISA method. Three experiments were performed in triplicate on a single 96 well plate. The average optical density, standard deviation and percentage error were then calculated. The intra-assay variability was 2.9- 23.5 % (Table 2.5).

Table 2.5. The intra- assay variability of the RBP4 ELISA. Data from three RBP4 standard curves produced in 1 experiment were analysed to calculate variability and it was expressed as a percentage of the average optical density (n=9).

RBP4 Conc (ng/ml)	Average absorbance at 490nm	Standard Error of the mean	Percentage Error (%)
0	0.00	0.00	0.00
1.25	0.25	0.06	23.5
2.5	0.37	0.01	3.63
5	0.60	0.02	2.90
10	0.85	0.03	3.24
20	1.06	0.03	3.16
40	1.25	0.05	3.90
80	1.31	0.06	4.59

2.3.4.4.2. Inter-Assay Variability

ELISA experiments were repeated on five different days and the average optical density, standard error of the mean and percentage error of the results of these experiments were used to calculate the inter-assay variability. This ranged between 15.9% - 22.2 % (Table 2.6).

Table 2.6. The inter- assay variability of the RBP4 ELISA. Data from RBP4 standard curves produced in 5 experiments were analysed to calculate variability and it was expressed as a percentage of the average optical density (n=5).

RBP4 Conc (ng/ml)	Average Absorbance at 490nm	Standard Error of Mean	Percentage Error (%)
0	0.002	0.001	
1.25	0.187	0.041	21.7
2.5	0.304	0.068	22.2
5	0.483	0.099	20.4
10	0.696	0.111	15.9
20	0.901	0.145	16.1
40	1.026	0.167	16.3
80	1.102	0.180	16.4

2.3.4.5 Stability of the Coating Antibody

The stability of the antibody coated ELISA plate was investigated to minimise any variability due to deterioration of the plate. Five plates were coated on the same day and the RBP4 ELISA standards were generated on days 1, 5, 6, 14 and 21. This experiment showed that the absorbance of the plate decreased as time from coating increased. The most robust results would be obtained by coating the plate the night before the experiment (Figure 2.11).

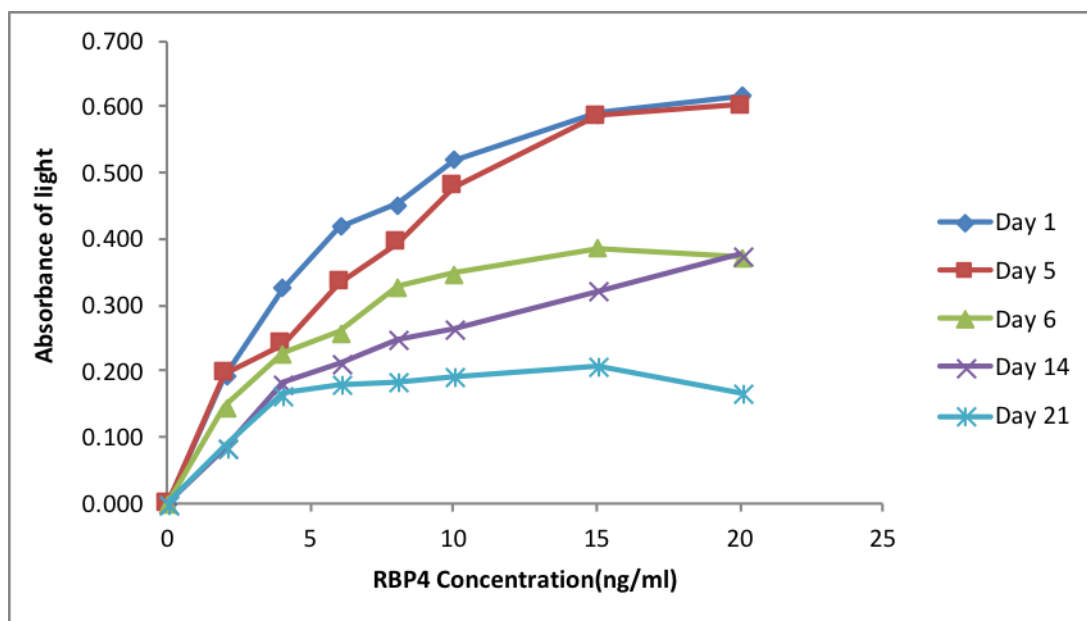


Figure 2.11. The optimal absorbance of a batch of RBP4 coated ELISA plates: on day 1, 5, 6, 14, 21 post coating with the antibody. As time from coating increases, the absorbance decreased. This was statistically significant between plates coated on Day 1 and Day 21 ($p=0.006$ by Kruskal-Wallis analysis of ranks).

2.3.4.6. Concentration of RBP4 secreted into the media and in the ESFT cell extract

Levels of RBP4 protein were measured in protein extracts from ESFT cell lines and the accompanying media that was collected from cells and concentrated (Section 2.2.4). The level of RBP4 protein in the cell extracts and concentrated media were analysed on the same 96 well plate. This was below the lower limit of detection for the ESFT protein extracts and the accompanying media; the positive control HEP G2 and accompanying media were positive for RBP4 protein (Table 2.7). The detection of RBP4 in HEPG2 cell extracts and the media from these cells confirm that the RBP4 ELISA had worked. Failure to detect RBP4 in ESFT cell extracts is consistent with the results of the western blot (Figure 2.5).

Table 2.7 RBP4 concentration in the six ESFT cell lines (by ELISA) and the media collected from these cells. The HEPG2 cell line was used as a positive control (n=3). The results are expressed as the mean \pm (SEM)

Cell Lines	RBP4 concentration in cell extracts (ng/ml)	RBP4 concentration in media collected from cells (ng/ml)
A673	Undetectable	Undetectable
RDES	Undetectable	Undetectable
SKES-1	Undetectable	Undetectable
SK-N-MC	Undetectable	Undetectable
TC-32	Undetectable	Undetectable
TTC-466	Undetectable	Undetectable
HEP G2	55.8 \pm 2.6	54.2 \pm 5.1

2.4 Discussion

For the first time, I have demonstrated that ESFT cell lines express RBP4 mRNA, as detected by RTqPCR. The level of RBP4 mRNA was low compared to that expressed by the positive control line HEPG2. However, I was unable to detect RBP4 protein in the ESFT cell lines, using western blots or ELISA. The western blot method is highly specific, as it separates the protein based on the physical property of size, as well as, the specificity of the antibody (Duburcq, Olivier et al. 2004, Ma, Baruch et al. 2012). But it does, however, require relatively large sample volumes. In one study using 40µg of yeast protein lysate, the average protein abundance detected was 51,200 copies per cell with no protein detected with abundances of less than 1000 copies per cell (Gygi, Corthals et al. 2000).

The RBP4 protein is mainly synthesized in the liver but also known to be expressed in adipose tissue, kidney, lung, heart, skeletal muscle, spleen, eyes and testis (Noy 2000). Given that ESFT are small round cell tumours that originate from bone or soft tissue, it would not be surprising to find RBP4 protein to present in these cells. It is reassuring to note that the positive control cells (HEPG2 - liver adenocarcinoma cells) express the RBP4 target protein and this could be detected in the conditioned media of the cells. The absence of protein in the ESFT by western blot method questions whether the protein is indeed present but at a low concentration (i.e. below the threshold of detection of the western blot). While the western blot method is highly specific, it is not very sensitive, giving very crude approximations of quantification (Bass, Wilkinson et al. 2017).

I have attempted to answer this question by adapting and developing a RBP4 ELISA method. This is a plate-based assay technique designed for detecting and quantifying peptides, proteins, antibodies or hormones. Although the ELISA would be less specific than the western blot (dependent on the antibody), it would be much more sensitive and allow for more accurate quantification (Duburcq, Olivier et al. 2004, Ma, Baruch et al. 2012). The RBP4 sandwich ELISA that was developed was a 5 step method. Meticulous care was taken to ensure the quality of the antibodies and proteins: they were aliquoted into single use aliquots to prevent freeze-thaw

cycles. OPD substrate and activation reagent were procured in the smallest available volumes in order to ensure that degradation of the compounds had not occurred before use in the ELISA. Purified RBP4 (E8018-K, Millipore, Hertfordshire, UK) with a concentration of 100ng/ml was utilised as a positive control for the generation of the standard curve. In addition, protein cell extracts and standards were prepared in RIPA buffer and media, in order to ensure that the diluents did not contribute to the optical density reading. This ELISA was optimised for the Nunc 96 well plates (on which it was performed) to ensure uniformity across the experiments. A single batch of plates were used for these experiments.

No ESFT cell extracts produced a result that was above the lower limit of my standard curve (2ng/ml). In order to determine whether this protein was in fact present in the cells (even in very low concentrations, < 2ng/ml), cell extracts and conditioned media were concentrated using centricon columns. The RBP4 ELISA experiments revealed that in the concentrated ESFT cell protein extracts and surrounding media (concentrated), RBP4 protein was not detectable.

The six ESFT cell lines express the RBP4 mRNA but not the protein. The reasons for this may be multi-factorial. The human genome and by extension mRNA codes for approximately 20,500 various proteins (International Human Genome Sequencing 2004, Siffroi and Chantot-Bastaraud 2004). However, the global relation between mRNA concentration and protein on mammalian cultures cells is poor, with only a 40% predictive value from cellular mRNA measurements (Table 2.8).

Table 2.8. Summary of studies for the relationship between mRNA and protein concentration in mammalian cells. R^2 = co-efficient of determination; R_s = Spearman's correlation co-efficient; * = human cell lines.

Authors	Year	Cell Line	R^2 (R_s)
Tian et al	2004	Mouse EML cells	0.35
Vogel et al	2010	Medulloblastoma *	0.29 (0.46)
Lundberg et al	2010	Brain glioblastoma *	(0.43)
Lundberg et al	2010	Squamous cell carcinoma*	(0.42)
Lundberg et al	2010	Bone osteosarcoma *	(0.42)
Schwanhauser et al	2011	NIH3T3 mouse fibroblast	0.37 (0.41)
Average all values \pm SD			0.39 \pm 0.05

Post-transcriptional mechanisms including translation and post translational modification of a protein from mRNA is not well-defined or understood and there are many complex and complicated processes involved. mRNA binds to ribosomes at specific binding sites, called the Shine Dal-garno sequence (SD). These sequences are complementary to the 3'end of the 16S rRNA. Transcripts with a weak SD (not perfectly complimentary) are translated with a lower efficiency (Maier, Guell et al. 2009). In addition, the secondary and tertiary structure of mRNA are sensitive to temperature and small metabolites which can cause them to selectively sequester and expose the ribosomal binding site (Grossman, Zhou et al. 1985). Regulatory proteins and sRNAs are able to influence the evolution and stability of mRNA and this affects translational efficiency. In addition, ribosomal density and occupancy has a direct role to play in translational efficiency (Figure 2.12).

The major post-translational factors that affect protein expression within cells are protein degradation and its secretion from cells. The half- life of a protein is dependent on the intrinsic stability of the protein, the *N*-terminal amino acid of a protein (the *N*-end rule), post translation processing (phosphorylation, ubiquitination, methylation and acetylation) and the cellular localisation of the protein.

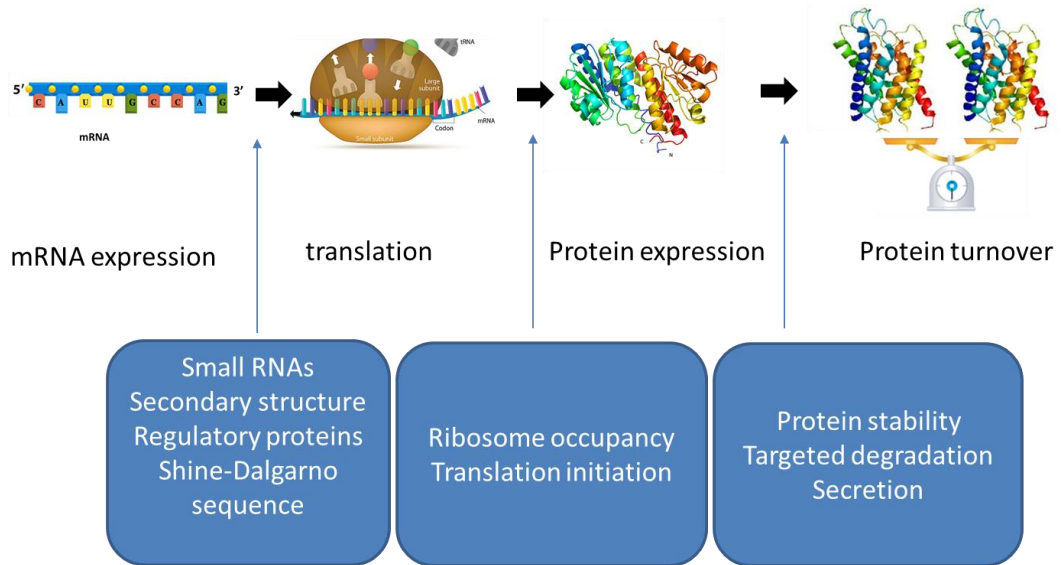


Figure 2.12. Post-transcriptional factors affecting protein formation from mRNA. Various biological and technical processes determine whether the target protein is formed, its structure and function. This diagram was adapted from Maier et al. 2009.

Although RBP4 protein plays a role in transporting of retinoids to cells (Alapatt, Guo et al. 2013), I have shown that it is not produced by the ESFT cells. Furthermore, RBP4 protein was not detected by western blot, in the non-cancer cell lines NHU and MSC. This is inconsistent with studies that have shown low levels of RBP4 protein in the undifferentiated human subcutaneous adipose tissue-derived mesenchymal stem cells (Winkler, Hempel et al. 2016).

Other non-ESFT cancer cell types were investigated for this target protein, which was not expressed by HT-29 (colon cancer), HMB2 and A375 (melanoma), T98G (glioblastoma), RT-4, RT-112 and T24 (bladder cancer) and MC7 (breast cancer). Four neuroblastoma cell lines with variable sensitivities to fenretinide (IMR-32= very sensitive to drug; SHEP-1, SK-N-SH, SH-SY-5Y= resistant to drug) were investigated for their RBP4 protein content. RBP4 protein was not detected in these neuroblastoma cell lines. This variable response to the drug fenretinide could not be attributable to any differences in binding to RBP4, as this protein does not appear to be present.

Of all the cell lines tested, RBP4 protein was only present in HEPG2. This is contrary to my expectation of RBP4 being produced and utilised locally by cells sensitive to the retinoids/retinamides. I investigated a varied panel of other cancer cell lines, in order to determine whether this observation was specific to ESFTs. There have been numerous studies describing increased and decreased RBP4 levels, dependent upon the cancer type (see Section 1.4.1 and 2.1). I have therefore investigated 2 non cancer cell lines, one of which was the MSCs. The ESFTs are purported to originate from MSC (von Levetzow, Jiang et al. 2011). It would be an interesting observation to determine whether this protein was present in the cell of origin but undetected in ESFT. This did not appear to be the case.

It is much more likely that the transport protein is produced in the liver and released into circulation, in order to perform its exocrine function (Makover, Soprano et al. 1989, Newcomer and Ong 2000). ESFT cell studies have shown that cell death approached 90% with fenretinide (10 μ M). Therefore it is highly unlikely that the modulation of a protein that is efficiently transported from its distant site of production to the peripheral tissue where it is needed to initiate cell death, would result in any significant improved local outcome.

2.5 Future work

While detection of the absolute RBP4 protein content in the ESFT cell lines was of great significance, it would be important to consider that said cells could demonstrate a heterogeneous protein expression within its population. This would not be detectable by ELISA as it is not sensitive enough to quantify protein production at the cellular level. The Enzyme-Linked ImmunoSpot (ELISPOT) assay is widely used and can be up to 400 times more sensitive than the conventional ELISA because detected protein is captured directly before having time to be diluted in culture or captured by adjacent cells (Rininsland, Helms et al. 2000). I would use this technique to visualise and quantify the secreted protein (RBP4) from individual cells within a population (ESFTs).

Finally, I would like to translate this laboratory based characterisation of RBP4 protein to one in which patient plasma samples at diagnosis could be investigated (ELISA) for the RBP4 content of tumour cells. This could then go on to form the basis of the next generation of strategies against ESFTs.

Chapter 3

Intracellular Lipid Binding Proteins

3.1 Introduction

3.1.1 Cellular Retinol Binding Proteins

Cellular Retinol Binding Proteins (CRBPs) are small cytosolic proteins which are members of the intracellular lipid-binding protein (iLBP) superfamily. They include CRBP-I, CRBP-II, CRBP-III and CRBP-IV. Other members of the iLBP superfamily include Cellular Retinoic Acid Binding Proteins (CRABPs) and Fatty Acids Binding Proteins (FABPs) (Ong 1987).

Within the internal milieu of cells, retinol binds to CRBP-I (Ong 1987, Shingleton, Skinner et al. 1989, Napoli 1993). Retinol and fenretinide are structurally similar (Figure 1.2 and Figure 1.3). They contain identical β -ionone rings and isoprenoid backbones but the alcohol group in retinol is replaced by an amide group attached to a benzene ring (the alcohol group is attached to the benzene ring) in fenretinide. In interactions with RBP4 protein, retinol and fenretinide have been shown to occupy the same binding pocket. CRBP-I has been identified as an internal protein transporter for retinol, and it is possible that fenretinide is transported intra-cellularly by this protein as well (Harada, Miki et al. 1995). There are several other transport protein candidates. These are CRBP-II, CRBP-III and CRBP-IV (that belong to the iLBP superfamily) and share a high degree of homology (Li and Norris 1996, Artimo, Jonnalagedda et al. 2012). As a result, I have hypothesised that CRBP-I is a likely transporter of fenretinide/fenretinide-like molecules intracellularly, but it may be possible for one or more of these iLBPs to also serve as alternative candidate transporters.

While ESFT cells have demonstrated increased sensitivity to fenretinide-induced cell death (Myatt, Redfern et al. 2005), there has been a variable response to this drug in other cancer cell lines. In addition, normal cells have not been susceptible to the effects of this drug (Villani, Appierto et al. 2006) (Formelli, Camerini et al. 2003, Freemantle, Spinella et al. 2003, Lovat,

Corazzari et al. 2004). My hypothesis is that these different effects of fenretinide might in part be dependent on the role of these intracellular lipid-binding proteins and their selective interaction with different nuclear receptors modifying chromatin structure, regulating gene transcription, thereby and inducing cell death or promoting survival. This hypothesis is supported by studies showing that CRABP2 selectively couples with nuclear retinoic acid receptor (RAR- α) to induce cell death (Schug, Berry et al. 2007) whereas FABP5 binds to peroxisome proliferator-activated receptor (PPAR) β/δ to induce cell survival (Schug, Berry et al. 2007). The characterisation of these proteins has not previously been defined in ESFTs (Figure 1.6).

The primary aims of this chapter are therefore:

- To examine the expression of the cellular retinol binding proteins in ESFT cells lines and tumours.
- To investigate the relationship between iLBPs expression and established clinical parameters.

3.2 Methods

3.2.1 Sub cellular Fractionation

Sub cellular fractionation was performed by differential centrifugation using a protocol adapted from Koya et al (2000). Cells were cultured and harvested at 70% confluency (washing in ice cold PBS), scraped and pelleted (Section 2.2.4.1).

The cell pellets were re-suspended in 50 μ l of iso-osmotic buffer (0.3 M sucrose, 10 mM Tris.HCl, 1 mM EDTA) and kept on ice. A sample (5 μ l) of the protein extract was taken for quantification of the total protein content (Section 2.2.4.2). The remaining cellular extract was centrifuged at 1000 g for 10 min at room temperature. In order to separate the nuclear component, the pellet was re-suspended in iso-osmotic buffer (as above). A 5 μ l aliquot was removed for protein quantification, and the remainder (of the sample) was added to an equal volume of loading buffer (2XSDS loading buffer, 200 mM DTT), aliquoted (50 μ l) and stored at -20 °C.

The supernatant was centrifuged at 8000 g for 10 min at 4 °C, in order to separate the membrane from the mitochondrial fraction. The remaining supernatant was then transferred to a Beckman centrifuge tube (Beckman Coulter, UK) and centrifuged at 100,000 g for 1 h at 4 °C. In order to pellet the membrane fraction, it was re-suspended in 50 μ l iso-osmotic buffer, the protein content quantified. The remaining sample was then added to loading buffer, aliquoted and stored as above. The supernatant following the 100,000 g centrifugation step was the cytoplasmic fraction; protein content of this fraction was quantified and the remaining sample mixed with loading buffer, aliquoted and stored as before (Figure 3.1).

The purity of the extracted fractions was confirmed by western blotting using cytochrome C (mitochondrial marker) (Ott, Robertson et al. 2002), Na,K-ATPase (membrane marker) (Klodos, Esmann et al. 2002) and Anti-TATA binding protein TBP antibody (nuclear marker) (Table 3.1).

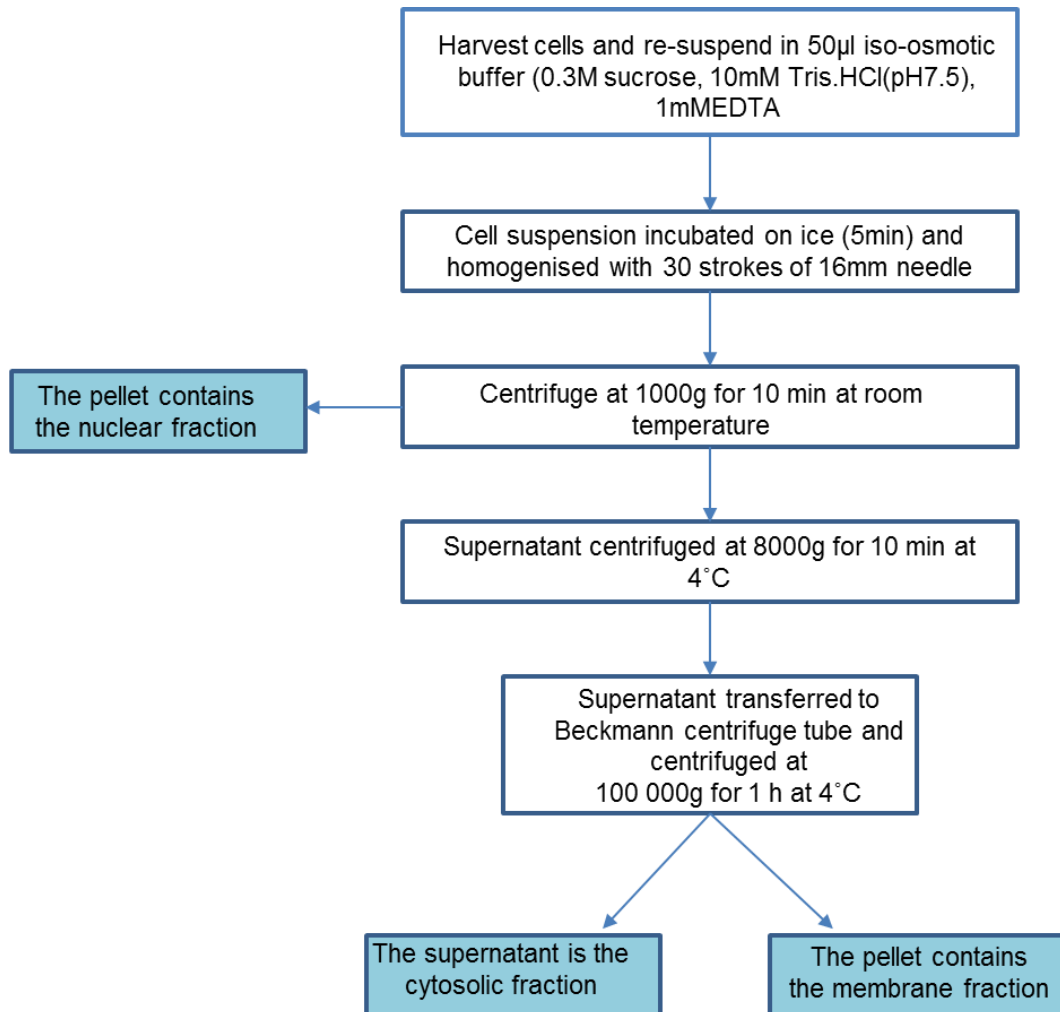


Figure 3.1 Summary of the subcellular fractionation method, that has been adapted from Koyal et al (2000).

Table 3.1 Details of antibodies used as subcellular fraction markers

Target	Antibody details and supplier	Antibody species	Concentration
Cytochrome C	4272, Cell Signalling (supplied by VWR)	Rabbit monoclonal	1:1000 (dilution) No concentration available
Sodium-potassium ATPase (Na,K-ATPase)	Ab 7671, Abcam Plc, Cambridge, UK	Mouse monoclonal	0.4µg/ml
Anti-TATA binding protein TBP antibody	Ab 63766, Abcam Plc, Cambridge, UK	Rabbit polyclonal	1mg/ml

3.2.3 Immunohistochemistry

3.2.3.1 Clinical samples and Tissues

All frozen tumour samples were taken at diagnosis from children attending Children's Cancer and Leukaemia Group (CCLG) centres throughout the UK. Positive control tissues were collected with the assistance of Mr Aidan Hindley, GIFT Research Tissue Co-ordinator. Informed consent was obtained for the use of tissue and tumour material in research and ethical approval was obtained from St James's University Trust Ethics Committee (LREC) and the Multi-Centre Research Ethics Committee (MREC/98/4/023, Trent MREC, CCLG samples from patients not on trial; MREC/98/044, MREC Scotland, patients registered on EUROE.W.I.N.G.99). Table 3.2 catalogues the clinical details of the panel of ESFT used in the immunohistochemistry experiments.

Table 3.2 Clinical details of patient tumour samples. These include the site of the tumour at presentation (site); age at diagnosis; metastatic or non-metastatic disease (Y=Yes; N=No); response to treatment (% necrosis): time to first event and current disease status (D=deceased; R= complete remission and A = alive with disease).

Tumour Number	Site of tumour	Age at diagnosis (Yrs.)	Metastatic Or non-metastatic	Response to treatment (%Necrosis)	Time to first event (days)	Current disease status
1	Sacro-iliac joint	19	Y	No data	75	D
2	Rib	9	N	>95%	3238	R
3	Soft tissue, lower limb, hip	13	N	No data		No data
4	Chest wall	8	N	95	296	D
5						
6	Femur	14	Y	100	1519	R
7						
8	Rib	14	N	No data	1290	D
9	Lt thigh	38	N	Viable tumour remains	1110	A with disease
10	Proximal Humerus	28	N	>95	546	D
11	Rt Para-vertebral	4	Y	<50	252	D
12	Rt distal femur	6	Y	No data	307	A with disease
13	Rt foot	12	Y	60	4536	R
14	Chest wall and	15	N	100	2655	R

	rib					
15	Ischio-pubic bone	15	N	100	325	D
16	Distal tibia	18	N	20	2154	R
17	Rib	9	N	100	1037	D
18	Rib	14	Y	100	2238	R
19	Iliac bone	16	N	No surgery	613	D
20	Rt posterior thoracic wall	10	N	No data	225	R

3.2.6.2 Preparing fresh frozen tissue for cryo-sectioning

The tumour and tissue samples were placed in Optimum Cutting Temperature (OCT) compound (Solmedia Supplying Science, Shrewsbury, UK), and then allowed to freeze on dry ice. A metal “chuck” was placed on dry ice in order to minimise differences in temperature between material and equipment. OCT of an amount slightly larger than the tissue sample was placed on the chuck. As the OCT began to freeze the tissue which was placed in it was overlaid with more, ensuring that the entire surface of the tumour was completely covered. The OCT block was completely frozen within 30s, after which, the embedded tissue was removed from the chuck. It was placed in a labelled cassette (Solmedia, Shrewsbury, UK) and stored in liquid nitrogen (BOC, Industrial Gases, UK).

Fresh frozen tissue mounted in OCT compound was placed onto a chuck in the pre-cooled cryostat (Leica: Milton Keynes, Buckinghamshire, UK) and

sections (5µm) were cut and mounted on super-frost plus glass slides (Thermo Scientific, Horsham, UK) for IHC.

3.2.6.3 Slide fixation methods

3.2.6.3.1 Methanol: Acetone

Cryo-sections (5 µm) were prepared on super-frost plus glass slides and placed in a metal slide rack (Solmedia, Shrewsbury, UK). The sections were fixed by submerging the slides in a glass dish (Solmedia) containing methanol: acetone (1:1: Merck Biosciences) for 2 min at room temperature in the fume hood (Holliday Fielding Hocking Ltd, Leeds, UK). Slides were then transferred to a second glass dish with clean methanol: acetone (1:1) for a further 2 min. These slides were allowed to air dry on filter paper for 10 min and then labelled.

3.2.6.3.2 Paraformaldehyde

Paraformaldehyde (4%w/v) was made by measuring 800mls of 1X PBS into a glass beaker and heating it to 60 °C on a stirring plate in the fume hood. Forty grams of paraformaldehyde powder was added to the heated PBS and stirred until the powder was dissolved. The final volume was made up to one litre with 1X PBS before being cooled and filtered (Nalgene™ Rapid-Flow™ Sterile Disposable Filter Units with PES Membrane, Thermo Fischer Scientific). The slides were then submerged in a dish containing 200 ml of fixing solution (4%w/v paraformaldehyde in 1X PBS) for 10 min. They were then washed under a running tap water for 10 min. Care was taken to prevent the slides from drying out by keeping them submerged in glass beaker with tap water.

3.2.6.4 Detection Methods

3.2.6.4.1 Standard

Endogenous peroxidase was quenched by treating the slides with hydrogen peroxide (0.6% in methanol: Sigma Aldrich Company Ltd.) for 10 min at room temperature. The slides were mounted and loaded directly onto the Sequenza slide racks (Thermo Scientific, Horsham, UK). Slides were rinsed

in running tap water for 10 min and care taken to ensure that the slides did not dry out. The slide were washed twice with TBS for 5 min at room temperature. Endogenous biotin or biotin binding proteins were blocked (using the Avidin Biotin block SP-2001: Vector Laboratories, Peterborough, UK) for 10 min, washed twice with TBS and followed by a 10 min incubation with 100 µl of biotin and a further 2 washings with TBS, each of 5 min duration. Non-specific antibody binding was blocked by incubating the sections with species specific serum (diluted 1:10 TBS, Dako UK Ltd, Cambridgeshire, UK) for 5 min at room temperature. The optimal antibody concentration (Table 3.3) was determined by incubating the positive control tumour sections with a range of antibody concentrations. The sections were incubated with 100 µl of antibody (diluted in antibody diluent, Dako UK Ltd, Cambridgeshire, UK) at room temperature for 1 h followed by incubation with 100 µl of the appropriate secondary antibody (Table 3.3), for 30 min at room temperature followed by two washes with TBS.

Sections were incubated with Streptavidin AB (200 µl: Thermo Scientific, Horsham, UK) for 30 min at room temperature and then washed twice with TBS. The Liquid DAB Substrate Chromogen System for peroxidase (Dako UK Ltd, Cambridgeshire, UK: 1 drop of 3,3' diaminobenzidine (DAB) chromogen per ml of Substrate Buffer, details are company propriety) was used to incubate the sections for 10 min at room temperature. Development of a brown precipitate was consistent with the expression of the protein of interest.

3.2.6.4.2 EnVision+ System-HRP

Cryo-sections (5 µm) were prepared as in section 3.2.6.2 and fixed by methods outlined in Section 3.2.6.3. Endogenous peroxidase was quenched by treating the slides with 100 µl Peroxidase Block (EnVision, Sigma Aldrich Company Ltd.) for 10 min at room temperature. The slides were rinsed in running tap water for 10 min and then loaded directly onto the sequenza

sliding rack. Non-specific antibody binding was blocked as in Section 3.2.6.4.1.

The optimal antibody concentration was determined and incubated as previously described (Section 3.2.6.4.1 and Table 3.2). Following this, the slides were washed twice in TBS. The slides were then incubated in 100 μ l of Peroxidase Labelled Polymer (EnVision+System-HRP (DAB) for 30min at room temperature and washed twice in TBS. The slides were incubated with the appropriate secondary antibody (Table 3.3), for 30 min at room temperature, followed by two washes with TBS. Sections were then incubated with Liquid DAB Substrate Chromogen System for peroxidase as previously described in Section 3.2.6.4.1.

3.2.6.4.3 Novo-Link

Cryo-sections (5 μ m) were prepared as in section 3.2.6.2 and fixed by methods outlined in section 3.2.6.3. Endogenous peroxidase was quenched by treating the slides with 100 μ l Peroxidase Block (RE7140-K, Novo Link Polymer Detection System: Leica Bio systems Newcastle Ltd.) for 5 min at room temperature. They were rinsed in cold water for 10 min before non-specific antibody binding was blocked by incubating the sections with Protein Block (RE7140-K, Novo Link Polymer Detection System: Leica Bio systems Newcastle Ltd.) for 5 min at room temperature. The slides were washed twice with TBS (5 min each) at room temperature. The optimal antibody concentration was determined by incubating the positive control tumour sections with a range of concentrations of the antibody (See Table 3.3). The sections were incubated with the optimum concentration of primary antibody and washed as in Section 3.2.6.4.1. The slides were incubated with Post Primary Block (Novo Link Polymer Detection System: Leica Bio systems Newcastle Ltd.) for 30 min before being washed twice in TBS for 5 min (each) at room temperature. The slides were then incubated in 100 μ l of Novo-Link Polymer (NovoLink Polymer Detection System: Leica Bio systems Newcastle Ltd.) for 30 min at room temperature and again washed twice in

TBS. Sections were then incubated with Liquid DAB Substrate Chromogen System for peroxidase as previously described in section 3.2.6.4.1.

Table 3.3 Details of the optimisation of IHC antibodies including the method of fixation (A+M= acetone+ methanol fixation method); primary antibody concentration and dilution.

Antibody	Detection method	Fixation method	Primary antibody Concentration and dilution	Duration of incubation with primary antibody (h)	Secondary Antibody
CRBP-I	EnVision+ System-HRP	A + M	sc-30106 0.4 µg/ml 1:50	1h	Anti-rabbit
CRBP-IV	Novo-Link	A + M	HPA034749 Sigma- 0.2mg/ml 1:200	Overnight	Anti-rabbit
CRABP2	Novo-Link	A + M	10225-1-AP Proteintech 0.2 µg/ml 1:50	Overnight	Anti-mouse
FABP5	Novo-Link	Paraformaldehyde	Ab 37267, Abcam Plc 0.4 µg/ml 1:400	1h	Anti-rabbit

Table 3.4 Negative and positive tissues used as controls in IHC of iLBPs. For CRABP2 and FABP5, tonsillar tissue was used as both the negative and positive control. This was because tonsils are made up of masses of lymphoid tissue, non-keratinizing squamous epithelium and connective tissue (Boyaka, Wright et al. 2000). These varied cellular types express FABP5 and CRABP2 differently. Human kidney sections were used as the positive control for CRBP-IV while human pituitary sections were the positive control for CRBP-I.

iLBPs	Positive Control	Negative Control
CRBP-I	Pituitary	Tonsil
CRBP-IV	Kidney	Tonsil
CRABP2	Tonsil	Tonsil
FABP5	Tonsil	Tonsil

3.2.6.5 Haematoxylin Staining

Sections were counter-stained with haematoxylin in a fume-hood. Sequential submersion in Meyer's haematoxylin (0.3%w/v haematoxylin, 2% v/v ethanol, 0.03% w/v sodium iodate, 0.1% w/v citric acid, 5% w/v chloral hydrate, 5% w/v aluminium potassium sulphate, 12% v/v glycerol in water (Sigma- Aldrich Company Ltd), for 15 s , followed by running tap water for 1 min and then by Scott's tap water (2% w/v Magnesium Sulphate, 0.35% w/v Sodium Bicarbonate in water: Sigma- Aldrich Company Ltd), for 1 min was carried out The sections were then submerged a third time for 1 min in running tap water. They were then dehydrated in 70% ethanol (Sigma-Aldrich, Dorset, UK), for 30 s, then 90% ethanol (Sigma- Aldrich, Dorset, UK), for 1 min and finally in 100% ethanol (Sigma- Aldrich, Dorset, UK) for 1 min.

Table 3.5 Protocol for Mayer's haematoxylin staining of frozen sections for IHC.

Haematoxylin staining solution	Incubation time
Running tap water	5min
Mayer's Haematoxylin(Merck Biosciences)	15s
Running tap water	1min
Scott's solution(2% magnesium sulphate, 0.35% sodium bicarbonate : Sigma Aldrich Company Ltd)	1min
Running tap water	1min
70% Ethanol	30 s
90% Ethanol	30 s
100% Ethanol	1min
Xylene (Merck Biosciences)	1min
Xylene	1min
Air Dry	Overnight in the fume hood

IHC sections were mounted by placing one drop of DePeX mounting medium (Sigma- Aldrich, Dorset, UK) on a glass cover slip and then gently adhering the cover slip (VWR International, UK) to the specimen, ensuring that there were no air bubbles. Sections were visualised by light microscopy (Zeiss Axioplan microscope; Zeiss, UK).

Tumours were confirmed as ESFT by IHC for membrane CD99/MIC2 protein, a marker of ESFT (Halliday, Slagel et al. 1998, Schiavo, Tullio et al. 2007).

3.2.7 Scoring and Statistical analysis

The ESFT panel along with the appropriate positive and negative controls were prepared and stained as described in section 3.2.6.4. Each slide was examined under high power magnification (100X) using a Zeiss Axioplan

microscope (Carl Zeiss Ltd, Cambridgeshire, UK). Ten random fields of vision were examined for each slide. A total number of 100 cells (for each high-powered field of vision) were counted, from which the numbers showing no staining (Intensity 0), weak staining (intensity 1), moderate staining (intensity 2) and heavy staining (intensity 3) were recorded. The H-score was calculated using the equation below (Detre, Saclani Jotti et al. 1995).

H-score= (% cells at intensity 1 X 1) + (%cells at intensity 2 X 2) + (%cells at intensity 3 X 3)

An independent marker scored a representative sample of slides, to act as quality control and to mitigate for bias. Statistical analyses were undertaken in R version 3.2.5 and the statistical significance were tested using ANOVA with a post-hoc Bonferroni process. Scatter plots were constructed to explore the relationships between the intra-lipid binding proteins. Variation were considered significant when $p < 0.05$. The H-scores of the ESFT were analysed for clinically significant prognostic markers (Cotterill, Ahrens et al. 2000, Meyers, Krailo et al. 2001, Grier, Krailo et al. 2003), and samples were compared using the Kruskal-Wallis comparison test.

3.3 Results

ESFT and non-ESFT cancer cell lines were investigated for the expression of iLBPs (CRBP-I, CRBP-II, CRBP-III, CRBP-IV, CRABP2 and FABP5) at the mRNA and protein levels.

Target mRNA was detected by RTqPCR. The cell lines and positive controls (Table 3.6) were amplified for the house keeping gene, β 2M. The β 2M mRNA was detected in all the cell lines. RNase free water was used as the negative control. There was no detection of amplified mRNA in samples in the absence of reverse transcriptase or in samples in which RNA was replaced with RNase free dH₂O. This was consistent with efficient and specific cDNA formation and amplification.

The proteins were detected by western blot with β -Actin as the loading control and the positive controls for each target protein as in Table 3.6. For each protein, I have shown a representative western blot and histogram summarising the densitometry or protein expression across 3 independent repeats.

Table 3.6 Details of the positive control RNA and protein lysate used in detecting iLBP targets by RTqPCR and western blot.

Target	Positive control cell lines
CRBP-I	HEP G2, CRBP-I lysate
CRBP-II	Human small intestine
CRBP-III	Human heart
CRBP-IV	Human heart, kidney
CRABP2	MCF-7
FABP5	HEP G2

3.3.1. CRBP-I

3.3.1.1 mRNA expression of Cellular Retinol Binding Protein I in ESFT cells

CRBP-I mRNA was expressed and detected in the 6 ESFT cell lines by RTqPCR. Expression was homogenous in 5 of the 6 cell lines examined. With the exception of A673, the ESFT cell lines had a similar levels of expression ($\Delta\Delta Ct=0-3.6$). The A673 cell lines had the lowest level of CRBP-I mRNA. ($\Delta\Delta Ct= 9.4$) This was statistically significant (Figure 3.2) ($p<0.0001$).

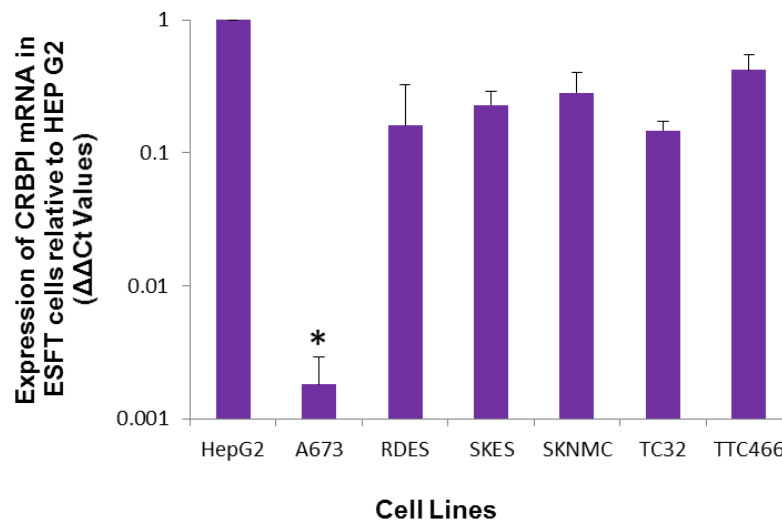


Figure 3.2 The expression of CRBP-I mRNA in ESFT cell lines relative to HEP G2 cells, after correction for $\beta 2M$ housekeeping gene. Each reaction contained 400ng/ μ l RNA (n=3). The CRBP-I mRNA level was lower in A673 as compared to the other ESFTs, and this was statistically significant by ANOVA.

3.3.1.2 Protein expression of CRBP-I in ESFT, other cancer and normal cell lines

CRBP-I protein (15 kDa) was detected in the cell extracts of the 6 ESFT cell lines and was detected in the recombinant CRBP-I protein lysate (293T Lysate, Santa Cruz Biotechnology, Inc., Texas, USA) and positive control cell line, HEP G2 (Figure 3.3). The 15 kDa protein product was

demonstrated (by densitometry) to be most abundant in SKES-1 and SK-N-MC cell lines and least abundant in the A673 (Figure 3.3).

Initially, protein loading was confirmed by probing the western blots for α -Tubulin (50 kDa). Since the positive control cell line did not appear to express α -Tubulin, a second loading control, β -Actin (42 kDa) was used. It was expressed by all types including the positive control cell line (HEP G2).

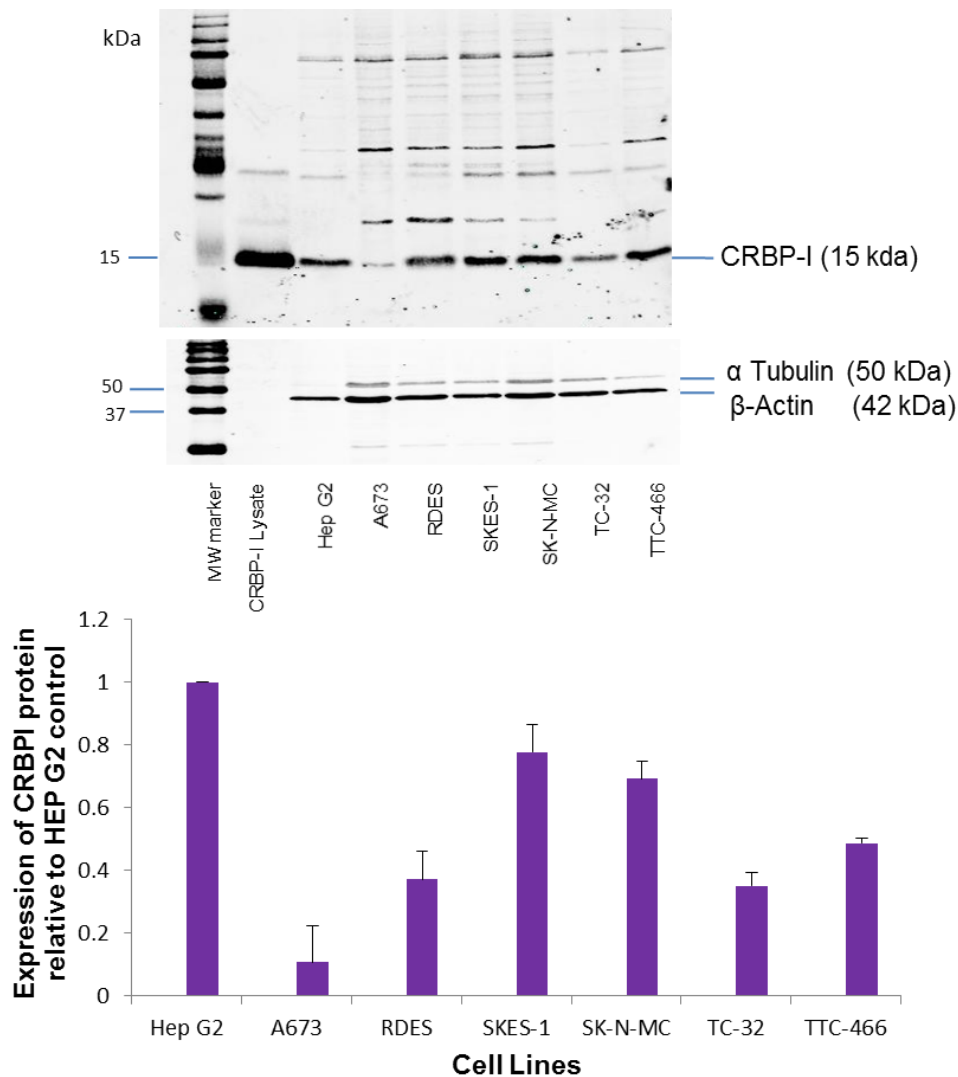


Figure 3.3 Western Blot analysis for CRBPI in ESFT protein extracts, using CRBPI transfected lysate and Hep G2 as positive controls. Initially α -Tubulin was used as the loading control. However HEP G2 cells are α -Tubulin negative. β -Actin was the preferable loading control. Bands were quantified by densitometry and expression levels calculated as the ratio of the CRBPI protein to β -Actin expression and normalised to the positive control cell line, HEP G2. MW=molecular weight marker in kDa.

Sub-cellular fractionation of ESFT cells revealed that CRBP-I was expressed in the cytoplasm (Figure 3.4) and this is consistent with the literature that CRBP-I is a cytosolic protein (van Aalten, Findlay et al. 1995).

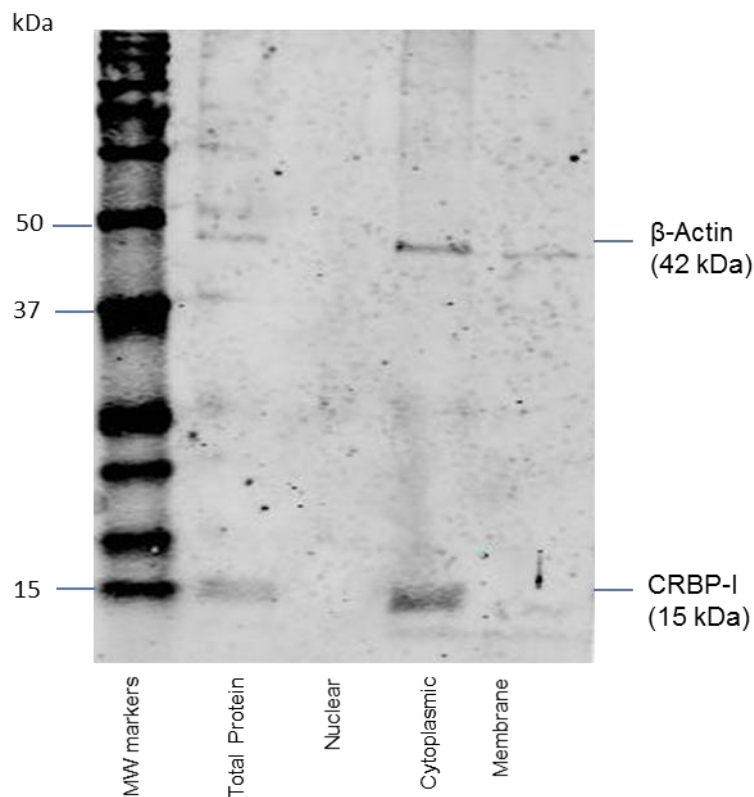


Figure 3.4 Western Blot analysis for CRBP-I protein in SKES-1 sub-cellular fractions produced by the method described in Section 3.2.5. Each sub-cellular fraction was confirmed by using membrane, cytoplasmic and nuclear markers.

CRBP-I protein was also characterised in the non-cancer cells lines NHU and MSC, where it was found to be absent (Figure 3.4). Fenretinide resistant neuroblastoma cell lines SHEP-1, SK-N-SH and SH-SY-5Y expressed the CRBP-I protein (Figure 3.5). HEPG2 were used as the positive control and β -Actin was the loading control.

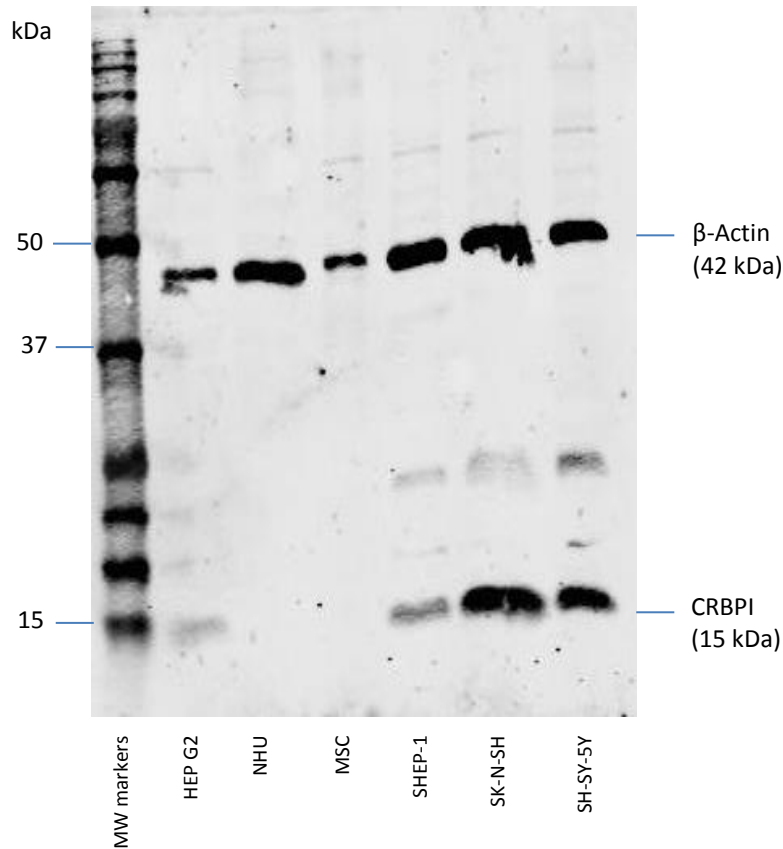


Figure 3.5 Western Blot analysis for CRBP-I protein normal non-cancerous cell lines (NHU and MSC) and three neuroblastoma cell lines (SHEP-I, SK-N-SH and SH-SY-5Y) that are known to be resistant to fenretinide. HEP G2 protein extract were used as the positive control and β -Actin as the loading control.

Other non ESFT cancer cell line protein extracts were also investigated for the CRBP-I protein. These included HT-29, HMB2, A375, T98G, IMR-32, RT-4, RT-112, T-24 and MCF-7. There was no CRBP-I protein detected apart from the HEP G2 cells (positive control). β -Actin (loading control) antibody showed uniform protein loading apart from MCF-7, which was under-loaded (Figure 3.6).

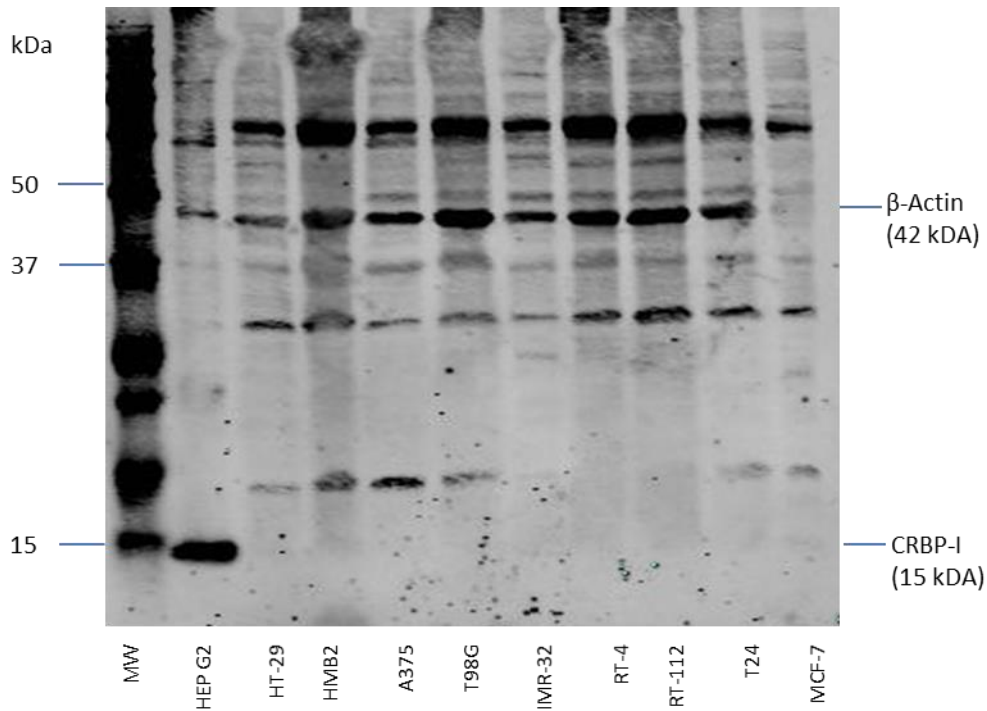


Figure 3.6 The expression of CRBP-II mRNA in ESFTs relative to human small intestine after correction for β 2M housekeeping gene. Each reaction contained 400ng/ μ l RNA (n=3). There was no statistical significance in levels of CRBP-II mRNA expression among the six ESFT cell lines, but the level of expression was significantly different to that of the positive control when using the ANOVA, post hoc Bonferroni test.

3.3.2 CRBP-II

3.3.2.1 mRNA expression of Cellular Retinol Binding Protein II in ESFT cells

CRBP-II mRNA was detected in all ESFT cell lines: its expression was homogenous. A673, RDES, SKES-1, SK-N-MC, TC-32 and TTC-466 showed similar levels of expression ($\Delta\Delta$ Ct= 20.5-23.5), that was not statistically significant ($p=0.46$) (Figure 3.6). Human small intestine RNA (636339: TakaraBio Europe/Clontech, California, USA) was used as a positive control and RNase free water as the negative control. The 6 ESFT cell lines expressed CRBP-II mRNA at a significantly lower level than the positive control cell line ($p<0.0001$) (Figure 3.7).

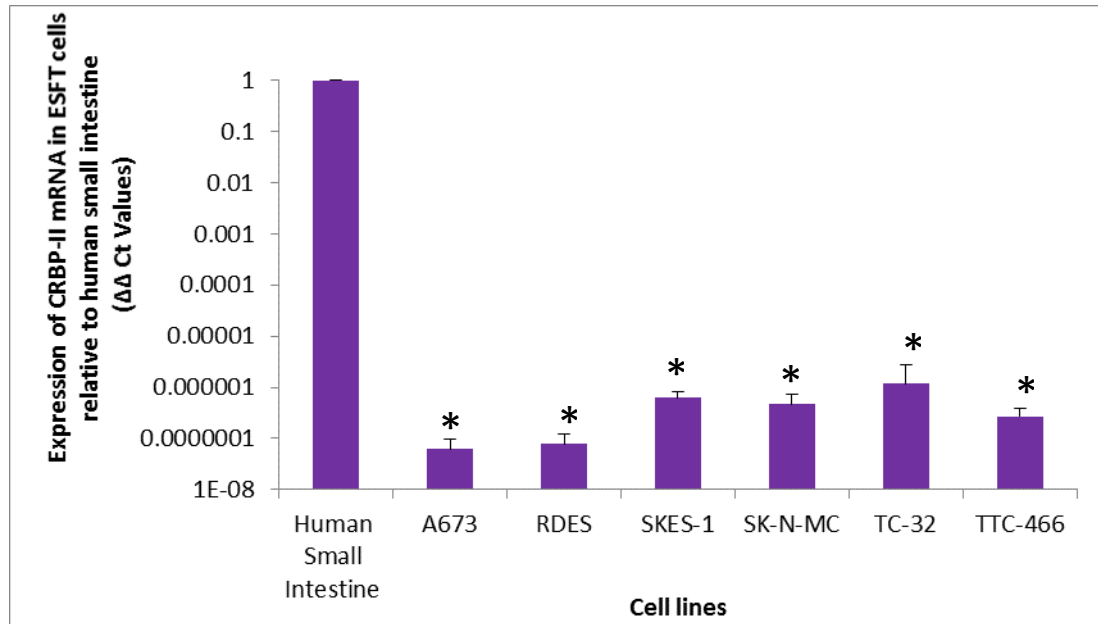


Figure 3.7 The expression of CRBP-II mRNA in ESFTs relative to human small Intestine, after correction for β 2M housekeeping gene. Each reaction contained 400ng/ μ l RNA (n=3). There was no statistical significance in levels of CRBP-II mRNA expression between the six ESFT cell lines, but this level of expression was significantly different to that of the positive control when tested using ANOVA, post hoc Bonferroni test.

3.3.2.2 CRBP-II Protein in ESFT cell lines

CRBP-II protein was not detected in its native form in any of the 6 ESFT cell line protein extracts, but the positive control demonstrated the expected band at 15 kDa. A larger protein, however, was detected at 30 kDa in all 6 ESFT cell lines (Figure 3.8). This was calculated by plotting the molecular weight against the migratory front of the dye. The size of the larger CRBP-II band is double that of the expected 15 kDa: this suggests that the protein band at 30 kDa is a dimer.

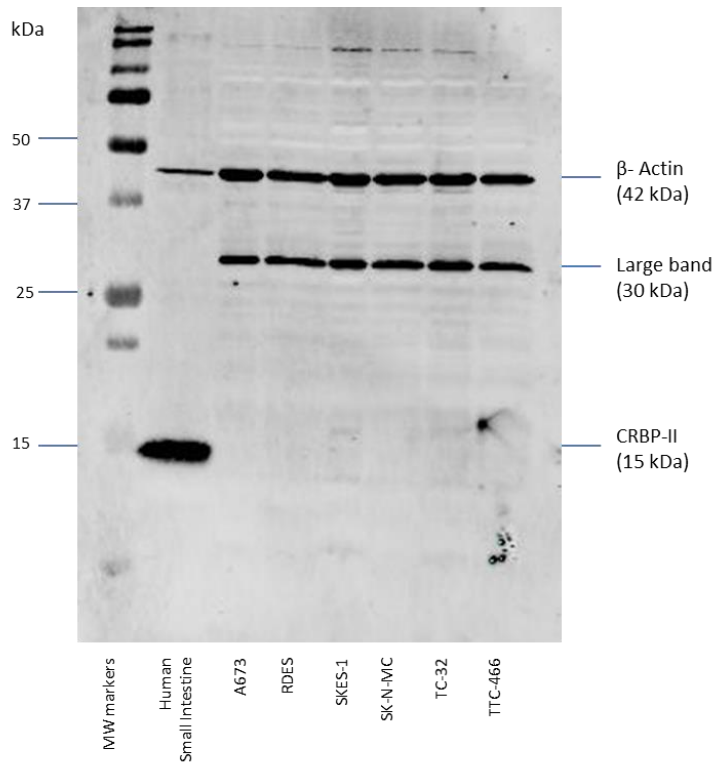


Figure 3.8 Western Blot analysis for CRBP-II in ESFT protein extracts , using human small intestine lysate as the positive control and β -Actin as the loading control. A mature band was demonstrated at an estimated molecular weight of 30 kDa, by plotting molecular weight against the migratory distance. The western blot is representative of three independent experiments. MW=molecular weight marker in kDa. (n=3)

CRBP-II protein was also not detected in any of the normal (NHU and MSC) or in the non ESFT cancer cell lines. However, the larger molecular weight protein (30 kDa band) was also seen in other cancer cell lines including bladder cancers (RT-4, RT-112, T-24, B-tert), breast cancer (MCF-7), colon carcinoma (HT-29), lung cancer (A549), glioblastoma (T98G), melanoma (HMB2, A375), neuroblastoma (IMR-32, SK-N-SH, SH-SY-5Y) and rhabdomyosarcoma (A204) (Figure 3.9).

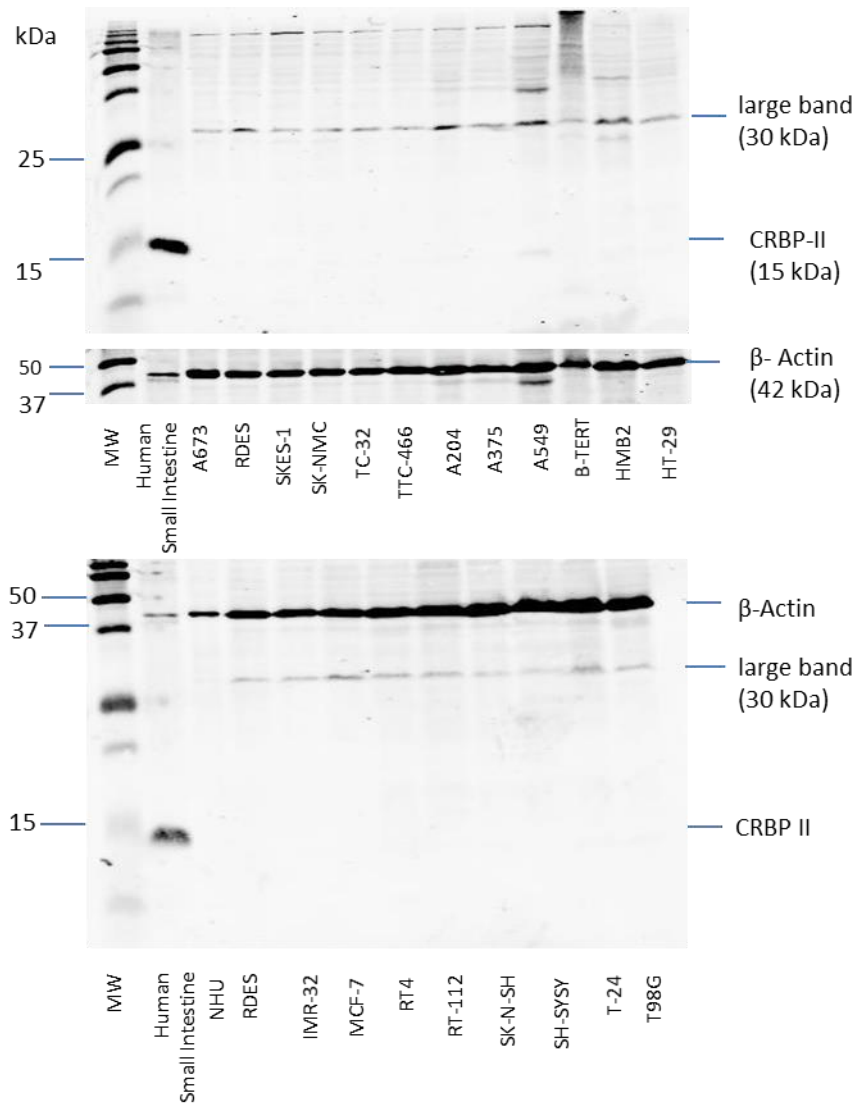


Figure 3.9 Western Blot analysis for CRBP-II protein in ESFT and non-ESFT cancer cell lines. Human small intestine lysate was the positive control and β -Actin, the loading control. The 6 ESFT cell lines were A673, RDES, SKES-1, SK-N-MC, TC-32, TTC-466. The non-ESFT cancer cell lines included A204 (Rhabdomyosarcoma), A375 (Melanoma), A549 (Lung cancer), B-TERT, HMB2 (Melanoma), HT-29 (Colorectal adenocarcinoma), IMR-32 (Neuroblastoma), MCF-7 (Breast cancer), RT-4, RT-112, T-24 (bladder cancer), SK-N-SH, SH-SY-5Y, IMR-32 (neuroblastoma), and T98G (Glioblastoma). There was one non-cancer cell line (NHU). MW=molecular weight marker in kDa.

3.3.3 CRBP-III

3.3.3.1 Cellular Retinol Binding Protein III mRNA in ESFT Cells

CRBP-III mRNA was expressed and detected in all ESFT cell lines. Human heart total RNA (636339: Takara Bio Europe/Clontech) was used as a positive control and RNase free water as the negative control. The 6 ESFT cell lines expressed CRBP-III mRNA ($\Delta\Delta C_t = 0.3-7.01$) with A673, expressing statistically significant lower levels than the other cell lines ($p=0.035$). All the ESFTs expressed CRBP-III mRNA at a lower level than that of the positive control. This was only significantly different for the A673 cell line ($p=0.002$) (Figure 3.10).

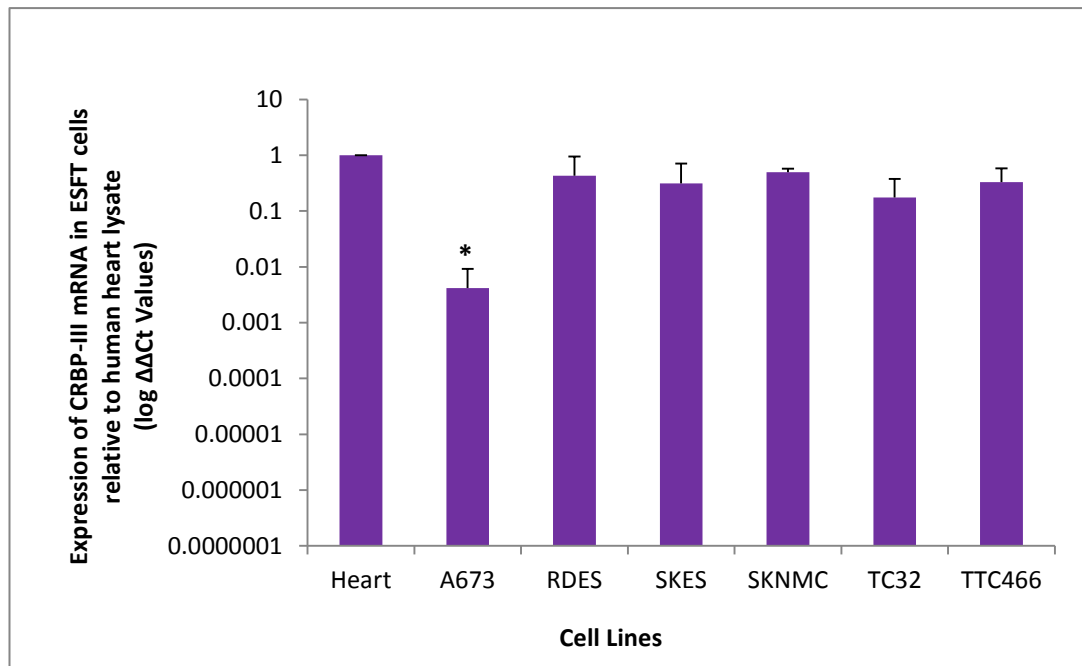


Fig 3.10 The expression of CRBP-III mRNA using the $\Delta\Delta C_t$ method, in 6 ESFT cell lines. $\beta 2M$ was used as the housekeeping gene and human heart RNA was the standard for reporting. Each reaction contained 400ng/ μ l RNA ($n=3$). The low level of expression in the A673 was statistically significant using ANOVA, Bonferroni post hoc test.

3.3.3.2 CRBP-III Protein in ESFT cell lines

CRBP-III protein was not detected in any of the 6 ESFT cell line protein extracts unlike the positive controls which demonstrated the expected band at 15 kDa (Figure 3.11). CRBP-III recombinant lysate and human kidney lysate were the positive controls and β -Actin was the loading control.

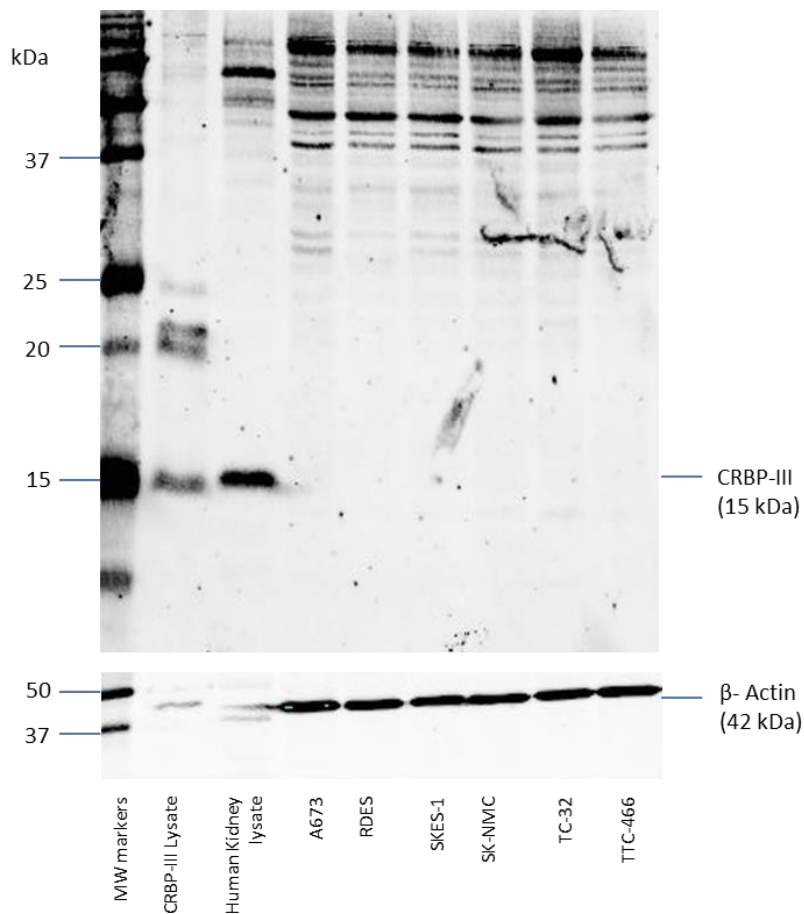


Figure 3.11. Western blots for CRBP-III protein in ESFT cell protein extracts . Recombinant CRBP-III lysate and Human Kidney lysate were used as positive controls and β - Actin as the loading control. The western blot is representative of three independent experiments. MW=molecular weight marker in kDa.

3.3.4 CRBP-IV

3.3.4.1 Cellular Retinol Binding Protein IV mRNA in ESFT Cells

CRBP-IV mRNA was expressed and detected in the 6 ESFT cell lines by RTqPCR. There was no statistical significance in the levels of expression between A673, RDES, SKES-1 and SK-N-MC ($\Delta\Delta C_t = -2.9-2.5$) ($p=0.15$) but, there was a significantly lower expression in TC-32 and TTC-466 ($\Delta\Delta C_t = 5.4-9.2$) with p value=0.0009. Human heart total RNA (636532: Takara Bio Europe/Clontech) was used as a positive control and RNase free water as the negative control (Figure 3.12).

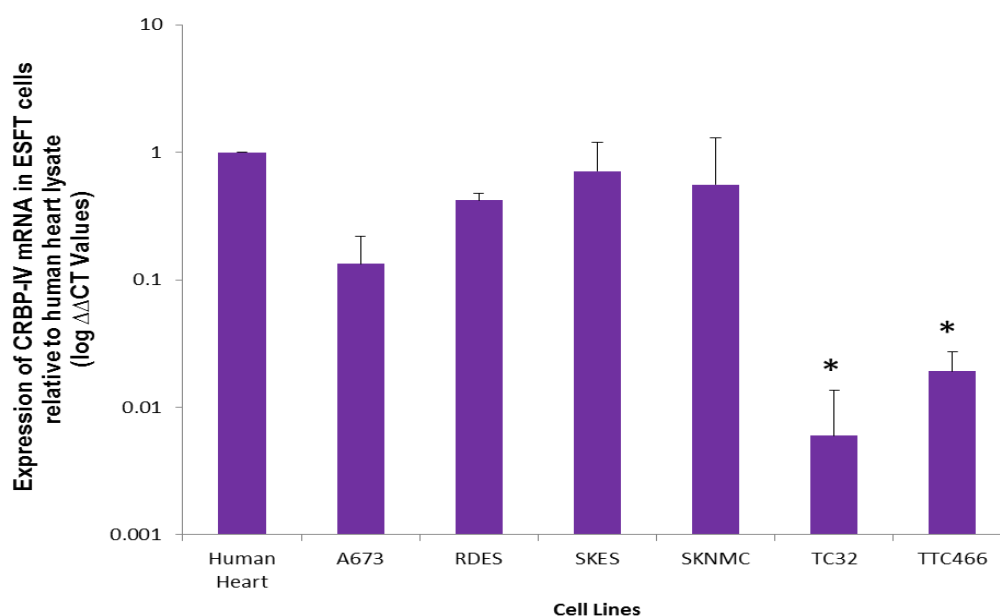


Figure 3.12 The expression of CRBP-IV mRNA using the $\Delta\Delta C_t$ method, in 6 ESFT cell lines. B2M was used as the housekeeping gene and human heart RNA was the standard for reporting. Each reaction contained 400ng/ μ l RNA. (n=3) CRBP-IV mRNA expression in TC-32 and TTC-466 were significantly lower than for the other 4 ESFT cell lines, by ANOVA, Bonferroni post hoc test.

3.3.4.2 Cellular Retinol Binding Protein IV in ESFT cell lines

CRBP-IV protein was detected in four of the ESFT cell lines (A673, RDES, SKES-1, and SK-N-MC) as well as in the positive controls (Human heart

(ab29431) and kidney lysate (ab30202): Abcam, Cambridgeshire, UK) demonstrated the expected band at 15 kDa (Fig 3.13). The 15 kDa protein product was demonstrated (by densitometry) to be of low abundance in the four ESFT cell lines when compared to that of the positive control and was undetectable in TC-32 and TTC-466. Protein loading was confirmed by probing the immune-blot for the loading control, β - Actin (42 kDa).

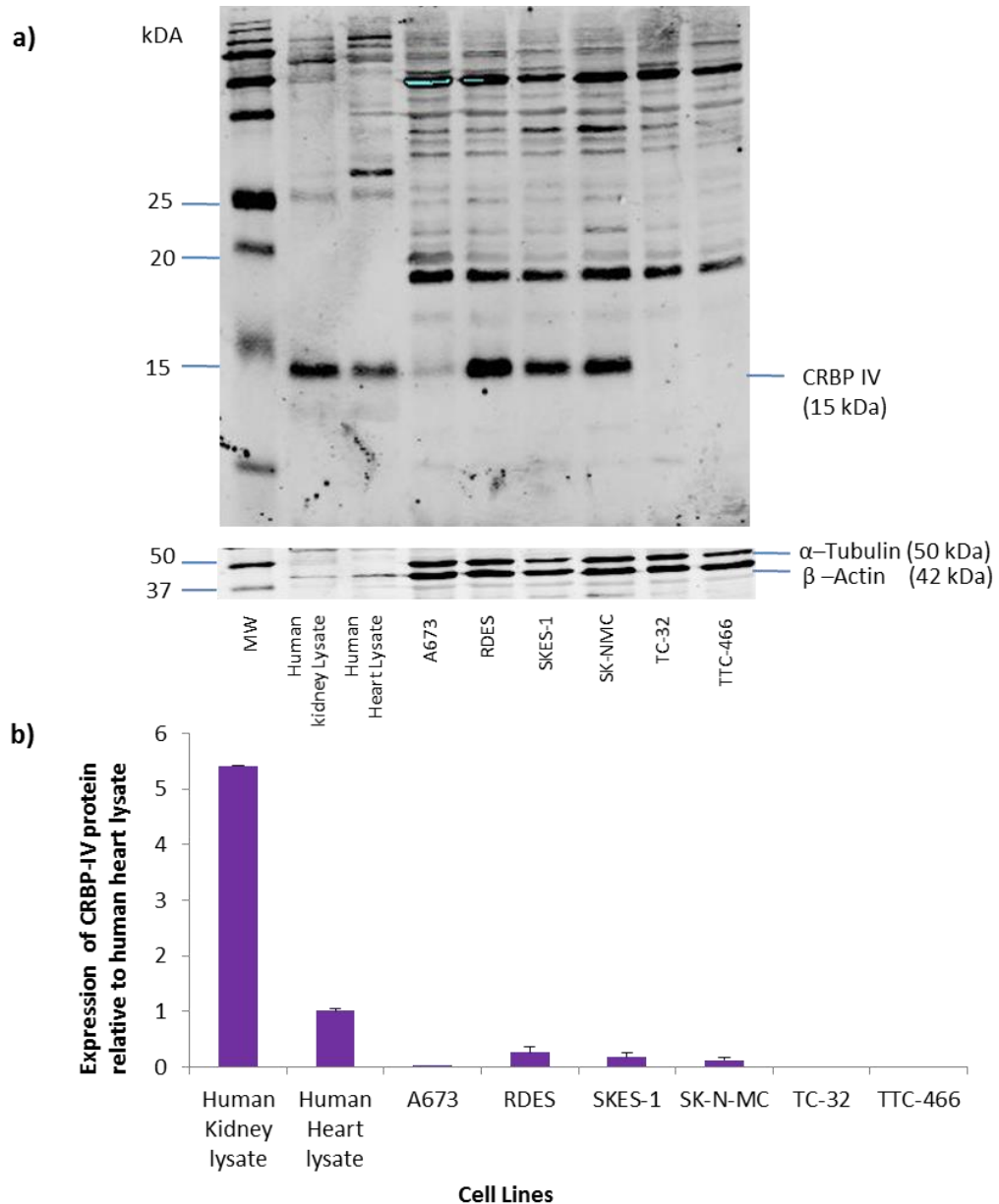


Figure 3.13 a) Western blot analysis for CRBP-IV protein in ESFT cell protein extracts , using human kidney and human heart lysate as positive controls and β - Actin as the loading control. **b)** Bands were quantified by densitometry and expression levels calculated as the ratio of the CRBP-IV protein to β -Actin expression (n=3). MW=molecular weight marker in kDa.

3.3.5 CRABP2

3.3.5.1 Cellular Retinoic Acid Binding Protein 2 mRNA in ESFT Cells

CRABP2 mRNA was expressed and detected in the 6 ESFT cell lines by RTqPCR. There were 2 groups of cell lines: the first group (A673, RDES, and TC-32) expressing CRABP2 at a low level with no statistical significant difference among them ($p=0.69$). This was also true for the highly expressing group (SKES-1, SK-N-MC and TC-32) which showed no significant difference. However, when the two groups were compared, there was a statistically significant difference, when using ANOVA, post hoc Bonferroni test ($p=0.0078$). SKES-1 and SK-N-MC demonstrated the highest level of expression ($\Delta\Delta Ct= 3.6-6.8$). All 6 ESFT cell lines expressed CRABP2 mRNA at a significantly lower level than MCF-7 (positive control) ($p<0.0001$) (Figure 3.14).

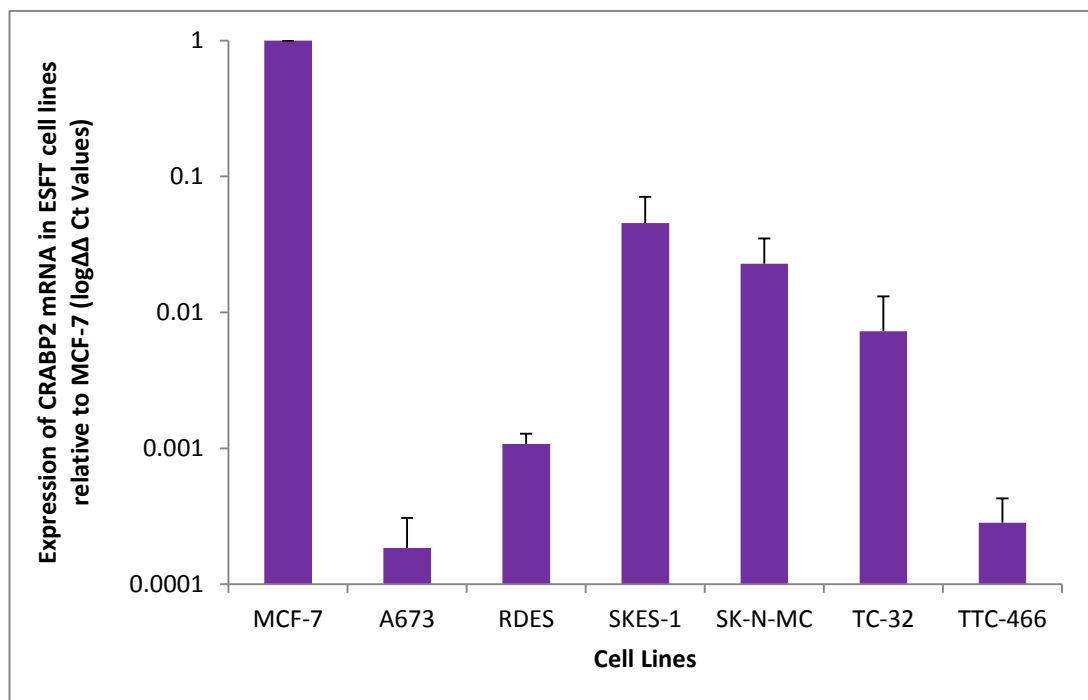


Figure 3.14. The expression of CRABP2 mRNA in the 6 ESFT cell lines, using MCF-7 cell line as the positive control and $\beta 2M$ as the housekeeping gene. Each reaction contained 400ng/ μ l ($n=3$). The lowest level of expression was in the A673 and the highest expression in SKES-1. There was no difference in expression between A673, RDES and TTC-466. The same was true for the group containing SKES-1, SK-N-MC and TC-32. Comparison of these two groups highlighted a statistically significant difference as did a comparison to the positive control cell line.

3.3.5.2 Cellular Retinol Binding Protein 2 in ESFT cell lines

CRABP2 protein (15 kDa) was detected in the cell extracts of the 6 ESFT cell lines, and in the protein extract of MCF-7 cells (positive control cell line). The 15 kDa protein product was demonstrated (by densitometry) to be expressed at low levels. Protein loading was confirmed by probing the western blots for β - Actin (Figure 3.15).

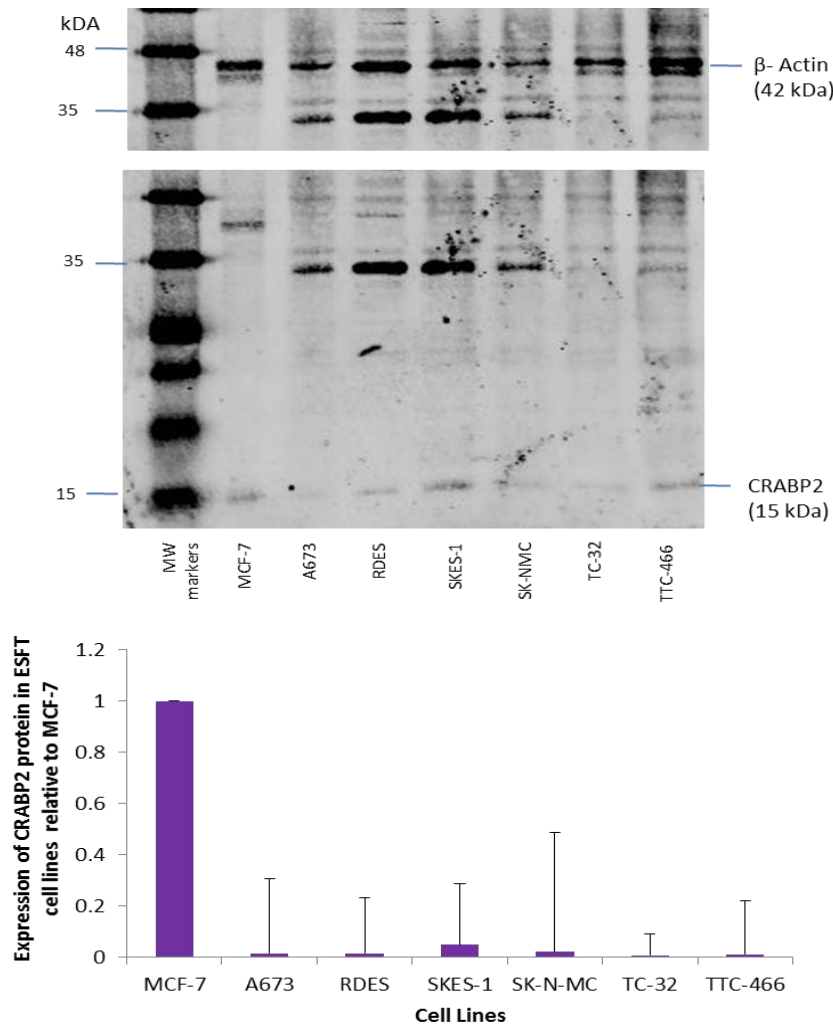


Figure 3.15. CRABP2 protein expression in ESFT cells protein extract using MCF-7 cells as the positive control and β -Actin as the loading control. Bands on the Western Blot were quantified by densitometry and expression levels calculated as a ratio of CRABP2 protein: β -Actin, which was then normalized to the positive control, MCF-7. MW=molecular weight in kDa (n=3)

3.3.5.3 CRABP2 protein in non ESFT cancer cells

CRABP2 protein was detected in most of the non ESFT cell lines as well as in the positive control, MCF-7, at the expected size (15 kDa) (Fig 3.16). The 15 kDa protein product was highly expressed in the HT-29 cell line, moderately expression in IMR-32 and RT-4; lowest expression in A375, T98G, and RT-112; and not at all in HMB2, T24 and HEP G2. Protein loading was confirmed by probing the immune-blot for the loading control, β - Actin (42 kDa). HEP G2 appeared to be under-loaded.

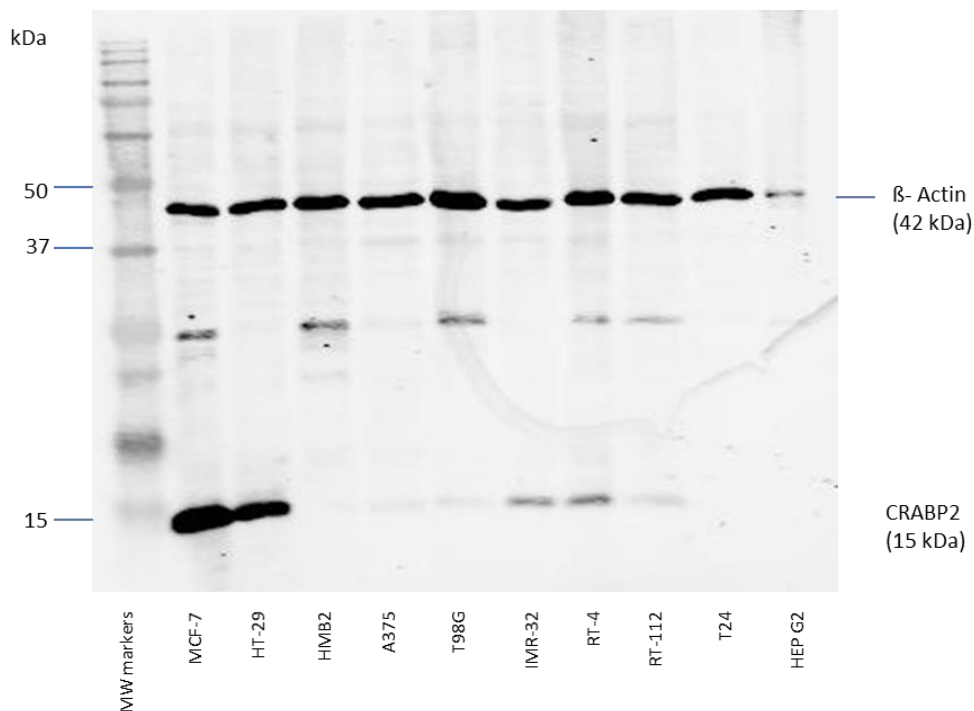


Figure 3.16 CRABP2 protein expression in non ESFT cancer cell lines extract, using kidney lysate as the positive control and β -Actin as the loading control. HEP G2 = Hepatocellular carcinoma , HT-29= Colorectal adenocarcinoma , HMB2 = Melanoma , A375= Melanoma, T98G= Glioblastoma, IMR-32= Neuroblastoma, RT-4= Bladder cancer, RT-112= Bladder cancer, T-24= Bladder carcinoma, MCF-7= Breast cancer

3.3.6 FABP5

3.3.6.1 Fatty Acid Binding Protein 5 mRNA in ESFT Cells

FABP5 mRNA was expressed and detected in all 6 ESFT cell lines by RTqPCR with the lowest expression demonstrated in A673 and TTC-466. ($\Delta\Delta C_t = -2.2-1.9$) SKES-1 and SK-N-MC had the highest level of expression, but this was not statistically significant ($p=0.068$). Interestingly, all the ESFT cells demonstrated a higher level of expression of the mRNA than did the positive control cell line (Figure 3.17).

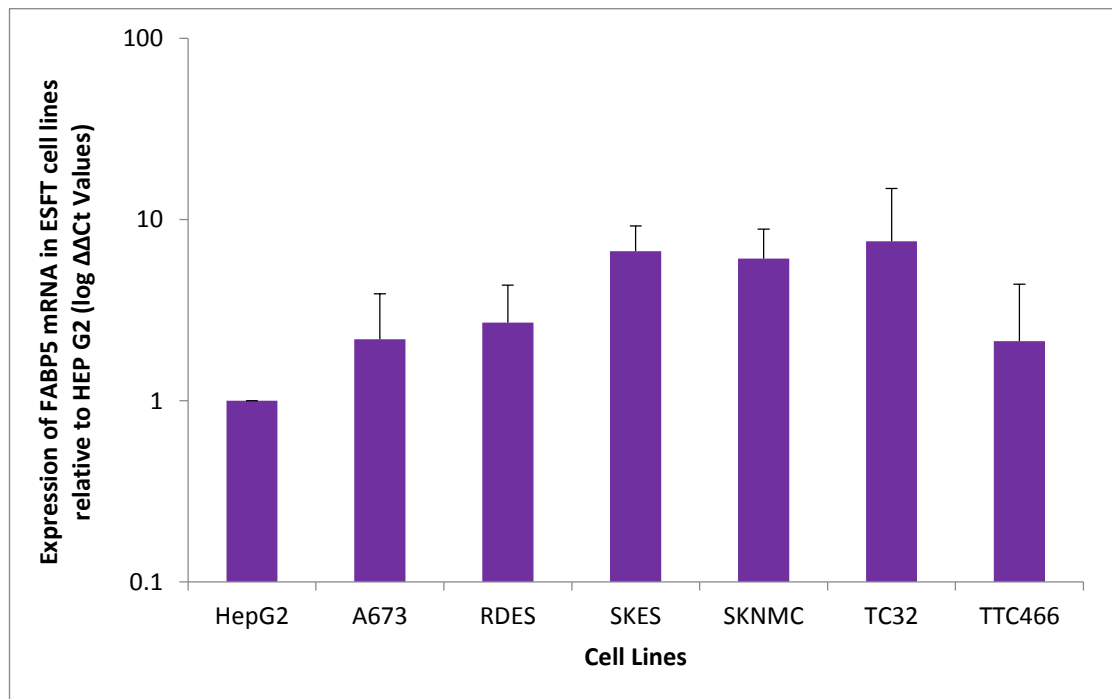


Figure 3.17 The expression of FABP5 mRNA in 6 ESFT cell lines using HEP G2 total RNA as the positive control and $\beta 2M$ housekeeping gene. Each reaction contained 400ng/ μ l ($n=3$). Comparison of the levels of FABP5 mRNA expression among the 6 ESFTs and the positive control did not reveal any significant differences by ANOVA, post hoc , Bonferroni.

3.3.6.2 Fatty Acid Binding Protein 5 expression in ESFT cell lines

FABP5 protein (15 kDa) was detected in the cell extracts of all 6 ESFT cell lines studied. The levels of FABP5 in ESFT cells were comparable to that in the HEP G2 cell protein extract (positive control cell line). The 15 kDa protein product was demonstrated (by densitometry) to be most abundant in SKES-1 (Figure 3.18). Protein loading was confirmed by probing the western blots for β -Actin (42 kDa). The HEP G2 protein appeared under-loaded in this blot.

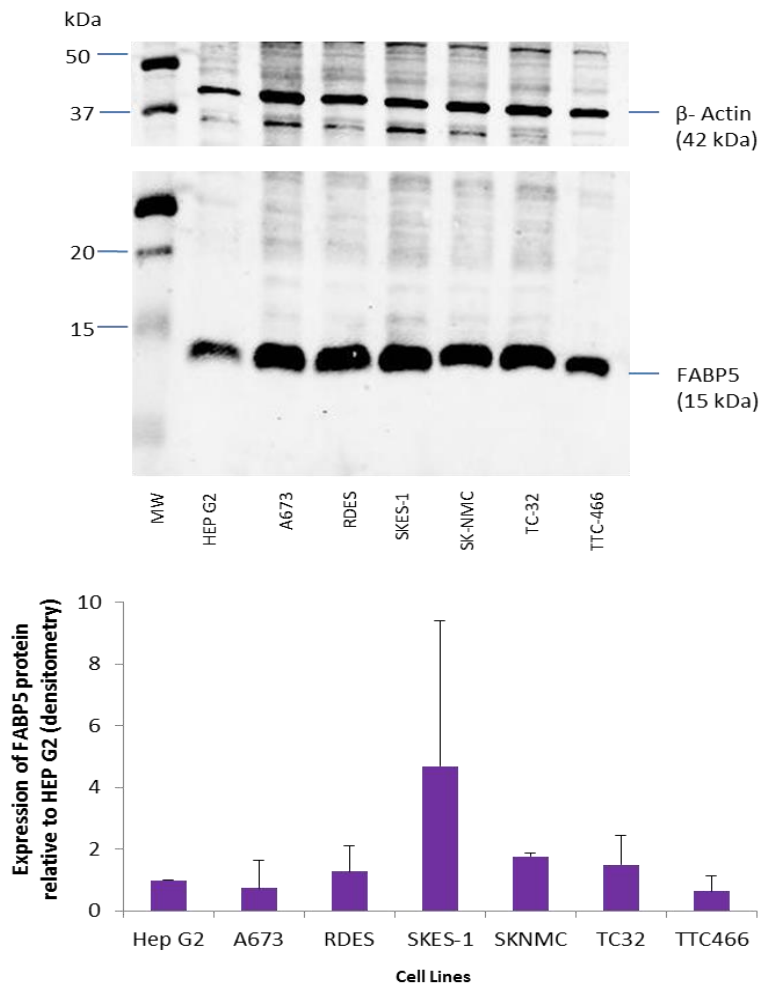


Figure 3.18 Western Blot analysis for FABP5 in ESFT cell protein extracts, using HEP G2 as positive control and β -Actin as the loading control. Bands on the western blot were quantified by densitometry and expression levels calculated as the ratio FABP5: β -Actin and normalised to the positive control HEP G2. MW=molecular weight markers in kDa (n=3).

3.3.6.3 FABP5 in non ESFT cancer cells

FABP5 protein was highly expressed in 7 of the 9 non ESFT cancer cell lines. It was not detected in either T98G or RT-112 cells. The expected 15 kDa band was also seen in the positive control (MCF-7) (Figure 3.19) Protein loading was confirmed by probing the immune-blot for β - Actin (42 kDa) and was found to be variable with the HEP G2 appearing under-loaded.

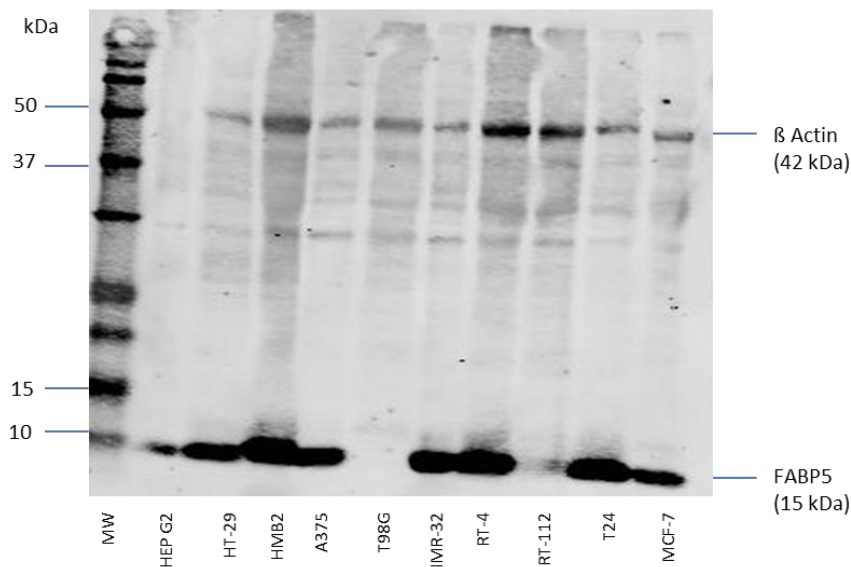


Figure 3.19 FABP5 protein expression in non ESFT cancer cell lines extract, using MCF-7 as the positive control and β -Actin as the loading control. HEP G2 = Hepatocellular carcinoma , HT-29= Colorectal adenocarcinoma , HMB2 = Melanoma , A375= Melanoma, T98G= Glioblastoma, IMR-32= Neuroblastoma, RT-4= Bladder cancer, RT-112= Bladder cancer, T-24= Bladder carcinoma, MCF-7= Breast cancer

The relative abundance of FABP5 mRNA compared to CRABP2

FABP5 and CRABP2 mRNA levels have been quantified in the 6 ESFT cell lines relative to HEP G2 in the former and MCF-7 cells in the latter. The expression of FABP5 mRNA was compared to CRABP2 using the Δ Ct

values, as the positive controls were different. The ratio was found to vary between 0.02 - 1.28 (Table 3.7).

Table 3.7 The FABP5: CRABP2 mRNA ratio in the 6 ESFT cell lines. This calculation has been performed using the Δ Ct values for FABP5 and CRABP2. This allows the data to be normalised to the housekeeping gene B2M but not for the positive controls which are different for the 2 proteins.

Cell Lines	Average FABP5 mRNA (Δ Ct value)	Average CRABP2 mRNA (Δ Ct value)	FABP5/ CRABP2 mRNA
A673	1.98	4.03	0.49
RDES	1.2	1.3	0.93
SKES-1	0.23	3.95	0.06
SK-N-MC	0.05	2.94	0.02
TC-32	0.64	0.5	1.28
TC-466	1.89	3.34	0.57

3.3.7 Immunohistochemistry

A pilot study was performed using a panel of 20 ESFTs. CRBP-I, CRBP-IV, CRABP2 and FABP5 proteins were characterized in these tissues and associations between these bio-markers expression (within clinically relevant sub-groups) were investigated. If the data implied any strong associations then a larger patient sample cohort would be analysed.

3.3.7.1 CRBP-I

Two CRBP-I antibodies were tested at various concentrations, using different methods of fixing (acetone/methanol and paraformaldehyde) at different incubation times (one hour and overnight) with the primary antibody. In addition, three methods of staining were investigated including using standard protocols, EnVision (Figure 3.20) and Novo-link kits (Figure

3.21). When using the amplification kits, extra steps of blocking for non-specificity with antibody appropriate animal serum at prolonged times were investigated. Despite these modifications, the background signal remained extremely high and so the immunohistochemistry studies for CRBP-I could not be interpreted.

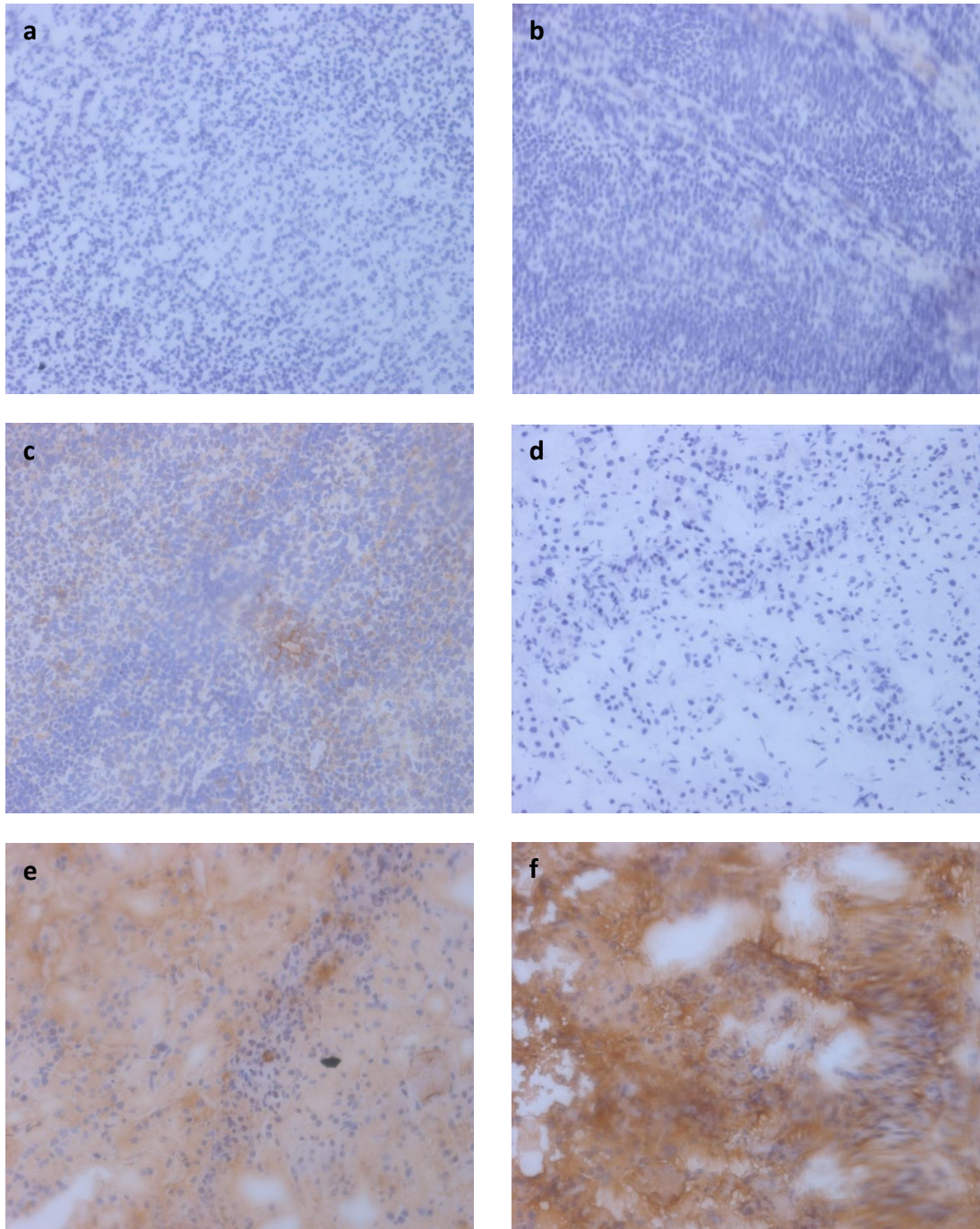


Figure 3.20 Immunohistochemistry staining for CRBPI protein, using the Envision protocol, in negative control tissue (tonsil) and positive control tissue (pituitary). The primary antibody(sc-30106) incubation time was 1 h. a) Tonsil section with no primary antibody b) Tonsil section with antibody dilution 1:200 c) Tonsil section with antibody dilution 1:50 d) Pituitary section with no primary antibody e) Pituitary section with antibody dilution 1:200 f) Pituitary section with antibody dilution 1:50. (Magnification X100)

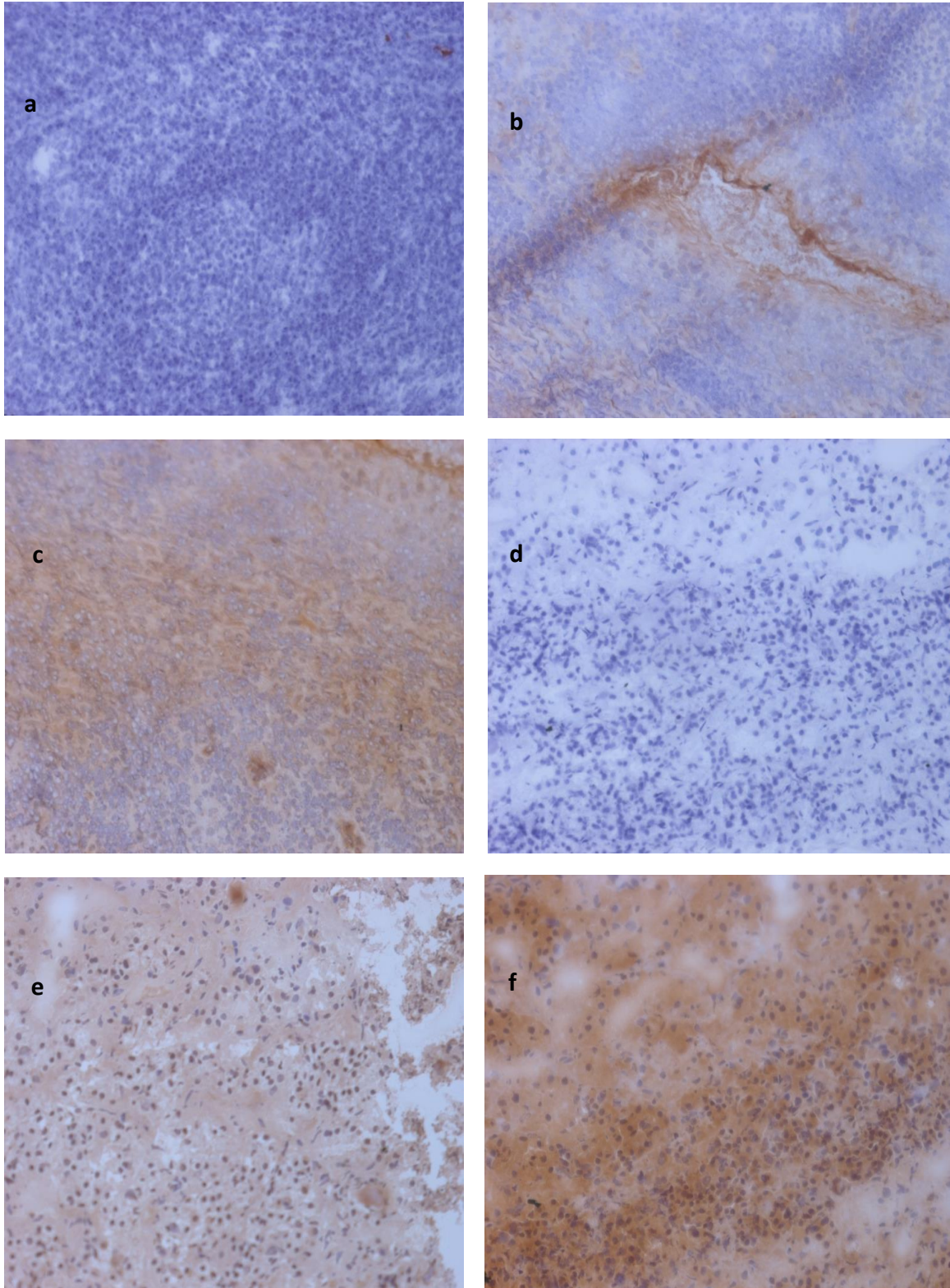


Figure 3.21 Immunohistochemistry staining for CRBP-I protein, using the Novo-Link protocol, in negative control tissue (tonsil) and positive control tissue (pituitary). The primary antibody(sc-30106) incubation time was 1 h. a) Tonsil section with no primary antibody b) Tonsil section with antibody dilution 1:200 c) Tonsil section with antibody dilution 1:50 d) Pituitary section with no primary antibody e) Pituitary section with antibody dilution 1:200 f) Pituitary section with antibody dilution 1:50. (Magnification X100)

3.3.7.2 Comparison of CRBP-IV, CRABP2 and FABP5 in a panel of ESFT tumours

CRBP-IV, CRABP2 and FABP5 antibodies have been optimised for IHC. Since these proteins showed relatively low abundance, amplification methods were needed for optimal detection. The conditions for immunohistochemistry of the target protein have been defined in Table 3.2. Sections were stained with no-primary antibody, antibody specific isotype and the target antibody. Comparison of the no-primary staining and the antibody specific isotype for CRBP-IV, CRABP2 and FABP5 revealed that there was no difference between the two (Figure 3.22). In future experiments was therefore carried out using the antibody specific isotype as a valid negative control.

Expression of CRBP-IV, CRABP2 and FABP5 were compared with reported clinical prognostic factors that are well recognised in ESFTs (Duchman, Gao et al. 2015). These include site of tumour, age at presentation, metastatic staging, and response to treatment and time to first event. Pelvic/central tumours (Paulussen, Ahrens et al. 2001, Grier, Krailo et al. 2003), older age (Cotterill, Ahrens et al. 2000, Grier, Krailo et al. 2003), metastatic disease (Bacci, Ferrari et al. 2000), poor response to treatment and shorter time to first event have all been associated with a poorer outcome.

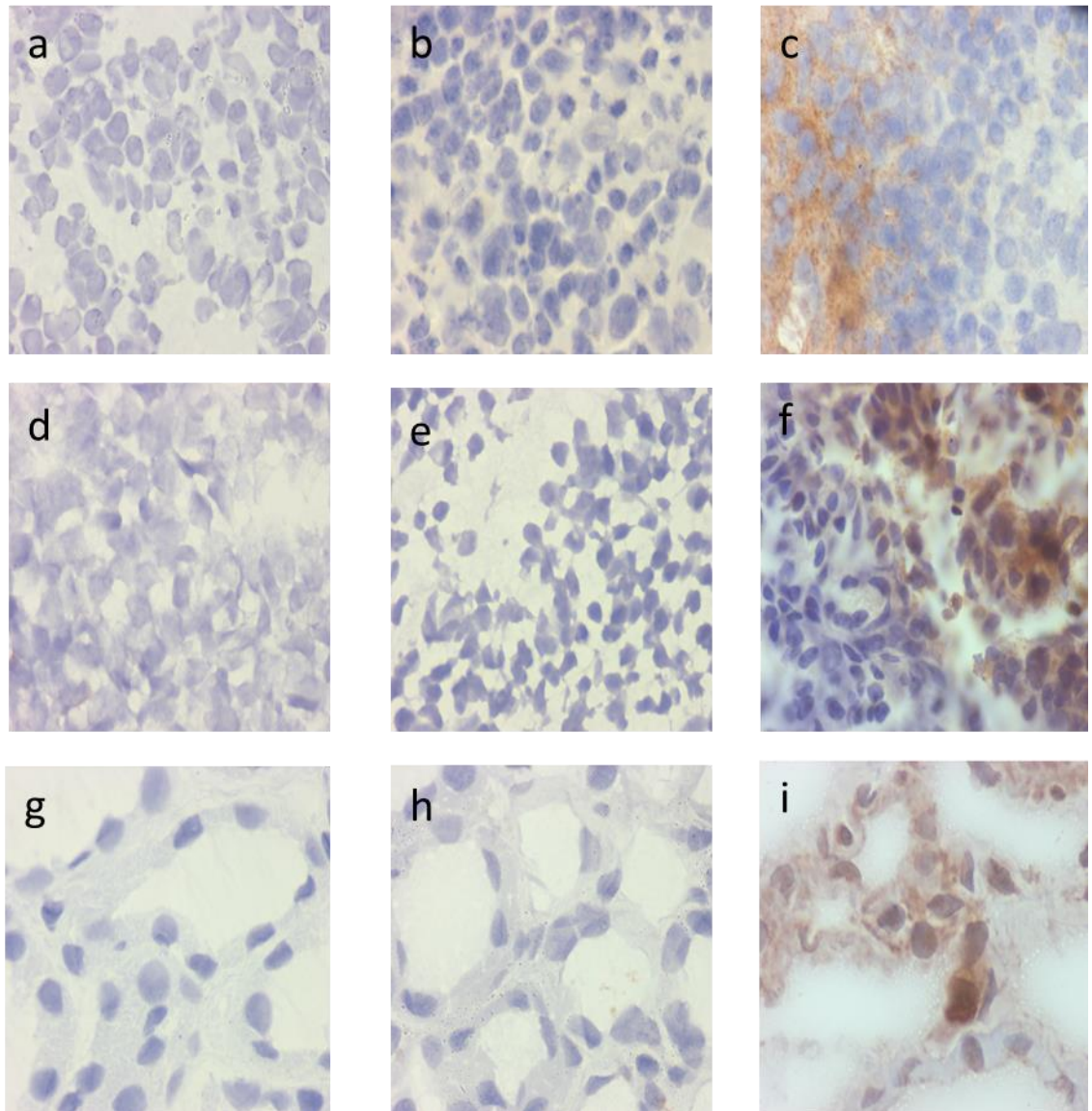


Figure 3.22 A comparison of no primary antibody, antibody specific isotype for particular antibody and positive control for each of the three target proteins. IHC for CRABP2 protein : **a)** tonsil with no primary antibodies **b)** tonsil tissue with CRABP2 antibody specific isotype **c)** tonsil tissue with CRABP2 antibody. IHC for FABP5 protein **d)** no primary FABP5 antibody **e)** FABP5 antibody specific isotype **f)** tonsil with FABP5 antibody. IHC for CRBP4V **g)** kidney with no primary antibody **h)** kidney with antibody specific iso-type and **i)** kidney with CRBP4V antibody staining were performed.

The CRABP2 and FABP5 markers appeared to be expressed at low levels in this panel of ESFT with the median H-score (Section 3.2.7) for both groups being similar (median CRABP2 H-score = 8; median FABP5 H-score=9). The expression of CRBP-IV however, was significantly greater in these tumours as evidenced by the larger H-scores (Figure 3.23) and this expression was statistically significantly different when compared to CRABP2 and FABP5 ($p=0.000$).

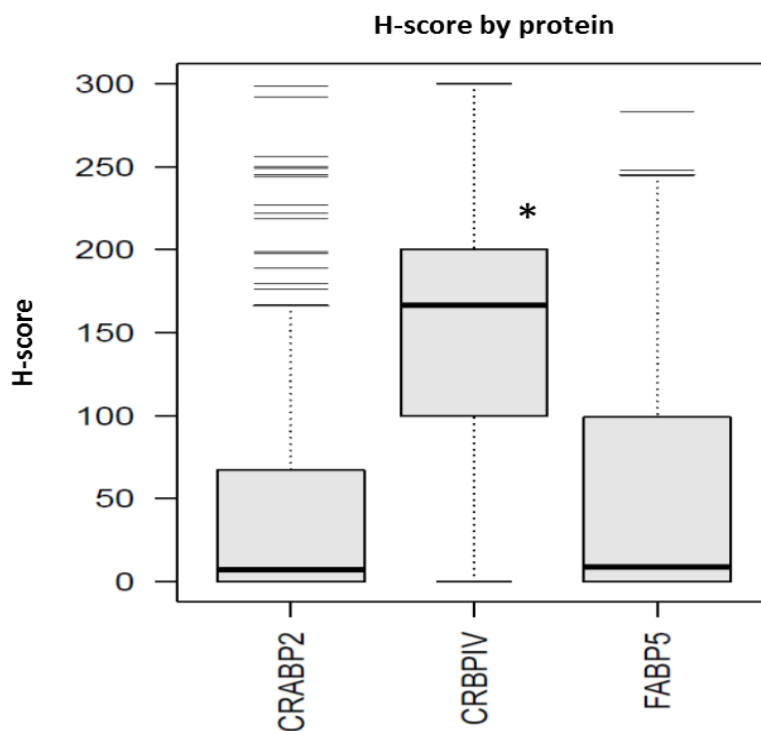


Figure 3.23 The expression of CRABP2, CRBP-IV and FABP5 proteins in a panel of ESFT, detected by IHC. H-scores were calculated for the target proteins and represented in the box and whisker plot using the R software. The bold line in the box represents the median, while the 1st and 3rd interquartile range are represented by the hinges. Outliers were defined as lying 1.5 times the interquartile range above the upper quartile and below the lower quartile. CRBP-IV expression was significantly different from CRABP2 and FABP5, using the Kuskal-Wallis test ($p=0.000$) *= statistically significant.

There was no apparent direct relationship between the expression of CRABP2, CRBP-IV and FABP5, when their H-scores were plotted against each other (Figure 3.23).

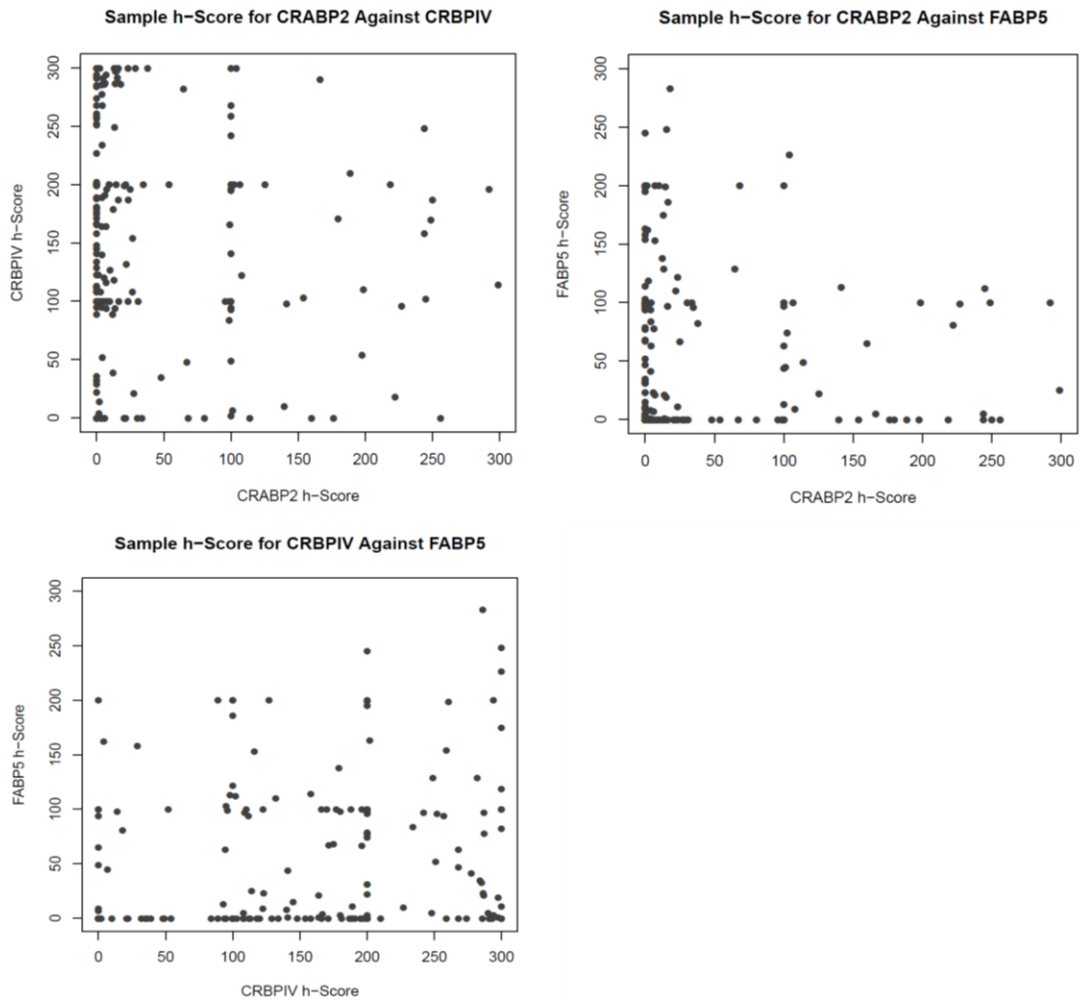


Figure 3.24 The relationship between the three target proteins in ESFTs. The H-scores for each protein was plotted against each of the remaining 2 proteins (in a scatter plot) to reveal any direct or linear relationship. The panel consisted of 20 ESFTs. In order to ensure that there was representative sampling for H-scoring, 10 independent fields of vision were examined for each tumour, resulting in 200 H-scores for each protein.

3.3.7.3 CRABP2 protein expression in the ESFT panel.

CRABP2 protein was expressed in 16 of the 19 ESFTs (84%). Of these 16 tumours, 8 expressed CRABP2 in the cytoplasm at low levels (50%) (Intensity 1: Section 3.2.7; Fig 3.26b). In all of the 8 tumours with low CRABP2 expression, there was protein localised to the cytoplasm. In 3 of these 8 tumours, CRABP2 was also expressed in the nucleus of all cells; a further three tumours revealed nuclear staining in 60% of the cells. In the 2 remaining tumours with low CRABP2 expression, nuclear staining was only present in 38% of the cells. There were 6 tumours (38%) with moderate CRABP2 protein expression (Intensity 2; Section 3.2.7.) (Fig 3.26c). In all of these tumours CRABP2 was detected in the cytoplasm, with three of these also containing nuclear CRABP2. There was a high level of protein expression in 2 tumours (13%) out of the panel of 19 (Intensity 3: Section 3.2.7; Fig 3.26d). One of those two tumours had a uniformly high expression in both cytoplasm and nucleus. In the second tumour, however, CRABP2 was expressed in only 35% of the cells in both the cytoplasm and the nucleus. CRABP2 was detected (by IHC) in the cytoplasm of 84% (16/19) tumours but only 69 % (13/19) of these tumour samples contained nuclear CRABP2 (Figure 3.25).

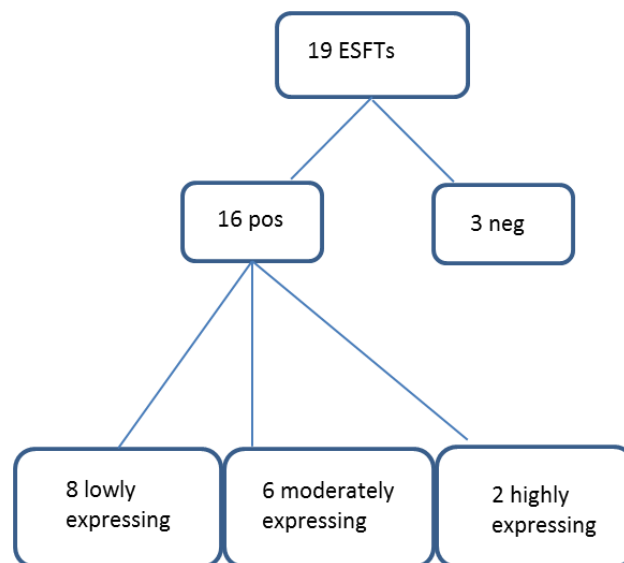


Figure 3.25 Relative expression of CRABP2 protein in the ESFT panel

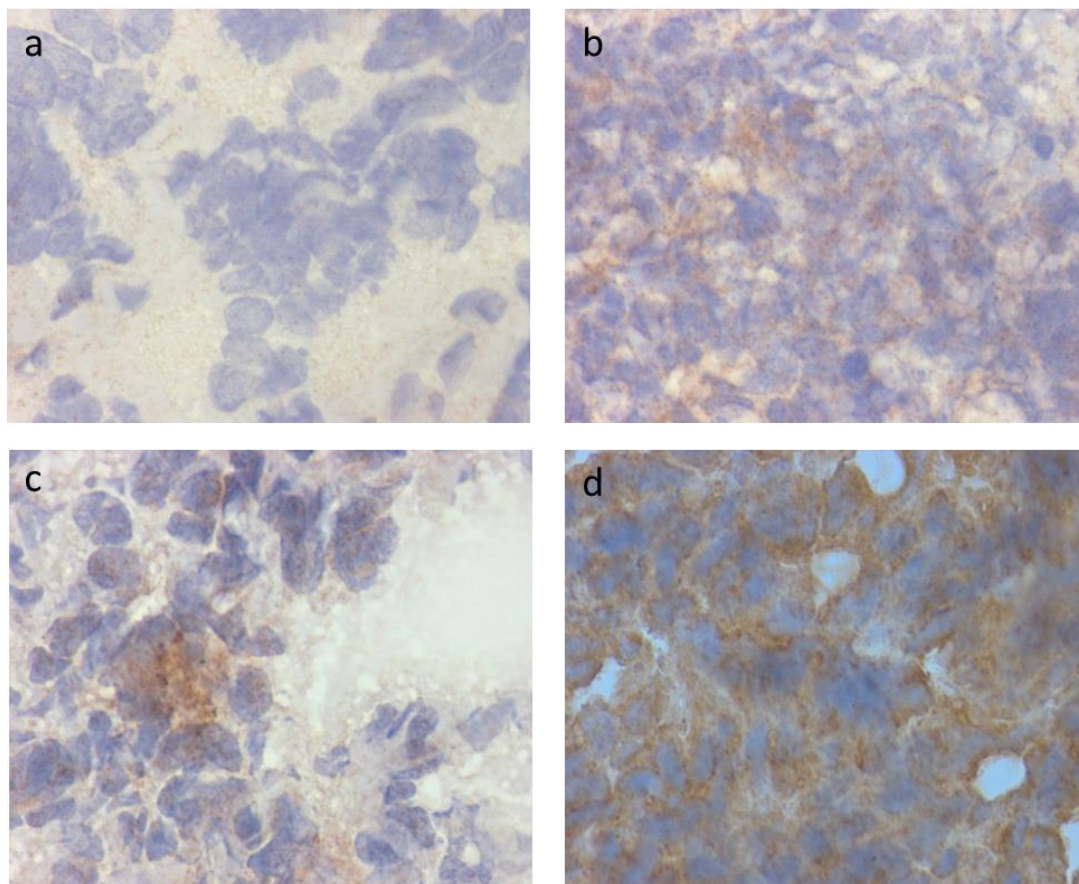


Figure 3.26 Immunohistochemistry staining of CRABP2 in a panel of ESFTs. It demonstrates variable intensities of staining **a)** ESFT cells with no staining designated as intensity 0 **b)** ESFT cells with weak staining designated as intensity 1 **c)** ESFT cells with moderate staining designated as intensity 2 and **d)** ESFT cells with heavy staining designated as intensity 3. Magnification X100.

For these 19 tumours, 190 fields of vision (see Section 3.2.7) were assessed and scored (H-score). The median H-score of the fields of visions that contained cytoplasmic CRABP2 was 5, while the median score for those in which cytoplasmic CRABP2 was absent was 150. This was statistically significant using Kruskal-Wallis test. ($p=0.04$). There were only 6/190 fields of vision in which there was no cytoplasmic staining.

When fields of vision with nuclear CRABP2 localisation ($n=65$) were compared for H-scores against those without ($n=95$), the groups were found

to be statistically different by the Kruskal-Wallis test. ($p=0.0003$). The median H-score for the former group was 2 while that of the latter group was 15. Generally nuclear expression of CRABP2 was higher than cytoplasmic (Fig 3.27).

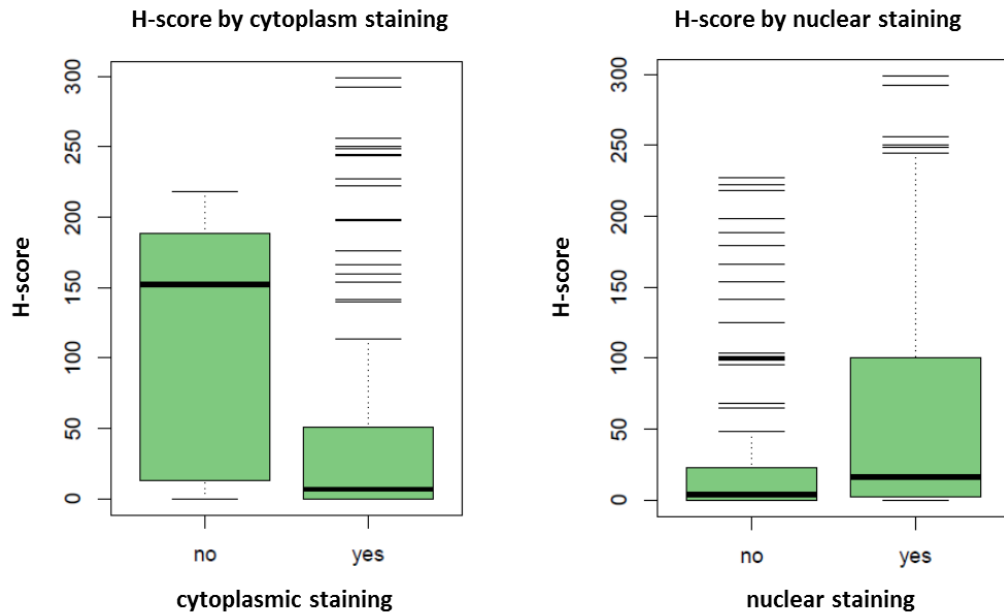


Figure 3.27 Sub-cellular localization of CRABP2 protein expression, calculated by the H-score. The expression in the cytoplasm and nucleus compartments were investigated. They were found to be statistically significantly different by the Kruskal-Wallis test with nuclear staining localization containing higher levels than cytoplasmic.

When the CRABP2 H-scores of the fields of vision were compared for the age at presentation, there was no statistical significance between the two groups (less than 15 years; more than or equal to 15 years) (Kruskal-Wallis test $p=0.6$). The patients who were younger than 15 years had tumours with a median H-score=9 and the older group had a median H-score=7 (Figure 3.28). There were eleven patients in the younger age group and seven in the older group. The age of two of the patients was unknown. Although there was no discernible difference between these groups, it is important to remember that the sample size is small, which may not make for clinically meaningful correlations.

When the site of the tumour was compared for the CRABP2 H-scores, it was found to be statistically significant (Kruskal-Wallis test $p=0.0001$). The median H-scores for centrally located tumours were highest (H-score= 12) and those tumours that were proximal had the lowest scores (H-score=1). The ESFT that were located distally had a median H-score of 10 (Fig 3.28). Of the panel, 12/18 tumours were central, with 5/18 sited proximally with only 1/18 was distal. The data for 2 tumours were unavailable.

The CRABP2 H-scores were compared for the metastatic staging of the tumours at presentation (metastatic or non-metastatic). There were six metastatic and twelve non-metastatic tumours; the data was unknown for two tumours. The H-score was higher in the non-metastatic group, and this was statistically different (Kruskal-Wallis, $p=0.0002$) (Figure 3.28).

The response of ESFT to chemotherapy has been defined as a good response ($>95\%$ tumour necrosis), intermediate response (71-95% tumour necrosis) and poor response ($<70\%$ tumour necrosis) (Subbiah, Chuang et al. 2017). When CRABP2 H-scores were compared for these clinical groups, the good responders had a higher median score when compared to the other 2 groups (intermediate responders). This was statistically significant (Kruskal-Wallis test=0.003) (Figure 3.28). The numbers in the various groups were small with 8 tumours having a good response, 1 producing an intermediate response and 3 showing a poor response. There were 8 tumours for which the data was unknown.

Another category that was evaluated was the time to first event (the number of interval days from diagnosis to first event: recurrence, progression, secondary tumour, infection and even death). There are 2 groups that are recognised as having clinical implications: early first event (less than two years) and late first event (more than or equal to two years) (Bacci, Ferrari et al. 2000). There were 8 tumours with a shorter time to first event, nine with a longer time to first event and three for which the data was unknown. There were no statistically significant difference in the CRABP2 staining (H-score) in the groups (Kruskal-Wallis $p=0.11$) (Figure 3.28). It may be that no difference was seen due to small sample size or that there could have been no correlation with CRABP2.

Finally, the CRABP2 staining (H-score) was compared for the patient survival outcomes. There were 2 patients who were alive with disease, 8 who were deceased (due to disease), 7 who were in remission and 3 for whom the data was unknown. When these 3 groups were compared, they were significantly different (Kruskal-Wallis $p=0.000$). Those who were in remission and alive with residual disease had a significantly lower median H-score when compared to those that were deceased (Figure 3.28).

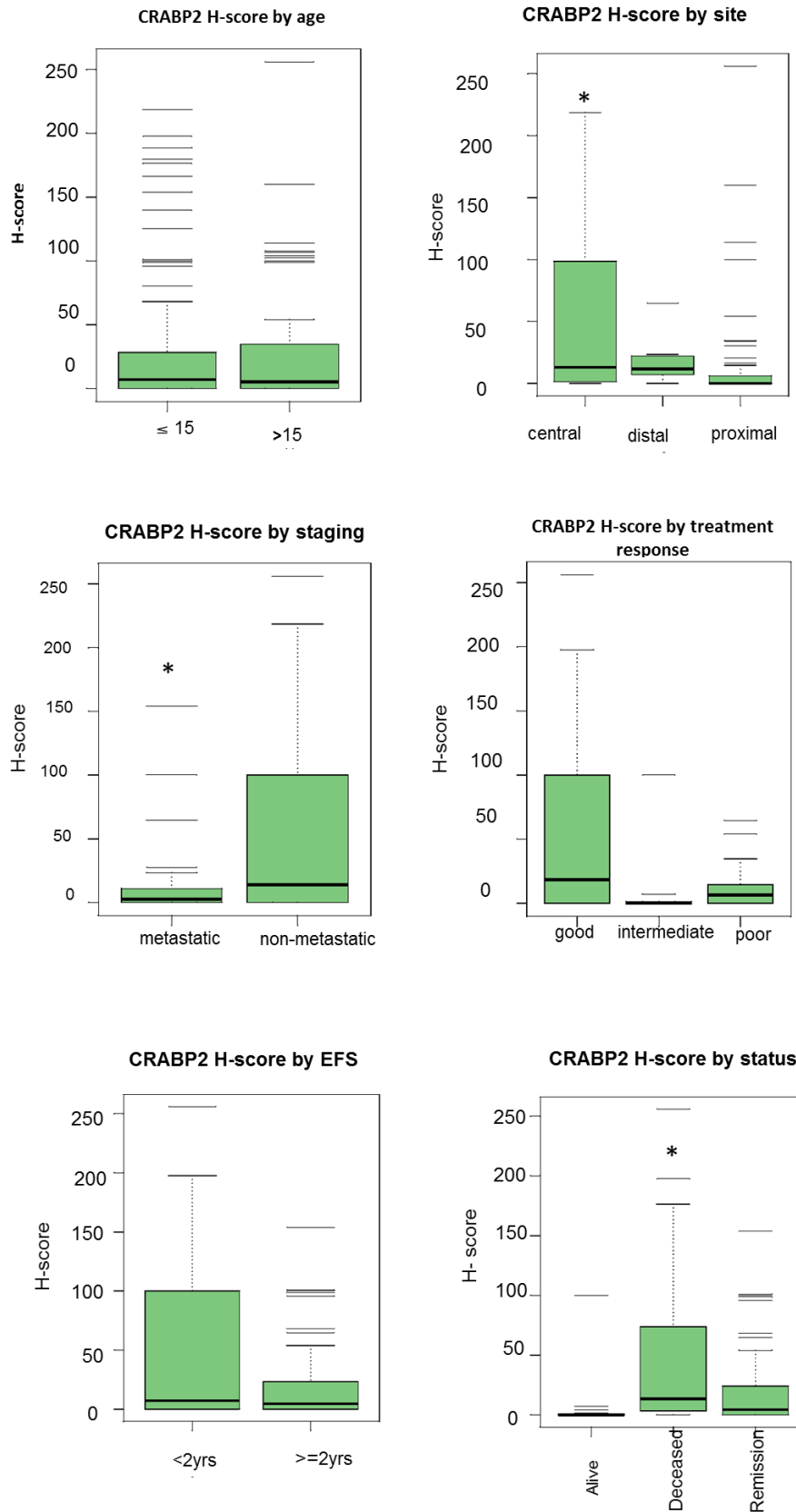


Figure 3.28 The CRABP2 protein expression (H-scores) in the ESFTs when stratified for recognized clinical prognostic factors. These include by a) site of the tumour: central (chest, thorax, ribs), proximal (arm, femur) and distal (feet, forearm, hands); b) metastatic staging ; c) response to training (good, intermediate and poor) ; d) age at presentation (<15 yrs, >15 yrs) ; e) time to first event (<2 yrs, >2 yrs)

FABP5 protein

FABP5 was expressed in 15 (83%) of the 18 ESFT samples. A low level of protein expression was observed in nine (50%) of the eighteen tumours (Intensity 1: Figure 3.30). All of the 9 tumours contained FABP5 in the cytoplasm. Five of these nine demonstrated nuclear staining of the FABP5 protein in 70 % of cells in the fields of vision (Figure 3.30).

A moderate level of expression of the FABP5 protein was observed in 5 (28%) tumour samples (Intensity 2: see Section 3.2.7; Figure 3.30c). All of these contained cytoplasmic protein staining. Two of these five also contained FABP5 in the nucleus of all cells. A further two tumours contained the protein in the nucleus of 42% of the cells and one tumour sample showed no nuclear staining.

Finally, 1 (6%) tumour from the panel was found to have a high level of FABP5 expression (Intensity 3: see Section 3.2.7; Fig 3.30d). The protein was present in both cytoplasm and nucleus, with all cells uniformly stained.

FABP5 was detected (by IHC) in the cytoplasm of 83% (15/18) tumours but only 56% (10 /18) of these samples contained nuclear CRABP2.

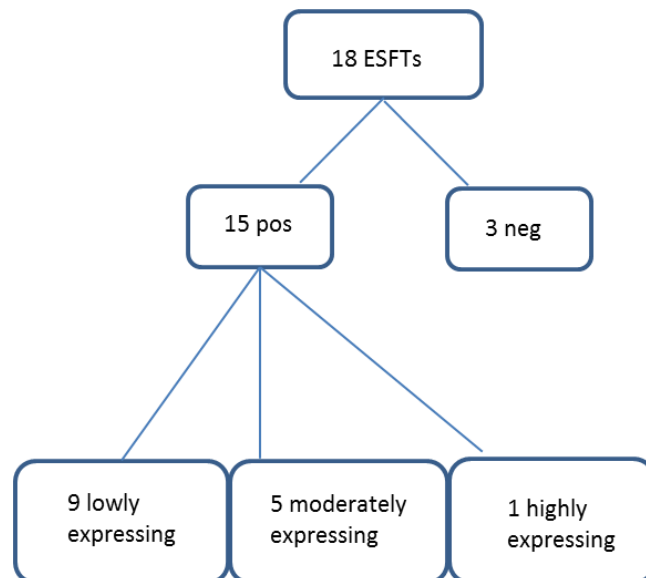


Figure 3.29. Relative expression of FABP5 protein in the ESFT panel

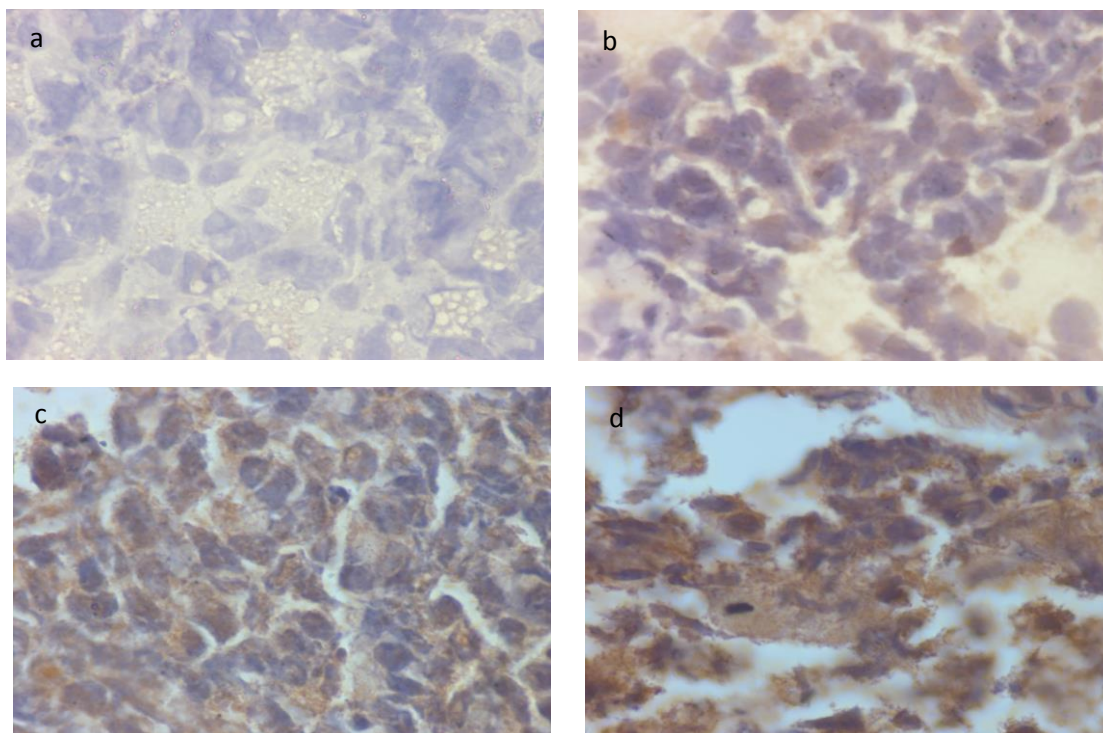


Figure 3.30. Immunohistochemistry staining for FABP5 in a panel of ESFTs demonstrating staining intensity. **a)** ESFT with no staining = Intensity 0 **b)** ESFT with weak staining= intensity 1 **c)** ESFT with moderate staining- intensity 2 **d)** ESFT with heavy staining= intensity 3. All slides were produced at 100 X magnification.

For these 18 tumours, 180 fields of vision (Section 3.2.7) were assessed and scored (H-score). All of the FABP5 positive tumours contained cytoplasmic protein. There was no statistical difference in the H-score of the tumours with nuclear FABP5 localisation, cytoplasmic localisation or a combination of cytoplasmic and nuclear ($p=0.17$) (Figure 3.31).

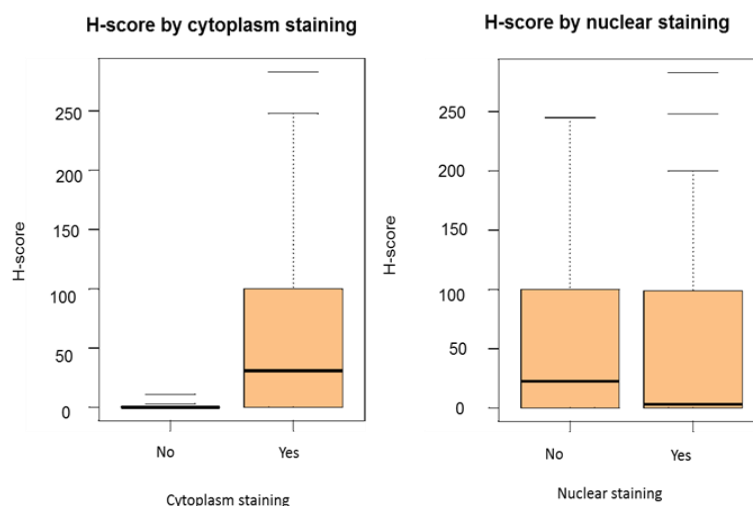


Figure 3.31. Sub-cellular localization of FABP5 protein expression calculated by the H-score. Expression in the cytoplasm and nucleus were investigated. The H-scores for sections in which there was cytoplasmic FABP5 were compared to those with no cytoplasmic FABP5. By Kruskal-Wallis, they were not found to be clinically significant.

The tumours were categorised into groups by the age at presentation (less than or equal to 15 years and more than 15 years). There were eleven patients in the younger group and seven in the older group, with the data for two patients unknown. There appeared to be a statistically significant difference (Kruskal-Wallis test, $p=0.0005$). Those patients presenting in the older groups (usually worse prognosis) had a higher median H-score (49), while the younger group had a median H-score of 1 (Figure 3.32).

When the H-scores for these tumours were grouped by tumour site, they were found to be statistically different, with the central tumours ($n=12$) having the lowest H-score (median H-score=1), followed by the proximal tumours ($n=5$; median H-score=55) and finally the distal tumour ($n=1$; H-score=128) having the highest concentration of FABP5 (Kruskal-Wallis $p=0.000$) There was no site data for two tumours (Fig 3.32). There appeared to be an association with tumours with the worse prognosis (centrally sited tumours) having the lowest level of FABP5.

Comparison of FABP5 H-scores for the ESFT panel grouped by metastatic staging (metastatic or non-metastatic) at presentation, found that the groups

were not statistically different (Kruskal-Wallis test ($p=0.73$)). There were 6 metastatic and 12 non-metastatic tumours (Figure 3.32).

Similarly, when the tumours were stratified according to response to chemotherapy (percentage tumour necrosis (Subbiah, Chuang et al. 2017)). There was no significant difference in the H-scores among the 8 good ($> 95\%$ tumour necrosis), 1 intermediate (71-95% tumour necrosis) and 3 poor ($\leq 70\%$ necrosis) responders (Kruskal- Wallis, $p=0.21$).

There was no statistical difference in the H-scores of the tumours when compared for time to first event after diagnosis (Kruskal-Wallis $p=0.67$). The samples were separated into two groups: a shorter time to first event (< 2 yrs) ($n=8$) and those with longer time to first event (2 years or more) ($n=9$). The data for three tumours was not available.

Finally, the FABP5 H-scores for the tumour samples were compared in three outcome groups: patients in remission, alive with disease or deceased. The H-score for the deceased group was lowest, followed by the group of patients that were in remission. Those patients alive with the disease had the highest mean H-score. This was significantly different (Kruskall-Wallis $p=0.03$) (Fig 3.32). This was however, a small sample with seven patients in remission, two in the group alive with the disease and eight in the deceased group. Data was unavailable for three patients. This finding needs further investigation in a study using a larger number of patient samples, as potentially FABP5 may be a bio-marker for outcome in ESFTs.

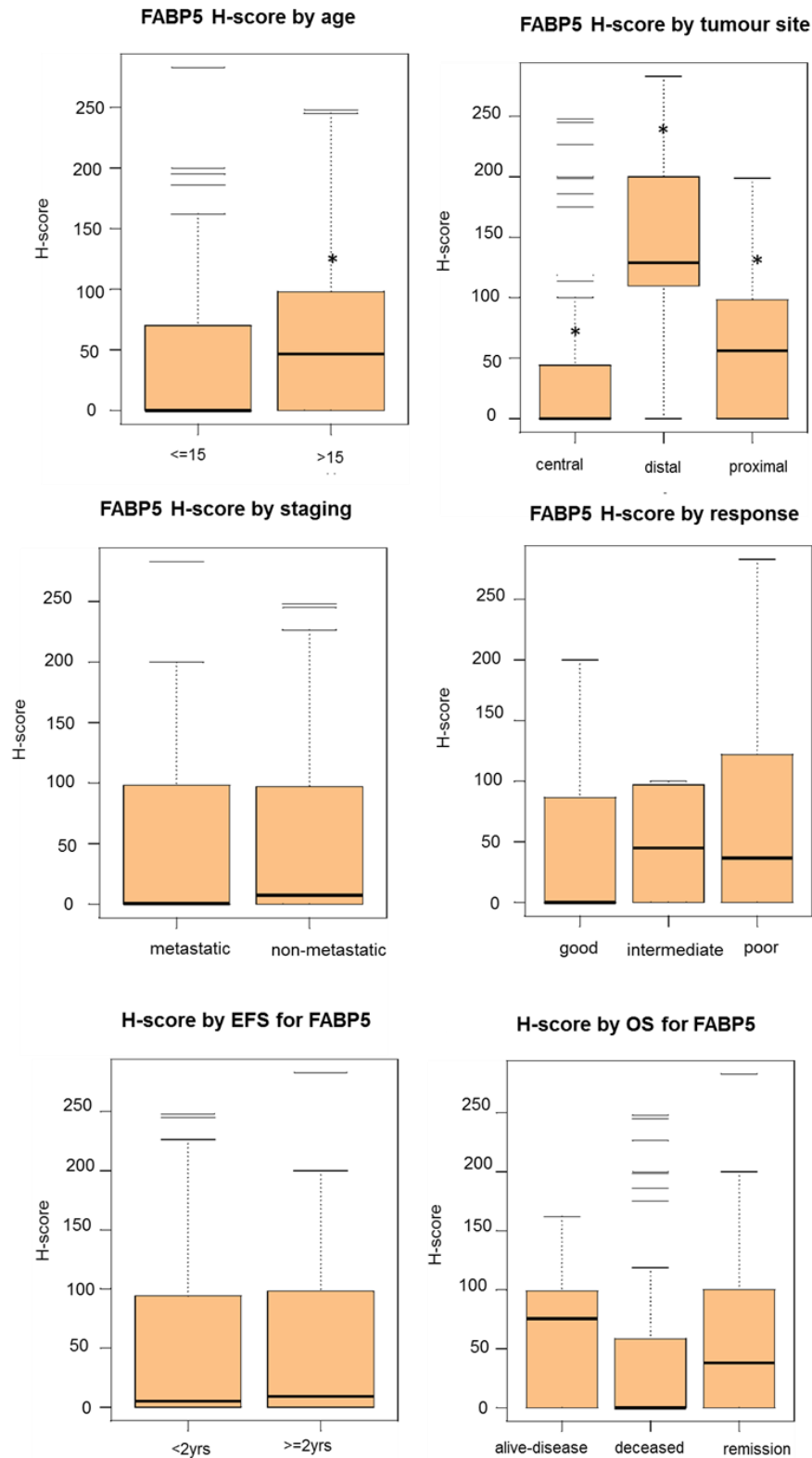


Figure 3.32. The FABP5 protein expression (H-scores) in the ESFTs when stratified for recognized clinical prognostic factors. These include by a) age at presentation (< 15 yrs , > 15 yrs) b) site of the tumour: central (chest, thorax, ribs), proximal (arm, femur) and distal (feet, forearm, hands); c) metastatic staging ; d) response to training (good, intermediate and poor) ; e) time to first event (< 2 yrs, > 2 yrs) and f) survival outcomes. The data was then analysed using the Kruskal-Wallis test to determine statistical significance.

3.3.7.5 CRBP-IV protein

CRBP-IV was detected in all of the 18 (100%) ESFT tumours. Only 2 (11%) of these showed a low level of protein expression (Intensity 1: Section 3.2.7; Fig 3.34). In 1(6%) of these tumours, the protein was cytoplasmic in location while the other tumour showed that the protein was localised in the nucleus.

Moderate CRBP-IV protein expression was observed in 10 (56%) of the 18 tumour samples (Intensity 2, see section 3.2.7; Fig 3.34c). Only 2 (11%) tumours demonstrated cytoplasmic staining while 8 (44%) tumours found the protein to be localised in the nucleoli (Figure 3.34e), and 1 (6%) tumour showed that the protein of interest was present in both the cytoplasm and nucleus.

Finally 6 (33%) tumours demonstrated a high level of CRBP-IV expression (Intensity 3: see section 3.2.7; Fig 3.34d). All 6 of these contained nuclear CRBP-IV protein, and five of these particularly showing staining of the nucleoli of the cells (Figure 3.34e). The other tumour contained generalised nuclear staining. Four of these six tumours contained CRBP-IV staining in both the cytoplasm and nucleus.

Only 39% of the tumours demonstrated cytoplasmic protein whereas 72% of these tumour samples contained CRBP-IV localised to the nucleoli and 11% of samples demonstrated generalised nuclear CRBP-IV (Figure 3.33).

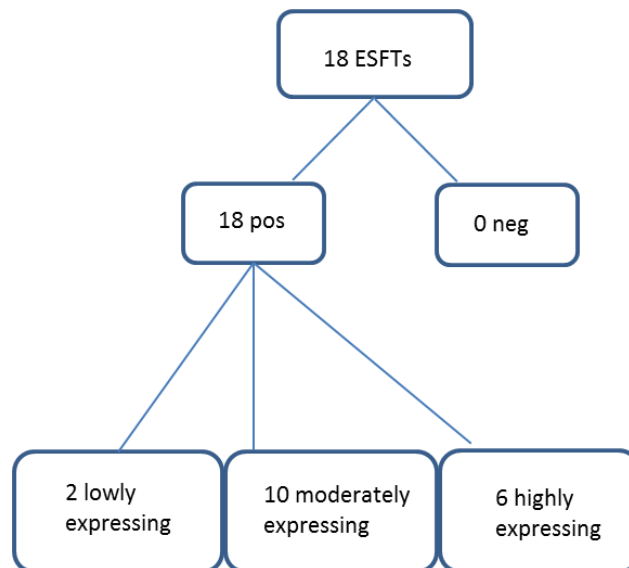


Figure 3.33 Relative expression of CRBP-IV protein in the ESFT panel

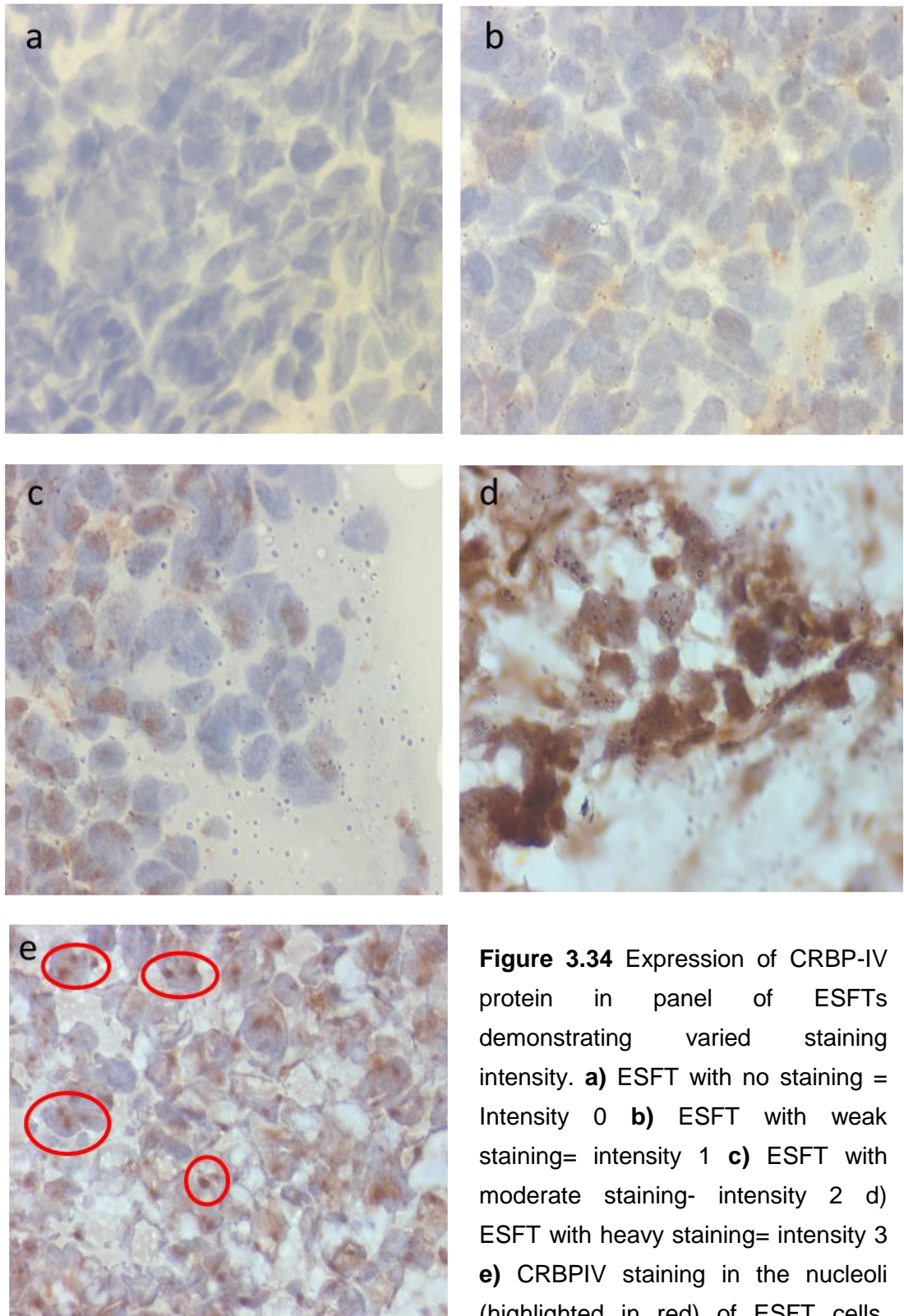


Figure 3.34 Expression of CRBP-IV protein in panel of ESFTs demonstrating varied staining intensity. **a)** ESFT with no staining = Intensity 0 **b)** ESFT with weak staining= intensity 1 **c)** ESFT with moderate staining- intensity 2 **d)** ESFT with heavy staining= intensity 3 **e)** CRBP-IV staining in the nucleoli (highlighted in red) of ESFT cells, giving it a speckled appearance. All slides were produced at 100 X magnification.

As previously, 10 fields of vision were assessed for each of the 20 tumours, resulting in CRBP-IV H-scores for 200 fields of vision (Section 3.2.7).

Clinically relevant categories (identical to those used in CRABP2 and FABP5 analysis), were used to evaluate the H-scores for CRBP-IV. When the data was grouped by age at presentation, the older patients (older than 15 yr.; n=12) had a statistically significantly different H-score when compared to the younger group (≤ 15 ys; n=6) (Kruskal-Wallis, $p=0.002$) (Figure 3.35). The median H-score for the older patients was 200, while the median H-score for the younger patients was 113. The ages of the patients for 2 tumours were unknown. Generally, the older group had a poorer clinical outcome (Grier, Krailo et al. 2003).

The H-scores for this panel of twenty tumours were then grouped by site of tumour (central, proximal and distal). There were twelve tumours in the centrally sited tumours, five tumours proximally and one tumour located distally. Data was unavailable for a further two tumours. There was no statistical difference between the three groups for CRBP-IV staining (Kruskal-Wallis, $p=0.067$) (Figure 3.35).

There was also no statistical difference in the H-scores for CRBP-IV staining when groups were compared for metastatic staging at presentation (Kruskal-Wallis, $p=0.07$). There were six tumours in the metastatic group and twelve in the non-metastatic group, with no data on two samples (Figure 3.35).

The CRBP-IV H-scores were compared by their response to chemotherapy. They were stratified as before into good responders (n=8) intermediate (n=1) and poor responders (n=3) (Subbiah, Chuang et al. 2017). Data was unavailable for 8 tumours. These three groups were statistically different from each other, with good responders having the lowest H-score, followed by the intermediate responders and the poorly responding tumours having the highest H-score (Kruskal-Wallis, $p=0.0004$).

There was no statistical difference in the H-scores of the tumours when compared for time to first event after diagnosis (Kruskal-Wallis, $p=0.787$). The groups were defined as a shorter time to first event (n=8) and those with longer time to first event (n=9). There was no information for three tumours (Figure 3.35).

Finally, the CRBP-IV H-scores for the tumours were compared in three outcome groups: patients in remission (n=7), patients with disease (n=2) and those deceased (n=8). There was no data for three tumours. There was no statistically significant difference (Kruskal- Wallis, $p= 0.129$) (Figure 3.35).

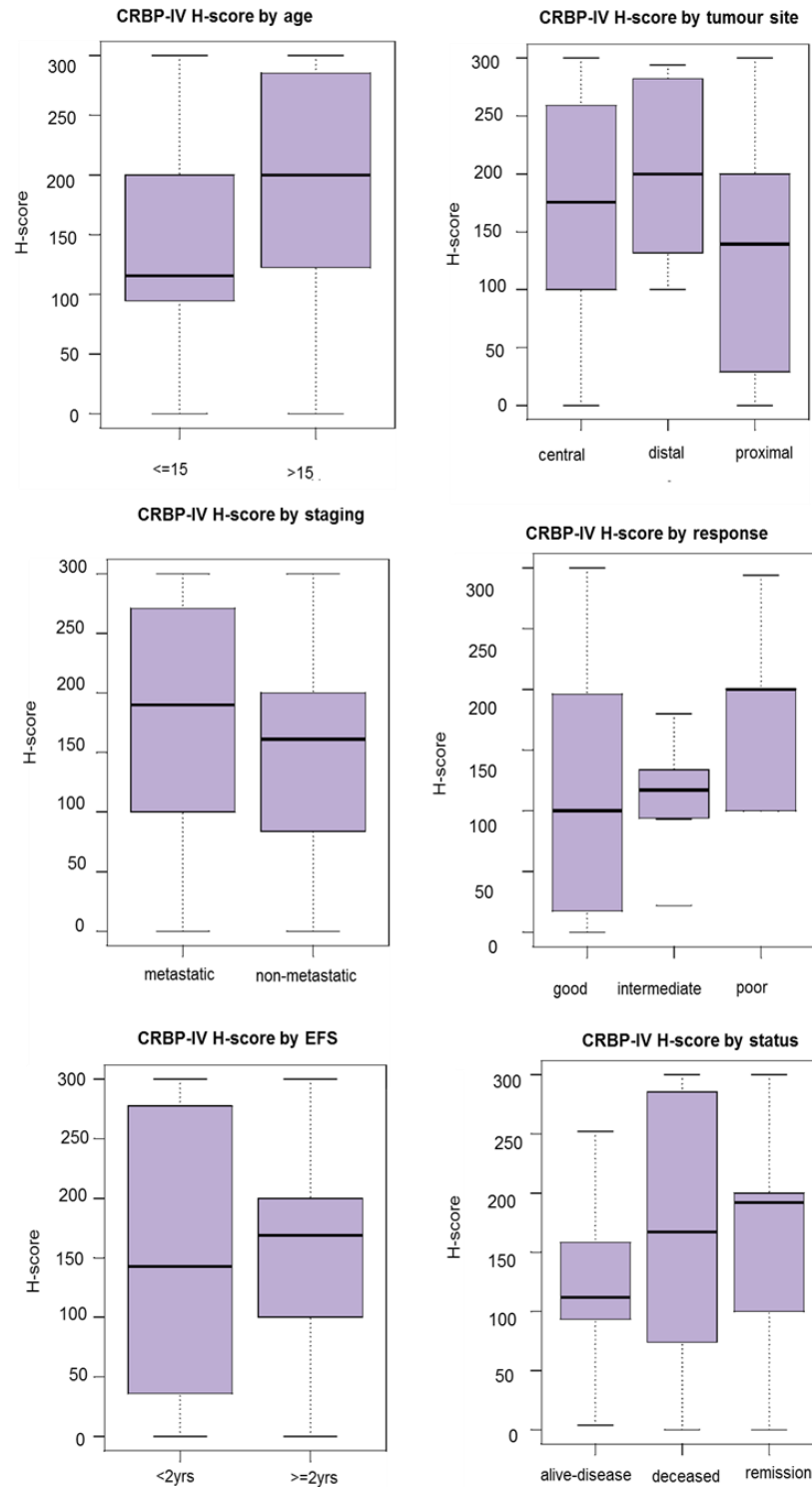


Figure 3.35. The CRBP-IV protein expression (H-scores) in the ESFTs when stratified for recognized clinical prognostic factors. These include by a) age at presentation (< 15 yrs , > 15 yrs) b) site of the tumour: central (chest, thorax, ribs), proximal (arm, femur) and distal (feet, forearm, hands); c) metastatic staging ; d) response to training (good, intermediate and poor) ; e) time to first event (< 2 yrs, > 2 yrs) and f) survival outcomes. The data was then analysed using the Kruskal-Wallis test to

3.3.8 Summary of Results

Table 3.8. Summary of the iLBPs expression in the 6 ESFT cell lines at the mRNA and protein levels. ✓ = present and X= absent

ESFT Cell Lines	Intra –Cellular Lipid Binding Proteins					
	CRBP-IV		CRABP2		FABP5	
	mRNA	Protein	mRNA	Protein	mRNA	Protein
A673	✓	✓	✓	✓	✓	✓
RDES	✓	✓	✓	✓	✓	✓
SKES-1	✓	✓	✓	✓	✓	✓
SK-N-MC	✓	✓	✓	✓	✓	✓
TC-32	✓	X	✓	✓	✓	✓
TTC-466	✓	X	✓	✓	✓	✓

3.4 Discussion

3.4.1 The value of prognostic markers in ESFT at diagnosis

ESFT is a rare cancer and so only a small number of studies have been performed in order to evaluate the prognostic factors. The presence of metastatic disease is the most unfavourable prognostic feature and accounts for 25% of patients at diagnosis (Casaroto, MB et al. 2017). Other unfavourable prognostic markers include poor responders (Schleiermacher, Peter et al. 2003, Avigad, Cohen et al. 2004) (Grier, Krailo et al. 2003), older patients (Grier, Krailo et al. 2003), larger (>200 ml) lesions and central tumour site (Paulussen, Ahrens et al. 2001, Grier, Krailo et al. 2003).

I have attempted to look at CRBP-IV, CRABP2 and FABP5 in these prognostic groups, in order to identify any relationship between the proteins and clinical outcomes. This pilot data was performed in a panel of 20 tumours and so, I accepted clinically informative cut-points defined (Rodriguez-Galindo, Navid et al. 2008). I have attempted to determine any relationship between these three proteins and the various clinical sub-categories. In some situations, the numbers in the sub-groups were too small to reasonably, reliably and accurately make statistical conclusions.

When compared with CRABP2 and FABP5, CRBP-IV had a higher preponderance in the panel of ESFT studied. All of the tumours in this panel were found to be positive for CRBP-IV, with 11 % having a low level of expression, 56% being moderately expressed and 33% having the highest expression of the protein. Only 39 % of the tumours demonstrated cytoplasmic protein whereas 72 % of these tumour samples contained CRBP-IV localised in the nucleoli and 11 % of samples demonstrated nuclear CRBP-IV. This was a very different pattern of distribution for CRBP-IV than previously described where it was reported to be restricted to cytoplasm (Alvaro, Alpini et al. 2002). It is therefore reasonable to consider that CRBP-IV may be acting as shuttle protein that transports various

ligands from the cell membrane to the nuclear membrane. Here the transported ligands bind to nuclear receptors and are potentially internalised within the highly metabolic organelle. It would be interesting to observe these samples using confocal microscopy, as this could provide more information on the sub-cellular localisation staining pattern observed.

Older patients who usually had a poorer prognosis (Jackson, Bittman et al. 2016) and the poorly responsive tumours represented a higher level of CRBP-IV protein. This was not noted in any of the other clinically prognostic groups evaluated. This is the first time that CRBP-IV protein has been suggested as a prognostic marker for disease. It has shown that in two different clinical sub-categories, patients with a poorer prognosis have a higher level of CRBP-IV. This particular trend would definitely need further evaluation and this can be done by increasing the size of the tumour panels. If higher levels of expression are then detected in more sub-groups of patients with a worse prognosis, CRBP-IV may indeed be playing a role as a prognostic biomarker.

CRABP2 protein expression in this panel of tumours was generally of low abundance (as evidenced by H-scores). Of all the tumours, 84% contained CRABP2 protein: 50% demonstrated a low level of expression while 38% moderately expressed the protein but with only 13 % contained a high level of CRABP2. While all the tumours that expressed CRABP2 contained the protein within the cytoplasm, only 69% showed it in the nucleus. This is in keeping with studies that have demonstrated the localisation of this protein in the cytoplasm and the nucleus (Majumdar, Petrescu et al. 2011). Those cells in which there was nuclear CRABP2 contained more CRABP2 (as evidenced by H-scores) than in those with cytoplasmic CRABP2. These findings could be further qualified with confocal microscopy, in order to determine whether this nuclear CRABP2 was in fact within the nucleus or at the nuclear membrane. This is important because it may provide further information about the role of CRABP2 downstream from binding to the nuclear RAR receptors.

Higher CRABP2 levels were seen in the tumours from a central site and from deceased patients (poorer prognostic groups). In direct contrast to this, more CRABP2 protein was detected in non-metastatic tumours and tumours with a good response to treatment (better prognostic groups). There was no statistical difference in CRABP2 levels based on age of presentation and time to first event. This analysis did not provide any obvious conclusions about CRABP2 levels in ESFT tumours but this may have been because the sample size was too small and further sub classifications made the groups much too small to reliably draw any conclusions. As was the case of CRBP-IV, this analysis could also benefit greatly by increasing the sample size.

Generally, the ESFT panel demonstrated a low level of expression of the FABP5 protein. All of the tumours in this panel were found to be positive for FABP5: 60% having a low level of expression; 33 % having moderate expression and 7% having high expression of the protein. Of all the tumours, 66% demonstrated nuclear FABP5 protein. Those tumours that demonstrated cytosolic localisation of the protein had higher levels when compared to those with those with nuclear FABP5. This is opposite to that shown by CRABP2. Since FABP5 is known to be cytosolic, and also found bound to down-stream nuclear membrane receptors, it is not a surprising observation (Song, Hou et al. 2014). However, the use of confocal microscopy could provide more useful information in determining the sub-cellular localisation of the nuclear FABP5 (at the nuclear membrane or within the organelle).

With respect to this particular protein, patients with centrally sited tumours as well as deceased patients (poorer prognosis) appeared to have the lowest levels of FABP5. Inconsistent with this observation was the fact that it was the older patients (poor prognostic group) that showed the highest level of FABP5. Metastatic staging, response of the tumour to treatment and the time to first event were equivocal when FABP5 levels were compared. No clear correlation (for this protein) could be deduced from the tumour panel. Although this small panel of tumours have provided some information about

FABP5 in ESFT tumours, trends in protein levels could be better analysed using a larger sample.

3.4.2 Expression of intra-cellular lipid binding proteins in cell lines

Since its discovery in 1973, CRBP-I protein has been found, but not abundantly, to be widely distributed within many different cell types. One of its richest source is the liver where it represents only 0.02% of the soluble proteins (Ong 1987). It has been found in developing embryo, liver, kidney, lung, adult ovary, pancreas, pituitary gland, adrenal gland, reproductive organs, retinal pigment epithelium cells of the eye, and brain (Porter, Fraker et al. 1983, Ong and Page 1986, Levin, Li et al. 1987, Rajan, Blaner et al. 1990, Folli, Calderone et al. 2001, Silvaroli, Arne et al. 2016).

For the first time, I have demonstrated that the 6 ESFT cell lines express CRBP-I mRNA, with the lowest level being in A673. The CRBP-I protein expression has mirrored that of the mRNA, with the lowest levels seen in the A673 line. Sub-cellular fractionation of the ESFT cells demonstrated that the CRBP-I protein was localised to the cytoplasm. CRBP-I has been reported in the cytosolic component of rat lung tissue, liver, kidney, testis and intestinal mucosa (Bashor, Toft et al. 1973). Therefore my findings in the ESFT are consistent with the literature. More recent studies with confocal microscopy conclude that CRBP-I localizes to lipid droplets (Jiang and Napoli 2013) within the cytoplasm. The cytosol component without the lipid droplets appear to have very little CRBP-I protein (Farias, Ong et al. 2005).

CRBP-I protein was detected in HEPG2, SHEP-1, SK-N-SK and SH-SY-5Y cell lines. This is not surprising given that this protein is generally ubiquitous and only known to be absent from small intestine and skin fibroblasts (Shirakami, Lee et al. 2012). During my studies, I did not detect the CRBP-I protein in a variety of other cell lines including MSC, NHU, HT-29 (colorectal adenocarcinoma), HMB2, A375, (melanoma), T98G (glioblastoma), IMR-32 (neuroblastoma), RT-4, RT-112, T-24 (bladder cancer) and MCF-7 (breast cancer) cell lines. Previous studies have shown MSC to express CRBP-I (Xu, Song et al. 2012). In addition, ESFT cell lines express the CRBP-I

protein and the cell of origin for ESFTs is thought to be the MSC (Riggi, Suva et al. 2010). These results are not consistent with the published literature. Failure of detection (by western blot), may have been because the low levels of CRBP-I protein present in the cells are below the limit of detection (Section 2.4).

The reduction or loss of CRBP-I expression is a frequent but not universal change in the early progression of cancer (Farias, Ong et al. 2005, Doldo, Costanza et al. 2014). Lower CRBP-I expression in breast cancer (Jing, Zhang et al. 1996) and loss of expression in other breast cancers (Kuppumbatti, Bleiweiss et al. 2000), nasopharyngeal (Kwong, Lo et al. 2005), oesophageal, renal cancer (Morris, Dreixler et al. 1999), ovarian (Cvetkovic, Williams et al. 2003), endometrial (Orlandi, Ferlosio et al. 2004), cervical, larynx cancer, astrocytic gliomas (Esteller 2002) and leukemic cells (Lehmann, Paul et al. 2002) have been demonstrated. Failure to detect CRBP-I in the cancer cell lines, above, may have been because of epigenetic silencing, via hypermethylation of CpG island of the promoter region of this gene (Lee and Goldberg 1996, Doldo, Costanza et al. 2014).

Another interesting observation involved CRBP-I expression in 4 neuroblastoma cell lines (non ESFT cancer cell lines). The 3 neuroblastoma cell lines SK-N-SH, SHEP-1, SH-SY-5Y expressed this target protein, but the IMR-32 cell line did not. These former 3 cell lines have previously been reported to be resistant to fenretinide (Myatt, Redfern et al. 2005) while IMR-32 cell line is fenretinide sensitive (Di Vinci, Geido et al. 1994, Reynolds, Wang et al. 2000). This has now been attributable to MYCN gene status (amplified or non-amplified) of the tumours and associated cell growth suppression (Wei, Song et al. 2008).

Clearly, some cell lines continue to express CRBP-I, while others lose this ability. In the former, the oncogenic process may be driven by a pathway that is not compromised by CRBP-I action. Another theory is that CRBP-I expressing cell lines may have inactivated the retinol metabolism/RAR pathway by the epigenetic inactivation of other genes (Farias, Ong et al. 2005). In the cell lines that have lost the ability to produce CRBP-I, there is compromise of retinol metabolism and transport, resulting in the blocking the down-stream activation of RAR receptors, leading to loss of cellular

differentiation and tumour progression (Mendoza-Rodriguez, Arreola et al. 2013) .

Cellular retinol binding protein II is reported to be specifically expressed in the cells of the small intestine and appears to be adapted for dealing with higher levels of retinol found in the digestive tract (Demmer, Birkenmeier et al. 1987, Ong 1987).

For the first time, I have characterised CRBP-II in ESFTs. Using RTqPCR, I have shown that the mRNA is present in all six ESFT cell lines, albeit, at low levels. Whilst I could not detect CRBP-II in its native form in the cell lines studied, a band of 30 kDa was detected in all cell lines, except those of the small intestine lysate (positive control). This larger band may be due to non-specific binding or alternatively may be detecting a dimer of the CRBP-II protein. It is surprising that this larger band was found to be absent in the small intestine lysate sample, where the native CRBP-II protein was known to be present and functional.

The absence of this protein in the normal cells, ESFTs, and non ESFT cancers is not surprising, as these cells are not subjected to increased levels of retinol (Demmer, Birkenmeier et al. 1987, Ong 1987) and they therefore do not require specifically adapted proteins. These results suggest that in ESFTs, CRBP-II is not important for the internal transport and metabolism of retinoids and retinamides, because the protein is not expressed in its functional form. However, it would be interesting to investigate the expression of CRBP-II in ESFT cells that have been exposed to high levels of fenretinide. The ESFTs may be induced to produce CRBP-II protein which may be an adaptive response to regulate homeostasis of cells in conditions of high retinol.

During this study, I have produced a positive control cell line for CRBP-II. Caco2 cell lines (colorectal adenocarcinoma cell line) possess the ability to differentiate into cells that are morphologically similar to cells of the small intestine (Levin 1993). The Caco2 cells do not express CRBP-II protein but the differentiated cells do so at high levels (Ong 1987). The role of this protein is poorly understood and so it would be enlightening to examine the

impact of knock down and over-expression of CRBP-II protein in Caco2 cells. The response of these modulated cells to fenretinide induced death could be translated for use in the ESFT system.

I have demonstrated for the first time that cellular retinol binding protein III is absent (by western blot) from the six ESFT cell lines. Interestingly, the CRBP-III mRNA is present in the ESFTs at comparable levels to the positive control. Possible explanations for the discordance between mRNA and protein levels within cells, have been discussed in Section 2.4. CRBP-III protein is primarily expressed in kidney and heart tissue (Folli, Calderone et al. 2001) and it is not therefore surprising that it is absent in the ESFTs. This absence of the protein supports the theory that CRBP-III is also not primarily important in ESFTs.

I have shown by RTqPCR, that cellular retinol binding protein IV mRNA was detected in all of the six ESFT cell lines, with the lowest level of expression in TC-32 and TTC-466 cell lines. CRBP-IV protein was detected in 4 of the 6 ESFT cell lines, but undetectable in TC-32 and TTC-466. CRBP-IV protein expression is heterogeneous in the ESFT population and this observed variation in protein expression may lend itself to discerning the role of CRBP-IV in ESFTs. I am particularly interested in whether it has any functional role in retinol/retinamide transport or fenretinide induced cell death in the ESFTs.

The CRBP-IV protein was present in many non ESFT cancer cell lines including HT-29, HMB2, A375, T98G, RT-4, RT-112, T-24, MCF-7, IMR-32, SK-N-SH, SHEP-1 and SH-SY-5Y. CRBP-IV was detected in nearly all tissues and cell lines examined, with the highest abundance in adult kidney, followed by heart, transverse colon, foetal heart, foetal spleen, lymph node, appendix, and the ascending colon (Alvaro, Alpini et al. 2002).

3.4.3 CRABP2

This is the first time that cellular retinoic acid binding protein 2 expression has been investigated in ESFTs and I have demonstrated that CRABP2 mRNA is detected in all six ESFT cell lines. CRABP2 mRNA is known to be

expressed widely in many types of cell lines (Ruberte, Friederich et al. 1992).

CRABP2 protein was detected at extremely low levels in all 6 ESFT cell lines (Figure 3.14). There was variable expression of the protein amongst the non ESFT cancer cell lines: high levels in MCF-7 and HT-29; moderate expression in IMR-32 and RT-4; low level in RT-112, T98G, and A375 and absent from HMB2, T-24 and HEP G2. Studies have found that CRABP2 is abundantly (but transiently) expressed during embryogenesis (mouse models) but is predominantly expressed in the skin. (Giguere and Evans 1990). In addition, the protein has been found in the salivary glands, oral mucosa ,oesophagus (Yang, Wang et al. 2016), urinary bladder (Jin, Fu et al. 2013), prostate (Okuducu, Janzen et al. 2005, Napoli 2017), female reproductive tract (Stachurska, Loboda et al. 2011) and skin (Fischer-Huchzermeyer, Dombrowski et al. 2017).

It should be noted that the CRABP2 antibody optimisation was difficult. Despite published literature (Morris and Levenson 2013, Yao, Morales et al. 2014), I had to perform extensive optimisation of five different antibodies before a suitable one could be identified. CRABP2 has 4 different isomers and it is possible that the antibodies may have been raised to specific isoforms and so may not be capable of detecting all isoforms.

For the first time, I have also demonstrated that FABP5 mRNA is detected in the 6 ESFTs at a level comparable to the positive control (HEPG2). The protein is detected at high levels of expression in all cell lines. By comparison, other non-ESFT cancer cell lines had a more variable level of expression.

Studies have shown that FABP5 mRNA has been detected in nearly all tissue types with a particularly high expression in the oesophagus (Yanase, Shimizu et al. 2001). The protein has been detected in skin, liver, brain, mammary glands and, importantly, in adipocytes and macrophages (Furuhashi and Hotamisligil 2008). FABP5 is upregulated in some cancers including hepatocellular (Jeong, Choi et al. 2010),prostate (Adamson, Morgan et al. 2003, Kawaguchi, Kinameri et al. 2016), cervical (Wang, Jia et

al. 2014), colorectal (Kawaguchi, Kinameri et al. 2016), bladder (Bushue and Wan 2010) and breast cancer (Levi, Lobo et al. 2013, Powell, Nasser et al. 2015). The over-expression or up-regulation of this protein produces cell proliferation, invasion and metastases (Jing, Beesley et al. 2000) while FABP5 down-regulation suppresses cell proliferation and invasiveness (Adamson, Morgan et al. 2003, Jeong, Choi et al. 2010, Morgan, Kannan-Thulasiraman et al. 2010, Myers, von Lersner et al. 2016).

The responsiveness of cells to retinoic acid (cell death) has been linked to the ratio of CRABP2 to FABP5 (Schug, Berry et al. 2007, Schug, Berry et al. 2008). CRABP2 delivers retinoic acid (RA) to RAR, while FABP5 shuttles the ligand to PPAR β/δ receptors. The binding affinity of the CRABP2/RAR pathway for RA exceeds that of the FABP5/PPAR β/δ path. The interactions of RA with both CRABP2 / RAR are characterized by K_d in the 0.1–0.2 nM range (Dong et al., 1999; Sussman and de Lera, 2005), while both FABP5 and PPAR β/δ associate at a K_d of 10–50 nM ((Tan et al., 2002). It is therefore predicted that, in most cells, RA signalling through RAR will predominate, and that activation of PPAR β/δ will become apparent only in cells that exhibit a high FABP5/CRABP2 ratio. In the ESFTs, FABP5 is much more abundant than CRABP2, a high FABP5/CRABP2 ratio abolishes RA-triggered upregulation of RAR target genes, which mediate important biological responses, such as cell cycle arrest. This is consistent with the failure of retinoic acid to induce differentiation into ESFT cells (Myatt, Redfern et al. 2005). ESFT are poorly differentiated tumours and this may in part be related to the FABP5: CRABP2 ratio. It would be interesting to test whether the relationship between CRABP2 and FABP5 can extend to and explain findings in cells that are sensitive to other retinoic acid analogues like fenretinide.

3.4.4 Methodological considerations

The sensitivity of immunohistochemistry has improved enormously over the years because of signal amplification techniques. The amplification process has improved detection by 2-10 fold when compare to standard techniques

and are ideal for low abundance proteins (Kohler, Lauritzen et al. 2000), like the iLBP family of proteins (CRBP-I, CRBP-IV, CRABP2 and FABP5) .

I was unable to comment upon the immunohistochemistry for CRBP-I in this panel of tumours, as the two CRBP-I antibodies that I have used did not work. Initially, the Santa Cruz FL-135 (sc-30106), a rabbit polyclonal IgG, was used. This antibody has been successfully used in several studies (Shi, Zheng et al. 2012) (Lutz, Hennige et al. 2011). Following this, a CRBP-I mouse monoclonal antibody (sc-271208, Santa Cruz) antibody was tried as it had been successfully used in various tumour and tissues (Trasino, Benoit et al. 2015) (Trasino, Tang et al. 2015).

The next consideration was that the CRBP-I protein has three recognised isoforms 1, 2 and 3. The canonical CRBP-I is designated as isoform 1 and is full length while the other 2 isoforms are smaller (National Centre for Biotechnology Information) (www.ncbi.nlm.nih.gov/gene). Since the two antibodies that I have tried were raised to detect the full length CRBP-I, it is unlikely that the antibodies failed because they did not recognise the various isoforms. CRBP-I has also been characterised in mouse mammary epithelial cells (Farias, Ong et al. 2005), rat uterine cells (Zheng and Ong 1998), cervical cancer cells (Mendoza-Rodriguez, Arreola et al. 2013) and human ovarian cancer tissue (Williams, Cvetkovic et al. 2009) using immunohistochemistry, with an affinity purified anti-sera produced in rabbits against a specific peptide sequence (residues 68-83) of pure human CRBP-antibody for use in the ESFT panel as this protein continues be relevant and interesting to this research.

Since native CRBP-II and CRBP-III were not detected in ESFTs, this protein was not investigated by immunohistochemistry in the ESFT panel.

3.4.5 Future Work

I have shown that CRBP-IV may be developed as prognostic marker because it appears to be expressed at higher levels in 2 sub-groups of patients with poorer outcomes. Ideally I would extend this immunohistochemistry study to include a much larger panel of tumours. In this way, clinically relevant cut-points could be independently evaluated and

the sub-groups sufficiently powered to be able to draw conclusions. Such a study would assist in making more confident conclusions about the FABP5 protein. The work to date is inconclusive about FABP5 protein content and its relation to the clinical sub-groups. Immunohistochemistry studies of CRBP-I were unsuccessful but I have now identified an affinity purified polyclonal sera that appears promising.

I expect to take this work forward by using confocal microscopy to assist in the more accurate determination of the localisation of CRBP-I, CRBP-IV, CRABP2 and FABP5 in the ESFTs.

CRBP-I and CRBP-IV have been reported as epigenetically silenced (gene hypermethylation) in many types of cancer (Kwong, Lo et al. 2005). It is interesting to note that CRBP-IV is not expressed in the TC-32 and TTC-466 cell lines. In this case, it may be that these genes have been hypermethylated and this has prevented transcription. As a result, the determination of the methylation status of these genes may provide an explanation and this knowledge could allow modulation of protein levels and possibly conclusions to be drawn about the function of these proteins in the fenretinide pathway.

Another interesting finding was the presence of the larger 30 kDa protein band found when probing for CRBP-II. Protein sequencing would determine the protein homology and also give an answer as to whether it was indeed a dimer of the CRBP-II protein.

Finally I would like to explore the function of the CRBP-I and CRBP-IV proteins as it applies to the ESFTs and fenretinide induced cell death. Knock down and knock in experiments would be of paramount importance in determining this.

Chapter 4

Protein Interactions with retinamide and retinamide like compounds- *in silico* Modelling

4.1 Introduction

Fenretinide (4-hydroxy(phenyl)retinamide; 4-HPR) is a retinamide that was first synthesized in the late 1960s (Cazzaniga, Varricchio et al. 2012). Although it has shown significant promise in treating ESFTs (Myatt, Redfern et al. 2005), the effectiveness of this drug is significantly limited by its low aqueous solubility and poor bioavailability (Graves, Ledet et al. 2015). Indeed, no tangible progress has been made in the last fifty years to improve its bioavailability. As a result, fenretinide has not progressed from laboratory to clinical use in the treatment of Ewing's Sarcoma Family of Tumours.

Scientific discoveries have occurred through wet-bench and dry laboratories. The former is defined by those activities that use living cells or organisms, chemicals and drugs that are tested and analysed. A dry lab is one in which computational or applied mathematical analyses are done on a computer-generated model to simulate a phenomenon in the physical realm (Stather, MacEachern et al. 2012). The traditional approach of wet lab experiments has proven to be slow and expensive (Agarwal and Fishwick 2010). *In silico* modelling of the interaction of small molecules with biological targets has been established as a powerful tool in drug discovery (Ekins, Mestres et al. 2007). Computational modelling can be utilised to study virtual interactions between proteins and small molecules. The likelihood of these interactions occurring in the real system, can be scored, based on the fundamental principles of mathematics, physics and chemistry. The possible orientations (poses) in which a small molecule and its protein target can be bound are numerous. Multiple binding results are screened and those that satisfy the various constraints of the ligand, the binding pocket and solvent can be identified and then taken forward for biological evaluation.

In the present study, three software programmes were chosen for the evaluation of the interactions between small molecule and protein partners,

based on their varied approach to docking and simulation of the interactions. These were eHiTS, Autodock and Glide software.

eHiTS uses an exhaustive systematic search looking for interactions between small molecules and proteins. The small molecule is divided into rigid fragments and flexible chains. The rigid fragments are docked independently into the receptor molecule and then flexible chains refitted between the rigid fragments (Zsoldos, Reid et al. 2007).

Autodock is a genetic algorithm that performs the docking simulation and these conformations are subjected to energy minimisations that are used in further adjustments/iterations. The ligand and various parts of the target protein are treated as flexible (Seeliger and de Groot 2010). Glide follows a hierarchical protocol, which focuses the on-going search for small molecule-protein interaction. Protein–ligand configuration space is explored by use of a grid of site points and rotations of the ligands about the site point (Friesner, Banks et al. 2004).

The application of this approach to many areas of scientific research including the discovery of antibacterial agents, anti-HIV drugs and also anti-cancer agents has proved successful (Simmons, Chopra et al. 2010). It has allowed extensive and comprehensive investigation of protein and small molecule interactions without the prohibitive time and cost factor. However, this method has not been applied previously to the discovery of small molecule modulators of retinol binding proteins.

The aim of the research presented in this Chapter is to use *in silico* modelling to investigate the interactions of the retinol binding proteins, retinamides and retinamide analogues. This process would provide simulated solutions of interactions between small molecule and the protein of interest. Knowledge gained from these structures may provide a basis for making predictions about the likelihood of interactions between the proteins and small molecules and this could be used for directing further experiments.

Material and methods

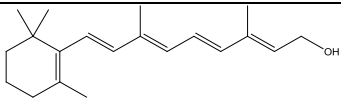
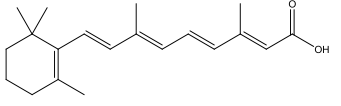
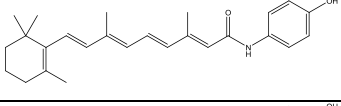
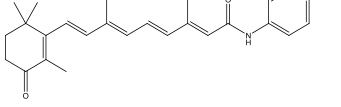
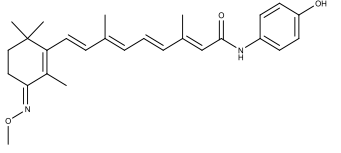
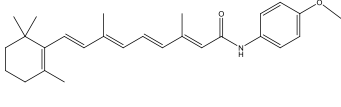
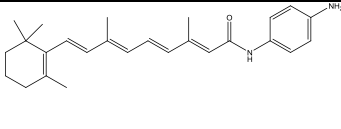
4.2.1 The Protein Structures

The Research Collaboratory for Structural Bioinformatics Protein Data Bank (PDB database, (www.rcsb.org)) was searched for crystal structures of the Retinol Binding Proteins (RBP4, CRBP-I, CRBP-IV, CRABP2, FABP5). The proteins (Table 4.3) were downloaded from the PDB database and imported into Maestro (version 9.2, Schrodinger, LLC, New York, NY, 2011). Maestro is the interface utilised within the Schrödinger software for visualising structures and providing analytical tools. It was used to virtually screen the docking results produced from the eHITS software. Water, solvent molecules and ligands were removed within the software and the protein file saved.

4.2.2 The Ligands

The structure of retinamides and retinamide-like compounds, used in the computational modelling are listed as in Table 4.1. The ligands were manually constructed and energy minimised, using the force field module in the Schrodinger Maestro programme (version 9.2, Schrodinger, LLC, New York, NY, 2011). The structure files were exported and saved as *file.sdf*.

Table 4.1 The chemical name, structure and assigned molecule number of the retinamide ligands used in modelling.

Chemical Name	Chemical Structure	Molecule Number
Retinol		4.1
Retinoic Acid		4.2
Fenretinide		4.3
4-oxo-fenretinide		4.4
RF21		4.5
N-(4-methoxyphenyl) retinamide		4.6
N-(4-aminophenyl)retinamide		4.7
Palmitic Acid		4.8

4.2.3 The computational tools

Three different molecular docking algorithms, eHiTS, Auto Dock and GLIDE were chosen in order to dock the chemical ligands (Table 4.1) within the retinol binding proteins (Table 4.3).

The various docking and scoring functions as well as the lowest energy conformations were assessed within all three software packages. Consensus scoring, a well-recognised strategy, was used to improve

predictions based on molecular docking (Oda, Tsuchida et al. 2006). The approach involved using the three independent scoring algorithms to identify binding affinities between protein and ligand. In the final analysis, more weight was given to a particular prediction if two or more of the software packages identified a particular ligand as having a strong binding affinity with the retinol binding proteins.

Protein Structural Homology using the Schrödinger Maestro software

The structural homology of the five retinol binding proteins (RBP4, CRBP-I, CRBP-IV, CRABP2, FABP5) were compared (in the Maestro programme) by superimposing the protein backbone and side chains. The proteins to be compared were imported into the workspace and were examined using the Superposition module.

4.2.4 eHiTS method

eHiTS software is a command-based programme that runs on LINUX computers. The directory was navigated and the prepared protein and ligand files (Section 4.2.1 and 4.2.2) were used in the docking algorithm. This produced the top ten solutions ranked for predicted binding ability of the individual seven chemical ligands docked (Table 4.1) into the RBP4 protein. This score was derived from an empirical scoring function. The accuracy of the docking process was set at 3 (high accuracy setting) to increase tolerance and accuracy of the pose generated. Accuracy settings range from 1 to 5. The lower the accuracy setting the more likely the algorithm is to include solutions that are not feasible. Similarly, if accuracy were set at 5, it would be likely that some solutions that were feasible would be discarded by eHiTS.

eHiTS docking within the retinol binding protein family required further refinement in the form of defining a 'clip' file (co-ordinates of the ligand within the binding pocket of the protein). This was necessary because initial

unconstrained dockings predicted binding of the small molecules with RBP4 in sites that were not consistent with the published binding site of the protein. For the proteins RBP4, CRBP-I, CRABP2 and FABP5, the crystal structure in the pdb database already possessed a co-crystallized ligand and so defining the 'clip' file was simple. In these cases, the ligand was removed from the protein structure, exported and saved as *protein_clip.pdb*. In the case of CRBP-IV (an *apo* protein) the 'clip' file was defined by manually constructing (using the Schrodinger Maestro software) a benzene ring with a short carbon chain backbone on either side and locating the 'dummy' ligand within the centre of the putative binding cavity.

The optimised command for docking in eHiTS was:

```
"eHiTS -select 10 -accuracy 3 -clean -ligand fenretinide.sdf -clip  
RBP4_clip.pdb -out fenretinide_RBP4.sdf -receptor RBP4.pdb."
```

4.2.5 Assessing the eHiTS docking

The Schrödinger Maestro software allowed visualization of the docked protein-ligand results and the predicted poses. In addition, the molecular surface module within Maestro was used in order to better visualize the three dimensional structure of the protein and ligand. This provided another method of assessing the viability of a docking conformations. Those that were clearly violating steric constraints (piercing the protein wall) were discarded (Figure 4.1). The eHiTS programme contains a scoring function based on a variety of empirical parameters. This function predicted the interactions between the small molecule and protein.

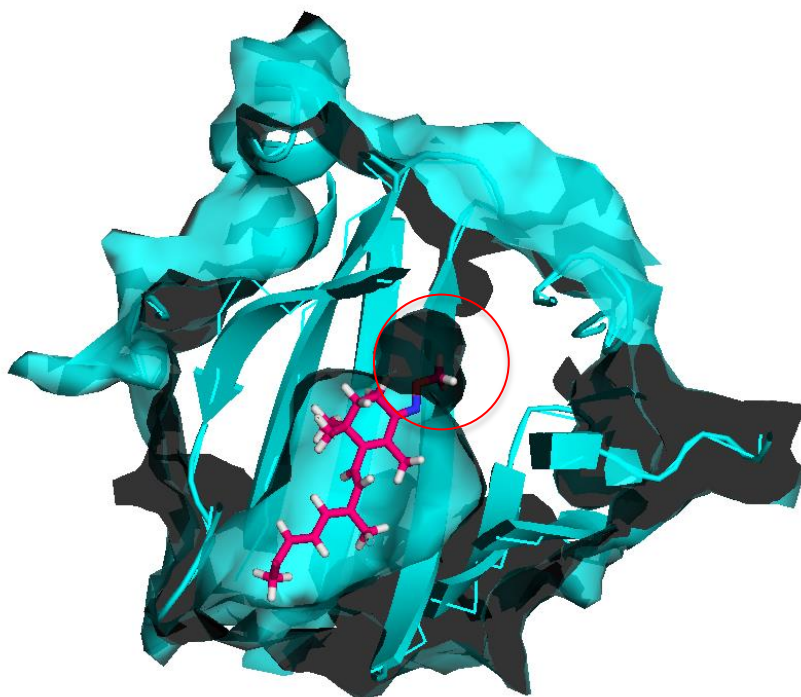


Figure 4.1 Schematic demonstrating RBP4 protein with molecular surface in blue and a retinamide compound in binding pocket with part of the side chain piercing the receptor pocket. (circled in red) This would produce significant steric hindrance and be energetically unfeasible.

4.2.5.1 Energy minimisation methods

Docked protein-ligand complexes were imported and analysed in Maestro. Of the top ten results, those that were docked in non-energetically feasible conformations (Section 4.2.5) were discarded. Of the remaining poses, the protein and appropriate ligand were highlighted, merged and the output file re-named. Using the Schrodinger Maestro interface, Macro Model was chosen and minimisation selected from the menu. The software default settings were used (force field-based methods; OPLS 2005, solution: water). For each situation, the ligand, protein and the docked complex were separately energy minimised. The thermal energies were compared using equation 1 below. The energy of the protein was denoted as $Energy_{Protein}$ and the energies of the retinamide ligands as $Energy_{Ligand}$. The energy

minimisation values of the protein-ligand complex were generated by the Maestro software and denoted $\text{Energy}_{\text{ProteinLigand}}$.

Equation 1

$$\text{Energy}_{\text{Binding}} = (\text{Energy}_{\text{Protein}} + \text{Energy}_{\text{Ligand}}) - \text{Energy}_{\text{ProteinLigand Complex}}$$

4.2.6 AUTODOCK method

Using a Linux operating system, the Autodock programme was accessed by opening a terminal and using the command “adt”. The ligands and proteins that were prepared and saved in the folders (Section 4.2.1, 4.2.2 and 4.2.4.) were imported into the AUTODOCK tool. Hydrogen atoms were added to the protein structure, checking torsion and ensuring that they were in the best energy conformation. These files were saved as output files.

The protein grid dimensions were defined as 50Å x 50Å x 50Å for the retinol binding proteins. Each point in the grid corresponds to an energy point. The docking command “run autogrid” was initiated. When this was completed, AUTODOCK was used to produce the top hundred poses. Finally the autodock tool was used to analyse the results and produce a graphical representation.

4.2.7 Glide method

Glide is a tool within the Maestro suite of programmes (version 9.2, Schrodinger, LLC, New York, NY, 2011) that allows docking of small molecules (Table 4.1) in the active site of a protein (Table 4.3). Since only seven ligands were being docked, the accuracy of scoring was set to the extra precision algorithm.

These ligands (Table 4.1) were imported into Glide after being manually constructed in Schrodinger Maestro and examined in the LigPrep module. This software produced high-quality three-dimensional structures in various ionization states and stereochemistry.

The retinol binding proteins (Table 4.3) were examined in the protein preparation module within the Glide software, in order to optimize intramolecular hydrogen bonds, ionise functional groups, produce tautomeric adjustments of amino acids and filling in missing side chains (Friesner, Banks et al. 2004).

Within the Glide docking module, the receptor grid was defined as the ProteinPrep output file and the ligand grid was the LigPrep output file. Small molecule-protein docking was performed using the default settings. The active site was defined as the centroid of selected residues in the *apo* protein. The programme gave a single best docking score for the named ligand and protein. In addition, the SiteMap programme (part of the Schrodinger Maestro suite of programmes) allowed visualisation of possible internal binding pockets within the protein. It provided a visual method of distinguishing between solutions, by the discarding those in which the binding pockets appeared to contradict published literature.

4.2.8. Appraising the scoring function

The docking scores can be equated to that of a representation of a 'virtual' K_i , which is analogous to the binding affinities of the interaction. The more negative the score, the higher the affinity between the protein and ligand. For instance, a score in the region of -9 for a particular ligand represented a 'virtual' K_i in the nM range of concentration, while those in the -6 region represented binding affinities in the μ M range and -3 in the M range. Using these values, any scores ranging from -0.01 to -2.00 were considered to represent non-binding interaction; -2.01 to -3.99 were very weak binders; -4.00 to -5.99 moderate binders and those with scores $>$ -6.00 to be strong binders, for the purposes of this modelling system. It is important to note that the absolute score values need to be interpreted with caution (Enyedy and Egan 2008).

4.2.9 Consensus docking approach

All Computational Modelling software algorithms use their own internal scoring function as a measure of predicted binding affinities. Various factors are weighted differently in the individual packages, thereby making certain algorithms better suited to docking of particular protein and their ligands. Consensus scoring is a well-recognised strategy that is used to improve predictions based on molecular docking (Oda, Tsuchida et al. 2006). The approach to this involves using multiple independent scoring algorithms to identify binding affinities between protein and ligand. This can enhance discrimination between the binding ligands. This utilised the programs eHiTS, AUTODOCK and GLIDE in order to give a consensus for design molecules. The prediction for binding of various small molecules to the protein of interest was designed around a majority agreement amongst the three software.

4.3 Results

4.3.1 The Retinol Binding Proteins

The PDB database was searched for the crystal structure of the five retinol binding proteins. Search strategies included both the *holo* and *apo* form and limited structures to those of *homo sapien* origin. Wherever there were multiple co-crystal structures, those with a retinoid or retinamide ligand were selected. Table 4.2 shows the search strategy for each protein and the outcomes.

Table 4.2 The search strategy for defining each protein form the PDB database and the outcomes

Protein symbol	Search terms	No. of hits	PDB ID of selected structure	Resolution (Å)
RBP4	Retinol binding protein, Retinol binding protein 4, Retinol binding protein IV, RBP4, RBPIV, rbp4,rbpIV	64	1RBP (<i>holo</i>) Cowan,S.W.,Newcomer, M.E., Jones, T.A. Journal: (1990) Proteins 8: 44-61 PubMed: 2217163 DOI: 10.1002/prot.340080108	2
CRBP-I	Cellular retinol binding protein1, Cellular retinol binding protein I, CRBPI,CRBP-I CRBP1,CRBP I, crbpl	18	1CRB (<i>holo</i>) Cowan, S.W., Newcomer, M.E., Jones, T.A. Journal: (1993) J.Mol.Biol. 230: 1225-1246 PubMed: 7683727 DOI: 10.1006/jmbi.1993.1238	2.7
CRBPIV	Cellular retinol binding protein 4, Cellular retinol binding protein IV, CRBPIV,CRBPIV,	1	1LPJ (<i>apo</i>) Folli, C., Calderone, V. Ramazzina, I., Zanotti, G., Berni, R. Journal: (2002) J.Biol.Chem. 277: 41970-41977 PubMed:	2

	CRBP IV, crbpIV		12177003 DOI: 10.1074/jbc.M207124200	
CRABP2	Cellular retinoic acid binding protein 2, Cellular retinoic acid binding protein II, CRABP2,CRABPII, crabp2, crabpII	10	2FR3 (<i>holo</i>) Vaezeslami, S., Mathis, E., Vasileiou, C., Borhan, B., Geiger, J.H. Journal: (2006) J.Mol.Biol. 363: 687-701 PubMed: 16979656 DOI: 10.1016/j.jmb.2006.08.059	1.48
FABP5	Fatty Acid Binding Protein 5, fatty acid binding protein5, FABP5,fabp5	32	1B56 (<i>holo</i>) Hohoff, C., Borchers, T., Rustow, B., Spener, F., van Tilbeurgh, H. Journal: (1999) Biochemistry 38: 12229-12239 PubMed: 10493790	2

4.3.1.1 Homology of Proteins

The homology of the extra-cellular RBP4 and the four Cellular Retinol Binding Proteins (CRBPs) were compared. The protein structures were obtained from the Protein Data Bank as outlined in the search above (Section 4.2.1).

RBP4 is composed of eight strands of anti-parallel β sheet with a single, short α - helical segment. The CRBPs contain ten β strands arranged into two anti-parallel β - pleated sheets and two α -helices (Newcomer, Jones et al. 1984). Comparison of RBP4 to the CRBPs revealed that the former was significantly structurally different to the latter group of proteins (Fig 4.3). The homology between RBP4 and the CRBPs is 9.34% (Zhang, Zhao et al. 2012) and superposition (Figure 4.2) reveal significant differences between the root mean square (rms) of the distances. The average rms was between 16.8- 18.1 Å (Table 4.4).

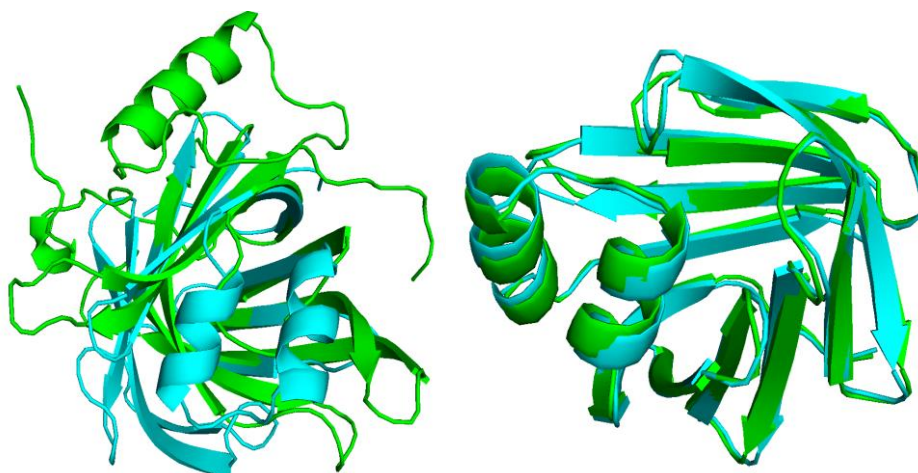


Figure 4.2 This computational modelling demonstrating the super-imposition of the retinol binding proteins. The first structure is the result of overlaying RBP4 (green) and CRBP-I while the second structure has CRBP-I (blue) and CRBP-IV (green) super-imposed on each other.

The intracellular proteins CRBPs, CRABP2 and FABP5 were more similar in structure when compared among themselves, as opposed to comparison with RBP4. The superposition function in Maestro demonstrated that the intra-cellular retinol binding proteins were very similar when their protein backbones were over-laid (Figure 4.2). The homology between the cellular retinol binding proteins is higher (49-58%)(Alvaro, Alpini et al. 2002) and visual examination of the superimposed structures do not demonstrate any major differences. Further detailed evaluation of the root mean square of the difference of the distance between the proteins showed that there were significant differences of distance between corresponding atoms in the compared protein molecules. This was attributed to variations in side chain structure (Figure 4.3). When each intra-cellular protein was compared with the other retinol binding proteins, the average distance between the protein backbones ranged from 11.21Å – 18.05 Å, while the maximal distance ranged from 26.77 Å – 39.46 Å (Table 4.4). This has implications for binding

with small molecules. Hydrogen bonds are usually of the order of 2-3 Å (the distance between the hydrogen within the donor and the acceptor atom) (Sweetman, Jarvis et al. 2014). If the root mean square value was 0 Å, this would be interpreted as the proteins being identical and hydrogen bonding ability with small molecules equivalent. However, if the distances were greater than 3 Å (as is the case in all the protein pair comparisons), it is likely that these differences would interfere with the ability to form hydrogen bonds.

Table 4.3 Comparison of structural differences between Retinol Binding Proteins when super-imposed on each other. The results were reported as the rms of the difference in distance between the corresponding atoms (Å= Angstrom).

Compared Protein Structures	Average Root Mean Square distance of the backbones (Å)	Maximal distance difference (Å)
RBP4 : CRBP-I	18.01	39.46
RBP4 : CRBPIV	17.78	38.75
RBP4 : CRABP2	18.05	39.46
RBP4 : FABP5	16.89	33.81
CRBP-I: CRBPIV	17.12	37.55
CRBP-I:CRABP2	11.21	26.77
CRBP-I : FABP5	16.15	34.87
CRBPIV:CRABP2	17.22	32.73
CRBPIV:FABP5	16.83	38.22
CRABP2: FABP5	15.89	35.78

4.3.1.2 Energy Minimisation of Proteins

An energy minimisation process was performed (using the MMF force field within the Maestro software) to determine the most energetically favourable conformation of the *apo* protein structures (Table 4.4). The calculated thermal energy of all structures were seen to decrease upon energy minimisation.

Table 4.4 Energy minimisation values of the proteins

Protein Structures	Energy before Minimisation (KJ/mol)	Energy after Minimisation (KJ/mol)
RBP4	-36 406.84	-41 680.78
CRBP-I	-30 692.00	-34 724.64
CRBP-II	-32 209.06	-36 634.70
CRBP-III	-20 813.53	-31 886.11
CRBP-IV	-24 113.48	-32 454.50
CRABP2	-26 153.96	-31 104.83
FABP5	-26 127.99	-32 003.55

4.3.2 Chemical Ligands and Energy Minimisation

Seven ligands were evaluated in terms of their ability to bind to the RBPs using the docking approach. These included: retinol (4.1), retinoic acid (4.2), fenretinide (4.3), 4-oxo-fenretinide (4.4), RF1-21 (4.5), N-(4-methoxyphenyl)-retinamide (4.6) and N-(4-aminophenyl)-retinamide (4.7) (Figure 4.1). Retinol and retinoic acid have been docked previously into the RBPs and they were used as a positive control for the various software docking solutions (Malpeli, Folli et al. 1996, van Aalten, de Groot et al. 1996, Kane, Bright et al. 2011). The energy minimisation values for these ligands are provided in Table 4.5.

Table 4.5 The Energy Minimisation Values of the seven chemical ligands, (both manually constructed and obtained from co-crystallized structures in the PDB database) used in computational modelling.

Chemical Ligands	Energy after minimisation (KJ/mol)
Retinol	+ 108.32
Retinoic acid	+ 24.69
Fenretinide	+ 28.49
4-oxo-fenretinide	- 4.58
RF1-21	+ 68.23
N(4-methoxyphenyl)-retinamide	+ 71.71
N(4-aminophenyl)-retinamide	+ 33.73

4.3.3 Docking Solutions of Retinol Binding Protein 4 and retinamide ligands

4.3.3.1 RBP4 and retinol

The PDB database provided a crystal structure for retinol docked in the RBP4 protein receptor (PDB id: 1RBP). As an internal experimental positive control, RBP4 protein and the retinol ligand (PDB id: 1RBP) were separated from the docked complex, energy minimised and scored by the eHiTS programme. Apo 1RBP was used to dock retinol (4.1). According to the eHiTS scoring function, retinol was predicted to bind to RBP4. This correlated well when it was compared with the positive control.

Thermal energies of binding for the top ten docking poses (generated by eHiTS) were calculated using equation 1 (Section 4.2.3.2.2). The protein-ligand complex would be energetically feasible if the energy of the docked complex was less than the combined energies of the minimised ligand and the protein. The more positive the energy of binding, the more likely it is that binding may occur. 1RBP produced positive binding energies for all ten retinol solutions ranging from +5.79 to +148.58 KJ/mol.

When retinol was docked using the Autodock software, it produced five energetically feasible groups of solutions. The predominant group contained 66 poses which were all visually very similar. Most solutions were in the same binding orientation within the pocket, as was in the eHiTS docked poses. The binding scores ranged from -9.8 to -8.25 kcal/mol (Figure 4.3). When a pose from each of the three most feasible energy groups was superimposed on each other, (See insert in Figure 4.3) there were no significant difference in orientation within the pocket.

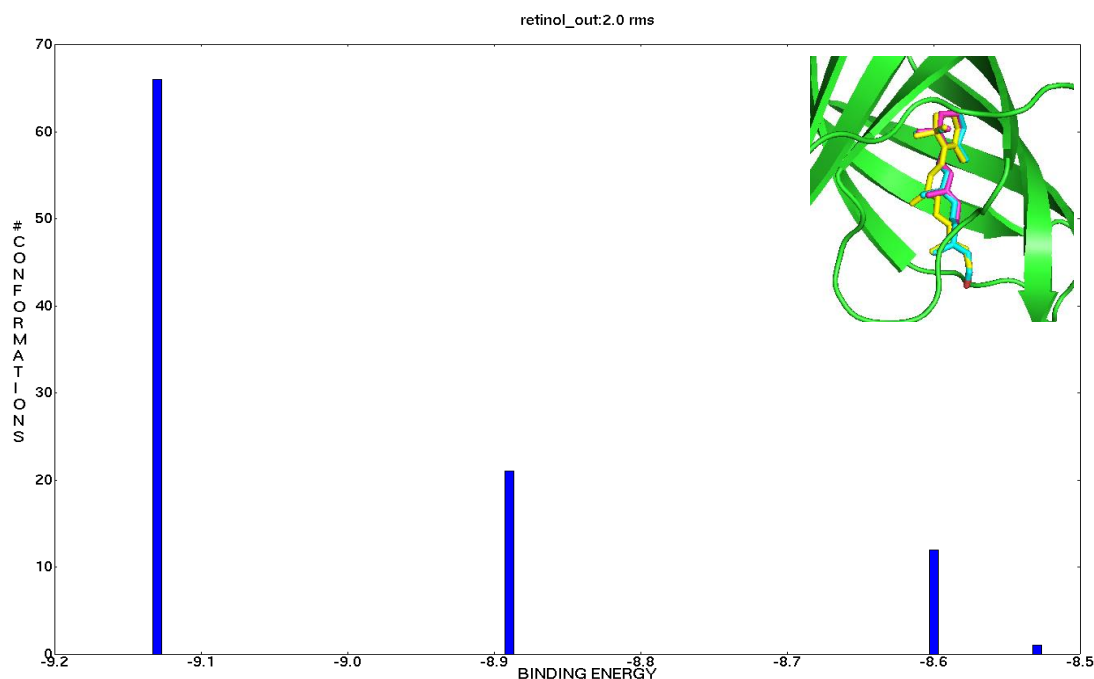


Figure 4.3. An Autodock graph showing the top hundred docking conformations of N-(4-methoxyphenyl)-retinamide in RBP4 protein and their respective predictive energies of binding.(kcal/mol) Of the top hundred poses, there were four populated binding groups The predominant group contained a possible sixty six solutions and had the maximal feasible binding energy(-9.8 kcal/mol). The next most energetically feasible group (binding energy: -8.9 kcal/mol) held twenty solutions. There were thirteen docked poses with a binding energy of -8.6 kcal/mol and one solution with energy of -8.52 kcal/mol. The insert in the top right hand corner shows a three poses of the retinol ligand within the protein-binding pocket. A single pose was taken from each of the three most energetically feasible binding groups and superimposed for comparison.

The GLIDE software produced possible binding solutions for RBP4 and retinol (GLIDE score -10.264).

In the three docking algorithms, there were no predicted H-bonding between retinol and RBP4. However, it is likely that there were hydrophobic interactions between retinol and this protein because of hydrophobic groups within the pocket and side chains. In addition, the complementary shape of the binding pocket and ligand also promoted interactions. Figure 4.4 shows possible hydrophobic interactions between retinol and phenylalanine, (residues 36, 61,135) and leucine (residue 35) in the receptor site. When the top docking poses of RBP4 and retinol in the eHiTS, Autodock and Glide software were compared they demonstrated that retinol was in the same

orientation and in almost identical poses (Figure 4.5). Thus, in this situation the prediction would be that RBP4 does bind to retinol.

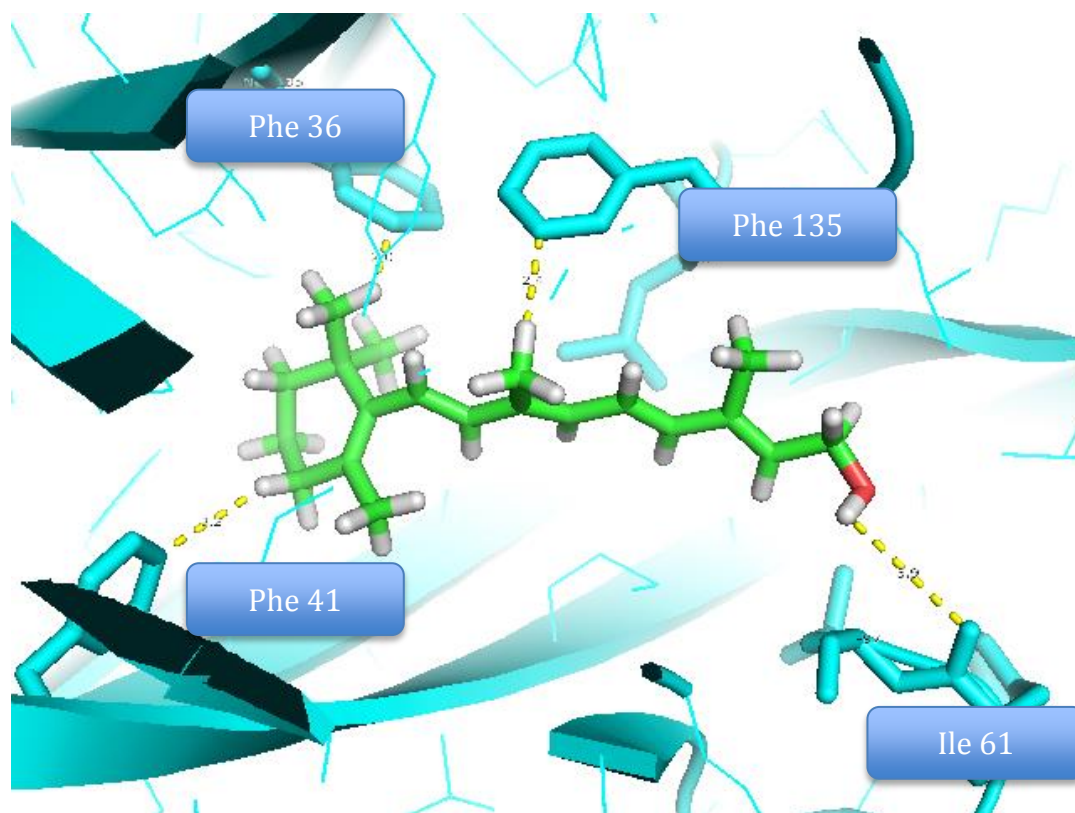


Figure 4.4. A computational modelling representation of retinol inside the binding pocket of the RBP4 protein. Potential hydrophobic interactions between retinol and amino acid side chains are represented in dashed yellow lines.

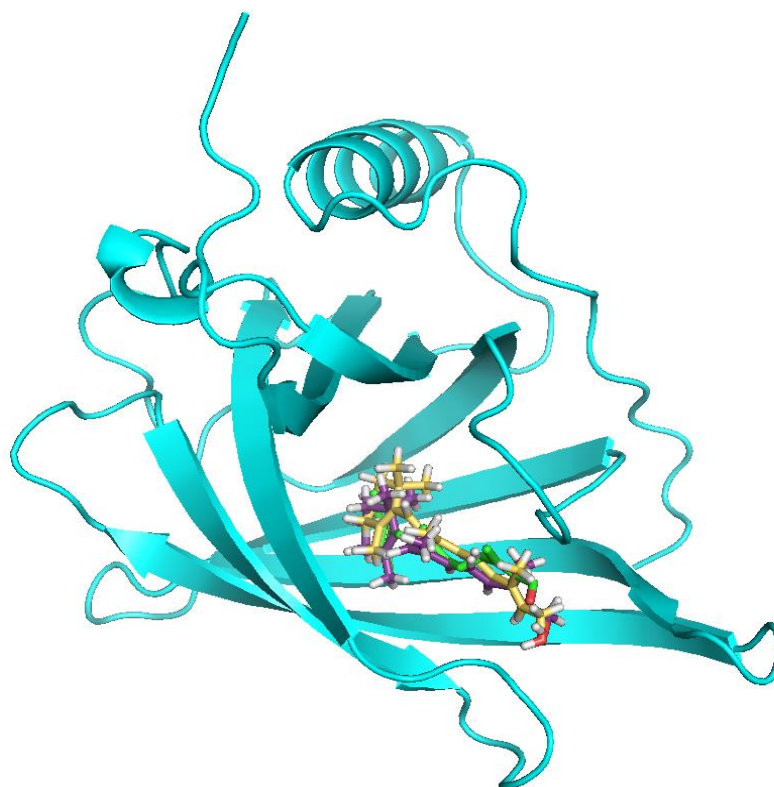


Figure 4.5. This computational modelling schematic shows the top docked poses for retinol in RBP4 according to the eHiTs (yellow), Autodock (green) and Glide (purple). The docking poses have been overlaid on each other.

4.3.3.2 RBP4 and fenretinide

When eHiTS was used to dock Apo 1RBP and fenretinide, the top ten poses included six with the benzene ring towards the outside of the protein and four having the benzene ring deep within the pocket. There were a series of eHiTS scores ranging from weak to strong binding affinities. The pose showing the strongest binding affinity had the benzene ring deep within the binding pocket.

Thermal energies of binding with fenretinide only produced one energetically feasible conformation of +82.42 KJ/mol. This was for one of the poses that exhibited weak binding affinity (eHiTS score) and had the benzene end of the fenretinide molecule facing the outside of the protein. The Autodock software showed that there were no energetically feasible binding outcomes

for RBP4 and fenretinide (Appendix 1). The Glide software did not produce any solutions for docking fenretinide in RBP4. On using a consensus docking approach, (see Section 4.2.3.6.) the prediction would then be that RBP4 does not bind to fenretinide.

4.3.3.3 RBP4 and 4-oxo-fenretinide

The eHiTS software produced ten solutions, nine of which were in the strong binding affinities range. Five of the ten solutions had the 4-oxo-fenretinide orientated with the benzene ring portion towards the opening of the binding pocket, while the remaining five contained the ligand with the benzene portion deep within the binding pocket. The thermal energies of binding (see section 4.2.3.2.2) with RBP4 and 4-oxo-fenretinide produced four energetically feasible conformations ranging from +3.3 to +105.6 KJ/mol.

The AUTODOCK software determined that there were no energetically feasible binding outcomes for RBP4 and 4-oxo-fenretinide. (See Appendix 4C) The Glide software did not produce any solutions for the docking of 4-oxo-fenretinide in RBP4. Using consensus docking, the prediction would be that RBP4 does not bind to 4-oxo-fenretinide.

4.3.3.4 RBP4 and RF21

The eHiTS software produced the top ten docking results for RBP4 and RF21 and predicted them to be all weak binders. Half of the solutions demonstrated that the benzene ring portion of RF21 was deep within the binding pocket while in the other five solutions, RF21 was docked in an orientation that was 180° compared the first five solutions. In this case, thermal energies of binding produced five energetically feasible poses which ranged from +0.67 to +484KJ/mol. The Autodock software determined that there were no energetically feasible binding outcomes for RBP4 and RF21 (Appendix 1). The Glide software did not produce any solutions for the

docking of RF21 in RBP4. The overall prediction is that RBP4 does not bind to RF21.

4.3.3.5 RBP4 and N-(4-methoxyphenyl)-retinamide

When the eHiTS software was used to dock N-(4-methoxyphenyl)-retinamide and 1RBP, the top ten solutions demonstrated strong binding affinities (eHiTS score – 9.4). Six of these poses had the methoxyphenyl portion of the ligand deep within the binding pocket while the other four solutions had the methoxyphenyl portion of the ligand near to the entrance of the binding pocket. Thermal energies of binding calculations did not produce any energetically feasible solutions. Both Autodock (Appendix 1) and Glide did not produce any energetically feasible docking solutions for RBP4 and N-(4-methoxyphenyl)-retinamide. On balance, RBP4 is predicted not to bind N-(4-methoxyphenyl)-retinamide.

4.3.3.6 RBP4 and N-(4-aminophenyl)-retinamide

Using the eHiTS software, N-(4-aminophenyl)-retinamide were docked into the structure of RBP4. The top ten poses contained five in which the aminophenyl part of the ligand was docked deep within the binding pocket while the remaining poses showed the aminophenyl portion of the ligand close to the entrance of the pocket. This ligand appeared to have a high affinity for RBP4 with an eHiTS score of -10.21. However, the thermal energies of binding calculations did not produce any energetically feasible docking solutions for RBP4 and N-(4-aminoyphenyl)-retinamide. In addition, Autodock (Appendix 1) and the Glide software predicted non-binding. As a result, RBP4 would not be predicted to bind to N-(4-aminoyphenyl)-retinamide.

4.3.4 Docking Solutions of Cellular Retinol Binding Protein 1 and retinamide ligands

4.3.4.1 CRBP-I and retinol

CRBP-I crystal structure (PDB id: 1CRB) was imported from the PDB database and the protein structure separated from the retinol ligand. These two separate components of the docked complex were energy minimised and scored using the eHiTS software (eHiTS score: -8.71). When the latter software was used to dock retinol in CRBP-I (1CRB), it produced the top ten poses with predicted strong binding affinity (eHiTS score: -7.65). 1CRB produced positive thermal binding energies for all ten docking solutions with retinol, ranging from +121.92KJ/mol to +140.27KJ/mol. The top four eHiTS poses contained the alcohol portion of the retinol ligand buried deep within the pocket, while the remaining six solutions had the retinol ligand docked with the benzene ring portion of the molecule buried deep within the binding pocket.

When retinol was docked in CRBP-I using the Autodock software, eight groups of solutions with different feasible energies of binding were produced. They ranged from -7.58 to -8.2 kcal/mol. The group with the lowest energy conformation (-8.2 kcal/mol) contained thirty one poses (Figure 4.6). Most solutions were in same binding orientation within the pocket as in the eHiTS docked poses. The binding scores ranged from -7.59 to -8.2 kcal/mol.

The GLIDE software produced feasible binding solutions for CRBP-I and retinol (GLIDE score -7.88). According to the three docking algorithms, there were no predicted hydrogen binding between retinol and CRBP-I. Figure 4.7 shows possible hydrophobic interactions between retinol, phenylalanine (Phe16, Phe57) and leucine residues (Leu26, Leu29, Leu117) in the receptor site.

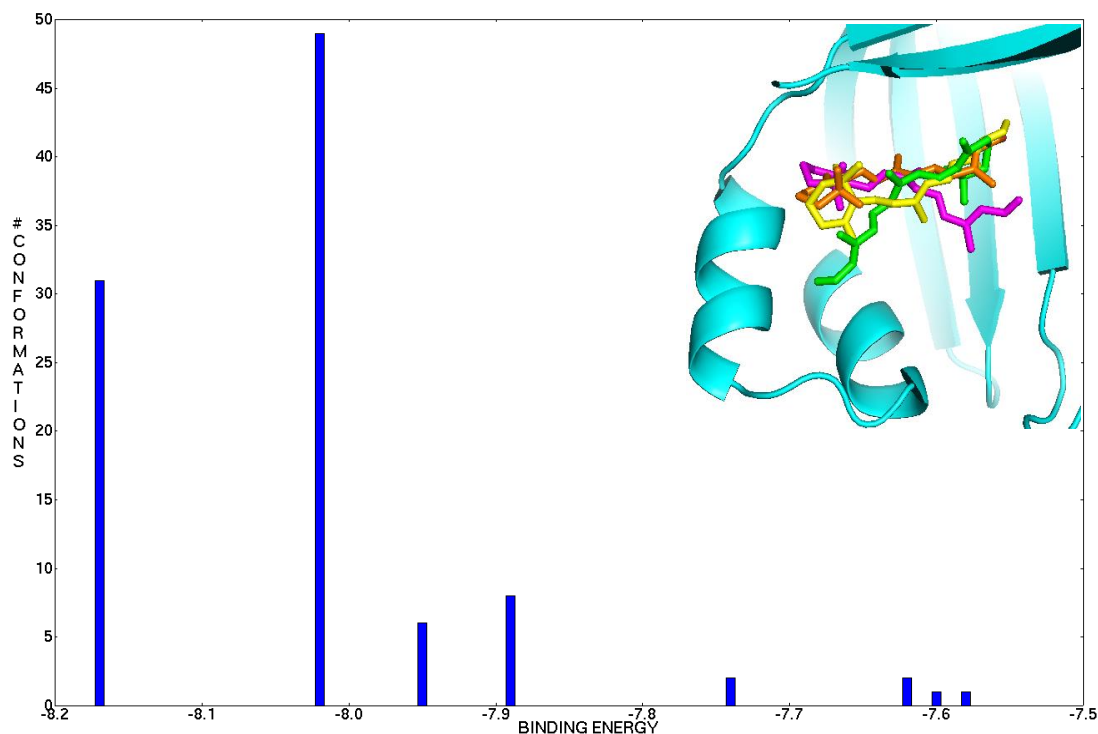


Figure 4.6. An Autodock graph showing the top hundred docking conformations of retinol in CRBPI protein and their respective predictive energies of binding. (Kcal/mol) The docking algorithm produced eight differently populated energy conformations. The lowest energy conformation was reported as -8.2 kcal/mol with thirty-one possible poses. The next lowest energy group were at -8.0 kcal/mol with forty-nine solutions. The remaining twenty solutions were scattered over six different conformations, with energy values ranging from -7.95 to -7.6 kcal/mol. There were five solutions with energy values of -7.95 kcal/mol; eight poses with energies at -7.9 kcal/mol; two solutions at -7.75 kcal/mol; three poses at -7.62 kcal/mol and one solution each at -7.6 kcal/mol and -7.59 kcal/mol. The insert at the top right hand corner contains tree top poses for retinol compared to the crystal structure in orange. Of the top three docked poses in autodock, two agree closely with the crystal structure.

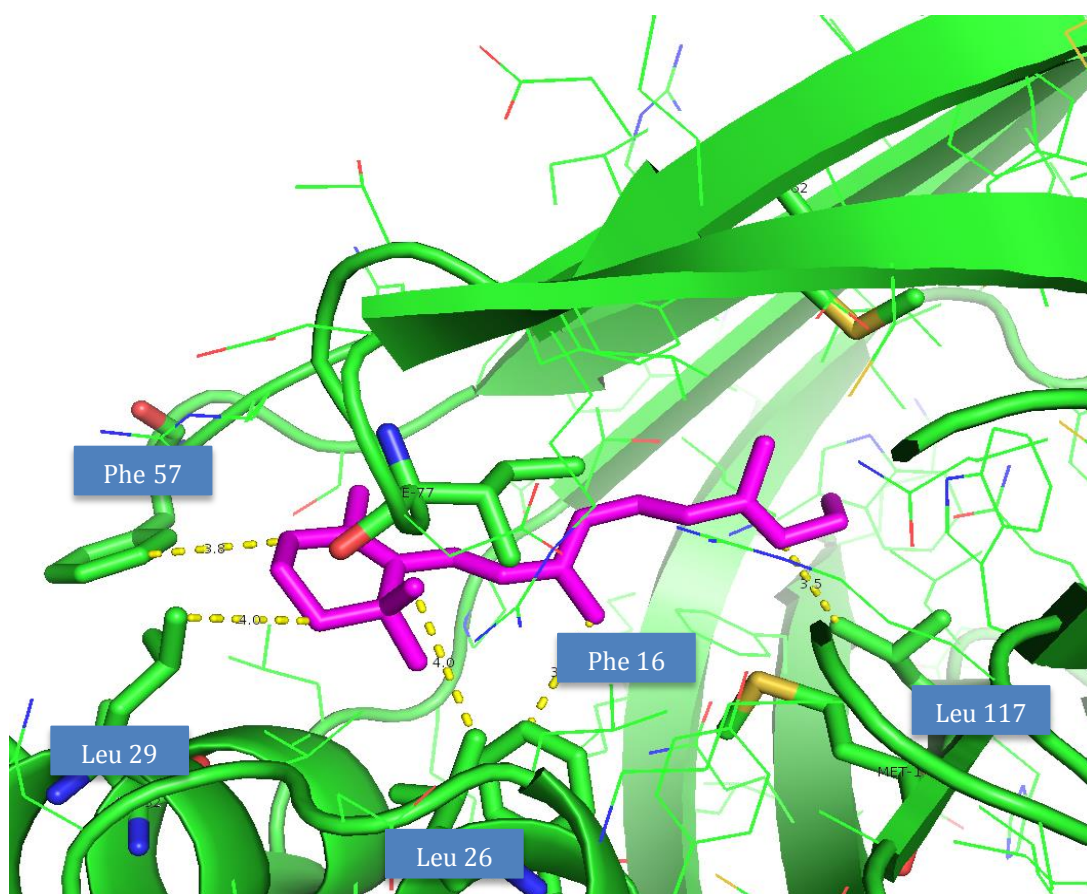


Figure 4.7 A computational modelling representation of retinol docked inside the binding pocket of the CRBPI protein. Potential hydrophobic interactions between retinol and amino acid side chains of CRBPI are represented as dashed yellow lines. Different parts of the retinol moiety may interact with Phenylalanine 16 and 57, as well as Leucine residues 26,29 and 117.

When the top docking poses of CRBP-I and retinol in the eHiTS, Autodock and Glide software were compared, they demonstrated that retinol was in the same orientation and in almost identical poses (Figure 4.8). The prediction therefore is that CRBP-I would bind to retinol.

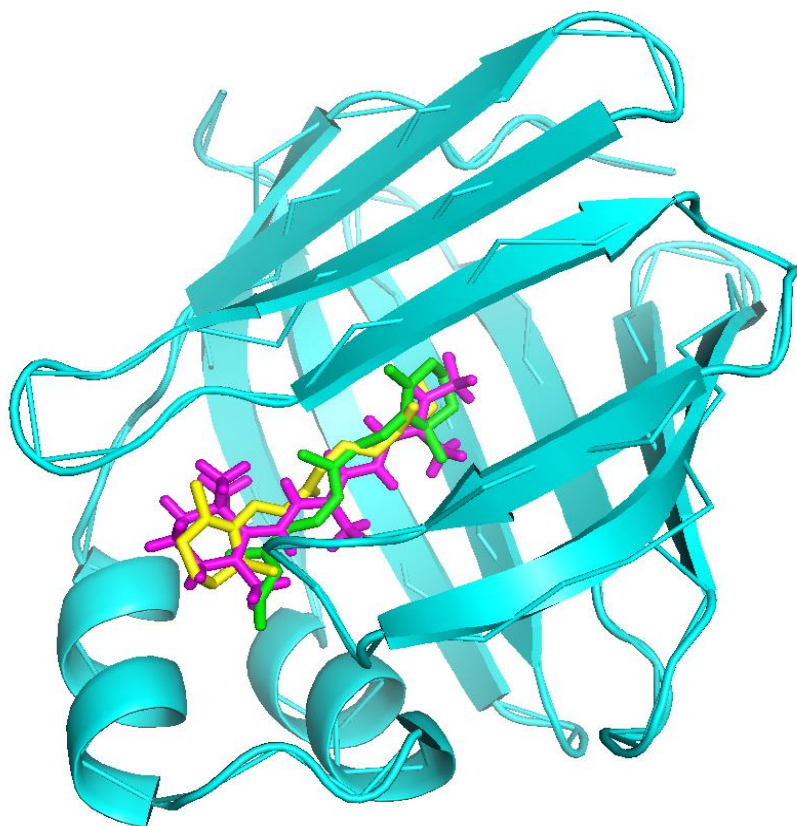


Figure 4.8 A computational modelling schematic showing the top docked poses for retinol in CRBPI according to the eHiTs (yellow), Autodock (green) and Glide (purple). The docking poses have been overlaid on each other. The Autodock pose for the top scoring docking shows retinol docked in an orientation within the binding pocket that is a 180° rotation to the top poses for eHiTS and Glide.

4.3.4.2 CRBP-I and fenretinide

When eHiTS was used to dock Apo 1CRB and fenretinide, the top ten poses included five poses with the benzene ring towards the outside of the protein

and the remaining five poses having the benzene ring deep within the pocket. The top eHiTS score for the predicted binding between CRBP-I and fenretinide was -2.65. For the purposes of this thesis, it was not considered a strong enough affinity for promoting binding (see Section 4.2.3.5). The thermal energy of binding calculation demonstrated that there were no energetically feasible conformations for CRBP-I and fenretinide. The Autodock software did not demonstrate binding between the ligand and protein as the most densely populated binding group was at a binding energy of -1.5kcal/mol. The groups with more feasible binding energies (weak to moderate binding) contained only fifteen of the top one hundred poses (Appendix 2). For the purposes of interpretation, Autodock was considered to predict no binding between CRBP-I and fenretinide. The Glide software did not produce any energetically feasible solutions for docking fenretinide in CRBP-I (Glide score= -1.44). Using consensus docking, CRBP-I was not predicted to bind to fenretinide.

4.3.4.3 CRBP-I and 4-oxo-fenretinide

The eHiTS software produced the top ten docking results for CRBP-I and 4-oxo-fenretinide showing that the small molecule would not be predicted to bind to the protein with a top eHiTS score of -1.58. However, the thermal energies of binding demonstrated that there were two energetically feasible solutions with binding energies of +39.43 KJ/mol and +41.81KJ/mol respectively. There were no predicted energetically feasible binding solutions for CRBP-I and 4-oxo-fenretinide when Autodock software was used (Appendix 2). The Glide software did not produce any energetically feasible solutions for docking 4-oxo-fenretinide in CRBP-I (Glide score= -0.718). Although, the eHiTS result was inconclusive, the overall prediction would be one of non-binding.

4.3.4.4 CRBP-I and RF21

When the eHiTS software was used to dock CRBP-I and RF21, the top eHiTS score produced was -0.98. This affinity of binding was not strong enough to produce binding between the small molecule and the protein. However when thermal energies of binding calculations for CRBP-I and RF21 were employed, (equation 1 in section 4.2.3.6) there were five thermally viable binding conformations ranging from +5.79- +83.37 KJ/mol. The Autodock software did not produce any energetically feasible docking solutions for CRBP-I and RF21 (Appendix 2). The Glide software did not produce any solutions for docking 4-oxo-fenretinide and CRBP-I. According to the principle of consensus docking, there would be no binding between CRBP-I and RF21.

4.3.4.5 CRBP-I and N-(4-methoxyphenyl)-retinamide

When the eHiTS software was used to simulate docking of N-(4-methoxyphenyl)-retinamide and CRBP-I, the top ten poses demonstrated that there would be weak binding, with the best eHiTS score being -3.65. The thermal energies of binding calculations did not produce any energetically viable solutions. The Autodock tool suggested that there were possibly fourteen different groups of binding solutions. Of the top one hundred poses, only thirty six were predicted to bind. Twenty seven of these were weak binders with binding energies of -3.0 and -4.0 kcal/mol. The remaining nine were moderate binders with binding energies of 5.0kcal/mol (Appendix 2). However, since the majority of the docking solutions (sixty four poses) were non binders and only nine poses were predicted to be moderate binders, the overall result was that Autodock did not predict that N- (4-methoxyphenyl)-retinamide would bind to CRBP-I. The Glide software did not produce any solutions for docking of N-(4-methoxyphenyl)-retinamide

and CRBP-I. The prediction was that CRBP-I would not bind to N-(4-methoxyphenyl)-retinamide.

4.3.4.6 CRBP-I and N-(4-aminophenyl)-retinamide

CRBP-I and N-(4-aminophenyl)-retinamide were docked using the eHiTS software. The eHiTS software produced the top ten docking results showing that the small molecule would bind strongly to the protein with a top eHiTS score of -8.18. Five of the solutions demonstrated that the benzene ring portion of the ligand was deep within the binding pocket while in the other five solutions, the retinamide was docked in an orientation that was rotated at 180° to that of first five solutions. However, there were no energetically feasible thermal energies of binding for CRBP-I and this substrate. Of the top hundred solutions produced in the Autodock software, ten poses were in the weak binding range (see section 4.2.3.5) with Autodock scores between -3.2 to -4.9kcal/mol. Only two poses were in the moderate binding range with an Autodock score of -5.2 kcal/mol. As a result, since eighty eight of the top one hundred poses did not demonstrate binding, Autodock was adjudged to predict no binding between CRBP-I and N-(4-aminophenyl)-retinamide (Appendix 2) The Glide software did not produce any solutions for docking N-(4-aminophenyl)-retinamide and CRBP-I. Using consensus docking, the prediction is that CRBP-I and N-(4-aminophenyl)-retinamide would not bind.

4.3.5 Docking Solutions of Cellular Retinol Binding Protein 4 and retinamide ligands

4.3.5.1 CRBP-IV and retinol

CRBP-IV crystal structure (PDB id: 1LPJ) was imported from the PDB database. There was only one structure for this protein, and it was crystallized in the *apo* form. An internal experimental positive control could not be performed as there was no co-crystallized structure. The binding

pocket was estimated, by producing a 'clip' file (Section 4.2.3.2). When eHiTS was used to dock retinol in CRBP-IV (1LPJ), it produced the top ten poses which predicted a strong binding affinity (eHiTS score: -8.15). In this group of solutions, there was discordance about the orientation of retinol within the binding pocket. Six solutions predicted that the alcohol moiety of retinol would be buried deep within the pocket, while the remaining four suggested that the benzene ring portion of the ligand would be located deep within the binding pocket. 1LPJ produced positive thermal binding energies for all ten docking solutions with retinol, ranging from +18.2 to +84.73 KJ/mol. The Autodock software produced the top one hundred docking solutions with all demonstrating strong binding affinity. There were nine groups of solutions of various energy conformations ranging from -7.04 kcal/mol to -7.64 kcal/mol. The group with the lowest energy conformation (-7.64 kcal/mol) contained the largest number of poses (forty eight) (Figure 4.9).

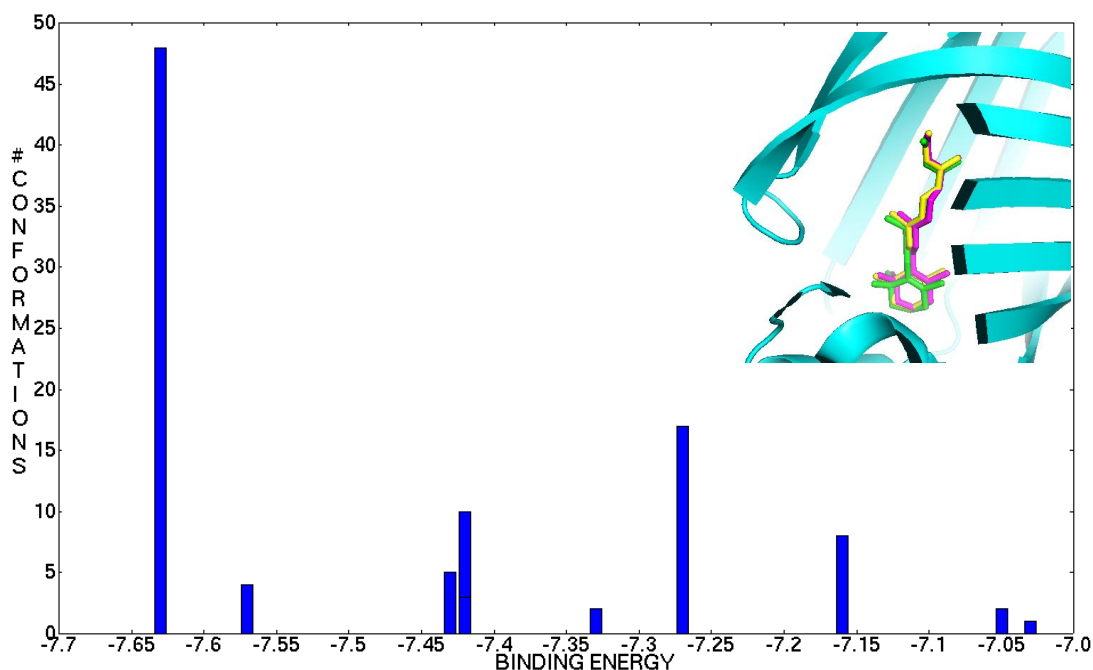


Fig 4.9 Autodock graph showing top hundred docking conformations of retinol in CRBPIV protein and their respective predictive energies of binding. (Kcal/mol) There were nine differently populated energy conformations. The predominant group with the lowest energy conformation was reported as -7.64 kcal/mol with forty-eight possible poses. There were two groups of approximately equal binding energies at -7.42 kcal/mol and -7.43 kcal/mol with ten and five solutions, respectively. At a binding energy of -7.34 kcal/mol, there were two possible solutions; seventeen poses with binding energies at -7.28 kcal/mol; eight results with binding energy at -7.15 kcal/mol; two results at -7.05 kcal/mol and one pose at -7.04. The insert at the top right hand corner shows the top three poses for retinol in CRBPIV (as per Autodock) superimposed for comparison.

The GLIDE software produced solutions for CRBP-IV and retinol that were strong binders (GLIDE score -7.30). The overall prediction here would therefore be one of high affinity of binding.

According to the three docking algorithms, there were no predicted hydrogen binding between retinol and CRBP-IV. Figure 4.10 shows possible hydrophobic interactions and pi-stacking in the receptor site, between retinol and tyrosines (Tyr 33, Tyr 86 and Tyr109), prolines (Pro 26 and Pro 29) and arginine residues (Arg 117).

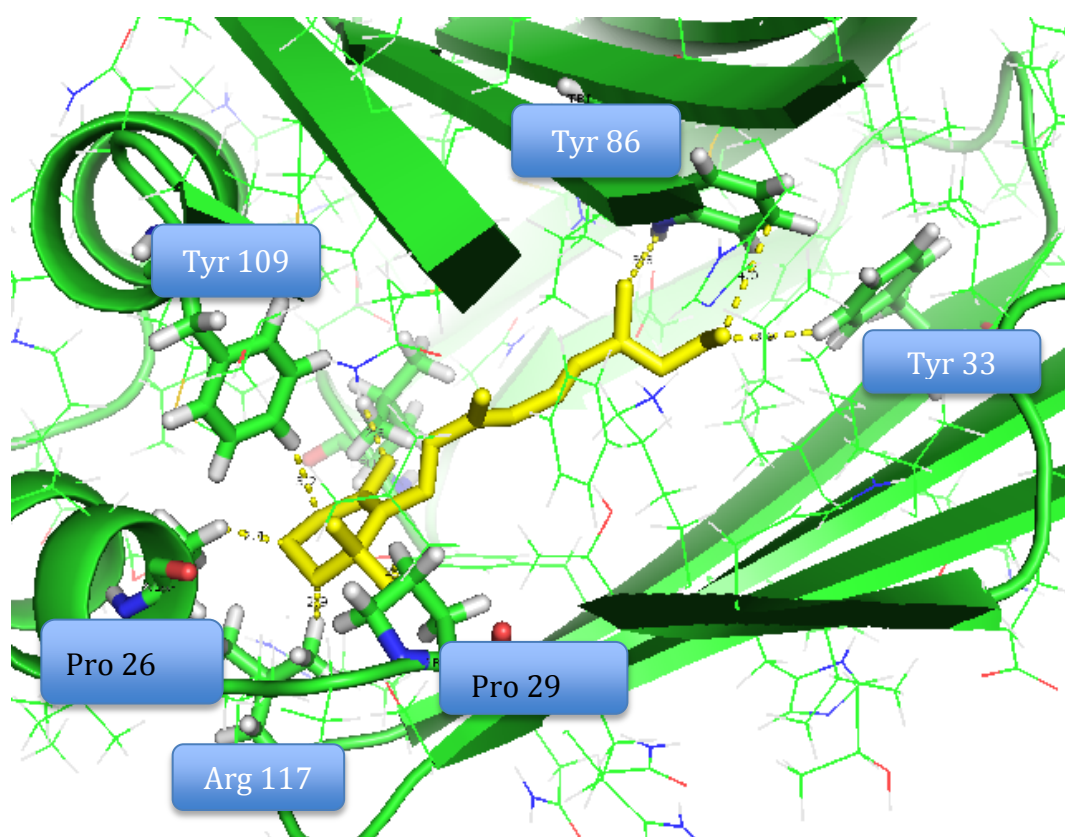


Figure 4.10 A computational modelling representation of retinol docked inside the binding pocket of the CRBP-IV protein. Potential hydrophobic interactions between retinol and amino acid side chains of CRBP-IV are represented as dashed yellow lines. There may be hydrophobic interactions and pi-stacking occurring between the retinol moiety and Tyrosine (33,86,109) , Arginine(117) and Proline (residues 26,29) .

When the top docking poses of CRBP-IV and retinol in the eHiTS, Autodock and Glide software were compared, they demonstrated that retinol existed in the same orientation, being in almost identical poses inside the binding pocket (Figure 4.11). The prediction is that binding would occur between CRBP-IV and retinol

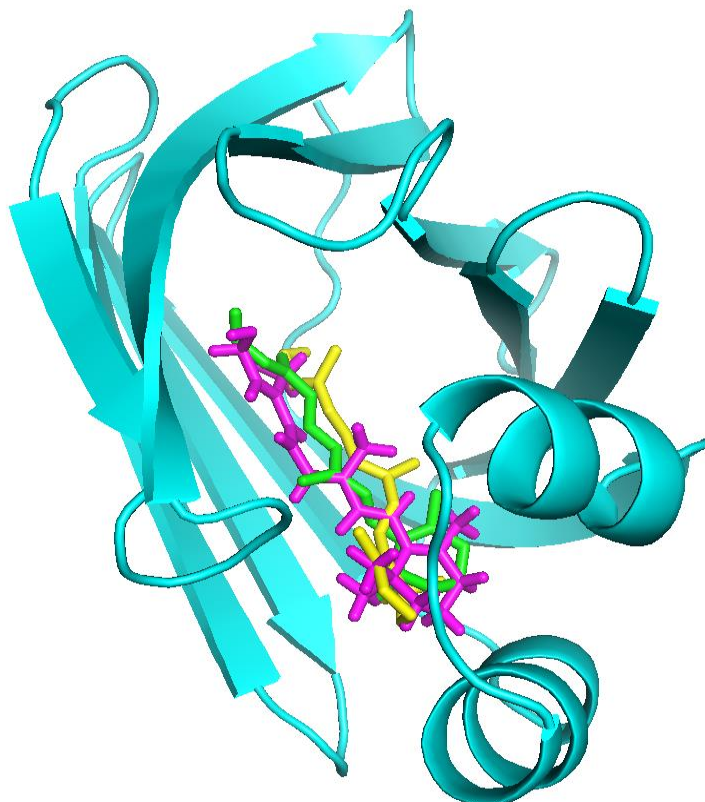


Figure 4.11 A computational modelling schematic showing the top docked poses for retinol in CRBP-IV according to the eHiTs (yellow), Autodock (green) and Glide (purple). The docking poses have been overlaid on each other. The three poses show that retinol is predicted to bind in the same area of the binding pocket and in the same orientation.

4.3.5.2 CRBP-IV and fenretinide

According to the eHiTS software, CRBP-IV is not predicted to bind to fenretinide. The top ten poses for the docking of this protein and small molecule produced a best eHiTS score of -2.30 (non-binder). However, thermal energies of binding produced one viable conformation of +32.47KJ/mol. When the Autodock software was used (as a docking algorithm), there were twelve possible energy conformational groups. None of these produced any energetically feasible poses (Appendix 3). The GLIDE software produced a feasible binding solution for CRBP-IV and fenretinide (GLIDE score -5.05), suggesting that it may exhibit moderate binding affinity.

Using consensus docking, CRBP-IV would not be predicted to bind to fenretinide.

4.3.5.3 CRBP-IV and 4-oxo-fenretinide

The top ten best poses produced by the eHiTS software for CRBP-IV and 4-oxo-fenretinide demonstrated that the small molecule was unlikely to bind to CRBP-IV (as the best eHiTS score was -1.43). The thermal binding energies calculation, however, produced feasible energies for the protein–ligand complex (between +2.53 and +35.26KJ/mol). The Autodock software did not produce any docking results that were energetically feasible (Appendix 3). Interestingly, Glide produced a docking result for this protein-ligand complex which suggested that they could bind moderately well (Glide score -5.62). As a result, the prediction would be one of non-binding between the protein and ligand.

4.3.5.4 CRBP-IV and RF21

When the eHiTS software was used to dock CRBP-IV and RF21, the top eHiTS score produced was -0.99. This level of binding affinity was not considered strong enough to produce binding between the small molecule and the protein. However, when thermal energies of binding calculations for CRBP-IV and RF21 were carried out using equation 1 (Section 4.2.4.1), there were two energetically viable binding conformations. The Autodock software did not produce any energetically feasible docking solutions for CRBP-IV and RF21 (Appendix 3). It was noteworthy, however, that the Glide software did produce docking solutions for RF21 and CRBP-IV, suggesting that they would bind moderately well (Glide score -5.98). In this case, the prediction is that CRBP-IV would not bind to RF21.

4.3.5.5 CRBP-IV and N-(4-methoxyphenyl)-retinamide

CRBP-IV and N-(4-methoxyphenyl)-retinamide were docked using the eHiTS software. The top ten docking poses were produced with an eHiTS score of 2.3. This suggests that all the solutions would be weak binders. (See Section 4.2.3.5) When thermal binding energies were calculated using equation 1 in section 4.2.3.2.2, there were no energetically feasible conformations for CRBP-IV and N-(4-methoxyphenyl)-retinamide (**4.6**). In addition, the Autodock software did not produce any energetically feasible docking solutions for this protein and the small molecule complex (Appendix 3). The Glide docking algorithm produced a binding solution that was of moderate affinity (Glide score of -5.92). Using consensus docking, there would be no binding between CRBP-IV and N-(4-methoxyphenyl)-retinamide.

4.3.5.6 CRBP-IV and N-(4-aminophenyl)-retinamide

CRBP-IV and N-(4-aminophenyl)-retinamide were docked using the eHiTS software. The eHiTS software produced the top ten docking results showing that the small molecule would bind strongly to the protein with a top eHiTS score of -7.14. Three of the solutions demonstrated that the benzene ring portion of N-(4-aminophenyl)-retinamide was deep within the binding pocket, while the other seven solutions contained the ligand oriented in a 180° rotation when compared with the first three solutions. However, there were no energetically feasible thermal energies of binding for CRBP-IV with this substrate. Of the top hundred solutions produced in the Autodock software, none demonstrated energetically feasible binding (Appendix 3). However, the Glide software produced docking solutions for N-(4-aminophenyl)-retinamide and CRBP-IV. The results suggested that they would bind, with moderate affinity (Glide score -5.72). This result was more difficult to interpret, and there was no obvious consensus or prediction to be made. The result was considered inconclusive.

4.3.6 Docking Solutions of Cellular Retinoic Acid Binding Protein 2 and retinamide ligands

4.3.6.1 CRABP2 and retinoic acid

The PDB database provided a crystal structure for retinoic acid docked in the CRABP2 protein receptor (PDB id: 2FR3). As an internal experimental positive control, 2FR3 protein and the retinoic acid ligand were separated from the docked complex, energy minimised and scored by the eHiTS programme. Apo 2FR3 was used to dock a manually constructed retinoic acid ligand (**4.2**). According to the eHiTS scoring function, retinoic acid was predicted to bind to CRABP2 with high affinity (eHiTS score -6.98). The re-scoring of 2FR3 and its crystallized retinoic acid (positive control) produced a score of -8.52. This was a difference of more than two orders of magnitude. Thermal energies of binding for the top ten docking poses generated by eHiTS, were calculated using equation 1 (see section 4.2.3.2.2). 2FR3 produced positive binding energies for all of the ten retinoic acid solutions ranging from +3.65 to +33.43KJ/mol. All of the docked poses contained the carboxylic acid portion of the molecule buried deep within the binding pocket.

When 2FR3 and retinoic acid was docked using the Autodock software, there were two energetically feasible groups of solutions. The predominant group contained ninety eight poses (Figure 4.12).

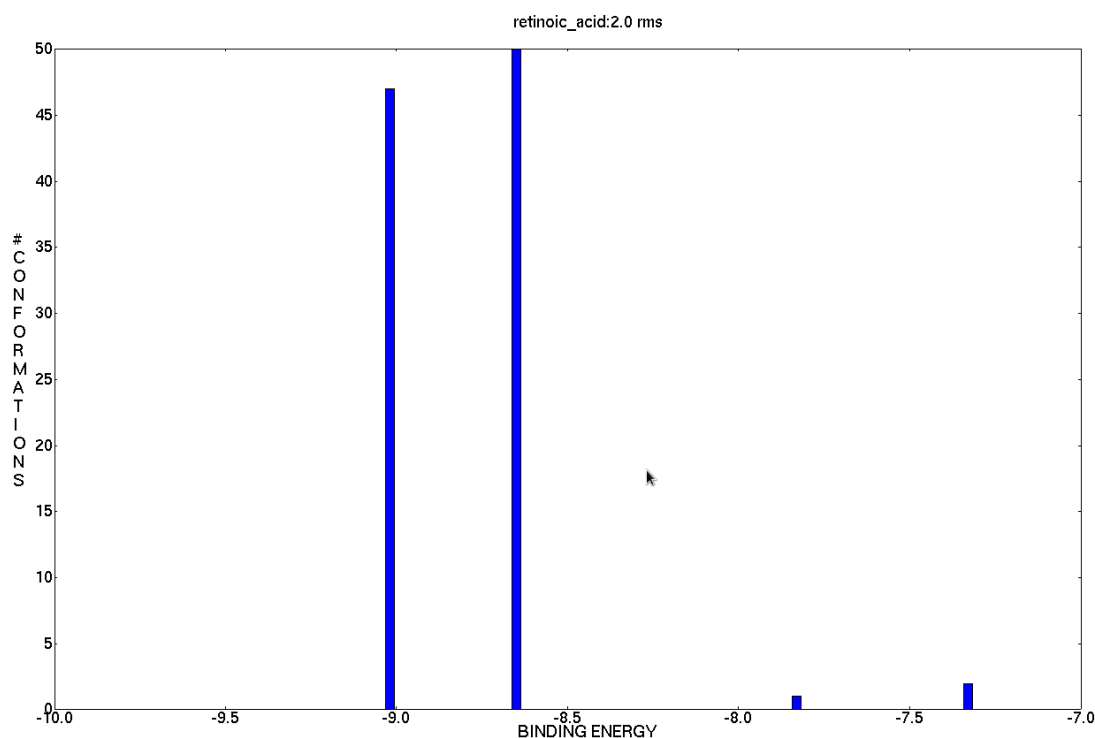


Figure 4.12. An Autodock graph showing the top hundred docking conformations of retinoic acid in CRABP2 protein and their respective predictive energies of binding. (Kcal/mol). The two predominant groups contain ninety-seven poses and are at binding energies of -9.0 and -8.5kcal/mol. The remaining three poses are still within the high affinity binding range between -7.4 and -7.8kcal/mol.

The GLIDE software predicted high affinity binding solutions for CRABP2 and retinoic acid (GLIDE score -10.04).

When the top docking poses of CRABP2 and retinoic acid in the eHiTS, Autodock and Glide software were compared, they demonstrated that retinoic acid was in the same orientation and in almost identical poses for eHiTS and Glide but the ligand docked by Autodock was significantly different (Figure 4.13).

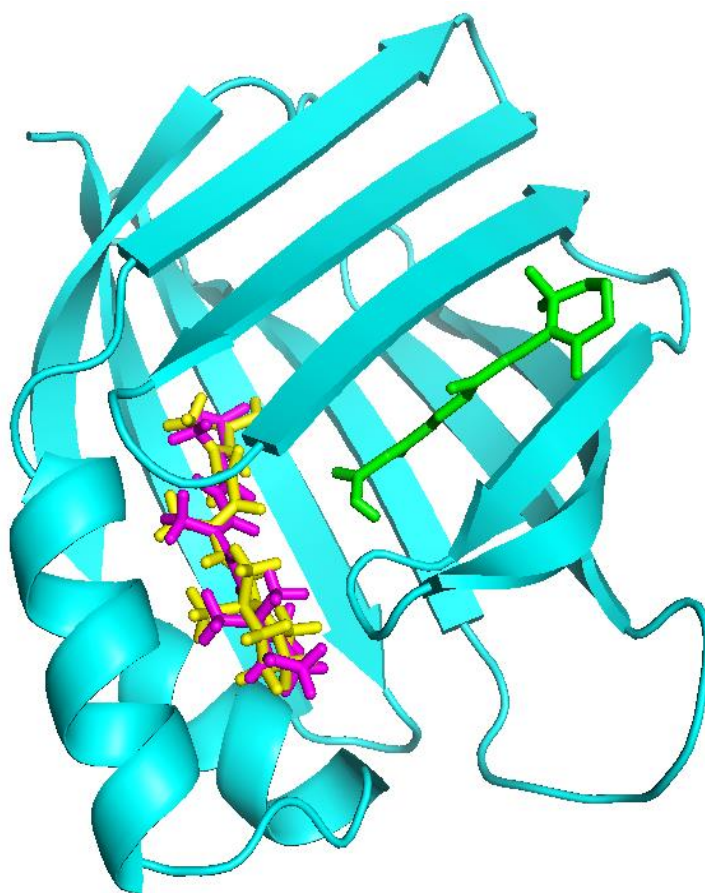


Figure 4.13 A computational modelling schematic showing the top docked poses for retinoic acid in CRABP2 according to the eHiTs (yellow), Autodock (green) and Glide (purple). The docking poses have been overlaid on each other. The three poses show that the docked retinoic acid ligand for eHiTs and bind in the same area of the binding pocket and in the same orientation. However the ligand docked by Autodock appears to be in a significantly different region and in a different orientation.

In the three docking algorithms, likely binding between the protein molecule and retinoic acid was potentiated by possible hydrogen bonding between the carboxylic group of retinoic acid and tyrosine134 as well as arginine132 residues of CRABP2 (Figure 4.14). In addition, hydrophobic interactions and the complementary shape of the binding pocket and ligand may also contribute to the binding. Clearly in this situation, all three algorithms agreed that CRABP2 and retinoic acid would bind strongly.

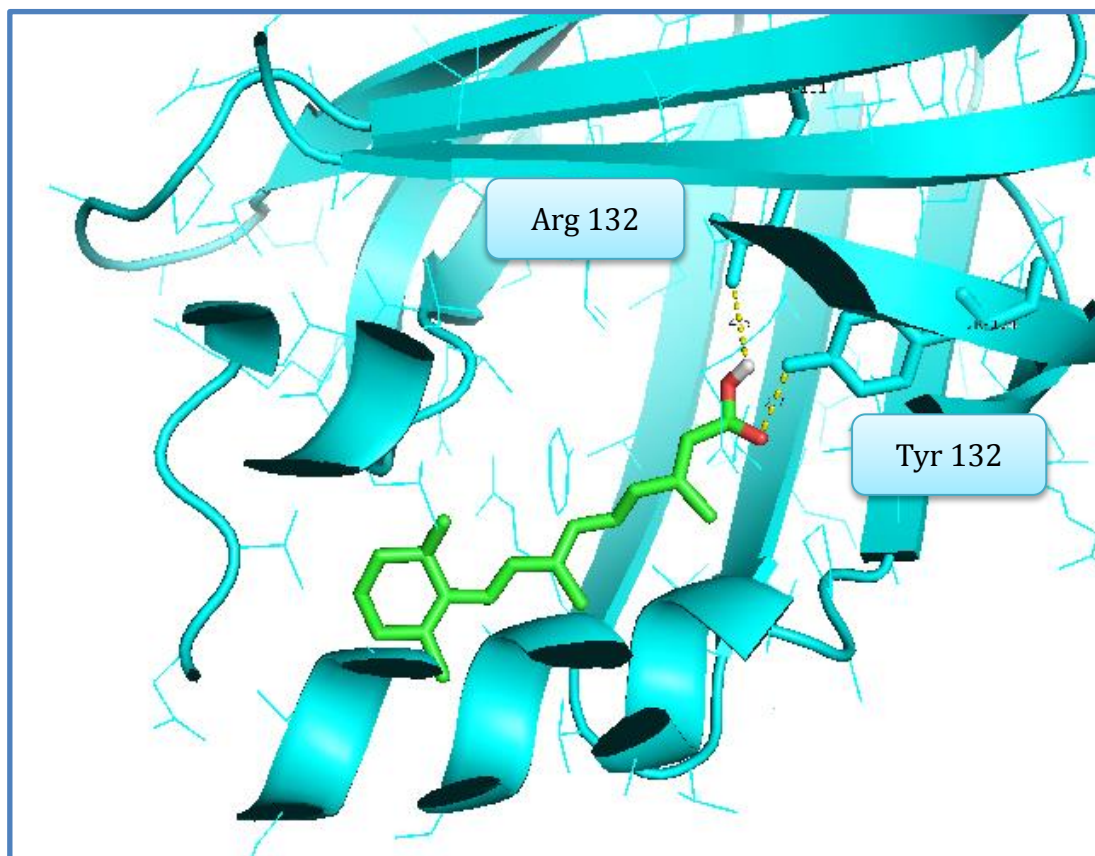


Figure 4.14 A computational modelling representation of retinoic acid docked inside the binding pocket of the CRABP2 protein. Potential hydrogen bonding between the carboxylic group of the retinoic acid and tyrosine 134 and arginine 132 are represented by dashed yellow lines.

4.3.6.2 CRABP2 and fenretinide

According to the eHiTS software, CRABP2 is predicted to bind to fenretinide. The top ten poses for the docking of this protein and small molecule produced a best eHiTS score being -6.40 (strong binder). However, there were no energetically feasible thermal energies of binding. When the Autodock software was used as the docking algorithm, there were multiple energy conformational groups, but none of these were energetically feasible (Appendix 4). The GLIDE software predicted a feasible binding solution with weak/moderate binding affinity, for CRABP2 and fenretinide (GLIDE score - 4.99). The interpretation of these results were not straightforward, and the

overall impression was that it was not possible to make predictions about binding.

4.3.6.3 CRABP2 and 4-oxo-fenretinide

The top ten best poses produced by the eHiTS software for CRABP2 and 4-oxo-fenretinide, demonstrated that the small molecule possessed a weak affinity for CRABP2, as the best eHiTS score was -4.25. The thermal binding energies produced several feasible values for the protein–ligand complex formation between +3.44 and +11.26KJ/mol. Autodock software did not produce any docking results that were energetically feasible (Appendix 4). Interestingly, Glide produced a docking result for this protein-ligand complex which suggested that they could bind moderately well (Glide score -5.65). The interpretation of these results was also not straightforward and the overall impression was that it was not possible to make a prediction about binding.

4.3.6.4 CRABP2 and RF21

When the eHiTS software was used to dock CRABP2 and RF21, the top eHiTS score produced was one of weak affinity (-4.34). The thermal energies of binding calculations for CRABP2 and RF21 produced energetically viable binding conformations ranging between +5.65 and +48.82 KJ/mol. The Autodock software did not produce any energetically feasible docking solutions for CRABP2 and RF21 (Appendix 4). The Glide software also did not produce any docking solutions for RF21 and CRABP2. Using the consensus docking approach, RF21 and CRABP2 were therefore not predicted to bind.

4.3.6.5 CRABP2 and N-(4-methoxyphenyl)-retinamide

CRABP2 and N-(4-methoxyphenyl)-retinamide were docked using the eHiTS software. The eHiTS software produced the top ten docking results showing

that the small molecule would bind to the protein with an eHiTS score of -4.99. The thermal energies of binding for CRABP2 and this substrate produced energetically feasible solutions in the range of +8.56 and +17.33 KJ/mol. Of the top hundred solutions produced in the Autodock software, none demonstrated energetically feasible binding (Appendix 4). The Glide software however did show docking solutions for N-(4-methoxyphenyl)-retinamide and CRABP2, suggesting that they would be weak binders. (Glide score -4.88) The overall impression was that there was not a high enough affinity for binding to occur between CRABP2 and N-(4-methoxyphenyl)-retinamide.

4.3.6.6 CRABP2 and N-(4-aminophenyl)-retinamide

CRABP2 and N-(4-aminophenyl)-retinamide were docked using the eHiTS software. The top ten docking poses were produced and these generated an eHiTS score of -6.43. This suggests that all the solutions would be strong binders (Section 4.2.3.5). The majority of the solutions (nine) demonstrated that the ligand was docked with amide group buried deep within the binding pocket. When thermal binding energies were calculated using equation 1 in section 4.2.3.2.2, there were energetically feasible conformations for CRABP2 and retinamide(**4.6**) ranging from +1.17 – 24.42 KJ/mol.

The Autodock software did not produce any energetically feasible docking solutions for this protein and the small molecule complex (Appendix 4). The Glide docking algorithm produced a binding solution that was a moderate binder with a Glide score of -5.27. Using consensus docking, the prediction is that CRABP2 and retinamide (**4.6**) are likely to bind with moderate to strong affinity.

4.3.7 Docking Solutions of Fatty Acid Binding Protein 5 and retinamide ligands

4.3.7.1 FABP5 and palmitic acid

FABP5 crystal structure (PDB id: 1B56) was imported from the PDB database and the protein structure separated from the palmitic ligand. The two components of the docked complex were energy minimised and scoring attempted using the eHiTS software. Unfortunately, the software was unable to produce a result as it found the ligand contained too many bonds (>16) for it to allow for scoring. When eHiTS was instructed to dock palmitic acid in FABP5, the top ten poses predicted non-binding (eHiTS score: -1.96 – 0.00). When palmitic acid was docked in FABP5 using the Autodock software, thirteen groups of solutions with different feasible energies of binding were produced. They ranged from -5.58 to -3.51 kcal/mol. The group with the lowest energy conformation (-5.58 kcal/mol) was the predominant one containing forty-six poses (Figure 4.15). There were a further thirty-one solutions distributed between two groups at binding energies of -5.5 and -5.35 KJ/mol. The remaining twenty-three were distributed among ten different energy groups.

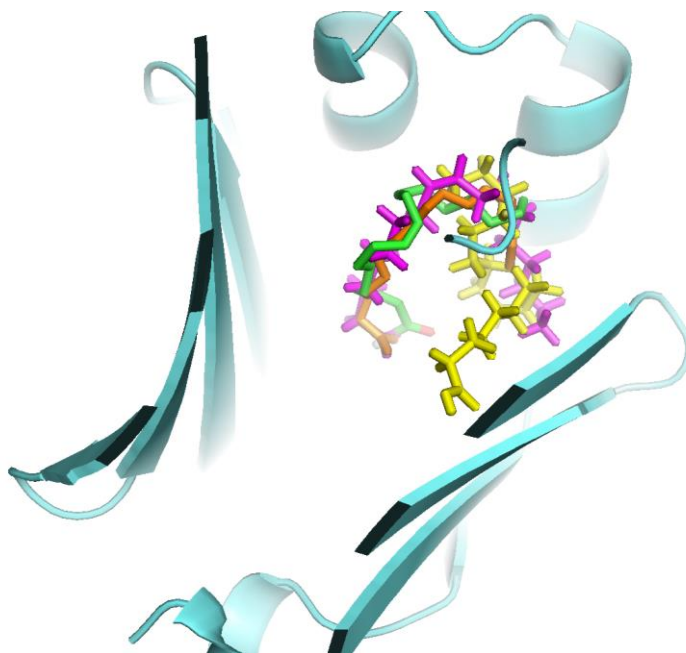


Figure 4.16. A computational modelling schematic showing the top docked poses for palmitic acid in FABP5 according to the eHiTs (yellow), Autodock (green) and Glide (purple). The native ligand from the PDB database has been included in orange. The docking poses have been overlaid on each other. The docked pose for Autodock, Glide and the native ligand are consistent with each other while the eHiTS pose appears significantly different from the other three. The former group demonstrates binding in the same area of the binding pocket and in the same orientation. However the ligand docked by Autodock appears to be in a different region and in a different orientation.

According to the docking algorithms and the pdb database, there would be hydrogen binding between the carboxylic acid portion of palmitic acid, arginine (129) and tyrosine (134) residues in the binding pocket of FABP5.

4.3.7.2 FABP5 and fenretinide

The PDB database was searched and a crystal structure for FABP5 protein receptor (PDB id: 1B56) was chosen. This structure contained oleic acid as the bound ligand. An internal experimental positive control could not be performed as the eHiTS programme could only reliably score ligands with a

length of less than or equal to eleven bonds. This co-crystallized ligand contained sixteen bond lengths. Apo 1B56 was used to dock a manually constructed fenretinide ligand (**4.3**) and according to the eHiTS scoring function, this ligand was predicted to bind to FABP5 with high affinity in three of the top ten poses (eHiTS score -9.38). The remainder of the top ten poses were non binders. Thermal energies of binding for the top ten docking poses generated by eHiTS, were calculated using equation 1 (see section 4.2.3.2.2). Fenretinide and FABP5 produced positive binding energies ranging from +5.54 to +109.86 KJ/mol. When the Autodock software was used as the docking algorithm, there were multiple solution groups, but none were energetically feasible (Appendix 5). In addition, the GLIDE software did not produce any energetically viable binding solutions for FABP5 and fenretinide. Using the consensus docking approach, FABP5 would therefore not bind to fenretinide.

4.3.7.3 FABP5 and 4-oxo-fenretinide

The top ten best poses produced by the eHiTS software for the docking of FABP5 and 4-oxo-fenretinide, demonstrated that only one of the poses possessed a strong binding affinity (eHiTS score: -8.71). The remainder of the solutions were not predicted to bind. The thermal binding energies produced feasible values for the protein–ligand complex between +6.6 and +78.35 KJ/mol. The Autodock software did not produce any docking results that were energetically feasible (Appendix 5). In addition, the Glide programme did not predict binding between FABP5 and 4-oxo-fenretinide (Glide score: -1.11). The prediction here is that FABP5 would not bind to 4-oxo-fenretinide.

4.3.7.4 FABP5 and RF21

When the eHiTS software was used to dock FABP5 and RF21, the top three eHiTS scores produced were of moderate affinity and the remaining seven

were non binders. The thermal energies of binding calculations for FABP5 and RF21 (see section 4.2.3.2.2.) produced energetically viable binding conformations ranging between +14.12 and +106.15 KJ/mol. The Autodock software did not produce any energetically feasible docking solutions for FABP5 and RF21 (Appendix 5) while the Glide software predicted non-binding. The overall assumption is that FABP5 would not bind to RF21.

4.3.7.5 FABP5 and N (4-methoxyphenyl)-retinamide

FABP5 and N-(4-methoxyphenyl)-retinamide were docked using the eHiTS software. This software produced the top ten docking results showing that the small molecule would either be non-binders or (at best) weak binders. (eHiTS score ranging from -0.01 to -3.59. The thermal energies of binding for FABP5 and this substrate produced energetically feasible solutions in the range of +18.55 and +42.84 KJ/mol. Of the top hundred solutions produced in the Autodock software, none demonstrated energetically feasible binding (Appendix 5). In addition, the Glide software predicted that FABP5 and N (4-methoxyphenyl)-retinamide would not bind.

4.3.7.6 FABP5 and N (4-aminophenyl)-retinamide

FABP5 and N-(4-aminophenyl)-retinamide were docked using the eHiTS software. The top ten docking poses were produced with only one being a strong binder (eHiTS score of -8.69). The remaining docked solutions were either non binders or weak binders. When thermal binding energies were calculated (using equation 1 in section 4.2.3.2.2), there were energetically feasible conformations for FABP5 and retinamide (**4.6**) in the range of +17.0 – 86.88 KJ/mol. However, neither the Autodock nor Glide softwares produced any energetically feasible docking solutions for this protein and small molecule complex (See Appendix 5). In this case, the small molecule N-(4-aminophenyl)-retinamide would not be predicted to bind to FABP5.

Protein	Ligands																				
	(4.1) Retinol			(4.2) Retinoic Acid			(4.3) Fenretinide			(4.4) 4-oxo-fenretinide			(4.5) RF21			(4.6) N-(4-methoxy-phenyl)-retinamide			(4.7) N-(4-amino-phenyl)-retinamide		
	E	A	G	E	A	G	E	A	G	E	A	G	E	A	G	E	A	G	E	A	G
hRBP4	✓	✓	✓	NA	NA	NA	✓	X	X	✓	X	X	X	X	X	*	X	X	*	X	X
hRBP-I	✓	✓	✓	NA	NA	NA	X	X	X	*	X	X	*	X	X	X	X	X	*	X	X
hRBP-IV	✓	✓	✓	NA	NA	NA	*	X	✓	*	X	✓	*	X	✓	X	X	✓	*	X	✓
hRBP2	NA	NA	NA	✓	✓	✓	*	X	✓	*	X	✓	*	X	X	*	X	✓	✓	X	✓
hABP5	NA	NA	NA	NA	NA	NA	✓	X	X	✓	X	X	✓	X	X	*	X	X	✓	X	X

Table 4.6 Summary of predictions of computational modelling between retinol binding proteins and retinamide ligands. The ligands are retinol (4.1), retinoic acid (4.2), fenretinide (4.3), 4-oxo-fenretinide (4.4), RF21 (4.5), N-(4-methoxyphenyl)-retinamide (4.6) and N-(aminophenyl)-retinamide (4.7). The computer software are represented as E=eHiTS, A=Auto Dock, G=GLIDE; ✓ = the software algorithm predicts binding between protein and ligand; * = the docking results from the algorithm are inconclusive and predictions about binding could not be made; X = the software predicts that the protein and ligand will not bind to each other, FABP5^x=Fabp5 protein was docked with palmitic acid as its native ligand and all three algorithms predicted binding.

4.4 Discussion

Advancement in the use of fenretinide in the clinical setting has been severely restricted by its bioavailability (Cooper, Hwang et al. 2011). Since its discovery almost sixty years ago, progress on modulating the drug (in wet laboratory experiments) in order to improve bioavailability has been slow and costly (Swinney and Anthony 2011). *In silico* modelling of the binding between proteins and small molecules has provided a different approach to this problem. This structure-based drug design tool can be used in three different ways: utilised as a high throughput screen searching large databases for three dimensional structures to find those fitting the binding pockets of the receptor, building *de novo* ligands (within the constraints of the binding pockets), and finally allowing optimization of known ligands by evaluating proposed analogues within the binding cavity (Kitchen, Decornez et al. 2004). The computational modelling within this research mainly utilises the optimization of ligands approach.

Identification of the binding site for the small molecule within the proteins is usually one of the first steps in this type of *in silico* modelling. It is reliant on the identification of complementary surfaces on the protein that can accommodate the small molecules but that also possesses the capacity to form interactions (hydrophobic and hydrogen bonding types) that drive ligand binding. The next step involves docking of candidate ligands into the protein molecule. Docking is simulated by various software and is a method that predicts the location and orientation of a small molecule binding to form a stable complex. Finally, a scoring function is applied which predicts the likelihood of binding or strength of binding affinity. Scoring functions vary and are specific to the software but most take into account hydrogen bonds, hydrophobic interactions, ionic bonds, Van der Waals forces, internal rotations, solvent effects, free energy due to vibrational mode as well as protein-ligand interaction and conformational changes (Genheden and Ryde 2015). The differences in scoring functions between software may be as a result of differential weighting of the various types of bonds outlined above.

There are two major challenges to the use of automated docking. Most systems allow flexibility of the ligand around bonds but keeps the protein

rigid within the docking. Molecular biology however, demonstrates that proteins are dynamic and as such, both protein and ligand are mobile. Published data use the crystal structure of proteins, as the gold standard (Improving X-ray crystallography modelling, FP7-PEOPLE - Specific programme "People" implementing the Seventh Framework Programme of the European Community for research, technological development and demonstration activities (2007 to 2013) (Simkovic, Ovchinnikov et al. 2017). The process of producing a crystal structure involves capturing structural data at one point in time and does not take into account movement either over time or in solution. The incorporation of protein mobility *in silico* is complicated (Leach 1994) and will involve more work before it can be optimised. It may be that *in silico* modelling has to operate with the protein structure held rigid and that allowances for protein mobility may have to be solved by molecular biology and proteomics. The second major challenge for computational modelling is the fact that it is difficult to thoroughly account for energy of solvation. This has typically been modelled as a function of accessible surface areas (Chothia 1974) (Eisenberg and McLachlan 1986). A recent volume-based method (Stouten *et al.*, 1993), successfully calculating solvation terms is more amenable to the conceptual framework of the grid-based energy evaluation of Auto Dock, but this has not been included in the other soft-wares.

This project utilised three different soft-ware programmes (eHiTS, AUTODOCK and GLIDE) for examining the interactions between the retinol binding proteins and various small molecule/ligands. It is essential to properly understand the strengths and limitations of each of these programmes before their predictions can be assessed. eHiTS is an exhaustive, systematic algorithmic docking programme. It is fully automated and does not require lengthy preparations of the ligands and protein before using it. However, it does require an education in basic computer programming commands, as well as, a special high processor speed computer unit (Linux systems). This system factors bond lengths and takes slices through the binding pocket at 0.5Å, ensuring that hydrogen bonds and hydrophobic interactions are affected as little as possible.(Zsoldos, Reid et al. 2006) In addition, aromatic ring stacking and metal ion interactions are

considered. The scoring function is based on empirical, as well as, knowledge based factors.

Auto Dock uses a genetic algorithm to produce docking solutions. It is especially reliable for docking of small molecules with less than or equal to six bond lengths but finds docking larger molecules, more challenging (Goodsell, Morris et al. 1996). It involves complex computer programming and requires lengthy preparations of the protein, ligand, as well as receptor grid generation and output files. It does however, produce results in the form of a histogram, which is easier to interpret. An ideal result would produce a single cluster of conformations at a low energy but this is often not the case, and a decision must be made between using the cluster with the lowest energy or that with the highest population number. Studies have supported that the cluster with the highest populations is a better predictor of binding. (Morris 1998, Lamarckian)(Figure 4.17)

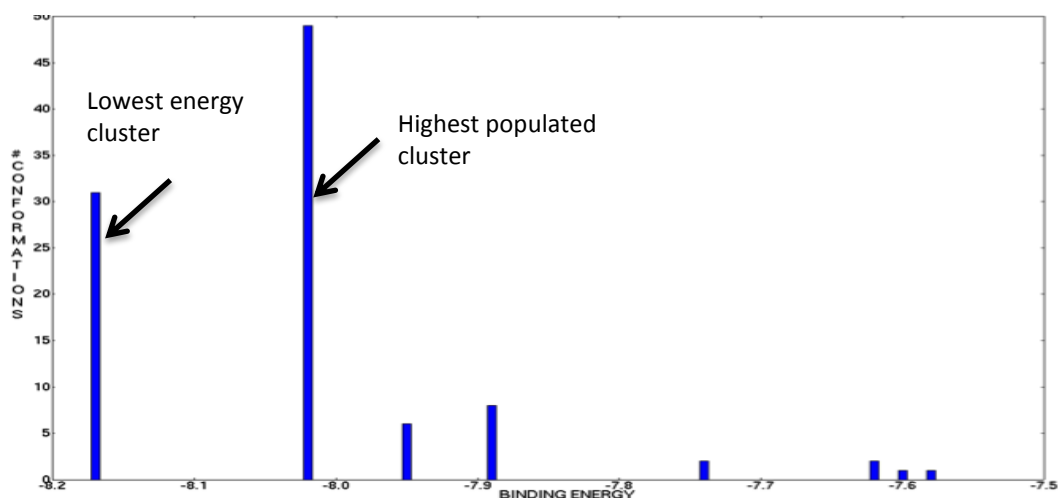


Figure 4.17. A representation of docking results in the AUTODOCK software. Solutions are presented as a histogram with the Binding Energy (kcal/mol) versus the number of conformations in each orientation. The binding group with the greatest number of solutions is not the one with the lowest energy conformation.

Auto Dock uses simulated annealing for searching conformations, allowing several torsional degrees of freedom in a flexible ligand. The limitation to this is that it may not always find the global minimum conformation. There were

no specific optimisations required for using this software with the retinol binding proteins. The presence of heavy metal ions were not prohibitive. Glide employed a systematic approach to conformational, orientation, and positional space of the docked ligand. Initially, the ligand is roughly posed and scored before flexible energy minimization is used to refine the process. The best poses were re-defined by Monte-Carlo sampling and a model energy function. Docking accuracy and errors in top-ranked poses were less than 1 Å in nearly half of the cases (Kawatkar, Wang et al. 2009). Size of the ligand and number of bonds has an impact on the accuracy of the docking. Glide was most reliable with ligands that have less than ten bonds but could perform docking on ligands with up to twenty bond length. This has significant implications for interactions. Glide does not perform docking on covalently attached ligands. The presence of heavy metal ions was not prohibitive.

Using Computational Modelling to assess protein homology and ligand interactions

The amino acid sequence homology is low between RBP4 and the intra-cellular binding proteins (Zizola, Frey et al. 2010). While the homology is higher among the cellular retinol binding proteins (Folli, Calderone et al. 2002) and the CRBPs appear extremely structurally similar, differences in side chains are large enough to mean that assumptions made about a single protein could not be generalised to all the CRBPs. This is especially relevant for CRBP-IV. Its crystal structure (1LPJ) is an *apo* protein and its binding pocket has not been previously defined. A 'clip file' from CRBP-I could not be used in CRBP-IV as the side chain positions would be very different and could potentially produce significant inaccuracies in predictions for the purpose of binding.

RBP4 Interactions

The RBP4 structure imported from the PDB database (PDB id: 1RBP) contained retinol as its co-crystallised ligand. During the initial docking of the retinol in RBP4 (using the eHiTS software), the binding pocket of the protein was not defined. When the generated results were compared to published literature, the ligands appeared to be docked in a position that was significantly different and this may have been due to the presence of an allosteric binding site. Since data had been published for this protein and its retinol ligand, subsequent dockings included defining a binding pocket ('clip file': x, y, z co-ordinates) within the command based programming. This optimisation produced results that supported previously published data and made predictions from unknown ligands more robust. The eHiTS scoring function allows the re-scoring of the composite parts of a protein-ligand complex without first having to re-dock. When the published co-crystallised RBP4-retinol complex was re-scored, the eHiTS score was significantly different from that of the independently docked and scored RBP4 with the manually constructed retinol. Since the proteins used were the same and the manually constructed retinol had been energetically minimised, there was an argument as to whether this difference was produced because the published crystal structure had not been energy minimised. After minimisation, the top eHiTS score for both situations were more consistent. This optimisation was used in all subsequent assessments of binding between the retinol binding proteins and the chemical ligands.

For RBP4 and retinol, the three software predicted binding and this was supported by published biological data (Soprano et al, 1994). However, in the case of RBP4 and fenretinide, Autodock and Glide agreed about non-binding. It was in fact, the eHiTS software that correctly predicted binding, as was demonstrated by Berni et al. eHiTS does predict binding of RBP4 to 4-oxo-fenretinide, while Autodock and Glide disagree. In this situation there is no published data. However, since fenretinide and 4-oxo-fenretinide are structurally very similar, it may be that eHiTS has predicted correctly and that Autodock and Glide have not. This goes against the consensus docking approach. With the RF21 ligand, there is only a prediction of weak binding.

The large bulky groups would possibly provide significant steric hindrance to binding. According to eHiTS, the N-(4-methoxyphenyl)-retinamide and N-(4-aminophenyl)-retinamide ligands binding to RBP4 with a high affinity, but does not show any feasible thermal binding energies. Both AUTODOCK and Glide agree on non-binding, but there is no data to support this.

On balance, none of the three computer programmes appear to be the perfect fit for RBP4 and the retinamide ligands. eHiTS accurately predicted that RBP4 would bind to fenretinide, while Autodock and Glide disagreed. Conversely, there were interactions in which eHiTS appeared too accepting and tolerant of ligands with bulky and polar groups (N-(4-methoxyphenyl)-retinamide and N-(4-aminophenyl)-retinamide). As such because there was no clear ideal docking algorithm, this approach was not discriminatory enough to inform biological experiments and so the interactions would need to be investigated experimentally.

CRBP-I Interactions

The CRBP-I structure imported from the PDB database (PDB id: 1CRB) contained retinol as its co-crystallised ligand. During the initial docking of the retinol in CRBP-I, the software (eHiTS) was unable to perform the docking exercise. Exploration of the crystal structure from the pdb database revealed that it contained two cadmium heavy metal ions. As metal interactions had not been factored in the eHiTS algorithm, results could not be generated until those heavy metal ions were manually removed in Schrodinger Maestro.

The three docking algorithms predict that CRBP-I would bind with high affinity to retinol (**4.1**). The eHiTS software, Autodock and Glide predicted that there would be no binding between CRBP-I and retinamide (**4.3**). According to the literature, CRBP-I binds to retinol (Levin 1988, Comparison of the ligand) but does not bind to fenretinide (Sani, Shealy et al. 1995).

Using consensus docking, CRBP-I and 4-oxo-fenretinide, RF21, N-(4-aminophenyl)-retinamide are not predicted to bind. The prediction for CRBP-

I and N-(4-methoxyphenyl)-retinamide is also that they do not bind to each other. In this case, all three algorithms agree.

The three *in silico* models predictions for binding between CRBP-I and retinol, fenretinide were consistent with the published data and that gave more weight to the predictions for ligands(4-oxofenretinide, RF-21, N-4-methoxyphenyl retinamide, N-4-aminophenyl retinamide) for which there was no published data.

CRBP-IV Interactions

The eHiTS and Autodock software performed their docking and scoring functions with the same previously defined constraints and optimisations. The Glide software had a preliminary step that involved defining the receptor grid. Since there was no published data on the protein binding pocket, and the pdb structure (PDB id: 1LPJ) is not co-crystallised with a ligand (*holo* structure), its docking co-ordinates were defined by using the centre of the protein as the centroid of the pocket. The reliable identification of unoccupied sites that have the potential to bind ligands with high affinity is non-trivial in this situation. As a result, docking results could not be verified by internal positive controls and may be erroneous because of the assumption outlined above.

The three docking algorithms predict that CRBP-IV would bind with high affinity to retinol (4.1). Consensus docking approach was used for CRBP-IV and N-(4-methoxyphenyl)-retinamide (4.6) and the prediction was that there would not be binding between protein and ligand. For the remaining ligands fenretinide (4.3), 4-oxo-fenretinide (4.4), RF21 (4.5) and N-(4-aminophenyl)-retinamide (4.7) the eHiTS software was inconclusive. Glide determined that there would be moderate binding while Autodock predicted no binding at all. This data was difficult to interpret and no clear consensus could be reached. Published literature demonstrates that CRBP-IV has low binding affinity for retinol (Folli,2002, Ligand binding). This interaction is unstable and difficult to co-crystallise, hence the published crystal structure is in the **apo** form. This is in direct contrast to the three modelling systems all predicting a strong interaction. The Glide software generally expected binding interactions

between CRBP-IV and all the retinamide ligands, while Autodock contradicted this prediction. eHiTS was largely inconclusive as its score and the thermal energies of binding did not support each other. Since there was no clear consensus, the approach would be to perform functional binding assays to determine whether binding occurs. In general, the computational modelling exercise did not work well for this protein.

CRABP2 Interactions

The three docking algorithms predict that CRABP2 would bind with high affinity to retinoic acid (**4.2**) and N-(4-aminophenyl)-retinamide (**4.7**). According to the software, CRABP2 would not bind to fenretinide, RF21 or N-(4-methoxyphenyl)-retinamide. The eHiTS programme demonstrated weak binding of CRABP2 to 4-oxo-fenretinide, being accompanied by energetically feasible thermal binding values. Autodock demonstrated no binding between CRABP2 and 4-oxo-fenretinide while Glide predicted that the ligand would bind to the protein with moderate affinity. This data (from the three docking algorithms) do not produce any consensus and as such makes it difficult to interpret or make predictions. This is a situation that could benefit greatly from further wet experiments (in order to determine binding).

According to published literature, retinoic acid (**4.2**) is the native ligand for the CRABP2 protein. All three docking algorithms agreed with this data, by identifying retinoic acid (**4.2**) as a high affinity binder. However, there is no published data for the other retinamide ligands binding to CRABP2.

When performing docking experiments with CRABP2, the Autodock programme appeared to be more intolerant and less accepting of binding to this protein (compared to the other two algorithms).

FABP5 Interactions

The FABP5 structure imported from the PDB database (PDB id: 1B56) contained oleic acid as its co-crystallised ligand. The eHiTS programme

predicted that FABP5 would bind very strongly to fenretinide, 4-oxo-fenretinide, RF21 and N-(4-aminophenyl)-retinamide (thermal binding energies calculations supports this). However, both Autodock and Glide failed to simulate binding between FABP5 and fenretinide (4.3) 4-oxo-fenretinide (4.4), RF21 (4.5) and N-(4-aminophenyl)-retinamide (4.7). Interestingly, the eHiTS algorithm was inconclusive when producing predictions about the binding of FABP5 that N-(4-methoxyphenyl)-retinamide (4.6). Autodock and Glide predicted no binding.

FABP5 is the natural transporter for fatty acids like oleic acid and palmitic acid (Armstrong, Goswami et al. 2014). There is however, no published literature on binding with retinamide ligands. Using consensus docking, FABP5 would not bind to any of the retinamide ligands (fenretinide, 4-oxo-fenretinide, RF-21, N-(4-methoxyphenyl)retinamide and N-(4-aminophenyl)retinamide). When eHiTS was used to simulate docking of oleic acid within FABP5, the software was unable to demonstrate high affinity binding. When an eHiTS score was attempted for the crystal structure, the programme was unable to score a ligand with more than 11 bond lengths. Glide and Autodock produced moderate affinity binding between the protein and oleic acid ligand. In this case, eHiTS does not appear to be suited for investigating binding between this protein and the ligands. Once again there is no published data and it would be useful (in the future) to investigate these binding relationships.

In conclusion, computational modelling is a very valuable tool in aiding future discoveries of interactions between proteins and small molecules. Advancement in this field has helped with the challenges of time and cost effectiveness that would otherwise plague this type of research. It is useful for looking at trends and patterns which can be invaluable in informing future research. It is however, important to remember, that this process is not without significant limitations including: accuracy, missing potential targets, and difficulty with the interpretation of individual software scores. Various packages have different strengths and it is not possible to pre-determine which soft-wares work well with the proteins of interest. This technique

requires improved computer processing power and large libraries (limited by published data) of available X-ray crystal structures. During this project, I was interested in retinamide interactions with the protein family of retinol binding proteins. eHiTS and thermal binding energies (in this situation) appeared not to be discerning enough to discriminate between potential interactions. However, Auto Dock and GLIDE appeared to be better programmes for predicting (this type of interaction) and there was a high degree of consensus between their independent results. In general, because there is no published literature for the majority of the retinamide ligands and the proteins, a consensus docking approach has been therefore been useful in eliminating biases within the individual programmes.

Chapter 5

The role of lipid binding proteins in fenretinide-induced cell death or cell fate

5.1 Introduction

The Cellular Retinol Binding Proteins (CRBPs) (Section 1.4.4) are a family of transport proteins which are integral for the intra-cellular transport and metabolism of retinol and retinol derivatives (Kane, Folias et al. 2011). For the first time, I have examined expression of the CRBPs in ESFT cell lines (Section 3.3.8), and found that CRBP-I, CRBP-IV, CRABP2 and FABP5 proteins were expressed. However, the role of these proteins in ESFTs is unknown.

CRBP-I protein binds to the Stimulated by Retinoic Acid 6 receptor (STRA6) at the internal cell membrane (Chen, Ke et al. 2016), facilitating transfer of retinol from extra-cellular RBP4 to the intra-cellular compartment by the process of diffusion through the protein channel (Marwarha, Berry et al. 2014). The *holo*-CRBP-I protein dissociates from STRA6, shuttles the retinol to lecithin:retinol acyltransferase (LRAT, an endoplasmic reticulum membrane protein) which then metabolises and modulates retinol storage (Marwarha, Berry et al. 2014). The relative amounts of *apo* and *holo* CRBP-I can affect retinoid homeostasis by manipulating downstream activation of retinoic acid receptors (RAR) (Kane, Folias et al. 2011).

CRBP-IV has a high level of structural similarity to that of CRBP-I (56-57%) and readily binds with retinol (Alvaro, Alpini et al. 2002). However, its potential function in transport, metabolism and retinoid homeostasis has not been clearly delineated. To date, this protein has only been investigated in other human cancer cell lines, but not in ESFTs (Kwong, Lo et al. 2005).

CRABP2 protein is a member of the intracellular lipid binding protein family (iLBPs). It acts as a cytosol-nuclear shuttling protein involved in the retinoid signalling pathway (Zhang, Vreeland et al. 2016). This protein performs

several functions: which includes binding to retinoic acid (retinoid) within the cytoplasm, and presenting this ligand to retinoic acid receptors at the nucleus, thereby inducing multiple anti-proliferative genes (Vreeland, Levi et al. 2014, Vreeland, Yu et al. 2014). Another function of CRABP2 has been to display oncogenic activities in other cancer cell lines (Yang, Wang et al. 2016).

FABP5 (like CRABP2) is a highly conserved cytosolic protein that belongs to the iLBP's (Armstrong, Goswami et al. 2014). This protein binds retinoic acid, long chain fatty acids and other hydrophobic ligands within the cytoplasm (Liu, Graham et al. 2011). Depending upon the nature of the bound ligand, different downstream receptors are targeted, and different signalling pathways are induced. These include the Peroxisomal Proliferative-activated receptor beta/delta (PPAR β/δ) in the nucleus (Yu, Levi et al. 2014). There has been extensive research on the role of FABP5 in human breast cancer cell lines (Liu, Graham et al. 2011) but not in ESFTs.

The primary aim of this chapter lies in determining of the function of the cellular lipid binding proteins (CRBP-I and CRBP-IV) in ESFT cells as they relate to the retinoid and retinamide signalling pathways. It would be informative to determine whether CRBP-I has a function in retinoid homeostasis in ESFTs and also whether these theories can be applied to fenretinide and retinamide transport and signalling pathways. In addition, the exploration of CRBP-IV function (within the ESFT environment) may provide valuable knowledge in its signalling pathway which can then be used in the treatment of ESFTs.

5.2 Material and Methods

5.2.1 Knock down experiments

5.2.1.1 ESFT cell growth in Accell culture media

SKES-1 cells (2×10^5 /well) were seeded in Mc Coy's 5A + 2mM glutamine + 15% FCS (pre-warmed to 37°C), and placed into eleven 6 well plates and left for 24 h. The media in six of these eleven plates were then replaced with Accell Delivery Media (3mls, GE Healthcare, Buckinghamshire, UK). After 72 h, one of the six plates containing Accell Delivery Media was replaced with Mc Coy's 5A + 2mM glutamine + 15% FCS (3mls, pre-warmed to 37°C). Cells were allowed to adhere to the primaria plate for 24 h before being harvested at time intervals of 0 h, 24 h, 48 h, 72 h and 96 h. The viable cell number was calculated using trypan blue exclusion assay (Vi-cell, Section 2.2.2). This experiment was repeated using the RDES and SK-N-MC cell lines.

5.2.1.2 Acell siRNA transfection

Cell culture was performed in a laminar flow cell culture hood under sterile conditions (Section 2.2.1) and RDES, SKES-1 and SK-N-MC cells were seeded in normal growth media, in triplicate in a 6 well plate (2×10^5 cells/well). After 24 h, the media was aspirated and replaced with 3 mls of pre-warmed Accell Delivery Media.

Si RNA Buffer (GE Healthcare), siRNA negative control (GE Healthcare) and siRNA targeted solution (GE Healthcare) were removed from -20 °C storage and placed on ice. The siRNA buffer was diluted by adding four volumes of sterile RNase free water. This was also used to prepare 100 µM siRNA negative control solution. The RNA concentrations were checked by spectrophotometry using the Nanodrop ND 1000.

Each cell type was incubated with RNase free buffer (30 µl), scrambled siRNA negative control (30 µl) and siRNA for the target (30 µl). The well contents were mixed gently by pipetting before incubating (37°C in 5%CO₂) for 72 h. Cells from each well were harvested, RNA extracted for

assessment by RTqPCR (Section 2.2.3.3), and protein extracted (Section 2.2.4.1.) and quantified by Bradford assay (Section 2.2.4.2). The target protein expression in these treated cells was determined by western blotting, SDS-PAGE (Section 2.2.4.3). RNAi knockdown experiments were performed for CRBP-I and the CRBP-IV genes (Table 5.1).

Table 5.1 Details of siRNA used in RNAi experiments

Target Protein siRNA	Product Code
CRBP-I	E-009825-00-0005
CRBP-IV	E-008654-00-0005
Scrambled siRNA (negative control)	B-002000-UB-100

5.2.1.3 The impact of RNAi on expression of other cellular retinol binding proteins

The down-regulation of CRBP-I and CRBP-IV proteins were quantified by both western blotting and densitometry (Section 2.2.4.3.). The protein extracts from cells treated with CRBP-I siRNA were analysed for RBP4, CRBP-II, CRBP-III, and CRBP-IV proteins whereas protein extracts from cells treated with CRBP-IV siRNA were investigated for RBP4, CRBP-I, CRBP-II and CRBP-III. Any positive bands were quantified by densitometry (target band relative to positive control) on LI-COR Odyssey CLx.

5.2.1.4 The effect of CRBP-I and CRBP-IV siRNA on viable cell number

SK-N-MC cells were seeded (2×10^5 cells/well) in triplicate in three 6 well plate with normal growth media. After 24 h, the media was aspirated and replaced with 3 mls of Accell Delivery Media. The cells were then treated with CRBP-I and scrambled siRNA (Section 5.2.1.2). After 72 h, cells were

collected from 3 wells, protein extracted, and the knockdown of CRBP-I confirmed by western blot. In the remainder of the wells, the Accell media was aspirated and replaced with normal growth media. These wells were then treated with 4-hydroxy (phenyl) retinamide (0-10 μ M) for 24 h, after which cells were harvested and the viable cell number determined by trypan blue exclusion (Section 2.2.2).

RNAi experiments for CRBP-IV were performed in SKES-1 cells. After careful checking to ensure that the protein had been down regulated, the cells were treated (as above) with 4-hydroxy (phenyl) retinamide. Viable cell number was counted as before (Section 2.2.2). This process was repeated in 3 independent experiments.

5.2.1.5 Treatment with fenretinide

RDES and SK-N-MC cells were seeded out in 10 cm² petri dishes and left overnight to adhere. The ESFT cells were then treated with fenretinide (10 μ M) over a time course of 0-48 h, after which cells were harvested by trypsinisation, and pelleted for protein extraction (Section 2.2.4.1). The proteins extracted at various time points (0h, 2h, 4h, 8h, 16h, 24h, 48h) were investigated for CRBP-I and CRBP-IV protein content by western blotting (Section 2.2.4.3), using 15% acrylamide gels. HEPG2 cell extracts (50 μ g) were used as the positive control for CRBP-I and human kidney lysate (50 μ g) as the positive control for CRBP-IV.

5.2.1.6 Subcellular fractionation of cells treated with siRNA

Since I was able to perform knockdown of CRBP-I and CRBP-IV proteins by RNAi experiments, it would be useful to know whether the protein modulation had altered cellular distribution of the target proteins. ESFT cells treated with siRNA were subjected to the same sub-cellular fractionation protocol as described in Section 3.2.1 and Figure 3.1. Purity of the extracted fractions was confirmed by western blotting, using the various markers

identified in Table 3.1. The intra-cellular distributions of CRBP-I and CRBP-IV were then compared to cells that had not been treated with siRNA.

5.2.2 Target gene activation with 5 aza-2'-deoxycytidine

5 aza-2'-deoxycytidine is an inhibitor of DNA methyl transferase activity and causes DNA demethylation (Kwong, Lo et al. 2005, Shutoh, Oue et al. 2005, Caren, Fransson et al. 2007). In some cancer cell lines where genes are silenced by methylation, they can be induced to express the gene product when it has been exposed to a demethylation agent like 5 aza-2'-deoxycytidine (Kwong, Lo et al. 2005).

RDES, SK-N-MC, SKES-1 and TC-32 cells lines were seeded (5×10^4 cells/well) in triplicate in 24 well plates (142475: Thermo-Fisher Scientific). They were left to adhere to the plate for 24 h. 5-Aza-2'-deoxycytidine (A3656: Sigma-Aldrich) (stored at -20°C) was used to make 10mM solution in DMSO. Serial dilutions of the stock were made to treat ESFT cells with 5 aza-2'-deoxycytidine (0.001 nM - 10 μM). The ESFT cell lines were treated with the six different concentrations of 5-Aza-2'-deoxycytidine for 72 h (Fulda, Kufer et al. 2001). The media with treatment doses of 5-Aza-2'-deoxycytidine were renewed daily, as the drug was known to be unstable (Lin, Momparler et al. 1981). A reduced concentration range of 0- 2 μM 5-Aza-2'-deoxycytidine was used to treat TC-32 cells. Cells were harvested at 72 h and viable cell number counted using the Vi-cell method (Section 2.2.2).

5.2.3 Surface Plasmon Resonance (SPR)

5.2.3.1 Desorbing and sanitizing

The Biacore maintenance Kit, type 2 (GE Healthcare Life Sciences, Buckinghamshire, UK) was retrieved from storage in the cold room (4°C) and the Sensor Chip Maintenance was inserted into the Biacore T200 machine (GE Healthcare Life Sciences, Buckinghamshire, UK). Desorbing protocols (Biacore Sensor Surface Handbook) were run prior to the commencing of

experiments and was repeated weekly thereafter. This protocol was performed at 25 °C for 20 min with the BIAdesorb solutions 1 (0.5% (w/v) sodium dodecyl sulphate (SDS)) and 2 (50 mM glycine-NaOH pH 9.5). The Biacore T200 was maintained by performing monthly desorbing and sanitizing procedure (<https://proteins.gelifesciences.com>)

5.2.3.2 pH scouting for RBP4 protein immobilisation

HBS-EP running buffer (10 mM HEPES, 3 mM EDTA, 150 mM NaCl, 0.5% Tween20- pH 7.4) was filtered through a 0.2 µm filter unit (Stericup Millipore, UK Ltd, Hertfordshire, UK) before use. A CM5 chip (BR-1005-30, GE Healthcare Life Sciences) was removed from the cold room and allowed to warm up to room temperature, prior to being inserted into the Biacore T200 (GE Healthcare Life Sciences, Buckinghamshire, UK). Sodium acetate buffers (10 mM) were made at pH 4, 4.5 and 5. RBP4 protein (1 mg, ABD Serotec, BIO-RAD, Oxfordshire, UK) was added to 476 µl of 10 mM sodium acetate (pH 4.5) to make a 1 mM RBP4 stock concentration. The RBP4 stock solution was then diluted in sodium acetate buffers (pH 4, 4.5, 5) to generate a 40 µM solution. The pH of the dextran CM5 chip is between 3-3.5 and the isoelectric point (pI) of RBP4 is 5.76. The optimum pH for immobilisation of this protein onto the CM5 chip lies between these two limits and so I evaluated the above conditions in order to determine the optimum pH for protein coupling to the chip. Using the immobilisation pH scouting wizard (Biacore T200 control software), the RBP4 protein samples (40 µM) at various pH's were inserted into 7 mm plastic vials (GE Healthcare Life Sciences) and covered with rubber caps type 3 (GE Healthcare Life Sciences). They were inserted into reagent rack type 1 (GE Healthcare Life Sciences) as directed by the wizard. NaOH (50 mM, Sigma-Aldrich) was used for regeneration of the chip surface. The pH buffer that facilitated the maximal number of binding response units (RU) for immobilisation of RBP4 to the CM5 chip was noted and thereby providing information which could be utilised in future experiments.

5.2.3.3 Preparing for RBP4 Protein Capturing onto the CM5 chip

The CM5 chip has four individual flow cells (flow cell 1= FC1; flow cell 2 = FC2; flow cell 3 = FC3 flow cell 4= FC4), to which variable levels of protein can be coupled. This allows the investigation of interactions between the same protein and ligand on the same chip simultaneously, under different conditions. A mathematical equation (see below) was used (prior to the capturing of the protein onto the chip surface) to estimate the amount of RBP4 required on each flow cell.

$$R_{\max}(\text{RU}) = \text{ligand/protein(kDa)} \times R_L(\text{RU}) \times S$$

Where R_{\max} = maximal response of binding between RBP4 and the ligand and is nominated as 100; R_L = immobilisation level of RBP4 required on the chip; S = stoichiometry of binding (assumed to be 1:1). In this equation the results are measure in response units (RU).

For $R_{\max} = 100$ with retinol (286 daltons) as the ligand and RBP4 (21kDa) as the protein:

$$100 = 0.286/21 \times R_L \times 1$$

$$100 = 0.0136 R_L$$

$$R_L = 7352.7 \text{ RU}$$

For a $R_{\max} = 100$ with another protein TTR (51kDA) as the ligand and RBP4 (21kDA) as the surface protein:

$$100 = 55/21 \times R_L \times 1$$

$$100 = 2.62 \times R_L$$

$$R_L = 100/2.62 = 38.1$$

These calculations highlight that the amount of protein needed to be captured on the CM5 chip varies widely, and is dependent upon the molecular weight of the protein.

5.2.3.4 CM5 chip surface preparation for amine coupling with RBP4 protein

A manual run module was used (Biacore Sensor Surface Handbook) to optimise conditions for the immobilisation of RBP4 on the CM5 chip using the Biacore Amine Coupling kit (GE Healthcare Life Sciences). Filtered, deionized water (10mls) was added to both the vial of N-Hydroxysuccinimide (NHS) and 1-Ethyl-3-(3-dimethylaminopropyl) carbodiimide hydrochloride (EDC) mixture, which were agitated until all the solids were dissolved. The EDC and NHS solutions were separately aliquoted and stored at -20 °C. Ethanolamine hydrochloride-NaOH pH8.5 (1M, GE Healthcare Life Sciences) was stored in the cold room (4° C)

EDC/NHS solutions were injected over the CM5 chip in order to activate/charge the dextran surface and allow coupling with an appropriately charged RBP4 protein. Pulsed injections of the protein demonstrated that the injection time needed for the required level of protein capture was 420 seconds. This information was used to produce an automated immobilisation method in the Biacore T200 wizard software which was subsequently used for the production of CM5 chips coated with RBP4 protein.

Using HBS-EP (as the running buffer at 37°C), equal volumes of EDC (GE Healthcare Life Sciences) and NHS (GE Healthcare Life Sciences) were mixed and injected for 360 s at a flow rate of 10µl/min over the chip surface. RBP4 (40µM) diluted in 10 mM sodium acetate at pH 4.5 was injected for 420 s at a rate of 10 µl/min until the required response units (2000-5000 RU) were achieved (Section 5.2.2.3). Ethanolamine hydrochloride-NaOH pH8.5 (1M:

GE Healthcare Life Sciences) was then injected over all flow cells for 420 s at a rate of 10 µl/min. This deactivated excess reactive groups and prevented further coupling of any protein/analyte with the chip.

5.2.3.5 Sample preparation

Scouting for Ligand Regeneration

The process of ligand regeneration involves removing the bound ligand from the sensor chip without destroying either the surface of the chip or the

activity of the protein immobilised upon it. The Biacore regeneration scouting kit (GE Healthcare Life Sciences) together with the scouting wizard in the Biacore T200 were used to determine ideal conditions for retinoid and retinamide ligand regeneration from the protein coated dextran chip. Reagent conditions that were explored included: 1mM NaCl; 10 mM glycine at pH 2.5- 3.5 and extended washes with HBS-EP buffer for 600 s. The ligand concentration was maintained constant at 100 nM retinol.

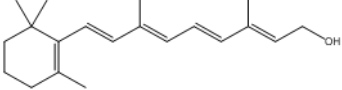
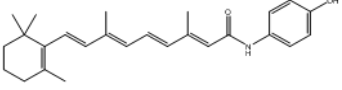
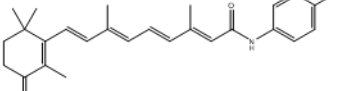
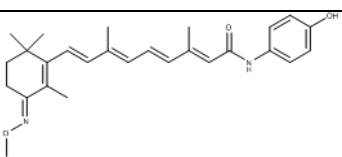
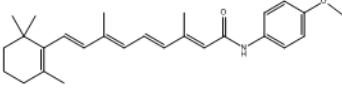
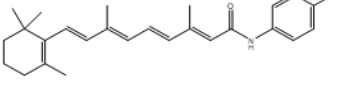
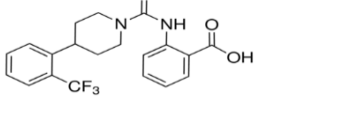
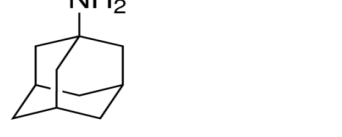
5.2.3.6 Solvent correction

The ligands of interest are all poorly soluble, and so were prepared in dimethyl sulfoxide (DMSO, Sigma-Aldrich). It was important to keep the concentration of DMSO to a minimum as the solvent could erroneously contribute to the binding responses measured. The optimal concentration of DMSO for preparation of the ligands was 1%. This was monitored by running DMSO (0.5-1.8%) over the chip surface, in order to correct for any binding contributions.

5.2.3.7 Preparing retinoid and retinamide derivatives for SPR

A panel of retinoid and retinamide-like small molecules were investigated for binding affinities with retinol binding proteins, using the Biacore T200. These included: retinol (Sigma-Aldrich, Dorset, UK), fenretinide (4-hydroxy (phenyl) retinamide), 4-oxofenretinamide, RF-21, N-(4-methoxyphenyl)retinamide and N-(4-aminophenyl) retinamide (Table 5.2). All compounds were synthesised by (MCCB group, Richard Foster, chemistry colleagues) with the exception of retinol, which was purchased. 10mM stock solutions of each compound were prepared (Table 5.2).

Table 5.2 Recipe for the production of retinoid, retinamide and other ligand stock solutions.

Stock Solution(10 mM) (Molecular Weight)	Chemical Structure	Retinamide(mg) added to DMSO(1ml)
Retinol (MW : 286 Da)		2.86mg
Fenretinide (MW : 391Da)		3.91mg
4-oxo Fenretinide (MW : 404 Da)		4.04mg
RF-21 (MW : 435 Da)		4.35mg
N-(4-methoxyphenyl)retinamide (MW : 405 Da)		4.05mg
N-(4-aminophenyl)retinamide (MW : 390 Da)		3.9mg
A1120 (MW : 392 Da)		3.92mg
1-adamantylamine (MW : 151 Da)		1.51mg

Serial dilutions of the 8 stock solutions were made to produce ligand concentrations of 0-100 μ M.

The effect of transthyretin on the interactions between RBP4 and the retinamide ligands was investigated by incubating transthyretin and the retinamide ligand together, and then passing the mix over the RBP4 coated CM5 chip. Serial dilution of stock TTR (200 μ M: P1742, Sigma) was used to produce a concentration curve of 0-100 μ M. Each TTR concentration was incubated with a fixed concentration of either retinol (40 μ M) or fenretinide

(40 μ M) on a shaker (88881102: Thermo Fisher Scientific) in the dark for 1h at room temperature.

5.2.3.8 pH scouting for cellular retinol binding proteins' immobilisation to the CM5 chip

CRBP-I

Commercially produced CRBP-I protein was available in 2 main forms: CRBP-I protein (GeneTex, CA, USA); or as a tagged (HIS, GST) protein. Initially the untagged protein was purchased and the isoelectric pH was estimated as 4.99 (using the ExPASy Bioinformatics Resource Portal www.expasy.org). The optimal pH for binding would be expected to lie between pH 3.5 (pH of CM5 chip) and pH 4.99. CRBP-I stock solution (126 μ M) was diluted with sodium acetate buffers (10mM) at pH 3.5-4.9 in order to generate 6.3 μ M solutions. The automated wizard in Biacore T200 was used (Section 5.2.3.4) and the pH buffer at which the maximal number of response units (RU) would be chosen for immobilisation of CRBP-I to the CM5 chip.

The second CRBP-I formulation was GST tagged (Abnova, Taipei City, Taiwan). The isoelectric pH for this protein was pH 4.89 (www.expasy.org). The expected optimal pH for binding of the GST tagged protein to the CM5 chip would be between pH 3.5- 4.99. Stock CRBP-I- GST tagged protein (8.7 μ M) was diluted with sodium acetate (10mM) at pH 3.6- 5 to generate 0.87 μ M solutions. In the Biacore T200, the pH buffer at which the maximal number (Section 5.2.2.3) of response units (RU) for immobilisation of CRBP-I-GST to the CM5 chip was chosen by using the immobilisation pH scouting wizard.

5.2.3.8.2 Preparing for CRBP-I Protein Capturing onto the CM5 chip

Using the formula:

$$R_{\max}(\text{RU}) = \text{ligand/protein(kDa)} \times R_L(\text{RU}) \times S \text{ (Section 5.2.2.3)}$$

For a $R_{\max} = 100$ with retinol (286 daltons) as the ligand and CRBP-I (15kDa) as the protein :

$$100 = 0.286/15 \times R_L \times 1$$

$$100 = 0.019 R_L$$

$$R_L = 5263.2 \text{ RU}$$

The capture of 5263.2 RU for CRBP-I would give an expected $R_{\max} = 100$.

The molecular weight of CRBP-I-GST = 41kDa and the molecular weight of small molecule retinol=0.286kDa and $R_{\max} = 100$.

In the second instance, when CRBP-I- GST tagged protein was being coupled to the chip, the molecular weight of the tagged protein was 41kDa. Using the formula as before:

For a $R_{\max} = 100$ with retinol (286 daltons) as the ligand and CRBP-I-GST (41kDa) as the protein :

$$100 = 0.286/41 \times R_L \times 1$$

$$100 = 0.00698 R_L$$

$$R_L = 14347.2 \text{ RU}$$

Therefore, to produce a $R_{\max} = 100$, there is the need to capture 14347.2 RU of CRBP-I-GST tagged protein. Since the GST tag is large when compared to CRBP-I protein (62.5 % of the total weight of the CRBP-I-GST molecule), correction was made for the contribution that the GST tag would make to the measured binding response. One of the flow cells of the CM5 chip was coated with GST to monitor these effects. The level of GST aimed for was 8967 RU (62.5% of the amount of CRBP-I-GST).

CRBP-IV

Commercially produced CRBP-IV protein was only available in a tagged form (HIS, GST) protein (Abnova). I attempted to cleave the GST tag from this protein using glutathione sepharose beads 4B (GE Healthcare Life Sciences). CRBP-IV protein (50 μ l) was diluted up to 1000 μ l with PBS

binding buffer pH7.3 (140 mM NaCl, 2.7 mM KCL, 10 mM Na₂HPO₄, 1.8 mM KH₂PO₄). The Gluthathione Sepharose 4B was prepared by adding 5 mls of binding buffer to 1 ml of slurry and centrifuging at 500 g for 5 min. The supernatant was decanted and washed twice. 100 µl of beads was mixed with the CRBP-IV protein sample and allowed to incubate overnight (at 4°C), using gentle end over end rotation (Hybaid Shake'n'Stack 6241: Thermo Fisher Scientific). The following day the mixture was allowed to sediment after centrifuging at 500 g for 5 min. The supernatant was then carefully decanted and retained. Binding buffer (5 mls) was added to Gluthathione Sepharose 4B (1 ml) and inverted to promote mixing. The mixture was centrifuged at 500g for 5 min and the supernatant was collected (wash 1). The washing and centrifugation processes were repeated three times to produce three washes. The bound protein was eluted from the beads by mixing glutathione sepharose 4B slurry (1 ml) with Elution buffer (0.5 ml: 50mM Tris-HCL, 10 mM glutathione, pH 8.0). The mixture was incubated at room temperature for 10 mins by gentle end over end agitation (Hybaid Shake'n'Stack 6241: Thermo Fisher Scientific). The medium was then sedimented after centrifugating at 500 g for 5 min. The collected supernatant contained the eluted protein (eluent 1). The process was repeated a further two times to produce eluent 2 and 3. The protein concentrations of the supernatant, the three washes and three elutions were checked by Bradford assay (Section 2.2.4.2), and the sample purity determined by western blot (Section 2.2.4.3.).

Following this, I purchased CRBP-IV (Abnova), that had been commercially purified to remove the GST tag. The purity (checked by western blot) using GST antibody (G7781: Sigma) was used at 1µg/ml concentration. According to the ExPASy tool (www.expasy.org), the isoelectric point of CRBP-IV protein is 7.07, and so the expected optimum pH for binding would be between pH 3.5- 7.0. CRBP-IV stock solution (7.33 µM) was diluted with the sodium acetate buffers (10 mM) at pH 4 - 6.5 to generate 1.5µM solution. Using the Biacore T200 pH scouting wizard, the pH buffer at which the maximal number (as determined by the equation in section 5.2.3.3) of response units (RU) for immobilisation of CRBP-IV to the CM5 chip was chosen for future experiments.

Finally, I attempted to couple the CRBP-IV- GST tagged protein (Abnova, Taipei City, Taiwan) to the CM5 chip. The isoelectric point of this GST tagged protein was 7.74 (www.expasy.org). Therefore the expected optimal pH for binding of the protein to the chip would be between pH 3.5 – 7.7. Stock CRBP-IV- GST tagged protein (8.7 μ M) was diluted in sodium acetate (10 mM) at pH 3.6- 5 to generate 0.87 μ M solutions. Using the immobilisation pH scouting wizard (Section 5.2.3.4) in the Biacore T200, the pH buffer at which the maximal number (as determined by the equation in section 5.2.3.3) of response units (RU) for immobilisation of CRBP-IV-GST to the CM5 chip was chosen for future experiments.

5.2.3.8.7 Preparing for CRBP-IV Protein Capturing onto the CM5 chip

Using the equation in Section 5.2.2.3:

For a R_{max} =100 with retinol (286 daltons) as the ligand and CRBP-IV-GST (41kDa) as the protein :

$$100 = 0.286/41 \times R_L \times 1$$

$$100 = 0.00698 R_L$$

$$R_L = 14347.2 \text{ RU}$$

The molecular weight of CRBP-IV-GST = 41kDa and the molecular weight of small molecule retinol=0.286kDa and R_{max} =100. As was in the case of CRBP-I-GST, corrections were also made for possible contributions of the large GST tag to the overall binding seen with the CRBP-IV-GST tagged protein.

5.2.3.8.8 Transthyretin

RBP4 is a small protein (21 kDa) that is a transporter of retinol (Saari, Futterman et al. 1978). Because of its small size, it can be easily filtered by the kidneys and removed from circulation (Quadro, Blaner et al. 1999). During circulation, *holo* RBP4 binds to TTR and this increases the size of the complex preventing it from being removed by the kidneys (Monaco 2000).It would be useful to determine whether binding of RBP4/retinol complex

would bind to TTR coated chip. In addition, I would like to investigate whether CRBP-I and CRBP-IV alone or in complex with retinoid ligands can bind to TTR.

As a result, I attempted to couple the TTR protein (Sigma Aldrich Company Ltd), to a CM5 chip. The isoelectric point of this protein was 5.17 (www.expasy.org).

Stock TTR protein (100 μ M) was diluted in sodium acetate buffers (10 mM) at pH 3.5- 5.6. to produce a 20 μ M solution. As before, the pH condition at which the maximal binding response (RU) was observed was chosen for binding of TTR to the chip in future experiments.

5.2.3.8.8.1 Preparing for TTR protein capturing onto CM5 chip

Using the equation in Section 5.2.3.3:

For a $R_{max} = 100$ with retinol (286 daltons) as the ligand and TTR (55kDa) as the protein :

$$100 = 0.286/54 \times R_L \times 1$$

$$100 = 0.0052 R_L$$

$$R_L = 18881 \text{ RU}$$

Using the formula above, in order to achieve $R_{max} = 100$, the CM5 chip would need to be immobilised with 18,881RU of TTR protein.

5.2.3.7.5 Biacore T200 procedure

The CM5 sensor chip and HBS-EP buffers ($\pm 1\%$ DMSO) were allowed to equilibrate to room temperature. The samples and DMSO correction controls were kept on ice. The CM5 sensor chip was inserted into the machine. The T200 was then primed with running buffer and temperature for interactions set at 37°C. The automated protein immobilisation wizard which was

developed in section 5.2.2.4 was initiated to produce covalent coupling of the protein to the CM5 chip surface. The method defined the flow cell (FC1-4), the contact time with protein (420s), the flow rate (10 μ l/min) and a dissociation time of 600 seconds (Section 5.2.3.4).

Before inserting the samples made in 1%DMSO, the running buffer was changed to HBS-EP + DMSO and the system primed. The T200 wizard was again used to set up a binding interaction analysis. The ligand and DMSO correction samples were loaded into the reagent rack (as defined by software) and the protocol was run. Solvent correction was carried out for each experiment using an appropriate DMSO range (0.5-1.8%). There was no carry over in these interactions between cycles and this step was removed from the wizard.

5.2.3.9 Analysis of SPR data

Surface Plasmon Resonance data was analysed using the Biacore T200 Evaluation software. The software package performed solvent corrections for each experiment, reviewed the baseline binding levels, compared binding responses to the reference chip, monitored binding stability and carry over. In addition, the software also helped in formatting a best fit curve and kinetics analysis where appropriate.

The Biacore systems determine the binding affinity in three independent ways: calculation from kinetic constants, measurement of steady-state binding levels and determination of affinity in solution.

5.3 Results

In this chapter, I attempted to answer the question of CRBP-I and CRBP-IV protein functionality within ESFTs by performing protein modulation experiments as well as investigating the direct binding with ligands (by SPR).

5.3.1 Protein Modulation experiments

5.3.1.1 Viable cell number of ESFTs in Accell media

Experiments performed using siRNA to decrease expression of a target protein required the ESFTs to be cultured in Accell media (serum free). It was important to determine what contribution this media would make to cell viability prior to its treatment with the siRNA.

These experiments were performed in RDES, SKES-1 and SK-N-MC cells lines. A growth curve for these cells in Accell media was produced over 0-96h. The mean viable cell number was plotted as a percentage of the total number of cells at 0h. All three cell lines demonstrated increasing cell death with increasing time in Accell media. The viable cell number decreased most between 72-96 h. After 72 h, the mean viable cell number for RDES, SKES-1 and SK-N-MC were $52.7 \pm 2.5\%$, $56.7 \pm 3.8\%$ and $50.8 \pm 4\%$ respectively (Mean \pm Std). However, at 96 h, they had decreased to $20.9 \pm 2.5\%$, $16.3 \pm 5.1\%$ and $25.5 \pm 2.2\%$. Future experiments will be maintained in Accell media for a maximum of 72 h, before transferring into cell specific media (Figure 5.1).

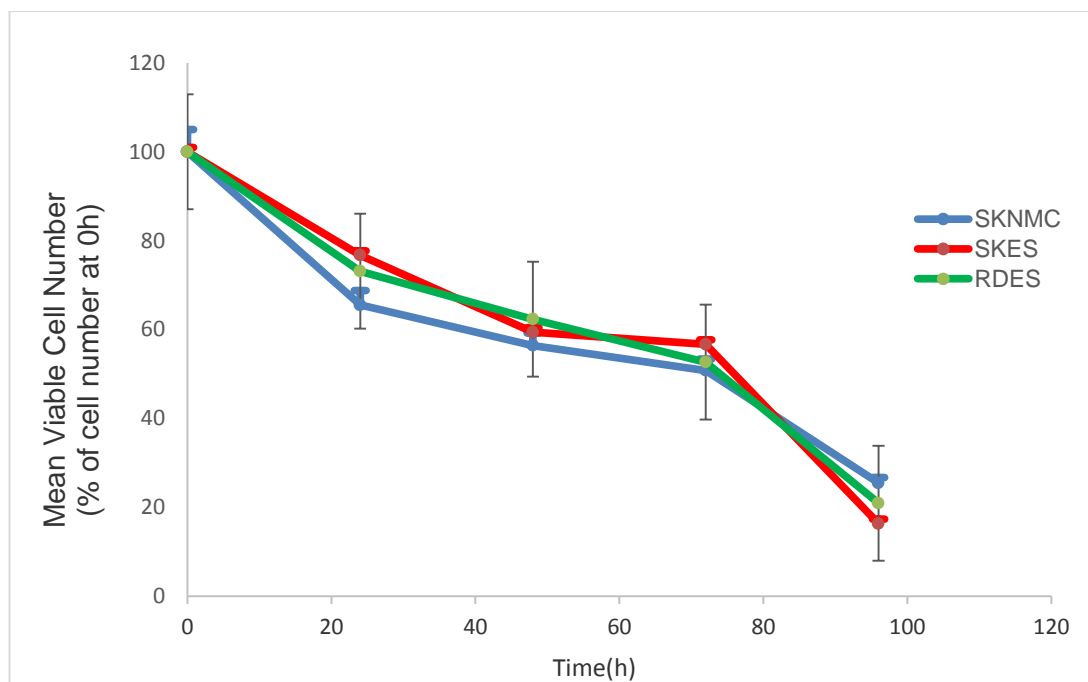


Figure 5.1. Effect of fenretinide on the viable cell number of SK-N-MC cells treated with siRNA for CRBP-I and scrambled control. These cells were treated with fenretinide (0-10 μ M) for 24 h. results are expressed as the mean \pm STD. The data was statistically analysed and the p value was not significant ($p = 0.22-0.79$) ($n=3$).

5.3.1.2 RNAi to knock down CRBP-I expression in ESFTs

Accell CRBP-I siRNA was used to knockdown CRBP-I protein expression in RDES, SKES-1 and SK-N-MC cell lines.

The RDES cells were treated CRBP-I siRNA over 72 h and demonstrated a decrease in CRBP-I mRNA after 48 and 72 h of treatment. At 48 and 72 h, the level of mRNA knockdown were similar in magnitude (84% and 88% respectively). When cell viability was investigated, it appeared that treating with siRNA for 72 h, the reduction of CRBP-I mRNA and protein were optimal (Figure 5.2). CRBP-I protein levels in the RDES cells were decreased to 35% of that of the control (measured by western blotting and densitometry) (Figure 5.3). Expression of the CRBP-I mRNA in both the SKES-1 and SK-N-MC cell lines (72 h) was reduced to 26% and 30% of that of the control cells respectively (Figure 5.2). It was not possible to confirm protein knockdown in the SKES-1 cells due to unequal loading of the blot with SKES-1 protein from both the scrambled and the target siRNA treated.

However, protein knockdown in the SK-N-MC cells were confirmed as being at 19% of that of the control (Figure 5.3).

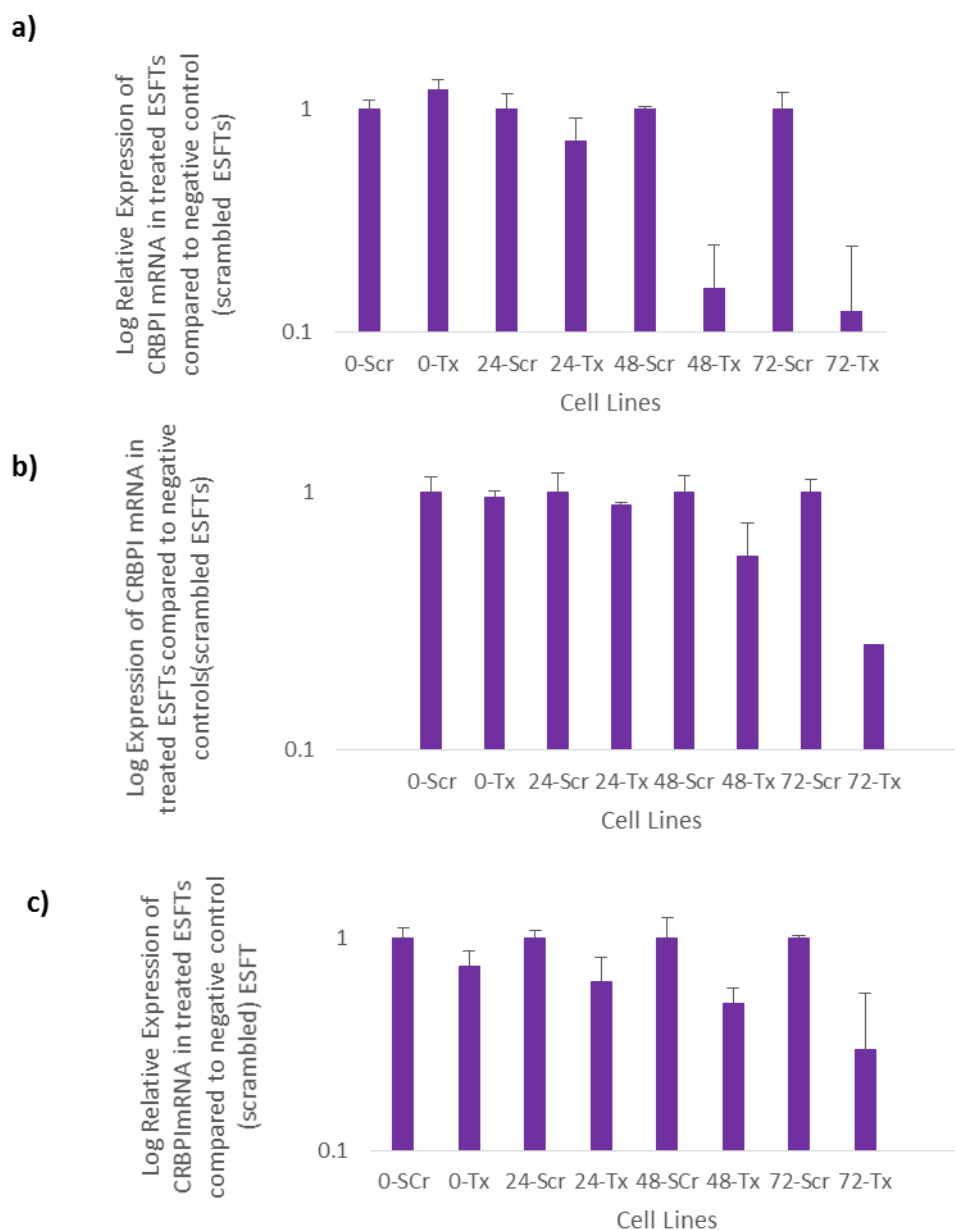


Figure 5.2 RTqPCR to detect CRBPI mRNA in **a)** RDES, **b)** SKES-1 and **c)** SK-N-MC cell lines that had been treated with CRBPI siRNA or scrambled siRNA (negative control) over a time course of 0-72 h. Results are shown as the mean \pm STD (n=2). 0, 24, 48 and 72= hours of treatment with siRNA. Scr= scrambled siRNA; Tx= target siRNA. (n=3)

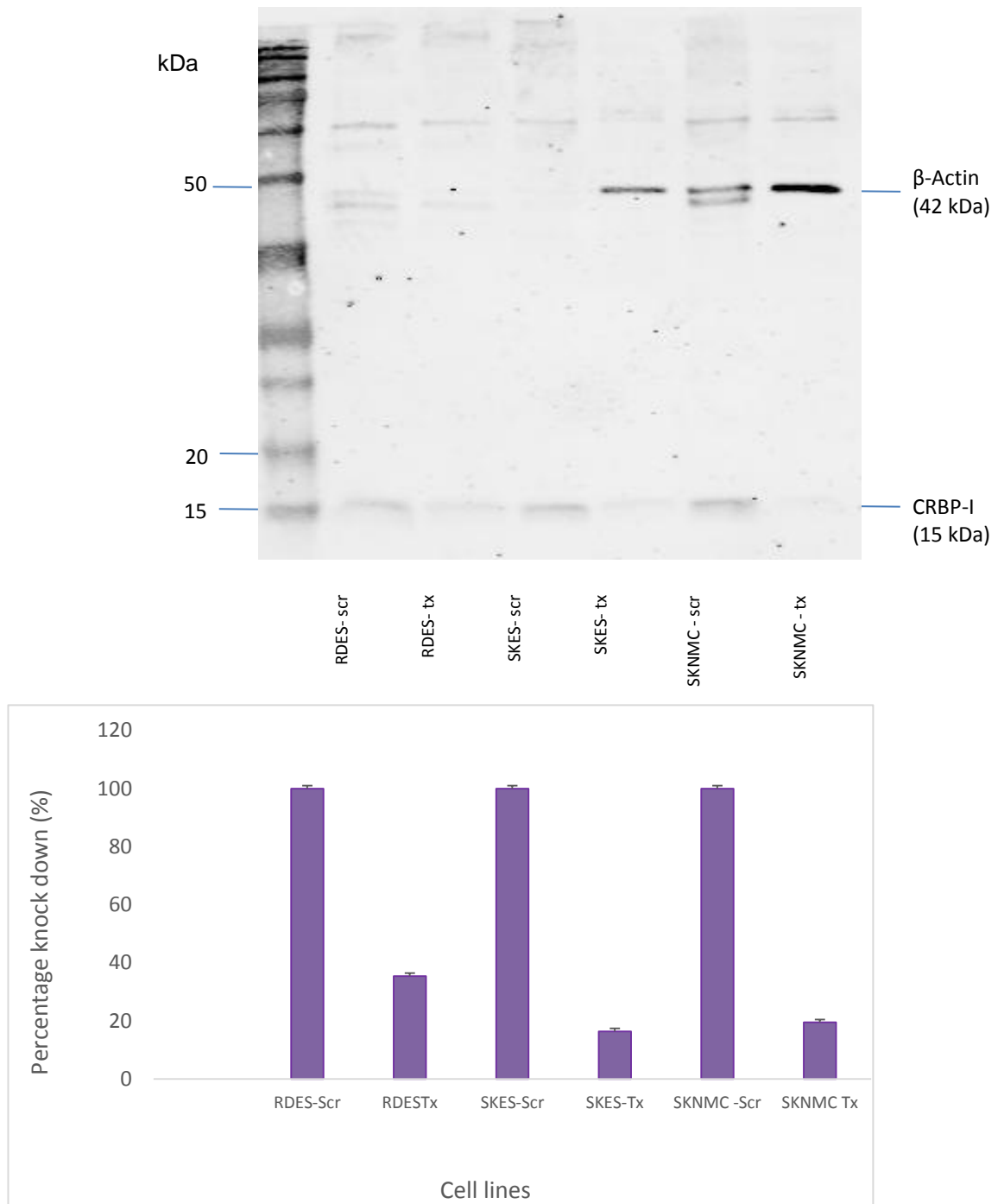


Figure 5.3 CRBP-I protein expression in cell lines (RDES, SKES-1 and SK-N-MC cells treated with CRBP-I siRNA in Accell media). The level of protein expression was quantified by densitometry (as shown in the red boxes) of the CRBP-I band relative to the loading control β - Actin to account for variability in loading. Scr=scrambled siRNA; Tx= treated with CRBPI siRNA (n=3).

5.3.1.3 Expression of retinol binding proteins in cells treated with CRBP-I siRNA

When the SK-N-MC cells were treated with CRBP-I siRNA, there was a decrease in mRNA and protein levels (Figure 3.2 and Figure 5.3). The specificity of this knockdown was confirmed by examining the expression of the other CRBPs (RBP4, CRBP-II, CRBP-III and CRBP-IV) by western blot. This demonstrates that although there is a decrease in CRBP-I protein content (Figure 5.4), the expression of RBP4 (Figure 5.5a), CRBP-II (Figure 5.5b), CRBP-III (Figure 5.5c) and CRBP-IV (Figure 5.5d) proteins remains unchanged in the SK-N-MC cells.

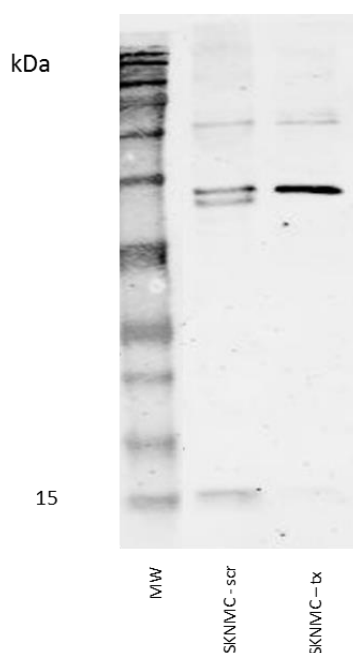


Figure 5.4 The knock-down of CRBP-I protein in SK-N-MC cells.

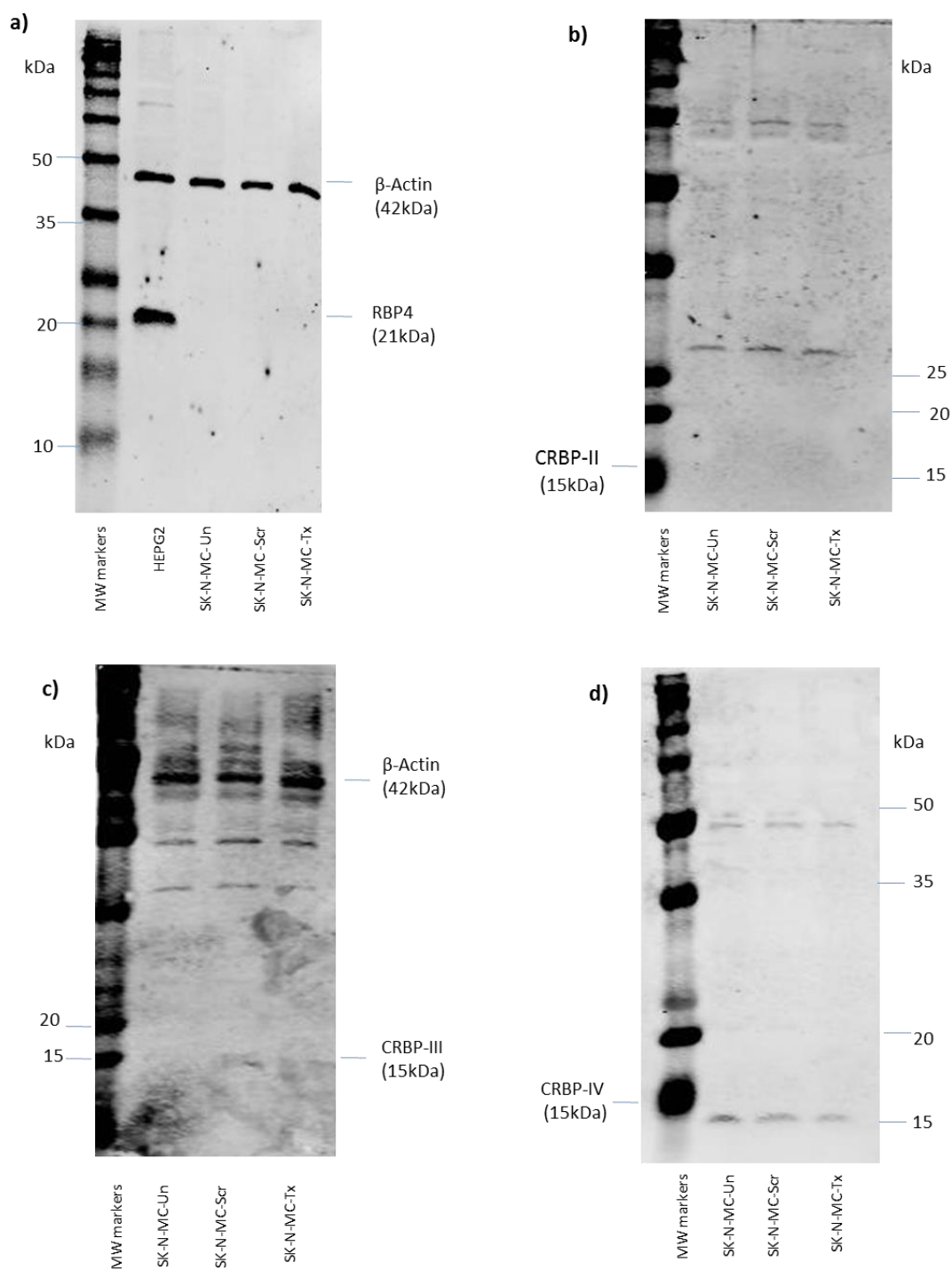


Figure 5.5 Expression of complementary CRBPs a) RBP4, b) CRBP-II, c) CRBP-III and d) CRBP-IV proteins by western blot, in SK-N-MC cells that have been treated with CRBP-I siRNA. (n=2).

5.3.1.4 Effect of fenretinide on SK-N-MC viable cell number (with reduced CRBP-I protein)

SK-N-MC cells in which CRBP-I had been decreased using target and scrambled siRNA were then treated with 4-hydroxy (phenyl) retinamide (0-10 μM). After 24 h the cells were harvested (Section 2.2.1) and the viable cell number counted (Section 2.2.2). There was no significant difference in the effect of 4-hydroxy (phenyl) retinamide on the viable cell number of the CRBP-I siRNA treated cells when compared to those treated with scrambled siRNA. The maximum treatment with fenretinide (10 μM) decreased viable cell number to $13 \pm 1.2\%$ (mean \pm STD) in SK-N-MC cells treated with CRBP-I siRNA and $17 \pm 0.76\%$ (mean \pm STD) in cells treated with scrambled siRNA (control) (Figure 5.6).

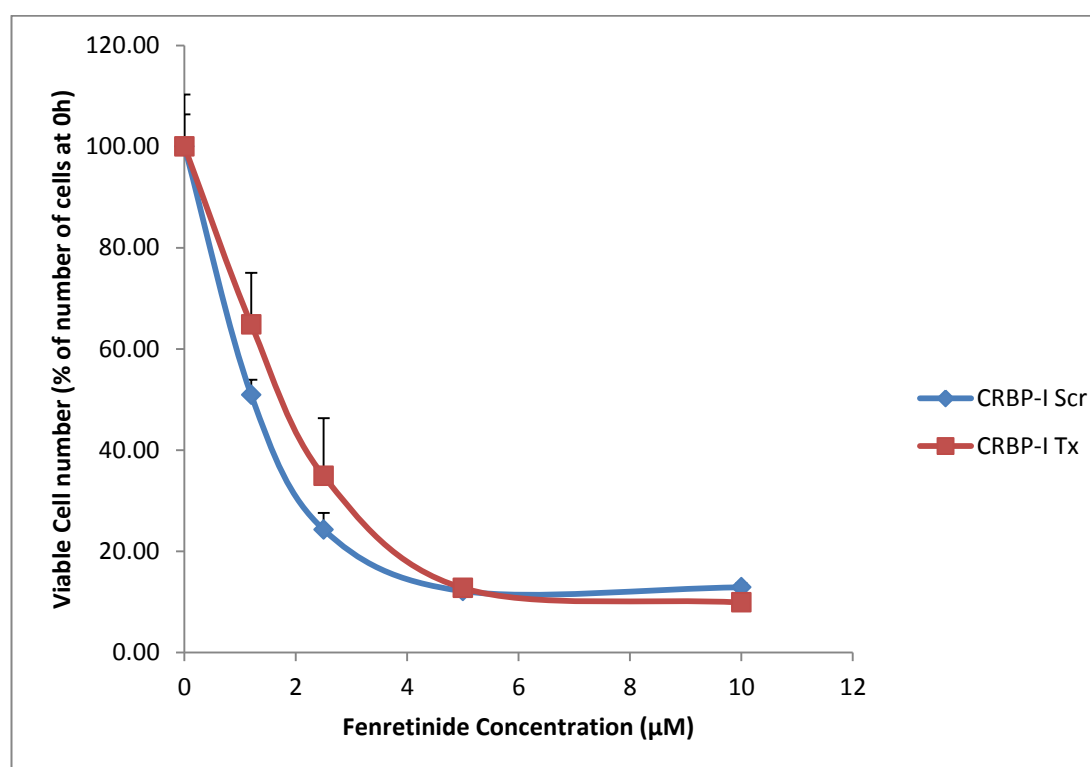


Figure 5.6 Effect of fenretinide on the viable cell number of SK-N-MC cells treated with siRNA for CRBP-I and scrambled control. These cells were treated with fenretinide (0-10 μM) for 24 h. results are expressed as the mean \pm STD. The data was statistically analysed and the p value was not significant ($p = 0.22-0.79$) ($n=3$).

5.3.1.5 Effect of fenretinide treatment on expression of CRBP-I protein

In order to establish whether levels of CRBP-I were modified by fenretinide, I treated RDES and SK-N-MC cell lines with 4-hydroxy(phenyl)retinamide for varying times (0-48 h), and the CRBP-I protein expression examined by western blotting. The protein loading was assessed using β -Actin, and densitometry then used to quantify relative expression. CRBP-I levels were normalised to the CRBP-I expression at 0 h. Relative expression of CRBP-I in the RDES cells varied between 40.7- 106 % the level found in RDES at 0 h of treatment. RDES cells treated for 8 h with fenretinide had the lowest levels of CRBP-I (40%) while those treated for 24 h showed the highest level (106%) (Figure 5.7).

The relative CRBP-I protein content in the treated SK-N-MC cells varied between 22 – 150%. Those cells that had been treated for 2 hours had the highest content of CRBP-I(150%), followed by those that had been treated for 24 hours(89%). The SK-N-MC cells that had been treated for 48 hours had the lowest levels of CRBP-I (22%). There did not appear to be any obvious trends in CRBP-I levels with fenretinide treatment in the ESFTs. (Figure 5.7)

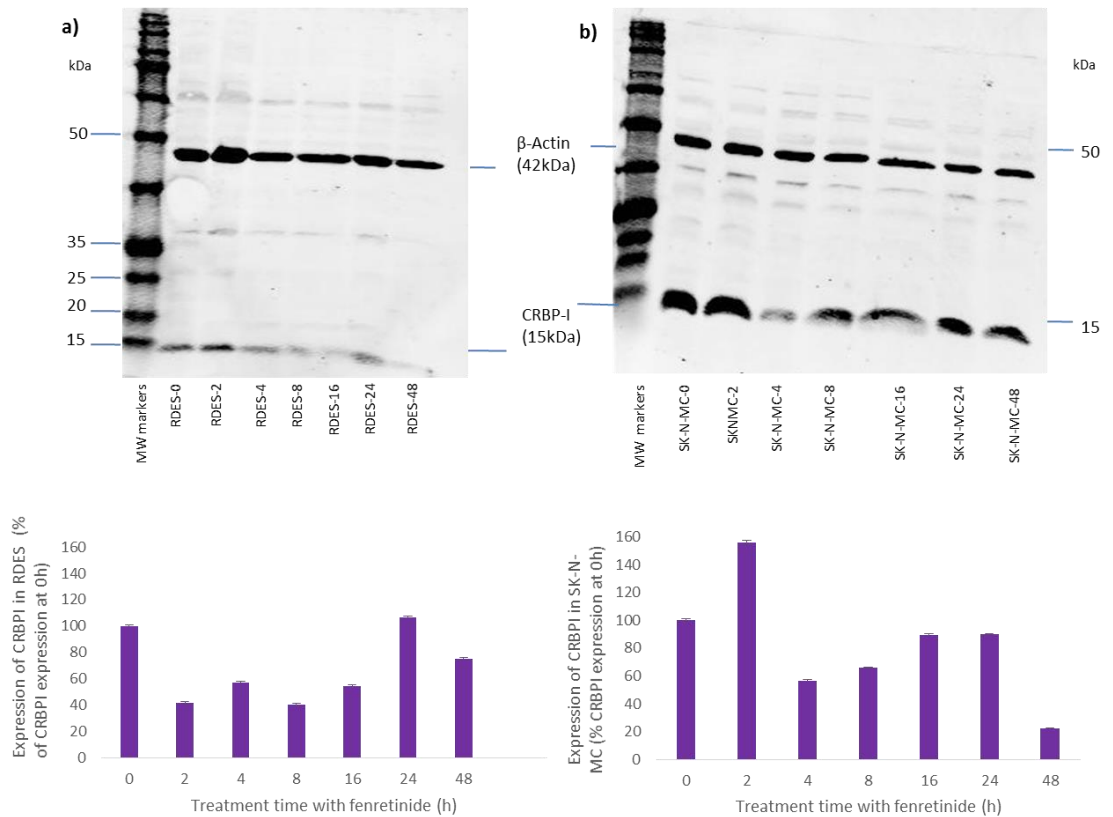


Figure 5.7. CRBP-I protein expression in **a)** RDES and **b)** SK-N-MC cell lines that have been treated with fenretinide over a time course of 0-48 h. The CRBP-I protein was expressed as a percent of the CRBP-I protein at 0h treatment. The level of protein was quantified by densitometry and corrected for β -Actin loading (n=2). MW=molecular weight

5.3.1.6 Sub-cellular expression of CRBP-I in SK-N-MC cells

The subcellular localisation of CRBP-I was examined in SK-N-MC cells after treatment with CRBP-I or scrambled siRNA (negative control). Using western blots, CRBP-I protein was found localised to the intra-cellular fraction of the control cells and this was consistent with published literature (Kane, Folias et al. 2011) (Figure 5.8).

After knockdown of CRBP-I by RNAi, CRBP-I protein was detected in the intra-cellular and the membrane fraction of the cells.

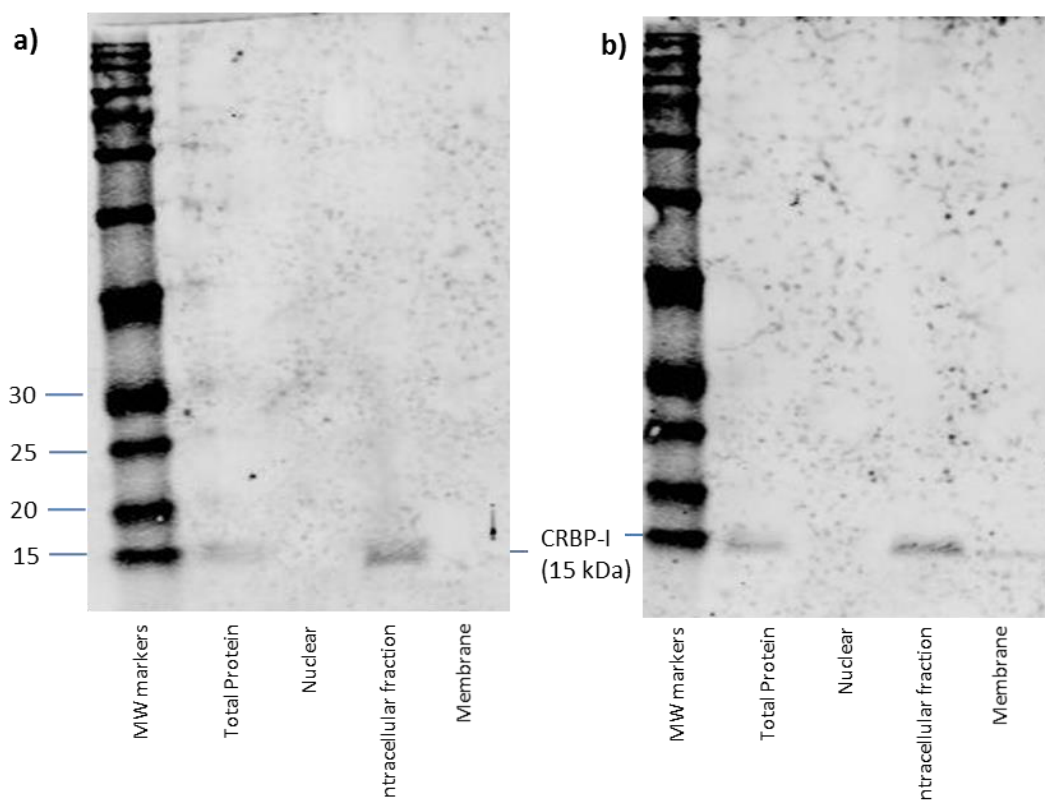


Figure 5.8 Subcellular fractionation of SK-N-MC cells treated with **a)** scrambled siRNA(control) and **b)** CRBP-I siRNA. Western blot to detect CRBP-I protein in various sub-compartments of the SK-N-MC cells. * = air bubble

5.3.2 CRBP-IV

5.3.2.1 RNAi to knockdown CRBP-IV expression in ESFTs

Accell CRBP-IV and scrambled siRNA (negative control) was used to decrease expression of CRBP-IV protein in RDES, SKES-1 and SK-N-MC cell lines.

The RDES cells were treated for 72 h and demonstrated the largest decrease in CRBP-IV mRNA was found after 24 h of treatment (to 22% of CRBP-IV level in the control). The knockdown was transient in this cell line, and partial recovery already evident at 48 h of treatment. It appeared that treating RDES cells with CRBP-IV siRNA for 24 h gave the largest decrease in the mRNA level (Figure 5.9). CRBP-IV protein levels were also decreased

to 52% of the control when measured by western blotting (quantified by densitometry).

Expression of the CRBP-IV mRNA in the SKES-1 also demonstrated a transient knockdown, with the largest decrease down to 42% of that of the control cells at 24 h of treatment. Western blotting also revealed (after 24 h of treatment), that there was a reduction in CRBP-IV protein level (35%) when compared to the cells treated with the control siRNA (Figure 5.10).

The CRBP-IV mRNA in the SK-N-MC cell lines at 72 h of treatment was reduced to 50% of the control cells. However, the protein knockdown in the SK-N-MC cells were confirmed as 65% of the scrambled control (Figure 5.10). This was determined by both western blotting and densitometry.

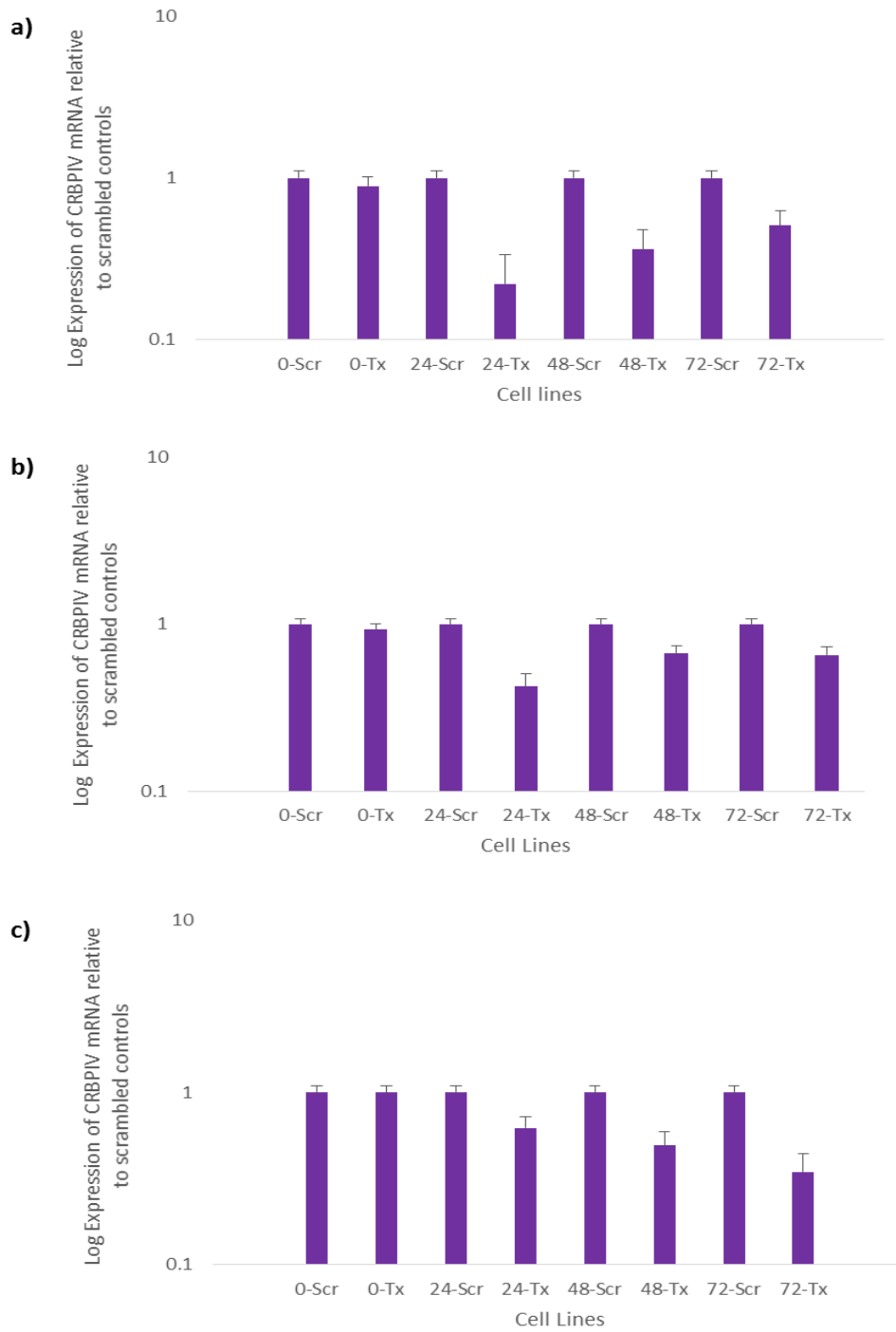


Figure 5.9 RTqPCR to detect CRBP-IV mRNA in **a) RDES**, **b) SKES-1** and **c) SK-N-MC** cell lines that had been treated with CRBP-IV siRNA over a time course of 0-72 h. The results for the cells treated with scrambled siRNA (Scr) and targeted siRNA (Tx) are shown. (n=3)

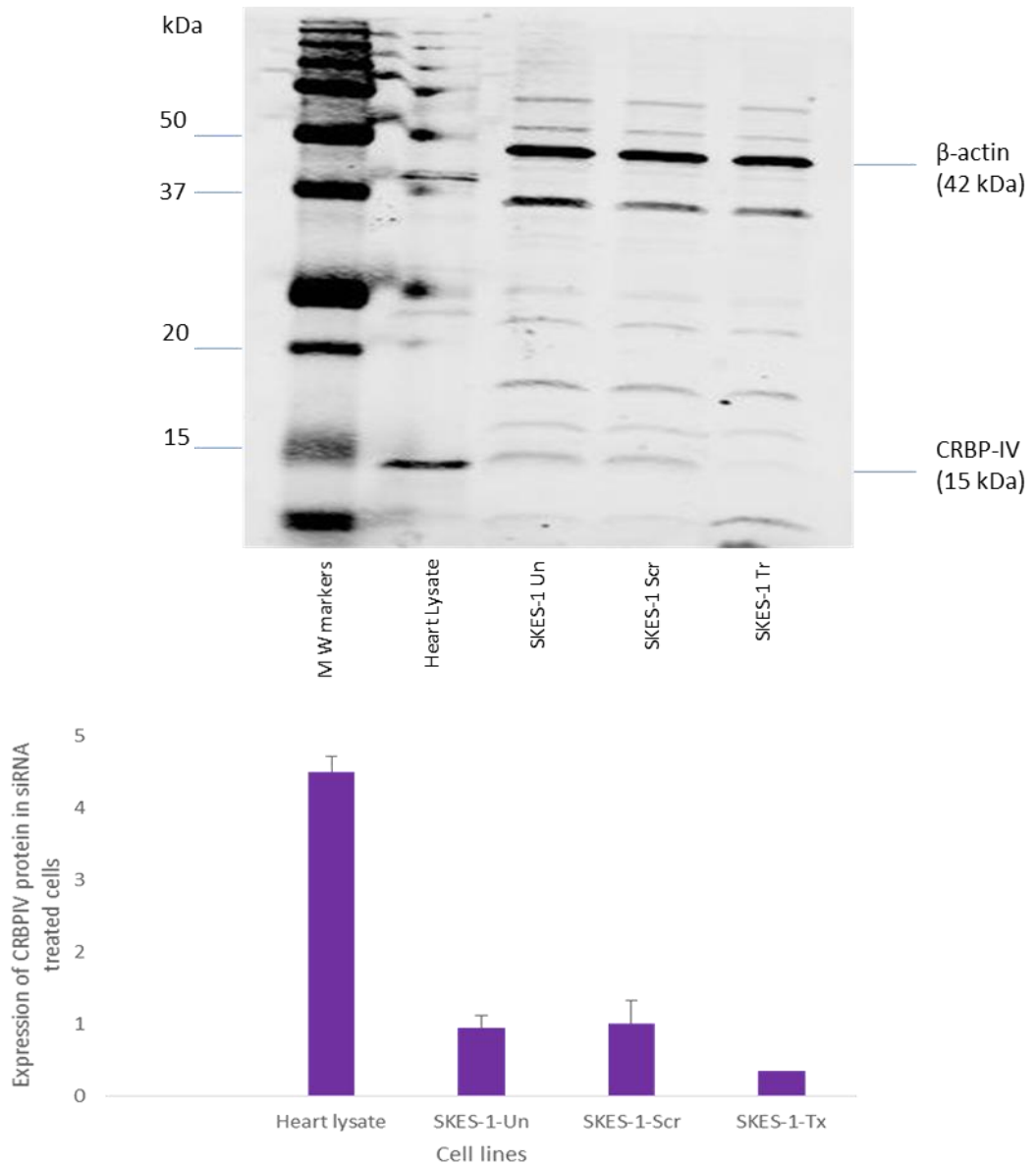


Figure 5.10 Western blot quantifying CRBP-IV protein in SKES-1 cells that have been treated with CRBP-IV siRNA. Densitometry was used to perform this quantification.

5.3.2.2 Expression of retinol binding proteins in cells treated with CRBP-IV siRNA

To establish whether the knockdown of CRBP-IV protein modulated the expression of other CRBPs (RBP4, CRBP-I, CRBP-II and CRBP-III), I examined the expression of these proteins using western blot. When CRBP-IV protein level was decreased in SKES-1 cells (Figure 5.9), the expression of RBP4 (Figure 5.11a), CRBP-I (Figure 5.11b), CRBP-II (Figure 5.11c) and CRBP-III (Figure 5.11d) proteins remains unchanged in the SKES-1 cells.

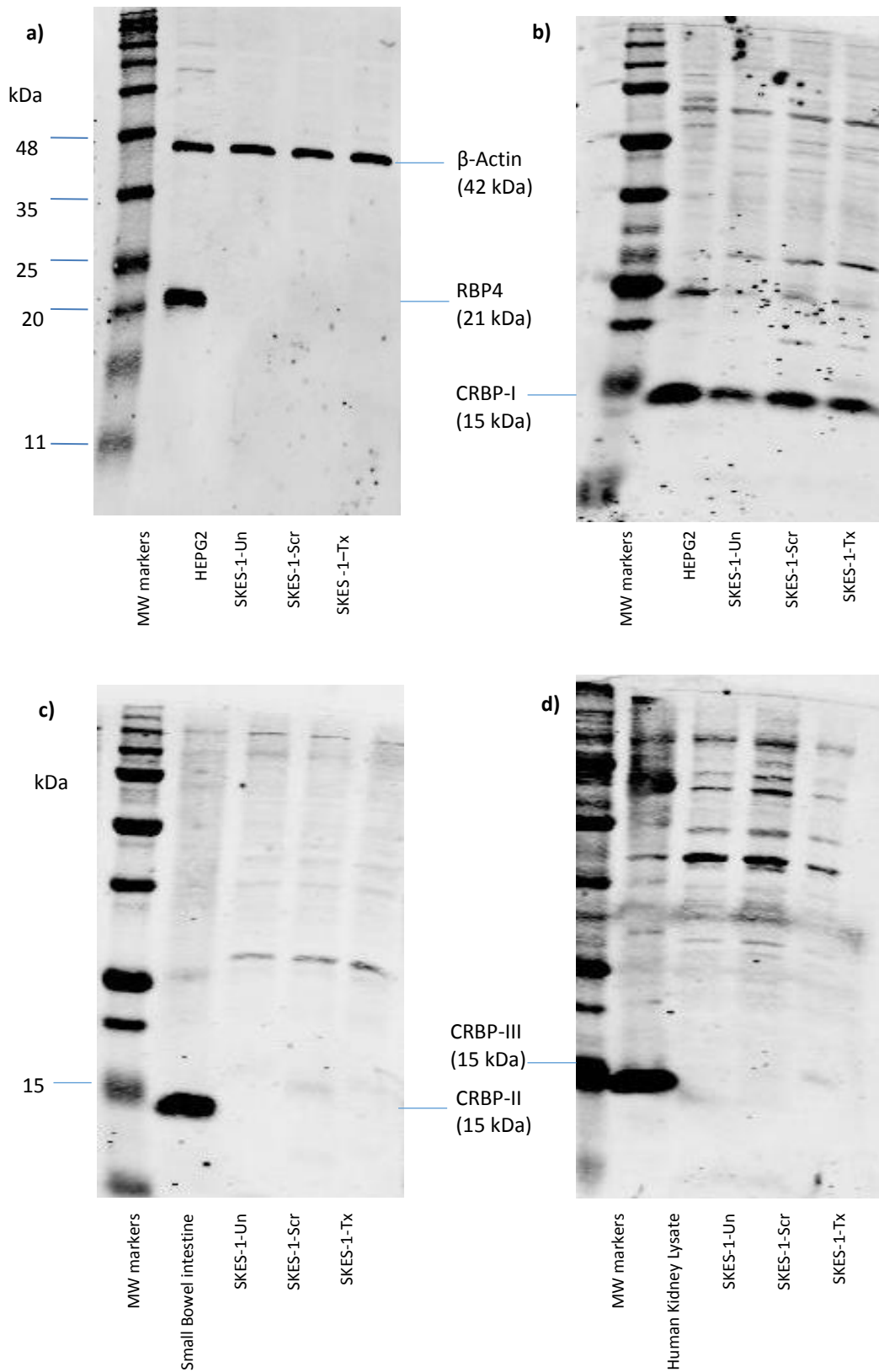


Figure 5.11. Expression of complementary CRBPs **a)** RBP4 protein **b)** CRBP-I **c)** CRBP-II and **d)** CRBP-III proteins by western blot, in SKES-1 cells that have been treated with CRBP-IV siRNA (n=3).

5.3.3.3 Effect of fenretinide on SKES-1 viable cell number (with reduced CRBP-IV protein)

SKES-1 cells were treated with CRBP-IV and scrambled siRNA for 24 h. These cells were then treated with fenretinide (4-hydroxy (phenyl)retinamide (0-10 μ M) for a further 24 h, and the viable cell number was counted (Section 2.2.2). There was no statistical difference in the cell's response to 4-hydroxy (phenyl)retinamide ($p=0.33$). The maximum concentration of fenretinide (10 μ M) decreased viable cell number to $20.1 \pm 7.2\%$ in SKES-1 (mean \pm STD) that had been treated with CRBP-IV siRNA and $21.4 \pm 4.8\%$ in SKES-1 cells treated with scrambled siRNA (Figure 5.12).

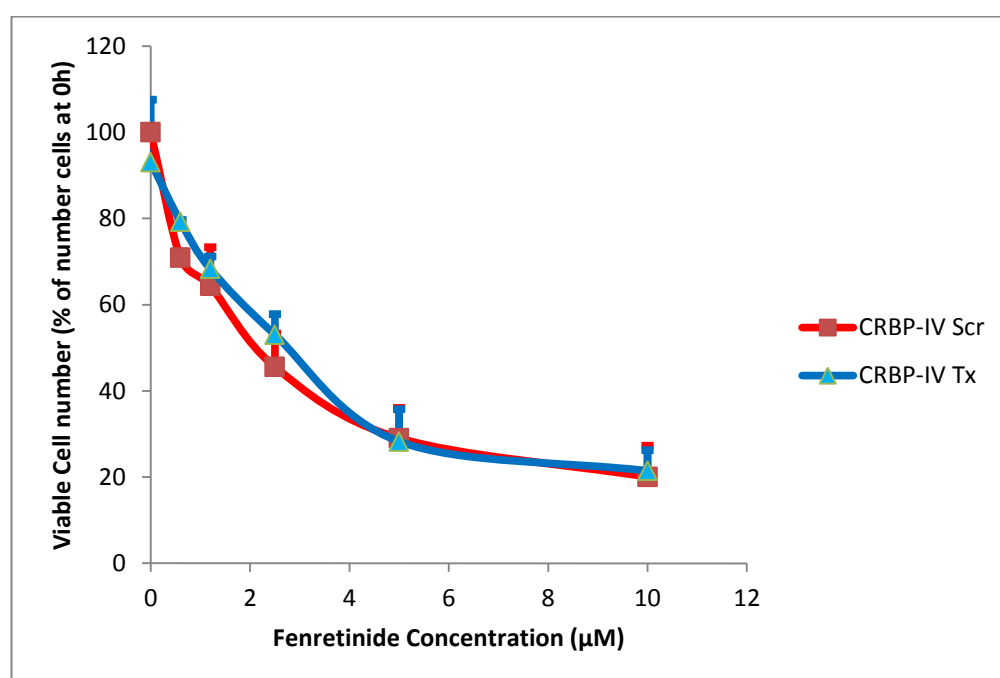


Figure 5.12 Effect of Fenretinide on the viable cell number of SKES-1 cells treated with siRNA for CRBP-IV and scrambled control for 24 h. These cells were treated with fenretinide (0-10 μ M) for 24 h. The results are expressed as the mean \pm STD. ($n=3$) The data was statistically analysed and the p value was not significant ($p =0.33$)

5.3.2.4 Effect of fenretinide on expression of CRBP-IV protein

In order to establish whether the level of CRBP-IV were modified by fenretinide, RDES and SK-N-MC cell lines were treated with 4-hydroxy(phenyl)retinamide over a time course (0-48 h) and the CRBP-IV protein expression then examined by western blotting. Protein loading was assessed using β -Actin and densitometry was used to quantify relative expression normalised to the CRBP-IV content at 0 h. CRBP-IV levels were expressed as a percentage of the CRBP-IV expression at 0h. The expression of CRBP-IV in the RDES cells varied between 16% and 52% (at 8h and 48 h respectively) of the level found in RDES which had not been treated (Figure 5.13). The CRBP-IV protein expression in the treated SK-N-MC cells varied between 22 % and 153% (at 48 and 2 h respectively) to that of the CRBP-IV levels at 0h of treatment with fenretinide. The CRBP-IV levels in cells treated for 24 h was almost identical to those cells not undergoing treatment. As in the case of CRBP-I, there did not appear to be any obvious trends in CRBP-IV levels with fenretinide treatment in the ESFTs (Figure 5.13).

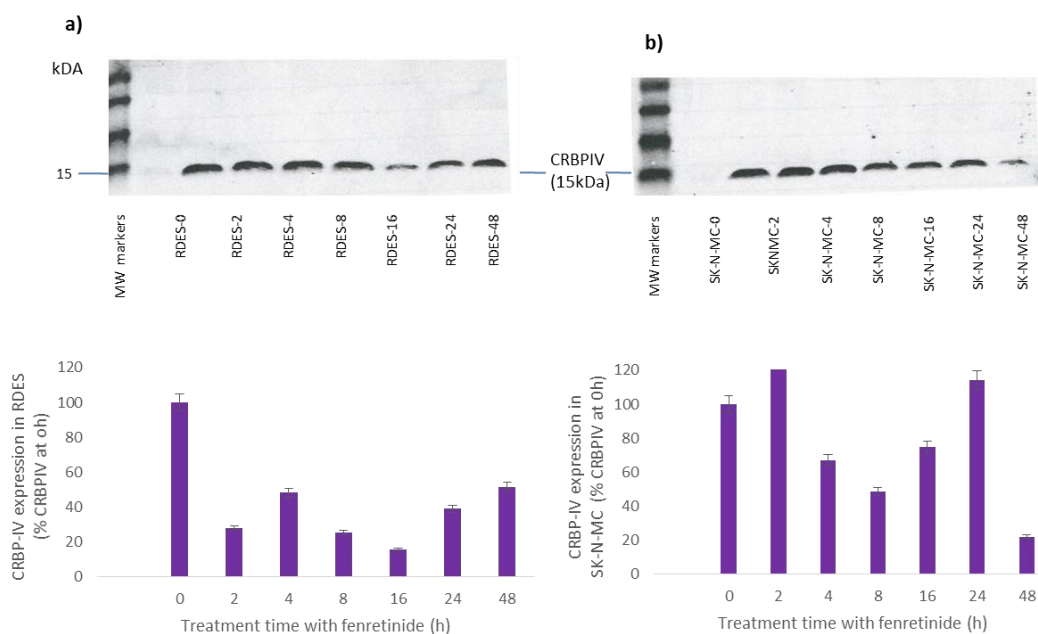


Figure 5.13. CRBP-IV protein expression in **a)** RDES and **b)** SK-N-MC cell lines that have been treated with fenretinide over a time course of 0-48 h. The CRBP-IV protein was expressed as a percent of the CRBP-IV protein at 0h treatment. The level of protein was quantified by densitometry (as measured in the red boxes) and corrected for β -actin loading. MW=molecular weight (n=2).

5.3.3 Demethylation of CRBPs

In many cancers cell lines, there have been reported silencing of CRBP-I and CRBP-IV proteins (Kane, Folias et al. 2011). This has been found to be as a result of hypermethylation of the CPG promoter regions in the corresponding genes. Some of these cancers have been shown to have altered vitamin A/ retinoid transport, metabolism and responsiveness. Lind et al has shown that by demethylating these genes (with 5-aza-2'-deoxycytidine), the cell lines can restart production of CRBP-I protein (Lind, Skotheim et al. 2006). Potentially, the induction of these cells to produce the CRBP proteins can also alter retinoid homeostasis and cause increased sensitivity to the retinoids. This theory can be extrapolated to CRBP-IV in the ESFTs. In particular, the TC-32 and TTC-466 lines which do not produce CRBP-IV protein, could be demethylated to manufacture this protein. This

would be particularly useful in order to determine whether this demethylation process can alter CRBP-I and CRBP-IV protein production in ESFTs and ultimately increase sensitivity to retinoids.

Effect of 5 aza-2'-deoxycytidine on viable cell number

SK-N-MC, SKES-1 and RDES were treated with 5 aza-2'-deoxycytidine in the concentration range of 0-10 μ M for 72 h (Lavelle, Sauntharajah et al. 2008). This highest treatment concentration of 5 aza-2'-deoxycytidine (10 μ M) decreased cell viable number (%) to $20.3 \pm 2.5\%$ (mean \pm STD) in RDES cells , $31.4 \pm 2.1\%$ in SKES-1 and $18.9 \pm 6.4\%$ SK-N-MC cells (Figure 5.14). Unfortunately, this reduced level of cell viability, and the sub-optimal conditions of the viable cells meant pursuing further experiments on these treated cells were of no benefit.

A reduced 5 aza-2'-deoxycytidine concentration range (0-2 μ M) in the TC-32 cell line was investigated but this also decreased viable cell number to $18 \pm 0.1\%$. This was similar to the results produced above and was therefore not of use in further experiments (Figure 5.14).

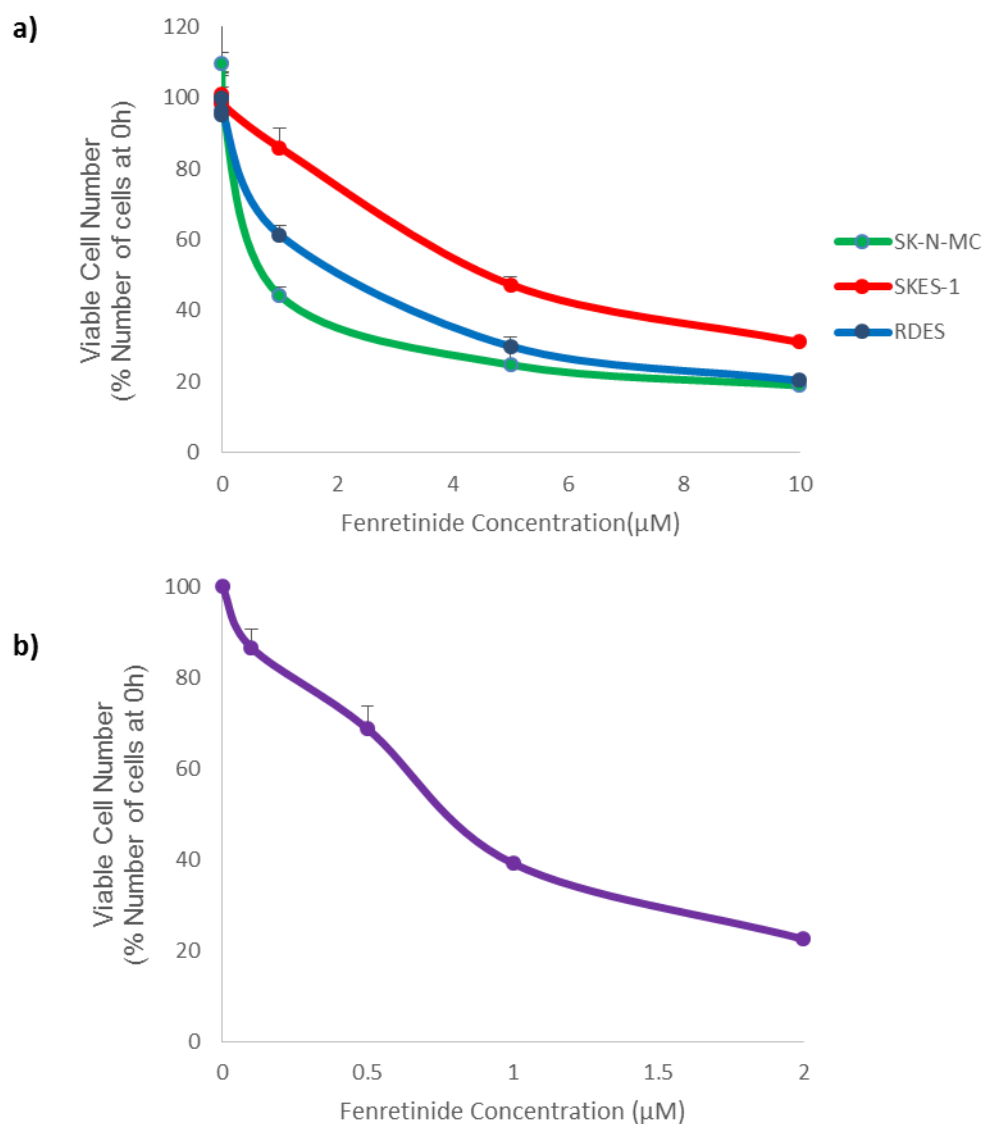


Figure 5.14 Effect of 5-Aza-2-deoxycytidine on the viable cell number of a) RDES, SKES-1 and SK-N-MC cells. These cells were treated with 5-Aza-2-deoxycytidine (0-10 μM) for 72 h; b) A reduced 5-Aza-2-deoxycytidine range (0-2 μM) was investigated in TC-32 cells. The results are expressed as the mean \pm STD. (n=4)

5.3.4 Surface Plasmon Resonance Preparation of a CM5 chip

Optimisation of RBP4 binding

The CM5 chip was chosen from among the other types of Biacore sensor chips, because this dextran coated chip allows proteins or peptides (that are not membrane associated) to be covalently coupled to it (www.gelifesciences). This chip has an isoelectric point (pI) 3.5 (REF), while the RBP4 protein has pI of 5.76 (www.ExPASy.com). The optimal pH for adherence of the protein to this chip would then be between these 3.5 and 5.76. There was no binding at pH < 4 or pH > 5 (results are not shown). The best condition for binding was at pH 4) (Figure 5.15).

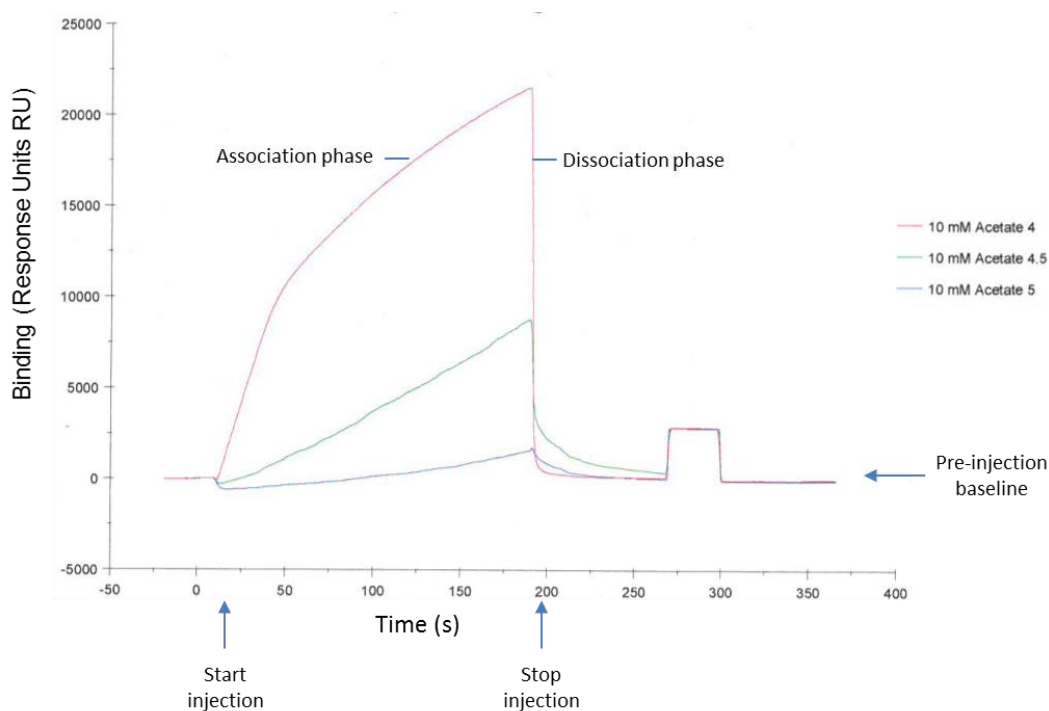


Figure 5.15. A binding profile of RBP4 protein onto a CM5 chip. Three RBP4 solutions at pH 4 (red), pH 4.5 (green) and pH 5 (blue) were injected over the CM5 chip, with the RBP4 pH 4 solution demonstrating the highest binding rate. The binding response is measured in response units (RU). One RU represents the binding of 1 pg of protein per square mm.

5.3.4.1 CRBP-I

The isoelectric point of CRBP-I protein (GeneTex GTX117328) is 4.99 (www.Expasy.com). The optimal pH binding conditions for this protein onto the dextran chip were determined by investigating interactions between pH 3.5 - 4.5. There was no binding observed under any of the evaluated conditions (Figure 5.16 a).

An alternative approach was therefore employed using a GST-tagged CRBP-I protein (Abnova : H00005947-PO1). The isoelectric point of this protein is 7.74. The optimal pH for binding of the protein to this dextran chip would be between pH 3.5- 7.7. The most successful binding condition was at and pH 4.5 (Figure 5.16 b). The attachment of the GST tag to this protein changed the isoelectric point of the protein and widened the range between the pI of the dextran chip and that of the tagged protein. This tag increased the affinity of the charged protein for the dextran coated chip (Costa, Almeida et al. 2014).

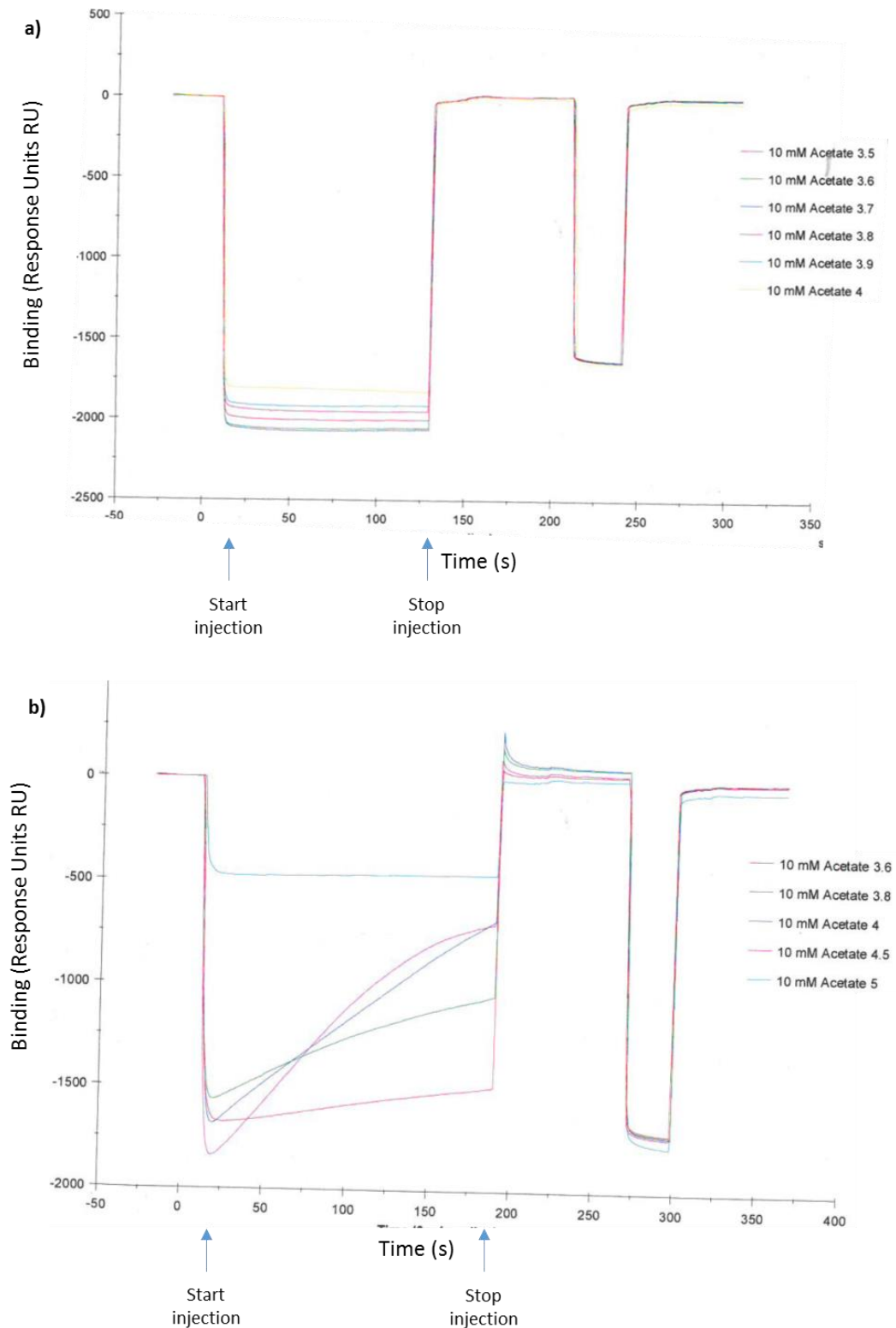


Figure 5.16. A binding profile of CRBPI protein onto a CM5 chip. a) Various CRBPI solutions at pH 3.5 (red), pH 3.6 (green), pH 3.7 (blue), pH 3.8 (pink), pH 3.9 (teal) and pH 4 (yellow) were injected over the CM5 chip, with no observed binding. b) this binding profile used CRBPI GST tagged protein and investigated pH conditions 3.6 (red), 3.8 (green), 4 (blue), 4.5 (pink) and 5 (teal). The optimal binding condition with this GST tagged protein was pH 4.5. The binding response was measured in response units (RU). One RU represents the binding of 1 μg of protein per square mm.

5.3.4.2 CRBP-IV

CRBP-IV protein was only commercially available with a GST-tag (Abnova H00116362-PO1). Attempts to cleave the GST tag from this protein using glutathione sepharose beads 4B was unsuccessful with the eluant not containing any measurable cleaved CRBP-IV protein.

Commercial cleavage was more successful and the isoelectric point of this untagged protein was 7.67. The expected optimal pH for binding of CRBP-IV protein to the chip would be between pH 3.5-7.5 (results not shown).

The isoelectric point of CRBP-IV-GST tagged protein is 7.74. I examined a range of pH conditions (pH 3.5-7.2) and concluded that the optimal binding pH is 4 (Figure 5.17).

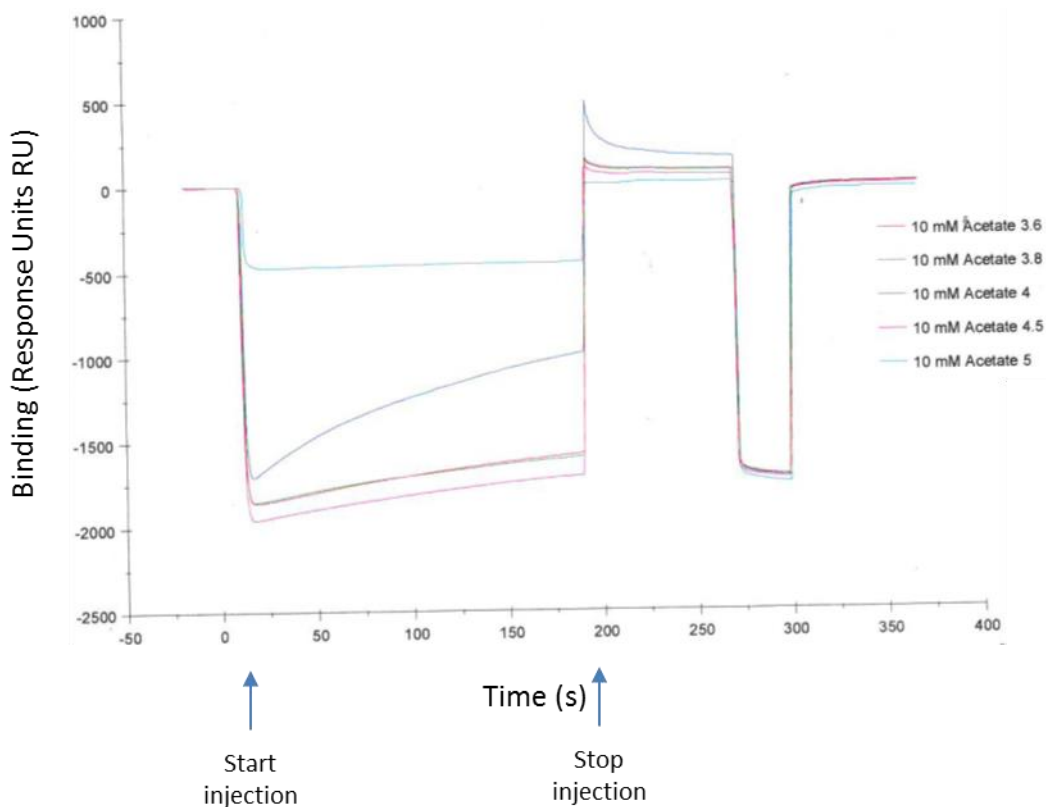


Figure 5.17. A binding profile of CRBP-IV protein onto a CM5 chip. Various CRBP-IV solutions at pH 3.6 (red), pH 3.8 (green), pH 4 (blue), pH 4.5 (pink) and pH 5 (teal) were injected over the chip, with the CRBP-IV pH 4 solution demonstrating the highest binding rate. The binding response is measured in response units (RU). One RU represents the binding of 1 pg of protein per square mm.

5.3.4.3 TTR

The isoelectric point of the transthyretin protein (Sigma: P1742) was 5.17. As a result, I would expect binding to the dextran chip to occur between pH 3.5-5. There was no binding at any of the pHs investigated in the above range (results not shown).

5.3.5. Optimisation of Ligand regeneration conditions

Ligand regeneration was optimised by evaluating reagent conditions: 1 mM NaCl, 10 mM Glycine pH 3.5, 10 mM Glycine pH 3, 10 mM Glycine pH 2.5 and washing with HBS-EP buffer for 600 s. The use of washes over an extended period (600 s) was sufficient to allow the small molecule to dissociate from the protein surface. Solvent corrections were performed for each protein and small molecule interaction, to compensate for any contributions to binding made by the DMSO vehicle.

Protein capture onto CM5 chip

The limit of protein capture was defined for each flow cell, using the immobilisation wizard in the Biacore T200 and the equations in Section 5.2.3.3. (Table 5.3).

Table 5.3. The level of protein captured (RU) on each of the four flow cells of the CM5 chips. Two separate CM5 chips (chip 1, chip 2) were coated for each protein. FC1 = flow cell 1; FC2= flow cell 2; FC3 = flow cell 3; FC4= flow cell 4.

Protein	Flow Cells	CM5 chip1	CM5 chip 2
RBP4	FC1	blank	Blank
	FC2- RBP4	2042	2680
	FC3- RBP4	2706	2539
	FC4- RBP4	2670	2679
CRBP-I	FC1	blank	Blank
	FC2-GST	2886	2763
	FC3-CRBP-I	4664	4376
	FC4-CRBP-I	4382	4484
CRBP-IV	FC1	blank	Blank
	FC2- GST	2168	2271
	FC3- CRBP-IV	4341	4422
	FC4- CRBP-IV	3886	4567

5.3.5.8 The binding affinities of RBPs

The interactions of RBP4 and retinamide small molecules

The small molecules (analyte) were prepared in 1% DMSO/HBP-ES (v/v), from which concentration ranges (0-100 μM) were produced. The samples were injected over the CM5 chip for 420 s at a flow rate of 10 $\mu\text{l}/\text{min}$. The 'off time' between successive injections of analyte was 600s.

The RBP4 retinol binding curves showed a maximal binding response as 17.9 response units (RU) at the concentration of 100 μM . The calculated $K_d = 105.2 \times 10^{-7}$ M. (95% C.I: 75-150 $\times 10^{-7}$ M; $R^2 = 0.89$) (Figure 5.18).

Fenretinide and RBP4 produced a saturated binding curve with a maximal binding response of 29.6 response units (RU) at 100 μM fenretinide. The estimated $K_d = 90.3 \times 10^{-7}$ M. (95% C.I: 43 – 110 $\times 10^{-7}$ M; $R^2 = 0.91$) (Figure 5.18).

The maximal binding response for RBP4 and 4-oxo fenretinide (100 μ M) was 13.7 response units (RU). The estimated $K_d = 287 \times 10^{-7}$ M. (95% C.I: 118 – 455.7 $\times 10^{-7}$ M; $R^2 = 0.97$). According to these calculations, 4-oxo fenretinide would bind to RBP4, but with a much lower affinity than retinol or fenretinide (Figure 5.18).

RBP4 and N-(4-aminophenyl) retinamide produced a binding curve with a binding response of 15.8 response units (RU) at maximal concentration (100 μ M). The estimated $K_d = 480 \times 10^{-7}$ M (CI :undefined). Given the low binding affinity, the wide confidence intervals and low R^2 value, it is unlikely that N-(4-aminophenyl)retinamide would bind to RBP4 (Figure 5.18).

The interactions between RBP4 and RF21 produced a linear, non-saturated binding curve with a maximal binding response of 5.4RU. The K_d could not be accurately calculated with wide confidence intervals and a low R^2 value. The prediction is that RF-21 would not bind to RBP4 (Figure 5.18).

The binding response between RBP4 and N-(4-methoxyphenyl) retinamide at maximal concentration (100 μ M) was 4.5 response units (RU). The estimated $K_d = 480 \times 10^{-7}$ M. (95% C.I : 60 – 1023 $\times 10^{-7}$ M; $R^2 = 0.88$). Given the low binding response and the low binding affinity with very wide confidence intervals, N-(4-methoxyphenyl)retinamide would not be predicted to bind to RBP4 (Figure 5.18).

1-adamantylamine is an organic molecule containing an adamantane backbone and an amino group substituted at one of the four methyne positions. Because of the shape of this molecule, it would not be expected to bind to RBP4 as the binding pocket cannot accept the bulky group. This interaction would be used as a negative control for RBP4 experiments. As predicted, there was no observed binding with a maximal binding response of 2.2RU (Figure 5.18).

A1120 is a non-retinoid RBP4 ligand which acts as a competitive inhibitor to displace retinol from RBP4, disrupting retinol-induced RBP4-TTR interaction, resulting in reduce serum RBP4 levels. In these experiments, A1120 samples produced a maximal binding response of 10.5 RU. $K_d = 6.2 \times 10^{-7}$ M (95% CI: 2.7- 9.7 $\times 10^{-7}$ M). This compound would bind with high affinity (greater than that of RBP4 and retinol) to RBP4 (Figure 5.18).

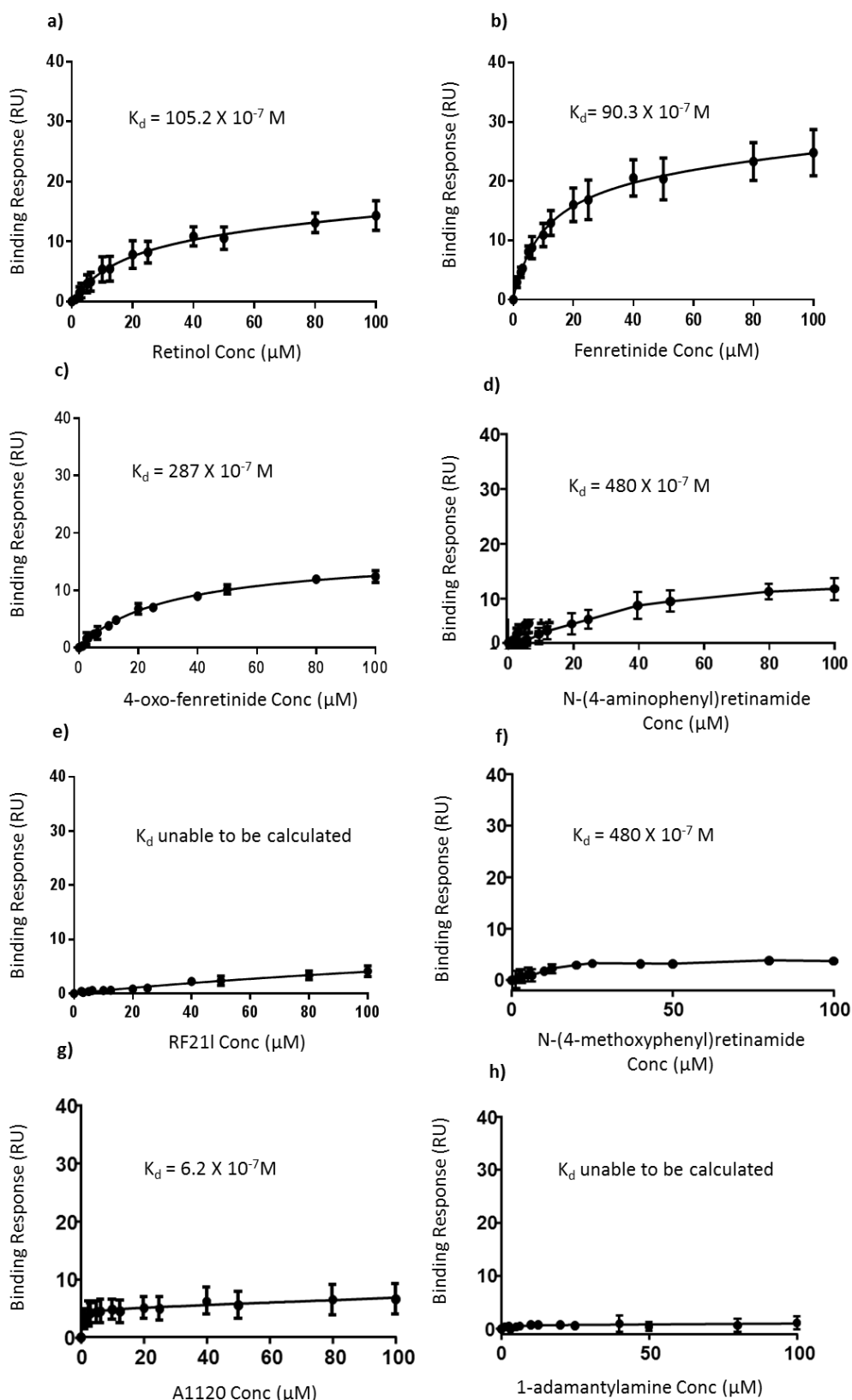


Figure 5.18 The interactions between RBP4 protein and retinoids and retinamides: **a)** retinol **b)** fenretinide **c)** 4-oxo-fenretinide **d)** N-(4-aminophenyl) retinamide **e)** RF21 **f)** N-(4-methoxyphenyl)retinamide **g)** A1120 **h)** 1-adamantylamine. The binding is measured in response units (**RU**) and further qualified by calculating the dissociation constant (K_d). The smaller the dissociation constant the greater is the binding affinity between RBP4 protein and small molecule.

The effect of TTR on the interaction of RBP4 and small molecules

Lyophilised transthyretin protein was dissolved to make 1 mM stock solution, from which a range of concentrations of TTR (0-160 μM) was produced. The binding curve demonstrated a maximal binding response (408.1RU) at the highest concentration of TTR (160 μM). The $K_d = 125 \times 10^{-7}$ M. The binding affinity was significantly different when compared to the affinity of RBP4 ($K_d = 105.2 \times 10^{-7}$ M) for retinol (t-test; $p = 0.000006 - 0.00000014$) (Figure 5.18). When varying concentrations of transthyretin (0-80 μM) and retinol (40 μM) were incubated together and injected over an RBP4 coated chip, the affinity of the TTR/ retinol mixture for the bound RBP4 was significantly greater ($K_d = 61.9 \times 10^{-7}$ M) than for retinol alone ($K_d = 105.2 \times 10^{-7}$ M) ($p = 0.0000002 - 0.001$). This was not so for TTR alone ($K_d = 125 \times 10^{-7}$ M) (t-test, $p = 0.17 - 0.42$). As the concentration of TTR/retinol increases, so does the binding response with a maximal binding response of 310 RU at the highest concentration of TTR/retinol (80 μM). Retinol therefore increases the binding response of TTR and RBP4 (Figure 5.19).

Similarly, varying concentrations of transthyretin (0-80 μM) and fenretinide (40 μM) were incubated and also injected over the CM5 chip. In this case, however, the affinity of the TTR/fenretinide mix for the bound RBP4 was significantly reduced ($K_d = 302.4 \times 10^{-7}$ M) when compared to fenretinide alone ($K_d = 90.3 \times 10^{-7}$ M) ($p = 0.00$). The maximal binding response of the TTR/fenretinide mixture was 183 RU at the highest concentration of TTR (80 μM). This data shows that fenretinide decreases the binding response of TTR and RBP4 (Figure 5.19).

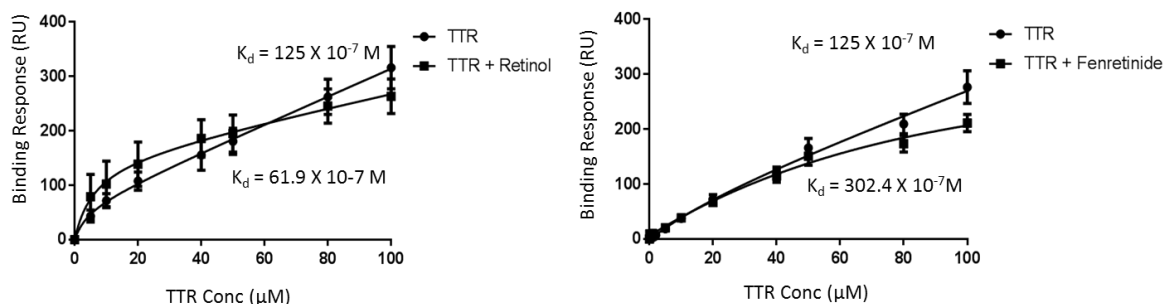


Figure 5.19 The effect of TTR on the interactions of RBP4 protein and **a)** retinol **b)** fenretinide The binding is measured in response units (RU) and further qualified by calculating the dissociation constant (K_d). The smaller the dissociation constant the greater is the binding affinity between RBP4 protein and small molecule.

5.3.5.2 The interactions of CRBP-I and retinamide small molecules

Retinol concentration range (0-100 μM) was prepared and injected over the CM5 chip. The binding curves showed a maximal binding response of 15.1 RU corresponding to that of retinol (100 μM) ($K_d = 0.99 \times 10^{-6} \text{ M}$) (Figure 5.20).

When fenretinide samples was injected, the binding appeared to be non-specific with a maximal binding response of 4.6 RU at a 50 μM concentration. The binding response ranged from 0.6 - 4.6RU and did not appear to be related to the concentration curve (n=4). Binding affinities could not be calculated and therefore (according to SPR) fenretinide would not bind to CRBP-I (Figure 5.20).

The interaction between 4-oxo fenretinide and CRBP-I showed a maximal binding response of 4.7 RU at a 4-oxo-fenretinide concentration of 100 μM (n=4). The binding curve demonstrated no interaction until a concentration of 50 μM 4-oxo-fenretinide had been reached. Although a K_d was calculated from this data, the confidence intervals were very wide and could not be defined. In addition, there was no confidence in the K_d , as the R^2 value was

extremely low ($R^2= 0.08$) and 4-oxo fenretinide would therefore not be expected to bind to CRBP-I (Figure 5.20).

N-(4-aminophenyl) retinamide demonstrated a concentration dependent binding response with a maximal response of 8.4RU (n=4). Although a K_d was calculated from this data, the confidence intervals were very wide and could not be defined. In addition, there was little confidence in the K_d , as the R^2 value was low ($R^2= 0.63$). This small molecule would not bind to CRBP-I (Figure 5.20).

The response of small molecule RF-21 was similar to that of 4-oxo fenretinide with a maximal binding of 2.8RU (n=5). The calculated K_d ($5.5 \times 10^{-6}M$) had wide undefined confidence intervals and demonstrated 'poor fit of data' ($R^2= 0.47$). Given that binding response was (within the margin of error for the T200, www.gelifesciences), and the low confidence in the 'fit of data', the prediction is that RF-21 would not bind to CRBP-I (Figure 5.20).

N-(4-methoxyphenyl) retinamide and 1-adamantylamine samples produced maximal binding response of 4.7RU (n=5) and 2.8RU (n=5) respectively. These responses were not concentration dependent and may have represented non-specific binding. The prediction is that neither of these two small molecules would bind to CRBP-I (Figure 5.20).

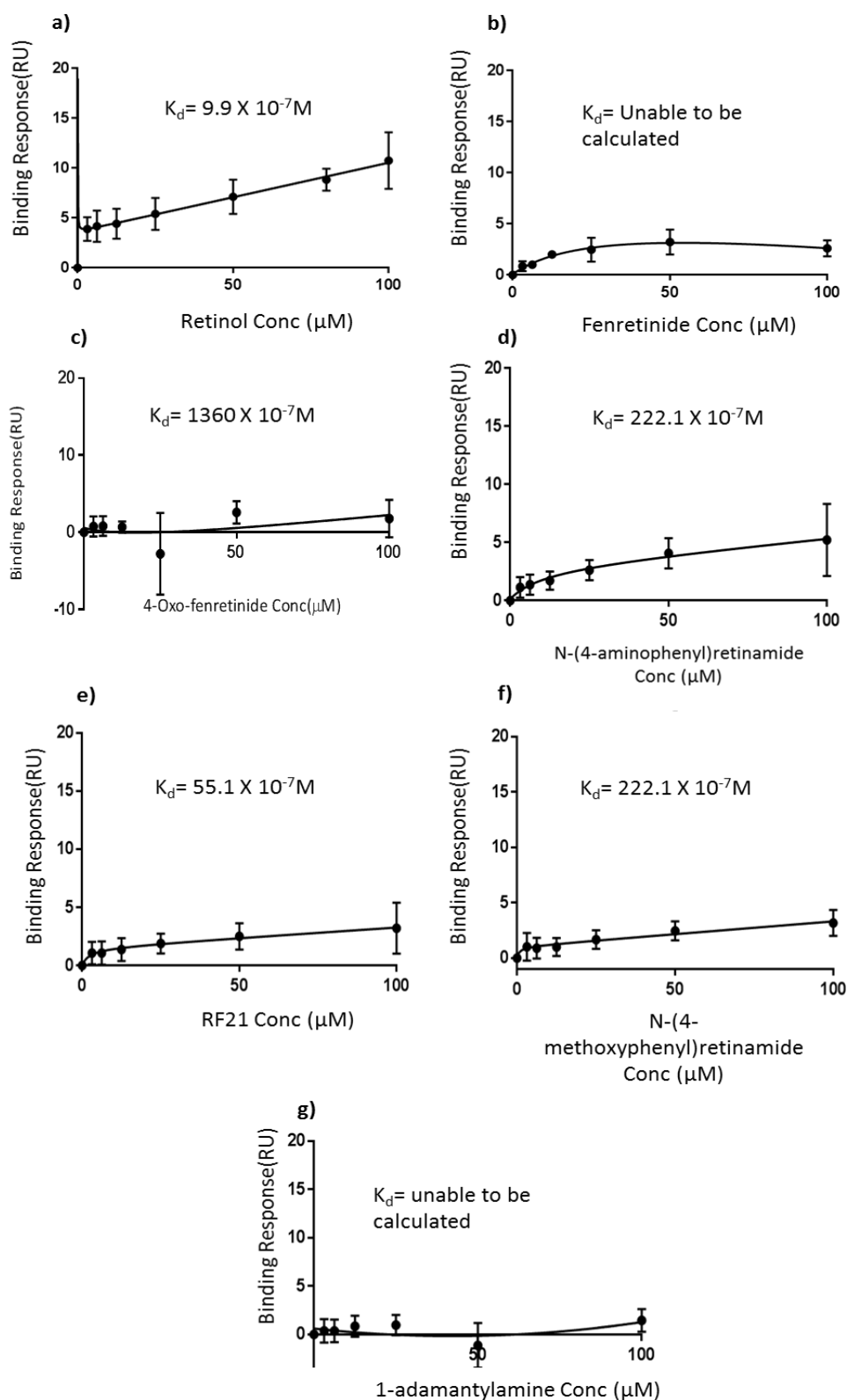


Figure 5.20 The interactions between **CRBPI** protein and **a)** retinol **b)** fenretinide **c)** 4-oxo-fenretinide **d)** N-(4-aminophenyl)retinamide **e)** RF21 **f)** N-(4-methoxyphenyl)retinamide **g)** A1120 **h)** 1-adamantylamine. The binding is measured in response units (**RU**) and further qualified by calculating the dissociation constant (K_d). The smaller the dissociation constant the greater is the binding affinity between CRBPI protein and small molecule.

5.3.5.3. The interactions of CRBP-IV and retinamide small molecules

A retinoic acid concentration curve was produced (see Section 5.2.3.7.5). There was concentration-dependent linear binding response with the maximal response of 68.8RU (n=7). As a result, the K_d could not be calculated (Figure 5.21).

Retinol and fenretinide were used to produce concentration curves (0-100 μ M). The binding responses did not appear to be concentration dependent. The maximal binding response was 3.2 RU for retinol (n=5) and 0.8 RU for fenretinide (n=5). These responses were within the range of sensitivity for the Biacore T200. According to this SPR data, retinol and fenretinide would not bind to CRBP-IV (Figure 5.21).

Concentration curves (0-100 μ M) were produced for 4-oxo fenretinide, N-(4-methoxyphenyl) retinamide, RF21, N-(4-aminophenyl)retinamide and 1-adamantylamine. The binding responses for each of these five small molecules were non-specific, and were not concentration-dependent and the maximal response demonstrated was still within the margin of error for the sensitivity of this machine. As a result, these compounds were not predicted to bind to CRBP-IV (Figure 5.21).

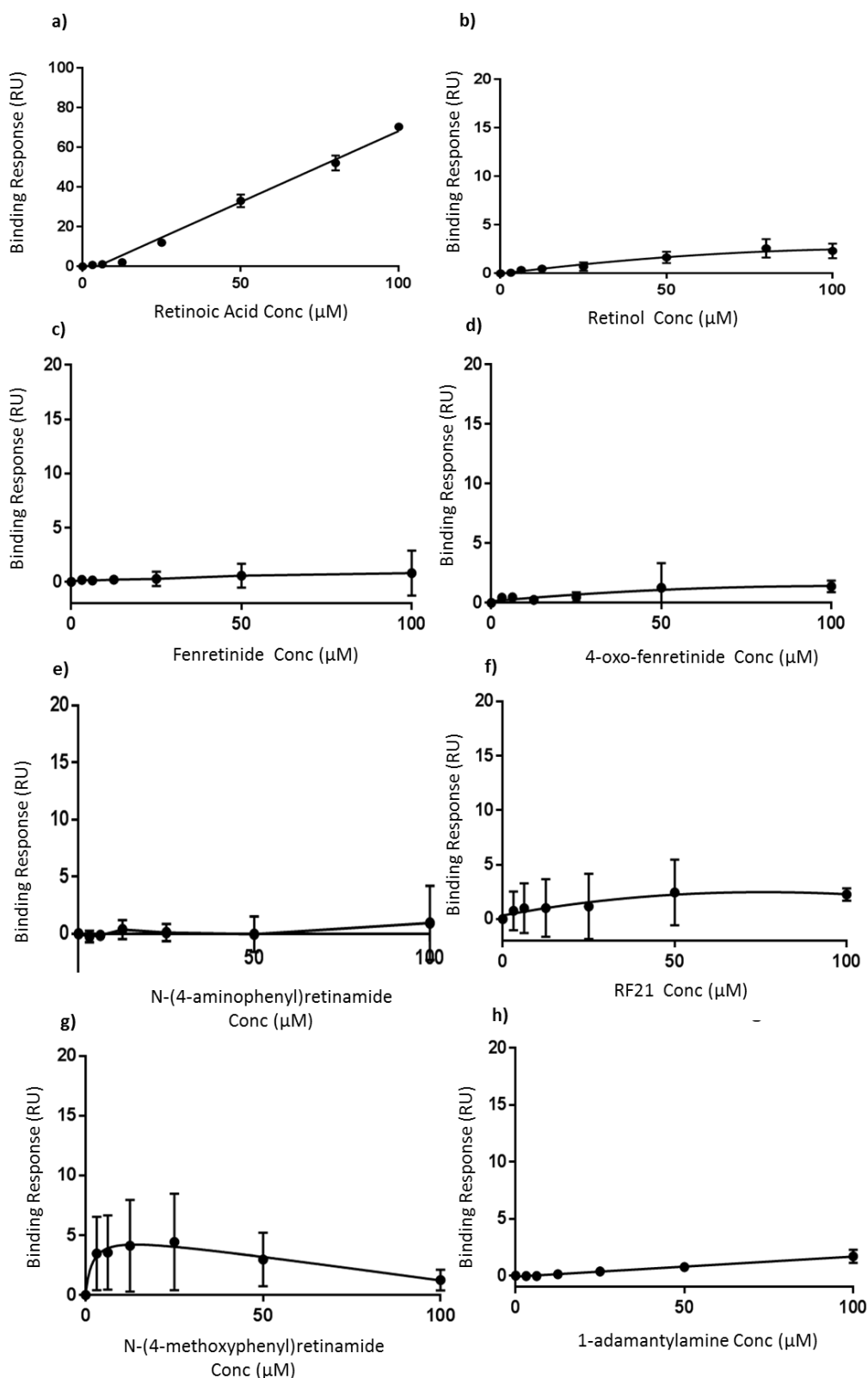


Figure 5.21. The interactions between **CRBP-IV** protein and **a)** retinoic acid ($n=3$) **b)** retinol ($n=5$) **c)** fenretinide ($n=5$) **d)** 4-oxo-fenretinide ($n=5$) **e)** N-(4-aminophenyl)retinamide ($n=5$) **f)** RF21 ($n=4$) **g)** N-(4-methoxyphenyl)retinamide ($n=5$) **h)** 1-adamantylamine ($n=3$). The binding is measured in response units (**RU**) and further qualified by calculating the dissociation constant (K_d). The smaller the dissociation constant the greater is the binding affinity between CRBP-IV protein and small molecule.

Table 5.4: Summary of binding predictions between retinol binding proteins and retinoids or retinamides using Surface Plasmon Resonance.

Ligand	RBP4	CRBP-I	CRBP-IV
Retinol	✓	✓	✓
Retinoic Acid	NA	NA	✓
Fenretinide	✓	X	X
4-oxo-fenretinide	✓	X	X
RF21	X	X	X
N-(4-methoxyphenyl)retinamide	X	X	X
N-(4-aminophenyl)retinamide	X	X	X
1-adamantylamine	X	X	X
A1120	✓	NA	NA

5.4 Discussion

5.4.1 Knock in and knock out experiments

In this chapter, the study demonstrated the knockdown experiments for target proteins using siRNA (Dharmacon, GE Healthcare, UK). During these experiments, cells were needed to be cultured in specialised (serum free) Accell Media. Tissue culture of ESFT cells were clearly sub-optimal (Figure 5.1) and growth curves showed that these cells should be limited to a maximum of 72h in the specialised Accell media. At that point, cell viability was approaching 60% (Figure 5.1). The reduced viability and sub-optimum condition of the remaining cells would limit any follow-on experiments.

As a result, 5 aza-2'-deoxycytidine was used in ESFT cell culture, in order to produce an alternative method for gene/protein modulation (Christman 2002). However, this process is non-specific, and therefore the demethylation would not be limited to the target genes. Any differences seen in the cellular function of the target proteins could be attributable to other unknown genes that had been de-methylated. When these experiments were performed with 5 aza-2'-deoxycytidine in the concentration range 0-10 μ M for 72 h (Colvin, Susanto et al. 2011), cell death approached 80%. On reducing the concentration range to 0-2 μ M, (Kwong, Lo et al. 2005, Caren, Fransson et al. 2007), cell death still approached 40%. This level was considered to be unacceptable for continuing further experiments. The ESFT cells were particularly sensitive to this compound and was unable to tolerate being cultured in a reduced treatment dose.

I have therefore successfully demonstrated the knockdown of CRBP-I (12 – 16 %) and CRBP-IV (23% - 50%) mRNA in ESFT cell lines (Figure 5.2 and Figure 5.14). The level of protein knockdown was reduced when compared to that of the mRNA, with CRBP-I protein being reduced to within 15-35% and CRBP-IV between 35-65% to that of normal levels (Figure 5.3 and 5.15). The success of the protein knockdown could be further qualified by investigating target genes downstream from CRBP-I and CRBP-IV (Taverner, Smith et al. 2004).

The reduced efficiency of the CRBP-IV protein knockdown may be due to the gene being partially methylated and therefore more resistant to down-regulation (Phillips, T et al 2008). Alternatively, the CRBP-IV protein may have a long half-life and even though the gene has been moderately down-regulated, the protein may still be present.

Since the cellular retinol binding proteins belong to the same family of intracellular lipid binding proteins, it is possible to hypothesise that when CRBP-I and CRBP-IV are downregulated, other family member proteins may be up-regulated to compensate for this. In the ESFT cell lines, however, the down regulation of CRBP-I and CRBP-IV did not alter the protein expression of the other CRBPs. In the original cells as well as those in which CRBP-I had been knocked down, RBP4, CRBP-II and CRBP-III were undetectable, while CRBP-IV was expressed. Similarly, in CRBP-IV knocked down and unaltered cells, RBP4, CRBP-II, and CRBP-III were found to be absent while CRBP-I was present. There has been studies (in mouse) suggesting that CRBP-I and CRBP-III may have a complementary relationship. In CRBP-I deficient mice, CRBP-III protein levels were up-regulated only in tissues that were known to express CRBP-III (Paik, Vogel et al. 2000). Since it has been shown that CRBP-III protein is not detected in ESFT cell lines, it follows that CRBP-III would not be up-regulated in ESFTs. Although these proteins share considerable homogeneity (49-58%) (Alvaro, Alpini et al. 2002), CRBP-II and CRBP-III do not appear to compensate for the loss of CRBP-I or CRBP-IV in ESFT cells.

CRBP-I is a ubiquitous protein which is localised to the cytoplasmic compartment of the cell (Napoli 1999). When the ESFT cells were treated with siRNA, and knockdown of the protein induced, CRBP-I protein appeared to be present in the cytoplasmic and membranous components. This observed change in the distribution of CRBP-I protein may be explained by the fact that when the protein level is reduced, it becomes more efficient at its shuttling function and then migrates from the cytoplasm to the membrane to await interaction with STRA6, for presentation of the ligand (Soni, Bala et al. 2007). It would be interesting to investigate any changes to sub-cellular localisation of CRBP-IV in ESFT cells in which CRBP-IV has been knocked down.

ESFT cells in which CRBP-I protein has been knocked down, respond in an almost identical manner to cells with a normal CRBP-I protein complement, when treated with fenretinide. It appears that the downregulation of CRBP-I protein in the ESFT cell lines do not alter fenretinide induced cell death. From this, it can be concluded that fenretinide is not dependent on the CRBP-I protein for induction of the cell death cascade. Similarly, ESFT cells in which CRBP-IV protein has been knocked down, respond in an almost identical manner to cells with a normal CRBP-IV protein complement when treated with fenretinide. In this case, however, the level of protein knockdown was not as successful as with CRBP-I siRNA and there was still a significant amount of the protein available. As such, it was difficult to draw any definitive conclusions about fenretinide induced cell death in ESFT cells containing only partially knocked down CRBP-IV protein.

5.4.2 Modulation of the CRBPs in ESFT cells by treatment with fenretinide

When ESFT cells were with treated with fenretinide (over a time course) and the CRBP-I and CRBP-IV protein content was quantified (by western blotting), there was no modulation of protein levels with time.

This was important to investigate as it provided further information for either the acceptance or refuting the hypothesis of this thesis. Since CRBP-I is known to accept retinol from the STRA6 receptor at the cell membrane and then shuttle it to various end organelles (for retinol homeostasis and metabolism), it would be reasonable to expect CRBP-I to function in a similar way with fenretinide. If this was the case, changes in CRBP-I content with fenretinide treatment would be observed. An example of such might be shown by a sustained progressive exhaustion of the finite CRBP-I protein pool as the protein becomes increasingly degraded after performing its function. Alternatively, increased fenretinide exposure may stimulate the cells to produce more CRBP-I protein for consumption.

The role of CRBP-IV is largely undefined in retinol metabolism. In this case, observations of CRBP-IV protein content (with increasing exposure to fenretinide) has not proven that there are any links between CRBP-IV and retinoid /retinamide metabolism pathways.

Thus for both these proteins, no conclusions could be drawn about the role of either CRBP-I or CRBP-IV in the fenretinide induced cell death within the ESFTs.

5.4.5 Biacore

As a part of determining their function, exploration of binding interactions and affinities between the retinol binding proteins (RBP4, CRBP-I and CRBP-IV) and fenretinide/fenretinide-like small molecules (Table 5.5.) have been carried out.

There are many ways of measuring binding interactions (such as, ELISA, gel-shift assays, pull-down assays, equilibrium dialysis, analytical ultracentrifugation, spectroscopic assays, Isothermal titration calorimetry (ITC) and Surface Plasmon Resonance (Pomorski, Kochanczyk et al. 2013). The use of surface plasmon resonance technology has become the method of choice for investigation of these type of reactions, as it does not require the labelling of any components and can be measured in real time (Myszka, He et al. 1998). Not only is this method quantitative, but it allows for high through-put screening, determination of binding strength, and modelling of binding reactions to determine the dynamic nature of the system (kinetic rate analysis).

The Biacore system utilises several different types of sensor chips (C1, CM3, CM4, CM5 and CM7), depending upon the type of interaction being studied. The CM5 chip has been identified as one, to which proteins/peptides which are not membrane-associated, (with or without GST tags), can be covalently coupled thereby fulfilling all the parameters of the interactions under investigation.

When performing the SPR experiments, the protein partner (ligand) was conjugated onto the surface of a sensor chip and the small molecules (analyte) were passed over the surface. This method is based on an optical detection system that monitors real-time changes in protein mass on the sensor surface. Binding events result in changes in protein mass which, in turn, alter surface plasmon resonance (an electro-magnetic phenomenon

that decreases the intensity of light reflected off of the surface of the sensor chip). The change of resonance angle resulting from analyte-ligand interaction is measured in resonance units (RU). A response of 1000 RU corresponds to a change of about 1 ng/mm² in surface protein concentration. Affinity values of analyte-ligand binding are then derived through fitting the resultant sensorgrams to those in a bank of well-characterised binding reactions (Zhang and Oglesbee 2003). At equilibrium, the rate of protein-small molecule complex formation is equal to the rate of dissociation into its components [protein] + [small molecule]. The measurement of the reaction rate constants can be used to define a dissociation constant (K_d). Since binding affinity is inversely related to the dissociation constant (Landry, Fei et al. 2011), it can be measured as $1/K_D$. The smaller the K_d value, the greater the affinity of the protein for its small molecule (Landry, Fei et al. 2011).

5.4.5.1 RBP4

According to the Biacore experiments, RBP4 can bind strongly to retinol and fenretinide and weakly to 4-oxo-fenretinide and N-(4-aminophenyl) retinamide. In fact, according to published studies, RBP4 is known to bind to retinol and fenretinide, but the binding affinities varied by 2 orders of magnitude when compared with that of my data (Table 5.17). It is important to note that those studies were produced using fluorescence resonance energy transfer (FRET) technology which measures energy transferred between chromophores. So, it is not surprising that various methodologies produce different results. This is potentially a reflection of the sensitivities of the method, or may be a reflection of altered states of activity of the protein. More importantly, however, both of these methods agree that there is binding between RBP4 and retinol as well as with fenretinide.

4-oxo-fenretinide is a polar metabolite of fenretinide which has been found to be present in the plasma of patients who were treated with fenretinide (Villani, Appierto et al. 2004). It is two to four times more efficient in inhibiting tumour growth when compared to fenretinide (Villani, Appierto et al. 2006). As a result, I would be expected that there will be binding between RBP4 and 4-

oxo-fenretinide. My data showed that binding did occur, but at a lower level. This may be explained by the fact, 4-oxo-fenretinide produces cell death by two independent signalling pathways (Tiberio, Cavadini et al. 2010) and such may have an alternative transport protein that it binds to with greater affinity.

The N-(4-aminophenyl) retinamide is another synthetic analogue with a polar amine group. SPR experiments predict binding but with a lower affinity than that of retinol, fenretinide and 4-oxo-fenretinide. However, when this compound was tested for biological activity (by my colleague, Dr Rachael Tenant, MCCB, University of Leeds), it demonstrated comparable activity to fenretinide with improved activity at 3 μ M concentration in TC-32 and TTC-466 cells. This compound has never before been examined in ESFTs and binding reactions with RBP4 has never been tested. It remains an interesting and exciting analogue because of its biological response as well as its chemical composition (contains a polar amine group which may make it more soluble).

RBP4 did not bind to RF21, N-(4-methoxyphenyl) retinamide, and 1-adamantylamine (negative control) (Table 5.5). This can be explained by the presence of the large bulky phenyl groups, which are unlikely to fit into the RBP4 binding pocket. When the biological activity of the former two compounds were investigated in ESFTs, the cell death activity for RF21 was comparable to that of fenretinide. N-(4-methoxyphenyl)retinamide, on the other hand, was ineffective in ESFT cell proliferation (Mehta, Hawthorne et al. 1998, Appierto, Cavadini et al. 2001). Therefore RF21 must be presented to the cell surface by an alternative transport protein.

RBP4 has also demonstrated binding with TTR. The binding affinity for TTR with retinol was greater than that for transthyretin protein alone. Conversely, the binding affinity for TTR and fenretinide was less than that for the TTR protein alone, as evidenced by the K_d . Malpeli et al demonstrated a six fold increase in affinity of retinol-RBP4 for TTR over apo-RBP4. By SPR, I have demonstrated a two fold increase in affinity for the same. In addition, Malpeli determined that fenretinide-RBP4 had negligible/no affinity for TTR. Biacore experiments have shown a five-fold decrease in affinity of fenretinide-RBP4 for TTR. The bulky phenyl ring at the end of the fenretinide molecule does

not allow it to sit completely inside the pocket and therefore conformational binding pocket loop changes cannot occur to allow binding with TTR (Berni and Formelli 1992).

Table 5.5 A comparison of the equilibrium dissociation constants (K_d). The interactions between RBP4, TTR and small molecules were investigated by surface plasmon experiments (SPR) and compared to published data, that had been performed under FRET.

Ligands	K_d by SPR	Published K_d
retinol	$1.05 \times 10^{-5} \text{ M}$	$2 \times 10^{-7} \text{ M}$ (Wysocka-Kapcinska, Campos-Sandoval et al. 2010) $1.9 \times 10^{-7} \text{ M}$ (Cogan, Kopelman et al. 1976)
fenretinide	$9.03 \times 10^{-6} \text{ M}$	$1.7 \times 10^{-7} \text{ M}$ (Berni and Formelli 1992)
4-oxo-fenretinide	$3.13 \times 10^{-5} \text{ M}$	No published data
N-(4-aminophenyl)retinamide	$4.8 \times 10^{-5} \text{ M}$	No published data
transthyretin	$12.5 \times 10^{-6} \text{ M}$	$0.33 \times 10^{-6} \text{ M}$ (Berni et al 1990 Bovine plasma) $1.2 \times 10^{-6} \text{ M}$ (Malpeli, 1995, Retinoid binding)
transthyretin + retinol	$6.19 \times 10^{-6} \text{ M}$	$0.2 \times 10^{-6} \text{ M}$ (Malpeli, 1995, Retinoid binding)
transthyretin + fenretinide	$30.24 \times 10^{-6} \text{ M}$	Negligible (Malpeli, 1995, Retinoid

		binding)
--	--	----------

5.4.5.2 CRBP-I

The Surface Plasmon Resonance experiments (Biacore) determined that CRBP-I-GST would bind well to retinol and less so to N-(4-aminophenyl)retinamide. This is consistent with Kane et al (Table 5.6) who has shown a high binding affinity between CRBP-I and retinol. N-(4-aminophenyl)retinamide, (a polar synthetic derivative which shows biological activity in cancer cells) (Section 5.4.5.1) appears to have a moderate binding affinity when investigated by SPR. However, it showed no binding with fenretinide, 4-oxo-fenretinide, RF21, N-(4-methoxyphenyl)retinamide and 1-adamantylamine. The absence of binding between CRBP-I and fenretinide or N-(4-methoxyphenyl)retinamide demonstrated in the Biacore experiments are consistent with the findings of Sani et al (Table 5.6). Although 4-oxo-fenretinide and RF21 are biologically active in ESFT cells, CRBP-I does not appear to be able to bind to them. Furthermore, computational modelling predicts that there would be no binding between these small molecules and protein (Section 4.3.8). This leads to the conclusion that the biological activity seen with 4-oxo-fenretinide and RF21 might be due to a different transport protein.

Table 5.6. A comparison of the equilibrium dissociation constants (K_d) for CRBP-I and small molecules by SPR and FRET studies.

Ligands	K_d by SPR	Published K_d
Retinol	$9.9 \times 10^{-7}M$	$11 \times 10^{-9}M$ (Kane, 2011, Binding affinities of CRBP-I and CRBPII for 9- <i>cis</i> -retinoids)
N-(4-aminophenyl)retinamide	$4.8 \times 10^{-5}M$	No published data

5.4.5.3. CRBP-IV

According to the SPR experiments, CRBP-IV-GST binds to retinoic acid, but did not produce a saturation curve as the binding responses were still within the linear portion of the graph. As a result, no kinetic analyses could be performed for this interaction. There was no demonstrated binding between this tagged protein and fenretinide, 4-oxo-fenretinide, RF21, N-(4-methoxyphenyl) retinamide, N-(4-aminophenyl) retinamide and 1-adamantylamine. These interactions of these synthetic retinoids and retinamides with CRBP-IV have never before been tested. Therefore predicted non-binding is not surprising, since these compounds have a bulky phenyl ring which make interactions with CRBP-IV are unlikely. Studies have already shown that this protein possesses an incompatible side chain that makes orientation of the B-ionone ring within the binding cavity difficult and unstable (Alvaro, Alpini et al. 2002). Further to this, CRBP-IV has been shown to bind retinoids in a different manner to other CRBPs (Alvaro, Alpini et al. 2002).

Thus after two different approaches (knock down experiments and SPR) to the functionality of CRBP-IV, there is agreement that this protein would bind to the positive controls retinol and retinoic acid but not to fenretinide and other fenretinide-like molecules. It does not appear to be the candidate transporter for these compounds.

5.4.6 Limitations and future work

5.4.6.1 Knockdown experiments

Although I was successfully able to demonstrate protein knock down with siRNA, culturing in Accell media produced ESFT cells that demonstrated reduced viability and was in a sub-optimal condition. A second method of modulating the proteins with a demethylating agent (5-aza-2'-deoxycytidine) was adapted in the ESFTs (Christman 2002). Initial experiments (with this reagent) demonstrated that ESFT cell survival was even more compromised

than with the Accell media (Figure 5.1 and 5.13). Furthermore, the demethylation is non-specific (not targeted) and so any changes seen in the functional element of the protein could not be attributed to modulation of that protein alone. It would be important to investigate other methods of knocking out target proteins, which does not have such a profound impact on cell viability. A short hairpin RNA (shRNA) is an artificial RNA molecule that can be used to silence target gene expression via RNA interference (RNAi). It is typically accomplished by delivery of plasmids, or through viral or bacterial vectors. shRNA is an advantageous mediator of RNAi in that it has a relatively low rate of degradation and turnover (Paddison, Caudy et al. 2002). However, it requires use of an expression vector, which can pose safety concerns and presents the need for acquiring of a new skill. Future work should also involve determining the methylation status of the CRBP-I and CRBP-IV gene, because this might present an alternative method of modulating these proteins.

I would therefore take this work forward by completing over-expression studies of CRBP-I and CRBP-IV in the ESFTs. In addition, I would continue to investigate my hypothesis by modulating CRABP2 and FABP5 proteins (using knockdown and over-expression experiments) in these cell lines. These could be achieved by viral and plasmid work (Moriya 2015). It would also be interesting to investigate whether treatment with fenretinide would affect CRABP2 and FABP5 protein levels (Villani, Appierto et al. 2004).

One of the most interesting findings of this chapter comes to the forefront when CRBP-I protein was knocked down, and the sub-cellular localisation of the protein was compared to cells with a normal CRBP-I protein content, some of the protein appeared to have migrated from the cytoplasm to the membrane. It would be useful to quantify the relative protein contents in these different fractions, potentially by ELISA, and to investigate co-localisation more thoroughly with confocal microscopy. This would then be extended to include CRBP-IV, CRABP2 and FABP5.

5.4.6.2. Biacore

While RBP4 protein was available in its native untagged form for use in SPR experiments, this was not the case for CRBP-I and CRBP-IV. There was one preparation of CRBP-I that was in its native form (GTX117328-pro, Gene-Tex, Inc. California, USA), but I was unable to immobilise this protein onto the CM5 chip. A GST tagged CRBP-I protein (H00005947-PO1, Abnova, Taipei City, Taiwan) was available and was successfully bound to the chip. The GST tag which was 26 kDa (larger than CRBP-I) alters the proteins isoelectric point, charge and solubility (Kimple, Brill et al. 2013). While the tag alters the primary structure of the protein, it can potentially alter both the secondary and tertiary structure as well. In addition, the GST tag possesses the ability to form a dimer, and that along with its charge and changes in the protein structure, may contribute to the binding interactions seen with CRBP-I (Kimple and Sondek 2004). Furthermore, the large GST tag may also bind to the small molecules non-specifically. Calculations for the level of protein to immobilise (Section 5.2.3.3.) are based on the assumption that all of the captured protein are active, and that they are orientated in such a way that it is feasible for binding with either small molecule/analyte or another protein. R_{\max} is a theoretical value and protein condition and orientation on the chip will affect it. In order to acknowledge any contributions to binding from the GST tag, one of the flow cells on the sensor chip was coated with GST and any non-specific binding seen was corrected. Potentially the Biacore chip could be coated with a specific GST antibody and the CRBP-I-GST protein could be used to coat the chip, with the GST portion of the protein binding to the sensor chip. In this way, the orientation of the protein could be assured. CRBP-IV protein could only be purchased in a GST tagged form (H00116362-Q01, Abnova, Taipei City, Taiwan). Attempts to cleave the tags from the protein were unsuccessful because a large concentration of the tagged protein (starting material) was required for producing sufficient native protein. This made it cost prohibitive. Commercial cleaving of the protein was performed but attempts at coating the CM5 chip was still unsuccessful. The process of cleaving the GST tag required eluting at various pHs, with

denaturing, reducing and non-ionic reagents (Kimple and Sondek 2004). As a result, the protein function and structure may have been affected and this contributed to the non-binding. CRBP-IV-GST was eventually coupled to the CM5 biosensor chip and corrections for methodologies were identical for CRBP-I-GST. The same argument with respect to the contribution of the GST tag, can be made about the binding interactions seen with CRBP-IV.

The TTR protein was obtained in a pure untagged form but attempts at coating the CM5 chip was also unsuccessful. The physiological pH for this protein was 5.2 but the pH of the chip was 4.5. This only provided a narrow window for optimisation and production of a charged TTR protein, that would allow binding to the sensor. As a result, (in the more complicated experiments), TTR was incubated with retinol and the solution then injected over a chip coated with RBP4. In order to mimic biological reactions (had time not been a factor), I would have continued attempts at producing a TTR coated chip. The RBP4 protein would have been incubated with retinol and the interactions with TTR explored. *Holo*-TTR (thyroxine) has been shown to be capable of being internalised in various cells within the body (Divino and Schussler 1990, Dekki, Refai et al. 2012, Landers, Mortimer et al. 2013). It would be interesting to investigate whether any interactions take place between TTR and the cellular retinol binding proteins (CRBP-I, CRBP-IV, CRABP2 and FABP5). My future work involves investigating (by SPR) interactions between CRABP2 and FABP5 proteins and the retinoid/retinamide molecules.

6 Discussion

In my thesis, I have tested the hypothesis that the binding of Retinol Binding Proteins with fenretinide or fenretinide-like compounds may result in or enhance cell death in ESFTs.

The main findings of this thesis are:

- CRBP-IV may be a prognostic marker for ESFTs. This protein was elevated in 2 sub-groups of patients with poorer outcomes.
- CRBP-IV was expressed in the ESFT cell lines and binds to retinol but not fenretinide or novel fenretinide-like compounds.
- CRBP-I is expressed by ESFTs but would not bind to fenretinide or novel fenretinide-like compounds.
- CRBP-II and CRBP-III were not detected in ESFTs.
- FABP5 is expressed at high levels and CRABP2 at lower levels in ESFTs. A high FABP5 to CRABP2 ratio has been associated with increased proliferation and metastasis (Campos, Centner et al. 2011), while low CRABP2 levels have been associated with poorly differentiated cells (Yang, Wang et al. 2016).
- RBP4 protein is not detected in ESFT cells, but will bind to retinol, fenretinide and the fenretinide metabolite, 4-oxo-fenretinide.

6.1 Intracellular Lipid Binding Proteins

To the best of my knowledge, ESFTs have not been characterised for the Cellular Retinol Binding Proteins. Immunohistochemistry of a panel of twenty ESFTs taken at diagnosis revealed that CRBP-IV protein was expressed at high levels in two groups of patients that have a poorer prognosis: older patients and poor responders. This is an extremely exciting finding, as it suggests that CRBP-IV may potentially be useful as a prognostic marker.

CRBP-IV has never before been identified as a prognostic marker for disease. It will be important to evaluate the independent prognostic value of CRBP-IV in a larger group of tumours in order to test whether this observation is statistically robust and adds to clinical data. Whether this relationship is also identified in other cancer types remains to be seen. If CRBP-IV does prove to be a bio-marker, it may have a significant impact on the treatment of this disease, by recognising patients (at diagnosis) with poorer outcomes who could benefit from more aggressive treatment options (Biswas and Bakhshi 2016) . This is especially useful in Ewing's sarcoma as there is a group of patients (that are staged as non-metastatic at diagnosis), who actually harbour micro-metastasis and go onto to develop early relapse. The outcome for this group is as poor as those with overt metastatic disease (Biswas and Bakhshi 2016) .

CRBP-IV protein demonstrates variable expression in the ESFTs being present in four of the six cell lines. Epigenetic silencing of the CRBPs has been reported in various cancers (Kwong, Lo et al. 2005) and it is possible that this protein has been silenced in these two cell lines. The down regulation of this protein did not have any discernible effect on fenretinide induced cell death. It will be interesting to determine whether this modulation affected cellular distribution and function of the protein. Computational Modelling and SPR determined that CRBP-IV would not bind to fenretinide and other fenretinide-like molecules and is therefore, not a candidate transporter protein for these molecules.

For the first time, I have also shown that CRBP-I is expressed in the ESFT cell lines. It is my prediction that this protein will be expressed by the primary ESFT panel if had it been possible to optimise the immunohistochemistry protocol. Future studies could use other antibodies, or alternative approaches such as peptide aptamers or *in situ* hybridisation. Subcellular localisation demonstrated that CRBP-I was expressed predominantly in the cytoplasm where it was most probably confined to lipid droplets in the cytoplasm (Farias, Ong et al. 2005).

Interestingly in ESFT cells in which protein expression was decreased (using siRNA), the protein was mobilised to the membrane compartment. As CRBP-I expression is reduced in the cells, it is possible that the protein is mobilised to the membrane as a response to the relative increase of retinol uptake into cells. Secondly, the downregulation of CRBP-I protein in ESFT cells did not have any effect on fenretinide induced cell death. Furthermore, computational modelling predicted, while SPR demonstrated that CRBP-I would bind to retinol but not to fenretinide or any of the fenretinide-like compounds. These results above provide strong evidence that CRBP-I is not an intra-cellular candidate transporter protein for fenretinide and fenretinide-like molecules.

I have for the first time shown that CRBP-II and CRBP-III proteins are not detected in ESFT cells. These observations are consistent with the published literature which demonstrate that while CRBP-II is expressed at high levels in the small intestine, it is virtually absent from other cell types (except foetal and peri-natal liver) (Ong 1984, Levin, Li et al. 1987), with CRBP-III protein that is highly expressed in the heart, muscle, adipose, and mammary tissue, and at a lower level in the spleen, lymph nodes and appendix. An interesting finding by Ghyselinck, Bavik et al, determined a possible compensatory role between CRBP-I and CRBP III. In CRBP-I deficient mice, CRBP-III protein levels were elevated in tissues that normally express CRBP-III. This suggested that CRBP-III could compensate for the absence of CRBP-I, possibly helping to maintain normal retinoid homeostasis (Ghyselinck, Bavik et al. 1999). However, this relationship was not present within the ESFTs, as when the CRBP-I protein was knocked down there was no increase in expression of CRBP-III. The absence of CRBP-II and CRBP-III proteins in the ESFT cells, makes it unlikely that they play any significant role in the fenretinide induced death cascade in ESFTs.

In my thesis, I have shown that CRABP2 protein is expressed at low levels in ESFT cell lines while FABP5 is highly expressed. These two protein have previously been investigated in other cell lines, but not in ESFTs (Barbus, Tews et al. 2011) (Campos, Centner et al. 2011). FABP5 is a strong and

independent prognostic factor for some cancers (Li, Zhang et al. 2011). Furthermore, cells with a high FABP5/CRABP2 protein ratio are highly proliferative with an increased tumorigenicity and metastatic phenotype (Campos, Centner et al. 2011). Therefore the high FABP5/CRABP2 protein ratio in ESFT cell lines is consistent with the fact that this tumour type has a poor clinical outcome.

A high FABP5/CRABP2 mRNA ratio (>3.5) in glioblastomas were associated with a poorer survival outcome (≤ 6 months), while a lower ratio (< 1.4) was linked to longer term survival (≥ 36 months) (Barbus, Tews et al. 2011). Applying the Δ CT method to the ESFT cell lines, the FABP5/CRABP2 mRNA ratio was low (0.01- 1.2). Accordingly, this would be associated with a better survival outcome.

In the immunohistochemistry experiments, FABP5 and CRABP2 proteins were equally expressed in the panel of ESFT samples. However, CRABP2 has a greater affinity for retinoic acid (being 100 times more) than that FABP5 and so, by competitive binding, the CRABP2-mediated pathway (which induces cell cycle arrest or apoptosis) is preferred. Therefore these tumours would be associated with a better prognosis.

The high FABP5/CRABP2 protein ratio in cell lines predict a poor outcome which is in direct contrast to both the mRNA ratio in cell lines and protein content in tumours. It would be interesting to carry out *in situ* hybridisation studies on the tumours, analysing for the FABP5/CRABP2 mRNA ratio by extending the protein and mRNA ratio quantification to include a larger tumour panel. This would be useful in determining whether Campos et al's hypothesis can be applied to ESFTs and assist in accepting or refuting the relationship between these two mRNAs and whether they are prognostic of outcomes.

CRABP2 and FABP5 continue to be of great interest to this search of transport proteins for the intra-cellular fenretinide pathway. CRBP-I and CRBP-IV do not appear to be the transport proteins for fenretinide, and as the search continues for the discovery of these intra-cellular transporters, it would be important to evaluate FABP5 and CRABP2 as candidates.

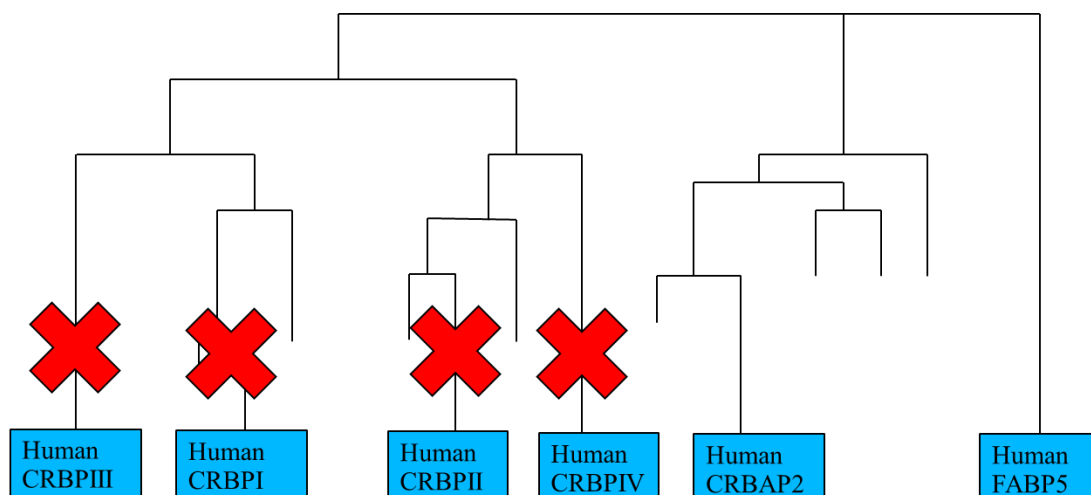


Figure 6.1 Candidate intra-cellular Lipid Binding Proteins transporters for fenretinide. This is the revised phylogenetic tree produced in Figure 1.5. At the end of this thesis, CRBP-II and CRBP-III proteins have been discounted as they were not found to be present in ESFTs. CRBP-I and CRBP-IV, although present in ESFTs, are also not the candidate transporters as they do not bind to fenretinide and its derivatives. Therefore, CRABP2 and FABP5 proteins have been identified as possible carriers and require further investigation.

6.2 Retinol Binding protein 4

I have demonstrated that the ESFT cell lines do not express or secrete the RBP4 protein. This was done using two independent methods (western blot and ELISA). Since ESFT cells do express the RBP4 mRNA, the absence of this protein may be the result of epigenetic alterations.

RBP4 is an adipokine that is known to suppress cytokine and insulin signalling, and so it is possible for this protein to also function in other signalling pathways that regulate cell proliferation and differentiation (Noy, Li et al. 2015). It may be possible for RBP4 to act as a tumour suppressor gene in mesenchymal stem cells (original lineage of ESFTs). When it is silenced as in ESFTs, it loses this function, and the cancer cells proliferate and differentiate in an unchecked manner.

The ESFT cells may never have expressed, or may have lost the ability to produce and secrete the RBP4 protein. Since this protein is in fact the plasma transporter for retinol and fenretinide (Cogan, Kopelman et al. 1976, Berni and Formelli 1992, Berni, Clerici et al. 1993, Coward, Conn et al.

2009), and ESFTs are sensitive to fenretinide (Myatt, Redfern et al. 2005, White and Burchill 2010), then the question to be asked is, how are the retinoid and retinamides presented to ESFTs? At the beginning of this thesis, my hypothesis was that ESFTs produce and secrete the RBP4 protein into the surrounding culture, where it would bind to retinoid/retinamide. This complex is then presented to the membrane transporter (STRA6) before it can become internalised and effect any response within the cell. The absence of RBP4 within the ESFTs required me to modify this hypothesis. Fenretinide and fenretinide-like molecules are most probably bound to RBP4 (produced in the liver and secreted into circulation: exocrine function) and carried to the ESFT cell surface for presentation and internalisation. The inability of ESFTs to produce RBP4 protein does not affect its response to fenretinide, and it is highly unlikely that the modulation of RBP4 protein levels (providing an exogenous source in chemotherapy protocols) would lead to any improved chemotherapeutic outcomes.

6.3 Binding Interactions

Due to time and cost constraints with respect to wet laboratory experiments, computational modelling was initially used to predict possible interactions between retinol binding proteins and various retinamides. I have compared three different theoretical binding tools in evaluating of retinamide binding affinities and interactions. The scoring function is based on the types of chemical bonds (differentially weighted in the programmes) which sometimes making particular algorithms better suited to docking of particular protein types and their ligands. I chose three algorithms (eHiTS, Autodock and Glide) and used a consensus docking approach to evaluate the results. The three algorithms predicted that RBP4, CRBP-I and CRBP-IV would bind to retinol while FABP5 and CRABP2 would bind retinoic acid. This is consistent with published literature where retinol is known to bind to CRBP-I (Ghyselinck, Bavik et al. 1999, Kawaguchi, Yu et al. 2011, O'Byrne and Blaner 2013) and CRBP-IV (Folli, Calderone et al. 2002). FABP5 and

CRABP2 are known to bind retinoic acid (Napoli 2017). There was also consensus among the three algorithms all predicting that RBP4 and RF21, as well as CRBP-I and fenretinide or N-(4-methoxyphenyl)-retinamide would not bind.

However, (in the case of RBP4), Autodock and Glide both predicted fenretinide, 4-oxo-fenretinide, RF21, N-(4-methoxyphenyl)-retinamide and N-(4-aminophenyl)-retinamide would not bind. eHiTS, on the other hand predicted binding with fenretinide and 4-oxo-fenretinide, but was inconclusive as to whether N-(4-methoxyphenyl)-retinamide and N-(4-aminophenyl)-retinamide would. Therefore, according to the principles of consensus docking, RBP4 would not bind to any of the candidate ligands apart from retinol. However, I and others have shown that RBP4 binds to fenretinide (Cogan, Kopelman et al. 1976, Berni and Formelli 1992, Berni, Clerici et al. 1993). Therefore the results of the consensus docking approach (for the three algorithms) to predict binding of RBP4 and retinamide ligands, is not accurate. Indeed, only one of the three software programmes (eHiTS) accurately predicted binding of RBP4 and fenretinide, which was consistent with my finding (using SPR) and the literature (Cogan, Kopelman et al. 1976, Berni and Formelli 1992, Berni, Clerici et al. 1993). This then makes interpretation of the other binding predictions more difficult. For instance, eHiTS is the only programme that predicts binding between RBP4 and 4-oxo-fenretinide, but this interaction has not been previously studied. Interestingly, eHiTS was the only programme to produce binding interactions that were classified as inconclusive (Table 4.8) because of inconsistent results within the algorithm. The eHiTS score showed an acceptable binding affinity but the thermal energies of binding results did not produce any feasible protein-ligand complex.

The docking results for CRBP-I and retinamide ligands 4-oxo-fenretinide, RF21, N-(4-methoxyphenyl)-retinamide and N-(4-aminophenyl)-retinamide also demonstrated inconsistencies. Autodock and Glide agreed that there was non-binding between the protein and ligands while eHiTS produced inconclusive results for the reason outlined above. According to consensus docking, this would be interpreted as non-binding. However, it is important to

consider that (in the case of RBP4), only one algorithm correctly predicted binding.

Docking results for CRBP-IV and CRABP2 correctly predicted binding with the respective targets (retinol and retinoic acid). The interactions of these proteins (CRBP-IV and CRABP2) with the test ligands fenretinide, 4-oxo-fenretinide, RF21, N-(4-methoxyphenyl)-retinamide and N-(4-aminophenyl)-retinamide were highly inconsistent and difficult to interpret. Glide predicted that all five retinamide ligands would bind to CRBP-IV and CRABP2; Autodock predicted no binding for all interactions; and eHiTS was inconclusive about its predictions for all interactions.

When the three algorithms were directed to investigate binding between FABP5 and the retinamide ligands, there was agreement that FABP5 would bind to palmitic acid. In this class of interactions, Autodock and Glide consistently agreed that there would be no binding between FABP5 and the ligands fenretinide, 4-oxo-fenretinide, RF21, N-(4-methoxyphenyl)-retinamide and N-(4-aminophenyl)-retinamide. eHiTS on the other hand predicted that there would be binding with fenretinide, 4-oxo-fenretinide, RF21 and N-(4-aminophenyl)-retinamide, but not with N-(4-methoxyphenyl)-retinamide. The same arguments about the robustness of these predictions also apply here.

As a rule, when all three algorithms agreed that there was binding between the protein and ligand, the prediction was usually robust and consistent with published data. There were three instances when all three programmes agreed that there would be no binding. One of these interactions (CRBP-I and fenretinide) had been previously studied and there was published literature that supported this (Sani, Shealy et al. 1995). The other two interactions have not been previously studied, but it is likely that these are also robust predictions given the chemistry of the ligands. The difficulty has been that in the majority of interactions there is disagreement, and some published literature agrees with the predictions of one out of the three algorithms. As such this makes the consensus docking approach (in the face of inconsistent predictions) an invalid one to be used in the interactions with this family of proteins.

My thesis incorporated a second independent methodology to explore and validate the interactions between the retinol binding proteins and the various retinamide ligands. Given that the computational modelling predictions of many of the novel retinamide interactions were inconclusive, their validation using surface plasmon resonance (SPR) has become important.

I have confirmed that RBP4 can directly bind to retinol and fenretinide, and this is consistent with both the modelling data from eHiTS and the literature (Cogan, Kopelman et al. 1976, Berni and Formelli 1992, Berni, Clerici et al. 1993, Coward, Conn et al. 2009). The 4-oxo-fenretinide compound was also shown to bind to RBP4 (SPR and eHiTS). This is a novel finding of my thesis as it has not previously been explored in published literature. It is not unexpected though, as 4-oxo-fenretinide is a known polar, active metabolite of fenretinide (Villani, Appierto et al. 2006, Poliakov, Samuel et al. 2017) that has been found to be at least two to four times more potent than fenretinide (Villani, Appierto et al. 2006), and may work synergistically with the parent drug. It is therefore plausible that its effects may be facilitated by the same extra-cellular transport protein as fenretinide. This, however, requires further investigation. The other retinamide analogues did not bind to RBP4. I have also confirmed that RBP4 will bind to A1120. This is a non-retinoid ligand that has been shown to displace retinol from RBP4 by disrupting the retinol-induced RBP4-TTR interaction (Dobri, Qin et al. 2013). During my experiments this was used as an additional positive control.

CRBP-I has been shown to bind retinol, but not any of the other retinamide analogues, including fenretinide. Ong et al (1994) have proven that retinol can indeed bind to CRBP-I. More recent studies have elucidated the pathway of cellular uptake of retinol from STRA6 (membrane protein) to CRBP-I before binding to further down-stream receptors (Kawaguchi, Yu et al. 2011, O'Byrne and Blaner 2013). Therefore CRBP-I was hypothesised to be a candidate for intra-cellular transport of fenretinide. Both computational modelling and SPR experiments disagree with this. Previous studies have shown that (by using fluorescence titration) CRBP-I does not bind to fenretinide (Malpeli, Stoppini et al. 1995, Sani, Shealy et al. 1995). Investigations of binding interactions for CRBP-IV revealed that it would only

bind to retinoic acid and retinol (weakly), but not to any of the other retinoid analogues. These two compounds have been reported to bind to CRBP-IV (Kwong, Lo et al. 2005, Napoli 2017). There is, however, very little published literature on CRBP-IV, which (in part) may be because it is one of the more recently identified cellular retinol binding proteins. CRBP-IV is unstable when bound to a ligand and dissociates very easily (Folli, Calderone et al. 2002), making study of such interactions more difficult.

My search for the intra-cellular transporters of fenretinide and its retinamide derivatives has led to the investigating of CRBP-I and CRBP-IV, as likely intra-cellular candidates. According to computational modelling and SPR experiments, these proteins are unable to bind to this class of compounds. It is possible that these methods are not very informative since they do not take into account the cellular milieu as well as the importance of co-factors for some binding reactions.

In order to overcome these limitations, I have attempted to qualify the interaction between iLBPs and retinamides by (siRNA) knocking down expression of selected target proteins. Knockdown was not 100%, or sustained and this explains why the approach has not been very informative. Alternative knockdown methods, such as Clustered Regularly Interspaced Short Palindromic Repeat (CRISPR), may be more useful tools to investigate this. Since these experiments were performed in cell culture (where co-factors necessary for binding would be present), and there were no differences seen, it is likely that CRBP-I and CRBP-IV are not the expected intracellular transporters.

6.4 Comparing the methodologies used in assessing binding interactions

Binding interactions between proteins and retinamide ligands were tested using two complementary but independent systems: computational modelling and surface plasmon resonance. The former is an *in silico* system that uses mathematical representations of the binding phenomenon and

scores it for 'goodness of fit' to a database. It is likely that multiple models can provide a good account of data. A good computational model will mirror the biological conditions and lead to novel understanding. They offer different perspectives to those provided by experiments and theory. At present, models have become a standard feature of scientific drug discovery and this new perspective along with experimental and theoretical knowledge may provide information upon which conclusions can be drawn (Brodland 2015).

Surface plasmon resonance are wet laboratory experiments that define and quantify the binding interactions between the target protein and analytes. While it is an artificial system, it is an interesting tool for examining potential interactions using small volumes of consumables. SPR is label free (labelling may impair binding ; be cost ineffective; require more reagent consumption) (Singh 2016), provides direct measurement of binding constant/affinity (Singh 2016) and produces results in real time (Homola, Yee et al. 1999, Singh 2016). In addition, the detection limits are low and it offers multi-channel performance. The biggest hurdles to this type of technology has been: portability of the hardware; improving sensitivities and limits of detection; and selectivity in complex biological solutions (Singh 2016). Current areas of research (within this field) include examination of protein interactions (with other proteins as well as DNA), structure-function examination (membrane) and T-cell receptor work (Homola, Yee et al. 1999).

Generally, the binding affinities produced in my studies were lower than that of the published binding affinities for the various reactions. Published binding affinities were produced by Fluorescence Resonance Energy Transfer (FRET), and differences in methods may have accounted for the variation noted. There was one interaction that was significantly different: with the binding affinity for RBP4 and retinol calculated as 2 orders of magnitude lower than that of published data.

When the binding affinity interactions were compared for the three software and there was agreement (binding or non-binding) between all computer programmes, SPR validated these results. For RBP4, however, only one

programme predicted binding with fenretinide and 4-oxo-fenretinide, and this was confirmed by SPR. In this case consensus docking approach did not work. For CRBP-I, consensus docking approach predicted binding with retinol alone (confirmed by SPR). With respect to CRBP-IV, computational modelling predicted binding to retinol and retinoic acid and SPR agreed. Predictions were inconclusive for this protein and the other retinamide ligands.

On balance, the use of computational modelling has not been as illuminating in characterising the interactions between this class of proteins and their target ligands. Some of the chosen soft-wares were too constrained and predicted non-binding in interactions that were known to occur (AUTODOCK and GLIDE predicted that RBP4 would not bind to fenretinide); GLIDE was too permissive; while eHiTS was inconclusive. Furthermore, the docking approach did not always agree with the published literature. As a result, I am of the opinion that consensus modelling with multiple programmes for the evaluation of these protein-protein interactions is of limited value. In future studies, I would utilise eHiTS (accepting the permissive rules) in combination with SPR for the identification of target proteins.

6.5 Modulation of fenretinide and the retinamides

Fenretinide exhibits a range of effects on cellular homeostasis, retinol binding, transport, cell survival, and apoptosis of cancer cells (Samuel, Kutty et al. 2006, Motani, Wang et al. 2009, Preitner, Mody et al. 2009, Tiberio, Cavadini et al. 2010, Bikman, Guan et al. 2012). Such a wide variety of effects of fenretinide (and potentially its derivatives) can only be achieved through interactions with multiple molecular targets. Apart from RBP4, other known fenretinide targets are: Beta-carotene oxygenase 1 (BOC1), Stearoyl-CoA Desaturase (SCD1) and Dihydroceramide desaturase-1 (DES1) (Kishi, Armstrong et al. 2014). CRBP-I and CRBP-IV do not appear to be a retinamide target. However, a wider search for the transport candidates may be directed at other members of the iLBP family, such as FABP5 and CRABP2. The identification of an elusive intra-cellular transporter of

fenretinide or fenretinide-like molecules may provide a strategy for modulating the effects of the retinamides.

Fenretinide activity can also be modulated by its delivery vehicle. Its use in clinical practice has been severely limited by poor aqueous solubility and low bioavailability. Initially, clinical trials used an oral gelatin capsule which contained fenretinide suspended in corn oil and polysorbate. The oral bioavailability was only 16% (Lui, 2007, emulsion) and increasing dosage levels meant that patients could be expected to take up to 42 capsules daily. This proved to be very challenging with respect to ensuring compliance. In addition, it was realised that increasing dosage did not result in increased plasma concentration levels and there was wide inter-patient variability in attained plasma concentrations. As a result, this formulation has not been recommended for future trials (Villablanca, London et al. 2011). Another oral formulation that delivers fenretinide in a lipid matrix (LYM-X-SORB) has been devised. This is reported to have up to a four-fold increase in plasma levels and up to seven fold increase in tissue concentration (when compared with the capsule delivery. It, however, has a bitter taste and the consistency of that of candle wax. This formulation has to be disguised to make it more palatable. This trial has been plagued by poor intestinal absorption (Cooper, Reynolds et al. 2017).

More recently, a newer intravenous formulation has been produced which delivers fenretinide as a lipid emulsion. This mode of delivery resulted in a three to ten-fold increase in tissue penetration with minimal toxicity. Hypertriglyceridemia has been one of the main toxicities observed. This has been attributed to the lipid emulsion vehicle, and can be reversed when the infusion is discontinued. There is currently a phase II study involving this formulation, that is accruing patients (Cooper, Reynolds et al. 2017).

At present, the fields of nano-technology and nano-medicine are developing alternative systems to improve the solubility and bioavailability of drugs. Micellar systems, acting as carriers, for fenretinide have also been investigated (Oriente, Zuccari et al. 2012). These particles contain a hydrophobic core that binds fenretinide and a hydrophilic outer shell that solubilises the drug. While aqueous solubility of fenretinide has been

increased by several orders of magnitude, fenretinide dissociation in this system is slow and inefficient (Orienti, Zuccari et al. 2012). Studies using a biodegradable fenretinide polymeric nanoparticle are currently under evaluation (Graves, Ledet et al. 2015). Preliminary data with a nano-encapsulated fenretinide formulation (glucosamine butyrate) demonstrates increased solubility, gastrointestinal absorption (due to interactions with mucosa) and almost 90% drug release (Pignatta, Orienti et al. 2015) The use of nanoparticles as a transport vehicle is continuing to yield promising results.

Fenretinide activity may also be modulated by altering its metabolic pathway. Studies have shown that fenretinide is extensively metabolised to its less polar primarily inactive 4-MPR metabolite and polar metabolites: 4-oxo-fenretinide; 4-hydroxy-fenretinide; and 4-fenretinide glucuronide metabolite (Illingworth, Boddy et al. 2011). The 4-oxo-fenretinide is two to four times as active as the parent drug and appears to work synergistically with fenretinide (Tiberio, Cavadini et al. 2010). This metabolite has been found to be effective in some fenretinide-resistant cells. This implies that while this drug shares a common cell death cascade pathway with fenretinide, it also appears to be able to produce cell death by another mechanism (mitotic arrest) (Tiberio, Cavadini et al. 2010). The effects of other newly identified polar metabolites have not been elucidated but this knowledge may provide an important avenue for altering fenretinide activity.

The *in vitro* metabolism of fenretinide is controlled by various hepatic cytochrome P450 (CYPs) enzymes. Metabolism to the active metabolite 4-oxo-fenretinide was carried out by CYPs 2C8 and 3A4 ; while conversion to 4-hydroxy -fenretinide, was catalysed by most CYPs (Marill, Cresteil et al. 2000) (McSorley and Daly 2000). Ketoconazole has been shown to inhibit fenretinide metabolism via these enzymes, leading to higher fenretinide plasma levels and improved clinical activity (Cooper, Hwang et al. 2011) (Mauerer, Lange et al. 2014). The discovery of inhibitors that prevent metabolism of fenretinide to its inactive metabolite, along with mimetics that potentially favour the pathway that producing the active metabolites would improve clinical outcomes.

Finally fenretinide bioavailability and activity can be modulated by modifying the chemical structure of the molecule. There continues to be ongoing research (in my laboratory and the wider scientific community) into the chemical modulation of the various moieties in the fenretinide molecule. Extensive work into altering the phenyl ring (Sabichi, Demierre et al. 2003) the amide group (Weiss, Alshafie et al. 2001) (Mershon, Anding et al. 2007) the cyclohexene ring (Patel, Huynh et al. 2004) and the isoprenoid backbone (Takahashi, Watanabe et al. 2008) have revealed several important principles that are integral to fenretinide's ability to induce cell death.

Studies performed by Dr Rachael Tenant (Lab G56, School of Chemistry, University of Leeds) in ESFT cell lines have determined that the presence of the NH or OH group at the 4-position of the phenyl ring is important for the fenretinide induced cell death. Incorporation of the NH₂ group at the ortho-position of the fenretinide structure was well tolerated as was the replacement of the 4-hydroxyphenyl group with a 4-pyridyl structure. To the best of my knowledge, the solubility of these particular compounds have not been improved when compared to the parent drug. Future work should be aimed at identifying additional analogues with comparable/better cytotoxic activity, and more importantly improved solubility whilst maintaining the minimal toxicity profile.

6.6 The future of cancer and ESFT therapeutics

Cancer and metastases is a complex and multi-step process, whereby abnormal cells proliferate in an unchecked manner to form a primary tumour which then proceed to invade the basement membrane and spread to distant sites. Progression and development of metastases accounts for the majority of cancer related deaths (Kang 2009; Ramis-Conde, 2009). As we continue to research and understand cancer in laboratories, it is essential that appropriate preclinical models are employed to investigate mechanisms and targets for the improvement of treatment outcomes.

Cell cultures (primary or immortalised cell lines) are extensively used for studying cancer biology and metastasis. They are simple, easy to establish, cheap and reproducible (Baumans and Van Loo 2013). However, these two-dimensional cultures suffer disadvantages associated with the loss of tissue-specific architecture, mechanical and biochemical cues, as well as, cell-to-cell and cell-to-matrix interactions, thereby making them relatively poor models for predicting drug responses (Fang, Roskies et al. 2017). The use of three-dimensional cell cultures (including multicellular spheroids, organoids, scaffolds, hydrogels, organs-on-chips, and 3D bio-printing) are advantageous in that they enable drug safety and efficacy assessment in a more *in vivo*-like context with the traditional 2D cell cultures. These models compensate for many of the deficiencies seen in monolayer cultures. They can develop gradients of oxygen, nutrients, metabolites, and soluble signals, thus creating heterogeneous cell populations (e.g., hypoxic vs. normoxic, quiescent vs. replicating cells). In addition, they have a well-defined geometry and optimal physiological cell-cell and cell-extracellular matrix (ECM) interactions. However, there are several practical challenges associated with spheroid culture, including the development, formulation and maintenance of the spheroids. In addition, the precise control of specific ratios of different cell types in spheroid when co-culture, and the lack of reliable, simple, standardized, and high-throughput compatible assays for drug screening using spheroids require further considerations and optimisations.

In addition to *in vitro* experiments, there has been mouse models used to mimic various types of cancer and metastases. While there has been no true mouse models of ESFTs, current animal studies employ a variety of approaches to producing a xenograft model. Sub-cutaneous models of ESFTs have been produced by injecting cells into the gastrocnemius muscle (Erkizan, Kong et al. 2009). Colonization and metastatic models have been produced by injecting into murine circulation through the saphenous or tail vein ((Vormoor, Baersch et al. 2001) (Kang 2009) and portal vein ((Kang 2009) while others have utilised intra-peritoneal administration (Okazaki, Fushida et al. 2017).

ESFT is a tumour of the tissue surrounding the bone and soft tissue and so a realistic model would be an orthotopic one, in which injections are performed in the soft tissue and periosteum. Recent advances in this field are exploring the injection of cells onto a scaffold before injecting into mouse models. This may provide us with a more realistic model of this disease.

Recently, several signalling pathways in ESFTs that have been identified as promising for targeted therapies. The EWS-FLI1 fusion gene is critical to the oncogenic process in ESFTs. It has not proven to be easily druggable". The small molecule YK-4-279 binds directly to the gene and inhibits RNA splicing. This is the first direct inhibitor described for the EWS-ETS fusion protein (Selvanathan, Graham et al. 2015). Other drugs are being evaluated that mimic the effects of EWS-FLI1 knock-down (RNA helicase A; protein kinase inhibitors). IGF1R antibodies (ganitumab) or small molecule inhibitors have produced dramatic but transient response in small numbers of patients (10%) with refractory disease (Garofalo, Mancarella et al. 2012). PARP1 inhibitors alone or in conjunction temozolamide have entered clinical trials (Brenner, Feng et al. 2012). Bevacizumab is an anti-vascular endothelial growth factor antibody that has been combined with vincristine, topotecan and cyclophosphamide in a phase II trial in patients with recurrent ES. Finally, the current Euro Ewing 2012 trial was meant to evaluate fenretinide and zoledronic acid in combination with first line chemotherapy for treatment of ESFT. However due to difficulties with drug formulation and lack of funding (from industry) to commit to the fighting of rare cancers, this arm of the study has been removed.

Since Ewing's sarcoma was first described almost 100 years ago, its treatment continues to rely upon multi-agent chemotherapeutic regimens alongside surgery and/or radiotherapy. This regimen is associated with significant acute and long term toxicities, giving rise to an urgent and compelling need to integrate novel agents in order to improve outcomes. Conventional chemotherapy that acts by mechanism different to the five drug backbone (currently in use), and targeted therapy at the EWS-FLI1 fusion gene or epigenetic changes are being considered for clinical trials. Fenretinide and its analogues continue to be a class of compounds that is

very exciting with regards to novel therapies for the treatment of ESFTs. It is well tolerated, with minimal toxicity and works by a mechanism that is different to drugs already in use. Future research and the next generation of clinical trials will ultimately determine whether this novel therapy can significantly improve outcomes for patients with Ewing's sarcoma.

6.7 Future Work

In my project I investigated both extra and intra-cellular retinol binding proteins as possible candidate transporters for fenretinide and its analogues. The determination of the specific plasma and intra-cellular transporters may allow for modulation of binding relationships and allow augmenting of the fenretinide induced cell death seen in ESFTs.

My ideas on progressing this body of work include:

Enzyme-Linked ImmunoSpot (ELISPOT) assay for RBP4 in ESFTs – to investigate the target protein content at a cellular level (Rininsland, Helms et al. 2000). This method has an extremely low level of detection (Schmittl, Keilholz et al. 2000) and results would allow for gating and characterisation of sub-populations of the ESFT cells that may express the protein.

RBP4 ELISA in patient plasma samples- If the protein were detected in the samples; the relationship between the protein levels and the patient outcome measures could be investigated.

RBP4 levels in mouse models treated with fenretinide. This could be measured by the established RBP4 ELISA.

Immunohistochemistry for CRBP-I in the panel of ESFTs using affinity purified anti-sera produced in rabbits against a specific peptide sequence (residues 68-83) of pure human CRBP-I (Eriksson, Hansson et al. 1987), or peptide aptamers or *in situ* hybridisation.

Confocal microscopy of the target proteins within the ESFTs to explore sub-cellular localisations. It would be useful to investigate whether modulation of protein levels altered the distribution of protein in cells.

Down-regulation of CRABP2 and FABP5 proteins within the ESFTs in order to determine whether these proteins play a role in the fenretinide induced cell death cascade. Alternative knockdown methods (CRISPR) with a more sustained approach to CRBP-I and CRBP-IV should be investigated

Over-expression of RBP4, CRBP-I, CRBP-IV, CRABP2 and FABP5 proteins – to explore the functionality of these proteins by over-expressing (using plasmids) in the fenretinide induced cell death cascade.

Binding interactions of CRABP2 and FABP5 proteins and the fenretinide analogues (SPR).

6.8 Final Conclusions

These studies have shown that RBP4 protein is not produced or secreted by the ESFT cells and therefore its function as a transporter of retinol and fenretinide is supported by its production in the liver and adipocytes. As a result, modulation of RBP4 protein in the ESFTs (fenretinide sensitive) are unlikely to alter the response to fenretinide. It would be important to consider whether modulation of circulating protein levels may have an impact on disease by investigating plasma studies.

Surface plasmon resonance determined that RBP4 would bind to 4-oxo-fenretinide. This is a novel finding and especially important as this compound is a polar, highly active metabolite of fenretinide. There may be benefit in exploring this relationship and determining whether any modulations with this compound (combination treatment or increased metabolism) can improve outcomes.

In addition, this study has also shown that CRBP-I, CRBP-IV, CRABP2 and FABP5 proteins are expressed in the ESFTs. Computational modelling and SPR determine that CRBP-I and CRBP-IV are unable to bind to fenretinide and its synthetic derivatives. Down regulation of these two proteins (using

RNAi) did not produce any change in the fenretinide induced death cascade. Therefore, it is highly unlikely that the former two proteins are candidates for the intra-cellular transport of this class of compounds. Interestingly though, CRBP-IV levels were found to be raised in ESFT patients with a poorer prognosis (older children, poorly responding tumours). This suggests that CRBP-IV should be further explored to determine whether it can be developed as a novel prognostic marker for this disease.

Although CRBP-I and CRBP-IV may not be the transport proteins for fenretinide and its derivatives, this study has also highlighted other potential candidate targets for the intra-cellular transport of fenretinide and its analogues: CRABP2 and FABP5. Further studies should investigate and explore the function of these proteins in the fenretinide induced cell death cascade.

List of Commercial Suppliers

Abcam Plc	Abcam Plc 330 Cambridge Science Park Cambridge, CB4 0FL www.abcam.com
Abnova	9 th Fl., No. 108, Jzouzh St. Neihu District, Taipei City 114 Taiwan www.abnova.com
Agilent Technologies	Agilent Technologies UK Ltd. 710 Wharfedale Road, Winnersh Triangle, Wokingham, Berkshire, RG41 4TP www.agilent.com
Amersham Biosciences	Amersham Biosciences (UK) Ltd. Amersham Place, Little Chalfont, Buckinghamshire, HP7 9NA www.amershambiosciences.com/uk
Applied Biosystems	Supplied by Life Technologies www.appliedbiosystems.com
ATCC	Supplied by LGC Promochem www.atcc.org
BD Biosciences	Becton Dickinson Biosciences 21 Between Towns Road, Cowley, Oxfordshire, OX4 3LY www.bdbiosciences.com
Beckman Coulter	Beckman Coulter (UK) Ltd.

Oakley Court,
Kingsmead Business Park, London
Road, High Wycombe, HP11 1JU

www.beckmancoulter.co.uk

Berthold Technologies, UK

Allied Business Centre
Coldharbour Lane
Harpenden, Herts AL5 4UT

www.berthold.com

Bio-Rad

Bio-Rad Laboratories Ltd.
Bio-Rad House, Maylands Avenue,
Hemel Hempstead,
Hertfordshire, HP2 7TD

www.bio-rad.com

Biosera Ltd

Supplied by Labtech International Ltd

www.biosera.com

Cambridge Biosciences

Cambridge Bioscience
Munro House, Trafalgar Way
Bar Hill, Cambridge
CB23 8SQ

www.bioscience.co.uk

Cole-Palmer, UK

Unit 3 River Brent Business Park
Trumpers Way Hanwell,
London W7 2QA

www.colepalmer.co.uk

**Corning Life Sciences
Supplies**

Supplied by Scientific Laboratory
Ltd.

www.corning.com/lifesciences

Dako, UK, Ltd

Supplied by Agilent Technologies UK
Ltd.

www.agilent.com

Eppendorf UK Limited	Eppendorf House Gateway 1000 Whittle Way Arlington Business Park Stevenage SG1 2FP www.eppendorf.co.uk
Falcon	Supplied by BD Biosciences
GE Healthcare	GE Healthcare Amersham Place, Little Chalfont, Buckinghamshire, HP7 9NA www.gehealthcare.co.uk
Geneflow	1 The Sycamore Tree Elmhurst Business Park Elmhurst Lichfield, Staffordshire WS13 8EX www.geneflow.co.uk
Gilson	Gilson UK 20 Charles Street, Luton, Bedfordshire, LU2 0EB www.gilson.com
Gibco	Supplied by Thermo-Fisher Scientific
Harlan Sera-Lab	Harlan Sera-Lab Ltd. Dodgeford Lane, Loughborough, Leicestershire, LE12 9TE www.harlanseralab.co.uk
Heidolph UK	Shire Hill Saffron Walden Essex, CB11 3AZ

www.heidolph-instruments.co.uk

Integra Biosciences

INTEGRA Biosciences AG
Tardisstrasse 201, CH-7205,
Zizers, Switzerland

www.integra-biosciences.com

Invitrogen Life Technologies

Invitrogen Life Technologies
3 Fountain Drive,
Inchinnan Business Park, Paisley,
Scotland, PA1 9RF

www.lifetech.com

Keison Products

P.O. Box 2124
Chelmsford
Essex CM1 3UP
England

www.keison.co.uk

Labtech International

Labtech International
1 Acorn House, The Broyle, Ringmer,
East Sussex, BN8 5NN

www.labtech.co.uk

LI-COR

LI-COR Biotechnology – UK Ltd.
St. John's Innovation Centre,
Cowley Road,
Cambridge, CB4 0WS

www.licor.com

Medical Air Technology Ltd

Mercury Way
Traffic Park
Manchester
M14 7LY

www.medicalairtechnology.co.uk

Merck Biosciences	Stanwell Road Feltham, Middlesex TW14 8NX www.merck.co.uk
MP Biochemicals	Supplied by Thermo Fisher Scientific www.mpbio.com
Merck Millipore	Suite 21, Building 6 Croxley Green Business Park Hertfordshire WD18 8YH www.merckmillipore.com
Nalgene Nunc International	Supplied by Thermo Fisher Scientific www.nalgene.com
New England Biolabs	New England Biolabs (UK) Ltd. 75-77 Knowl Piece, Wilbury Way, Hitchin, Hertfordshire, SG4 0TY www.neb.uk.com
Nunc	Supplied by Thermo Fisher Scientific www.nuncbrand.com
Olympus	Olympus KeyMed (Medical & Industrial Equipment) Ltd. KeyMed House, Stock Road, Southend-on-Sea, Essex, SS2 5QH www.olympuskeymed.com
Oxoid	Oxoid Ltd. Wade Road, Basingstoke, Hampshire, RG24, 8PW www.oxoid.com

Promega	Promega UK Delta House, Southampton Science Park, Southampton, SO16 7NS www.promega.com
Qiagen	Qiagen Ltd. Boundary Court, Gatwick Road, Crawley, West Sussex, RH10 9AX www.qiagen.com
R & D Systems Inc	614 McKinley Place NE Minneapolis, MN 55413 www.rndsystems.com
Sanyo Gallenkamp	Sanyo Gallenkamp Plc. Monarch Way, Belton Park, Loughborough, Leicestershire, LE11 5XG www.sanyogallenkamp.com
Scientific Laboratory Supplies Ltd	Wilford Industrial Estate Ruddington Lane Wilford, Nottingham NG11 7EP www.scientificlabs.co.uk
Sigma-Aldrich	Sigma-Aldrich Company Ltd. Fancy Road, Poole, Dorset, BH17 7NH www.sigmaaldrich.com
Thermo Fisher Scientific	Fisher Scientific UK Ltd. Bishop Meadow Road, Loughborough, Leicestershire, LE11 5RG

www.fisher.co.uk

**Thermo Hybaid
Ltd.**

Supplied by Thermo Fisher Scientific

Vector Laboratories

3 Accent Park
Bakewell Road, Orton, Southgate
Peterborough
PE2 6XS

www.vectorlabs.com

VWR International

VWR International Ltd.
14 Media Village, Liscombe Park,
Soulbury,
Leighton Buzzard, LU7 0GA

uk.vwr.com

Whatman

Supplied by GE Healthcare

www.whatman.com

Carl Zeiss Ltd

509 Coldhams Lane,
Cambridge
CB1 3JS

www.zeiss.co.uk

List of References

- Abola, M. V., C. L. Thompson, Z. Chen, A. Chak, N. A. Berger, J. P. Kirwan and L. Li (2015). "Serum levels of retinol-binding protein 4 and risk of colon adenoma." Endocr Relat Cancer **22**(2): L1-4.
- Abou-Issa, H., M. Moeschberger, W. el-Masry, S. Tejwani, R. W. Curley, Jr. and T. E. Webb (1995). "Relative efficacy of glucarate on the initiation and promotion phases of rat mammary carcinogenesis." Anticancer Res **15**(3): 805-810.
- Adamson, J., E. A. Morgan, C. Beesley, Y. Mei, C. S. Foster, H. Fujii, P. S. Rudland, P. H. Smith and Y. Ke (2003). "High-level expression of cutaneous fatty acid-binding protein in prostatic carcinomas and its effect on tumorigenicity." Oncogene **22**(18): 2739-2749.
- Agarwal, A. K. and C. W. Fishwick (2010). "Structure-based design of anti-infectives." Ann N Y Acad Sci **1213**: 20-45.
- Alapatt, P., F. Guo, S. M. Komanetsky, S. Wang, J. Cai, A. Sargsyan, E. Rodriguez Diaz, B. T. Bacon, P. Aryal and T. E. Graham (2013). "Liver retinol transporter and receptor for serum retinol-binding protein (RBP4)." J Biol Chem **288**(2): 1250-1265.
- Alkhouri, N., R. Lopez, M. Berk and A. E. Feldstein (2009). "Serum retinol-binding protein 4 levels in patients with nonalcoholic fatty liver disease." J Clin Gastroenterol **43**(10): 985-989.
- Alvaro, D., G. Alpini, P. Onori, A. Franchitto, S. S. Glaser, G. Le Sage, F. Folli, A. F. Attili and E. Gaudio (2002). "Alfa and beta estrogen receptors and the biliary tree." Mol Cell Endocrinol **193**(1-2): 105-108.
- Appierto, V., E. Cavadini, R. Pergolizzi, L. Cleris, R. Lotan, S. Canevari and F. Formelli (2001). "Decrease in drug accumulation and in tumour aggressiveness marker expression in a fenretinide-induced resistant ovarian tumour cell line." Br J Cancer **84**(11): 1528-1534.
- Armstrong, E. H., D. Goswami, P. R. Griffin, N. Noy and E. A. Ortlund (2014). "Structural basis for ligand regulation of the fatty acid-binding protein 5, peroxisome proliferator-activated receptor beta/delta (FABP5-PPARbeta/delta) signaling pathway." J Biol Chem **289**(21): 14941-14954.
- Arroyave, G. and M. Calcano (1979). "[Decrease in serum levels of retinol and its binding protein (RBP) in infection]." Arch Latinoam Nutr **29**(2): 233-260.
- Artimo, P., M. Jonnalagedda, K. Arnold, D. Baratin, G. Csardi, E. de Castro, S. Duvaud, V. Flegel, A. Fortier, E. Gasteiger, A. Grosdidier, C. Hernandez, V. Ioannidis, D. Kuznetsov, R. Liechti, S. Moretti, K. Mostaguir, N. Redaschi, G. Rossier, I. Xenarios and H. Stockinger (2012). "ExpPASy: SIB bioinformatics resource portal." Nucleic Acids Res **40**(Web Server issue): W597-603.
- Avigad, S., I. J. Cohen, J. Zilberstein, E. Liberzon, Y. Goshen, S. Ash, I. Meller, Y. Kollender, J. Issakov, R. Zaizov and I. Yaniv (2004). "The predictive potential of molecular detection in the nonmetastatic Ewing family of tumors." Cancer **100**(5): 1053-1058.
- Ayadi, L., C. Chaari, R. Kallel, K. Ayadi, A. Khabir, R. Jlidi, J. Daoud, M. Frikha, S. Makni and T. Sellami-Boudawara (2010). "[Ewing sarcoma osseous and extraosseous : a clinicopathologic study of 29 cases]." Tunis Med **88**(5): 301-305.

- Bacci, G., S. Ferrari, F. Bertoni, S. Rimondini, A. Longhi, P. Bacchini, C. Forni, M. Manfrini, D. Donati and P. Picci (2000). "Prognostic factors in nonmetastatic Ewing's sarcoma of bone treated with adjuvant chemotherapy: analysis of 359 patients at the Istituto Ortopedico Rizzoli." J Clin Oncol **18**(1): 4-11.
- Bacci, G., C. Forni, A. Longhi, S. Ferrari, D. Donati, M. De Paolis, E. Barbieri, E. Pignotti, P. Rosito and M. Versari (2004). "Long-term outcome for patients with non-metastatic Ewing's sarcoma treated with adjuvant and neoadjuvant chemotherapies. 402 patients treated at Rizzoli between 1972 and 1992." Eur J Cancer **40**(1): 73-83.
- Balagopal, P., T. E. Graham, B. B. Kahn, A. Altomare, V. Funanage and D. George (2007). "Reduction of elevated serum retinol binding protein in obese children by lifestyle intervention: association with subclinical inflammation." The Journal of clinical endocrinology and metabolism **92**(5): 1971-1974.
- Balamuth, N. J. and R. B. Womer (2010). "Ewing's sarcoma." Lancet Oncol **11**(2): 184-192.
- Barbus, S., B. Tews, D. Karra, M. Hahn, B. Radlwimmer, N. Delhomme, C. Hartmann, J. Felsberg, D. Krex, G. Schackert, R. Martinez, G. Reifenberger and P. Lichter (2011). "Differential retinoic acid signaling in tumors of long- and short-term glioblastoma survivors." J Natl Cancer Inst **103**(7): 598-606.
- Barlogie, B., B. Drewinko, D. A. Johnston and E. J. Freireich (1976). "The effect of adriamycin on the cell cycle traverse of a human lymphoid cell line." Cancer Res **36**(6): 1975-1979.
- Bashor, M. M., D. O. Toft and F. Chytil (1973). "In vitro binding of retinol to rat-tissue components." Proc Natl Acad Sci U S A **70**(12): 3483-3487.
- Bass, J. J., D. J. Wilkinson, D. Rankin, B. E. Phillips, N. J. Szewczyk, K. Smith and P. J. Atherton (2017). "An overview of technical considerations for Western blotting applications to physiological research." Scand J Med Sci Sports **27**(1): 4-25.
- Basu, T. K., U. M. Chan, A. L. Fields and T. A. McPherson (1985). "Retinol and postoperative colorectal cancer patients." Br J Cancer **51**(1): 61-65.
- Batten, M. L., Y. Imanishi, T. Maeda, D. C. Tu, A. R. Moise, D. Bronson, D. Possin, R. N. Van Gelder, W. Baehr and K. Palczewski (2004). "Lecithin-retinol acyltransferase is essential for accumulation of all-trans-retinyl esters in the eye and in the liver." J Biol Chem **279**(11): 10422-10432.
- Baumans, V. and P. L. Van Loo (2013). "How to improve housing conditions of laboratory animals: the possibilities of environmental refinement." Vet J **195**(1): 24-32.
- Berger, W. T., B. P. Ralph, M. Kaczocha, J. Sun, T. E. Balius, R. C. Rizzo, S. Haj-Dahmane, I. Ojima and D. G. Deutsch (2012). "Targeting fatty acid binding protein (FABP) anandamide transporters - a novel strategy for development of anti-inflammatory and anti-nociceptive drugs." PLoS One **7**(12): e50968.
- Berni, R., M. Clerici, G. Malpeli, L. Cleris and F. Formelli (1993). "Retinoids: in vitro interaction with retinol-binding protein and influence on plasma retinol." FASEB J **7**(12): 1179-1184.
- Berni, R. and F. Formelli (1992). "In vitro interaction of fenretinide with plasma retinol-binding protein and its functional consequences." FEBS Lett **308**(1): 43-45.

- Berry, D. C., C. M. Croniger, N. B. Ghyselinck and N. Noy (2012). "Transthyretin blocks retinol uptake and cell signaling by the holo-retinol-binding protein receptor STRA6." Mol Cell Biol **32**(19): 3851-3859.
- Berry, D. C., L. Levi and N. Noy (2014). "Holo-retinol-binding protein and its receptor STRA6 drive oncogenic transformation." Cancer Res **74**(21): 6341-6351.
- Berry, D. C., S. M. O'Byrne, A. C. Vreeland, W. S. Blaner and N. Noy (2012). "Cross talk between signaling and vitamin A transport by the retinol-binding protein receptor STRA6." Mol Cell Biol **32**(15): 3164-3175.
- Berry, S., T. Waldron, E. Winquist and H. Lukka (2006). "The use of bisphosphonates in men with hormone-refractory prostate cancer: a systematic review of randomized trials." Can J Urol **13**(4): 3180-3188.
- Bikman, B. T., Y. Guan, G. Shui, M. M. Siddique, W. L. Holland, J. Y. Kim, G. Fabrias, M. R. Wenk and S. A. Summers (2012). "Fenretinide prevents lipid-induced insulin resistance by blocking ceramide biosynthesis." J Biol Chem **287**(21): 17426-17437.
- Biswas, B. and S. Bakhshi (2016). "Management of Ewing sarcoma family of tumors: Current scenario and unmet need." World J Orthop **7**(9): 527-538.
- Blake, C. C., M. J. Geisow, S. J. Oatley, B. Rerat and C. Rerat (1978). "Structure of prealbumin: secondary, tertiary and quaternary interactions determined by Fourier refinement at 1.8 Å." J Mol Biol **121**(3): 339-356.
- Blaner, W. S. (1989). "Retinol-binding protein: the serum transport protein for vitamin A." Endocr Rev **10**(3): 308-316.
- Blaner, W. S. (2007). "STRA6, a cell-surface receptor for retinol-binding protein: the plot thickens." Cell Metab **5**(3): 164-166.
- Bluher, M., A. Tonjes and M. Stumvoll (2008). "Does retinol-binding protein 4 cause or reflect fatty liver disease?" Hepatology **48**(1): 4-6.
- Bos, J. L. (1989). "ras oncogenes in human cancer: a review." Cancer Res **49**(17): 4682-4689.
- Boya, P., M. C. Morales, R. A. Gonzalez-Polo, K. Andreau, I. Gourdiere, J. L. Perfettini, N. Larochette, A. Deniaud, F. Baran-Marszak, R. Fagard, J. Feuillard, A. Asumendi, M. Raphael, B. Pau, C. Brenner and G. Kroemer (2003). "The chemopreventive agent N-(4-hydroxyphenyl)retinamide induces apoptosis through a mitochondrial pathway regulated by proteins from the Bcl-2 family." Oncogene **22**(40): 6220-6230.
- Bray, F., A. Jemal, N. Grey, J. Ferlay and D. Forman (2012). "Global cancer transitions according to the Human Development Index (2008-2030): a population-based study." Lancet Oncol **13**(8): 790-801.
- Breccia, M., R. Latagliata, I. Carosino, L. Cannella, D. Diverio, A. Guarini, M. S. De Propriis, M. C. Petti, G. Avvisati, G. Cimino, F. Mandelli and F. Lo-Coco (2008). "Clinical and biological features of acute promyelocytic leukemia patients developing retinoic acid syndrome during induction treatment with all-trans retinoic acid and idarubicin." Haematologica **93**(12): 1918-1920.
- Brenner, J. C., F. Y. Feng, S. Han, S. Patel, S. V. Goyal, L. M. Bou-Maroun, M. Liu, R. Lonigro, J. R. Prensner, S. A. Tomlins and A. M. Chinnaiyan (2012). "PARP-1 inhibition as a targeted strategy to treat Ewing's sarcoma." Cancer Res **72**(7): 1608-1613.
- Broch, M., R. Ramirez, M. T. Auguet, M. J. Alcaide, C. Aguilar, A. Garcia-Espana and C. Richart (2010). "Macrophages are novel sites of expression

- and regulation of retinol binding protein-4 (RBP4)." Physiological research / Academia Scientiarum Bohemoslovaca **59**(2): 299-303.
- Brodland, G. W. (2015). "How computational models can help unlock biological systems." Semin Cell Dev Biol **47-48**: 62-73.
- Brohl, A. S., D. A. Solomon, W. Chang, J. Wang, Y. Song, S. Sindiri, R. Patidar, L. Hurd, L. Chen, J. F. Shern, H. Liao, X. Wen, J. Gerard, J. S. Kim, J. A. Lopez Guerrero, I. Machado, D. H. Wai, P. Picci, T. Triche, A. E. Horvai, M. Miettinen, J. S. Wei, D. Catchpool, A. Llombart-Bosch, T. Waldman and J. Khan (2014). "The genomic landscape of the Ewing Sarcoma family of tumors reveals recurrent STAG2 mutation." PLoS Genet **10**(7): e1004475.
- Burchill, S. A. (2008). "Molecular abnormalities in Ewing's sarcoma." Expert review of anticancer therapy **8**(10): 1675-1687.
- Burchill, S. A., P. A. Berry, F. M. Bradbury and I. J. Lewis (1998). "Contrasting levels of p21ras activation and expression of neurofibromin in peripheral primitive neuroectodermal tumour and neuroblastoma cells, and their response to retinoic acid." J Neurol Sci **157**(2): 129-137.
- Bushue, N. and Y. J. Wan (2010). "Retinoid pathway and cancer therapeutics." Adv Drug Deliv Rev **62**(13): 1285-1298.
- Campos, B., F. S. Centner, J. L. Bermejo, R. Ali, K. Dorsch, F. Wan, J. Felsberg, R. Ahmadi, N. Grabe, G. Reifenberger, A. Unterberg, J. Burhenne and C. Herold-Mende (2011). "Aberrant expression of retinoic acid signaling molecules influences patient survival in astrocytic gliomas." Am J Pathol **178**(5): 1953-1964.
- Caren, H., S. Fransson, K. Ejeskar, P. Kogner and T. Martinsson (2007). "Genetic and epigenetic changes in the common 1p36 deletion in neuroblastoma tumours." Br J Cancer **97**(10): 1416-1424.
- Casaroto, A. R., D. A. S. S. MB, C. T. Soares, D. A. S. S. PS, R. Y. F. Yaedu, J. H. Damante and V. S. Lara (2017). "Ewing's Sarcoma Family Tumors in the Jaws: Case Report, Immunohistochemical Analysis and Literature Review." In Vivo **31**(3): 481-491.
- Cazzaniga, M., C. Varricchio, C. Montefrancesco, I. Feroce and A. Guerrieri-Gonzaga (2012). "Fenretinide (4-HPR): a preventive chance for women at genetic and familial risk?" J Biomed Biotechnol **2012**: 172897.
- Chaiworapongsa, T., R. Romero, J. P. Kusanovic, P. Mittal, S. K. Kim, F. Gotsch, N. G. Than, S. Mazaki-Tovi, E. Vaisbuch, O. Erez, L. Yeo, S. S. Hassan and Y. Sorokin (2010). "Plasma soluble endoglin concentration in pre-eclampsia is associated with an increased impedance to flow in the maternal and fetal circulations." Ultrasound Obstet Gynecol **35**(2): 155-162.
- Chen, C. H., L. Y. Ke, H. C. Chan, A. S. Lee, K. D. Lin, C. S. Chu, M. Y. Lee, P. J. Hsiao, C. Hsu, C. H. Chen and S. J. Shin (2016). "Electronegative low density lipoprotein induces renal apoptosis and fibrosis: STRA6 signaling involved." J Lipid Res **57**(8): 1435-1446.
- Cheng, Y., C. Liu, N. Zhang, S. Wang and Z. Zhang (2014). "Proteomics analysis for finding serum markers of ovarian cancer." Biomed Res Int **2014**: 179040.
- Children's Oncology, G., J. G. Villablanca, M. D. Krailo, M. M. Ames, J. M. Reid, G. H. Reaman and C. P. Reynolds (2006). "Phase I trial of oral fenretinide in children with high-risk solid tumors: a report from the Children's Oncology Group (CCG 09709)." J Clin Oncol **24**(21): 3423-3430.

- Chothia, C. (1974). "Hydrophobic bonding and accessible surface area in proteins." *Nature* **248**(446): 338-339.
- Christman, J. K. (2002). "5-Azacytidine and 5-aza-2'-deoxycytidine as inhibitors of DNA methylation: mechanistic studies and their implications for cancer therapy." *Oncogene* **21**(35): 5483-5495.
- Cogan, U., M. Kopelman, S. Mokady and M. Shinitzky (1976). "Binding affinities of retinol and related compounds to retinol binding proteins." *Eur J Biochem* **65**(1): 71-78.
- Colvin, E. K., J. M. Susanto, J. G. Kench, V. N. Ong, A. Mawson, M. Pinese, D. K. Chang, I. Rooman, S. A. O'Toole, D. Segara, E. A. Musgrove, R. L. Sutherland, M. V. Apte, C. J. Scarlett and A. V. Biankin (2011). "Retinoid signaling in pancreatic cancer, injury and regeneration." *PLoS One* **6**(12): e29075.
- Cooper, J. P., K. Hwang, H. Singh, D. Wang, C. P. Reynolds, R. W. Curley, Jr., S. C. Williams, B. J. Maurer and M. H. Kang (2011). "Fenretinide metabolism in humans and mice: utilizing pharmacological modulation of its metabolic pathway to increase systemic exposure." *Br J Pharmacol* **163**(6): 1263-1275.
- Cooper, J. P., C. P. Reynolds, H. Cho and M. H. Kang (2017). "Clinical development of fenretinide as an antineoplastic drug: Pharmacology perspectives." *Exp Biol Med (Maywood)* **242**(11): 1178-1184.
- Costa, S., A. Almeida, A. Castro and L. Domingues (2014). "Fusion tags for protein solubility, purification and immunogenicity in Escherichia coli: the novel Fh8 system." *Front Microbiol* **5**: 63.
- Cotterill, S. J., S. Ahrens, M. Paulussen, H. F. Jurgens, P. A. Voute, H. Gardner and A. W. Craft (2000). "Prognostic factors in Ewing's tumor of bone: analysis of 975 patients from the European Intergroup Cooperative Ewing's Sarcoma Study Group." *J Clin Oncol* **18**(17): 3108-3114.
- Coward, P., M. Conn, J. Tang, F. Xiong, A. Menjares and J. D. Reagan (2009). "Application of an allosteric model to describe the interactions among retinol binding protein 4, transthyretin, and small molecule retinol binding protein 4 ligands." *Anal Biochem* **384**(2): 312-320.
- Craft, A. W., S. J. Cotterill, J. A. Bullimore and D. Pearson (1997). "Long-term results from the first UKCCSG Ewing's Tumour Study (ET-1). United Kingdom Children's Cancer Study Group (UKCCSG) and the Medical Research Council Bone Sarcoma Working Party." *Eur J Cancer* **33**(7): 1061-1069.
- Crompton, B. D., C. Stewart, A. Taylor-Weiner, G. Alexe, K. C. Kurek, M. L. Calicchio, A. Kiezun, S. L. Carter, S. A. Shukla, S. S. Mehta, A. R. Thorner, C. de Torres, C. Lavarino, M. Sunol, A. McKenna, A. Sivachenko, K. Cibulskis, M. S. Lawrence, P. Stojanov, M. Rosenberg, L. Ambrogio, D. Auclair, S. Seepo, B. Blumenstiel, M. DeFelice, I. Imaz-Rosshandler, Y. C. A. Schwarz-Cruz, M. N. Rivera, C. Rodriguez-Galindo, M. D. Fleming, T. R. Golub, G. Getz, J. Mora and K. Stegmaier (2014). "The genomic landscape of pediatric Ewing sarcoma." *Cancer Discov* **4**(11): 1326-1341.
- Cvetkovic, D., S. J. Williams and T. C. Hamilton (2003). "Loss of cellular retinol-binding protein 1 gene expression in microdissected human ovarian cancer." *Clin Cancer Res* **9**(3): 1013-1020.
- Darwiche, N., A. Hatoum, G. Dbaibo, H. Kadara, R. Nasr, G. Abou-Lteif, R. Bazzi, O. Hermine, H. de The and A. Bazarbachi (2004). "N-(4-

- hydroxyphenyl)retinamide induces growth arrest and apoptosis in HTLV-I-transformed cells." Leukemia **18**(3): 607-615.
- Davidoff, A. N. and B. V. Mendelow (1993). "Cell-cycle disruptions and apoptosis induced by the cyclophosphamide derivative mafosfamide." Exp Hematol **21**(7): 922-927.
- De Palo, G., U. Veronesi, T. Camerini, F. Formelli, G. Mascotti, C. Boni, V. Fosser, M. Del Vecchio, T. Campa, A. Costa and et al. (1995). "Can fenretinide protect women against ovarian cancer?" J Natl Cancer Inst **87**(2): 146-147.
- Dekki, N., E. Refai, R. Holmberg, M. Kohler, H. Jornvall, P. O. Berggren and L. Juntti-Berggren (2012). "Transthyretin binds to glucose-regulated proteins and is subjected to endocytosis by the pancreatic beta-cell." Cell Mol Life Sci **69**(10): 1733-1743.
- Delattre, O., J. Zucman, B. Plougastel, C. Desmaze, T. Melot, M. Peter, H. Kovar, I. Joubert, P. de Jong, G. Rouleau and et al. (1992). "Gene fusion with an ETS DNA-binding domain caused by chromosome translocation in human tumours." Nature **359**(6391): 162-165.
- Delia, D., A. Aiello, L. Lombardi, P. G. Pelicci, F. Grignani, F. Grignani, F. Formelli, S. Menard, A. Costa, U. Veronesi and et al. (1993). "N-(4-hydroxyphenyl)retinamide induces apoptosis of malignant hemopoietic cell lines including those unresponsive to retinoic acid." Cancer Res **53**(24): 6036-6041.
- Demmer, L. A., E. H. Birkenmeier, D. A. Sweetser, M. S. Levin, S. Zollman, R. S. Sparkes, T. Mohandas, A. J. Lusis and J. I. Gordon (1987). "The cellular retinol binding protein II gene. Sequence analysis of the rat gene, chromosomal localization in mice and humans, and documentation of its close linkage to the cellular retinol binding protein gene." J Biol Chem **262**(6): 2458-2467.
- Detre, S., G. Saclani Jotti and M. Dowsett (1995). "A "quickscore" method for immunohistochemical semiquantitation: validation for oestrogen receptor in breast carcinomas." J Clin Pathol **48**(9): 876-878.
- Di Vinci, A., E. Geido, E. Infusini and W. Giaretti (1994). "Neuroblastoma cell apoptosis induced by the synthetic retinoid N-(4-hydroxyphenyl)retinamide." Int J Cancer **59**(3): 422-426.
- Diamandopoulos, G. T. (1996). "Cancer: an historical perspective." Anticancer Res **16**(4A): 1595-1602.
- Divino, C. M. and G. C. Schussler (1990). "Receptor-mediated uptake and internalization of transthyretin." J Biol Chem **265**(3): 1425-1429.
- Dobri, N., Q. Qin, J. Kong, K. Yamamoto, Z. Liu, G. Moiseyev, J. X. Ma, R. Allikmets, J. R. Sparrow and K. Petrukhin (2013). "A1120, a nonretinoid RBP4 antagonist, inhibits formation of cytotoxic bisretinoids in the animal model of enhanced retinal lipofuscinogenesis." Invest Ophthalmol Vis Sci **54**(1): 85-95.
- Doldo, E., G. Costanza, S. Agostinelli, C. Tarquini, A. Ferlosio, G. Arcuri, D. Passeri, M. G. Scioli and A. Orlandi (2015). "Vitamin A, cancer treatment and prevention: the new role of cellular retinol binding proteins." Biomed Res Int **2015**: 624627.
- Doldo, E., G. Costanza, A. Ferlosio, D. Passeri, S. Bernardini, M. G. Scioli, D. Mazzaglia, S. Agostinelli, D. Del Bufalo, B. Czernobilsky and A. Orlandi (2014). "CRBP-1 expression in ovarian cancer: a potential therapeutic target." Anticancer Res **34**(7): 3303-3312.

- Donaldson, S. S., M. Torrey, M. P. Link, A. Glicksman, L. Gilula, F. Laurie, J. Manning, J. Neff, W. Reinus, E. Thompson and J. J. Shuster (1998). "A multidisciplinary study investigating radiotherapy in Ewing's sarcoma: end results of POG #8346. Pediatric Oncology Group." Int J Radiat Oncol Biol Phys **42**(1): 125-135.
- Dong, D., S. E. Ruuska, D. J. Levinthal and N. Noy (1999). "Distinct roles for cellular retinoic acid-binding proteins I and II in regulating signaling by retinoic acid." J Biol Chem **274**(34): 23695-23698.
- Donovan, M., B. Olofsson, A. L. Gustafson, L. Dencker and U. Eriksson (1995). "The cellular retinoic acid binding proteins." J Steroid Biochem Mol Biol **53**(1-6): 459-465.
- Dragnev, K. H., J. R. Rigas and E. Dmitrovsky (2000). "The retinoids and cancer prevention mechanisms." Oncologist **5**(5): 361-368.
- DuBois, S. G., M. D. Krailo, M. C. Gebhardt, S. S. Donaldson, K. J. Marcus, J. Dormans, R. C. Shamberger, S. Sailer, R. W. Nicholas, J. H. Healey, N. J. Tarbell, R. L. Randall, M. Devidas, J. S. Meyer, L. Granowetter, R. B. Womer, M. Bernstein, N. Marina and H. E. Grier (2015). "Comparative evaluation of local control strategies in localized Ewing sarcoma of bone: a report from the Children's Oncology Group." Cancer **121**(3): 467-475.
- Duburcq, X., C. Olivier, R. Desmet, M. Halasa, O. Carion, B. Grandidier, T. Heim, D. Stievenard, C. Auriault and O. Melnyk (2004). "Polypeptide semicarbazide glass slide microarrays: characterization and comparison with amine slides in serodetection studies." Bioconjug Chem **15**(2): 317-325.
- Duburcq, X., C. Olivier, F. Malingue, R. Desmet, A. Bouzidi, F. Zhou, C. Auriault, H. Gras-Masse and O. Melnyk (2004). "Peptide-protein microarrays for the simultaneous detection of pathogen infections." Bioconjug Chem **15**(2): 307-316.
- Duchman, K. R., Y. Gao and B. J. Miller (2015). "Prognostic factors for survival in patients with Ewing's sarcoma using the surveillance, epidemiology, and end results (SEER) program database." Cancer Epidemiol **39**(2): 189-195.
- Eisenberg, D. and A. D. McLachlan (1986). "Solvation energy in protein folding and binding." Nature **319**(6050): 199-203.
- Ekins, S., J. Mestres and B. Testa (2007). "In silico pharmacology for drug discovery: applications to targets and beyond." Br J Pharmacol **152**(1): 21-37.
- El-Mesallamy, H. O., N. M. Hamdy, A. S. Zaghloul and A. M. Sallam (2013). "Clinical value of circulating lipocalins and insulin-like growth factor axis in pancreatic cancer diagnosis." Pancreas **42**(1): 149-154.
- el-Shahawy, M., R. Tucker, H. Wahner and R. E. Smith (1971). "Hyperthyroidism and potassium." JAMA **217**(7): 969.
- Enyedy, I. J. and W. J. Egan (2008). "Can we use docking and scoring for hit-to-lead optimization?" J Comput Aided Mol Des **22**(3-4): 161-168.
- Eriksson, U., E. Hansson, H. Nordlinder, C. Busch, J. Sundelin and P. A. Peterson (1987). "Quantitation and tissue localization of the cellular retinoic acid-binding protein." J Cell Physiol **133**(3): 482-490.
- Erkizan, H. V., Y. Kong, M. Merchant, S. Schlottmann, J. S. Barber-Rotenberg, L. Yuan, O. D. Abaan, T. H. Chou, S. Dakshanamurthy, M. L. Brown, A. Uren and J. A. Toretsky (2009). "A small molecule blocking oncogenic protein EWS-FLI1 interaction with RNA helicase A inhibits growth of Ewing's sarcoma." Nat Med **15**(7): 750-756.

- Esteller, M. (2002). "CpG island hypermethylation and tumor suppressor genes: a booming present, a brighter future." *Oncogene* **21**(35): 5427-5440.
- Ewing, J. (1972). "Classics in oncology. Diffuse endothelioma of bone. James Ewing. Proceedings of the New York Pathological Society, 1921." *CA Cancer J Clin* **22**(2): 95-98.
- Fang, D., M. Roskies, M. N. Abdallah, M. Bakkar, J. Jordan, L. C. Lin, F. Tamimi and S. D. Tran (2017). "Three-Dimensional Printed Scaffolds with Multipotent Mesenchymal Stromal Cells for Rabbit Mandibular Reconstruction and Engineering." *Methods Mol Biol* **1553**: 273-291.
- Fang, J., S. J. Chen, J. H. Tong, Z. G. Wang, G. Q. Chen and Z. Chen (2002). "Treatment of acute promyelocytic leukemia with ATRA and As2O3: a model of molecular target-based cancer therapy." *Cancer Biol Ther* **1**(6): 614-620.
- Farias, E. F., D. E. Ong, N. B. Ghyselinck, S. Nakajo, Y. S. Kuppumbatti and R. Mira y Lopez (2005). "Cellular retinol-binding protein I, a regulator of breast epithelial retinoic acid receptor activity, cell differentiation, and tumorigenicity." *J Natl Cancer Inst* **97**(1): 21-29.
- Felsher, D. W. and J. M. Bishop (1999). "Reversible tumorigenesis by MYC in hematopoietic lineages." *Mol Cell* **4**(2): 199-207.
- Ferbeyre, G. and R. Moriggl (2011). "The role of Stat5 transcription factors as tumor suppressors or oncogenes." *Biochim Biophys Acta* **1815**(1): 104-114.
- Ferlay, J., I. Soerjomataram, R. Dikshit, S. Eser, C. Mathers, M. Rebelo, D. M. Parkin, D. Forman and F. Bray (2015). "Cancer incidence and mortality worldwide: sources, methods and major patterns in GLOBOCAN 2012." *Int J Cancer* **136**(5): E359-386.
- Fischer-Huchzermeyer, S., A. Dombrowski, C. Hagel, V. F. Mautner, J. Schittenhelm and A. Harder (2017). "The Cellular Retinoic Acid Binding Protein 2 Promotes Survival of Malignant Peripheral Nerve Sheath Tumor Cells." *Am J Pathol* **187**(7): 1623-1632.
- Flower, D. R. (1996). "The lipocalin protein family: structure and function." *Biochem J* **318** (Pt 1): 1-14.
- Flower, D. R., A. C. North and C. E. Sansom (2000). "The lipocalin protein family: structural and sequence overview." *Biochim Biophys Acta* **1482**(1-2): 9-24.
- Folli, C., V. Calderone, S. Ottonello, A. Bolchi, G. Zanotti, M. Stoppini and R. Berni (2001). "Identification, retinoid binding, and x-ray analysis of a human retinol-binding protein." *Proc Natl Acad Sci U S A* **98**(7): 3710-3715.
- Folli, C., V. Calderone, I. Ramazzina, G. Zanotti and R. Berni (2002). "Ligand binding and structural analysis of a human putative cellular retinol-binding protein." *J Biol Chem* **277**(44): 41970-41977.
- Formelli, F., T. Camerini, E. Cavadini, V. Appierto, M. G. Villani, A. Costa, G. De Palo, M. G. Di Mauro and U. Veronesi (2003). "Fenretinide breast cancer prevention trial: drug and retinol plasma levels in relation to age and disease outcome." *Cancer Epidemiol Biomarkers Prev* **12**(1): 34-41.
- Formelli, F., E. Cavadini, R. Luksch, A. Garaventa, V. Appierto and S. Persiani (2010). "Relationship among pharmacokinetics and pharmacodynamics of fenretinide and plasma retinol reduction in neuroblastoma patients." *Cancer Chemother Pharmacol* **66**(5): 993-998.
- Formelli, F., E. Cavadini, R. Luksch, A. Garaventa, M. G. Villani, V. Appierto and S. Persiani (2008). "Pharmacokinetics of oral fenretinide in

- neuroblastoma patients: indications for optimal dose and dosing schedule also with respect to the active metabolite 4-oxo-fenretinide." Cancer Chemother Pharmacol **62**(4): 655-665.
- Formelli, F., M. Clerici, T. Campa, M. G. Di Mauro, A. Magni, G. Mascotti, D. Moglia, G. De Palo, A. Costa and U. Veronesi (1993). "Five-year administration of fenretinide: pharmacokinetics and effects on plasma retinol concentrations." J Clin Oncol **11**(10): 2036-2042.
- Formelli, F. and L. Cleris (1993). "Synthetic retinoid fenretinide is effective against a human ovarian carcinoma xenograft and potentiates cisplatin activity." Cancer Res **53**(22): 5374-5376.
- Freemantle, S. J., M. J. Spinella and E. Dmitrovsky (2003). "Retinoids in cancer therapy and chemoprevention: promise meets resistance." Oncogene **22**(47): 7305-7315.
- Friesner, R. A., J. L. Banks, R. B. Murphy, T. A. Halgren, J. J. Klicic, D. T. Mainz, M. P. Repasky, E. H. Knoll, M. Shelley, J. K. Perry, D. E. Shaw, P. Francis and P. S. Shenkin (2004). "Glide: a new approach for rapid, accurate docking and scoring. 1. Method and assessment of docking accuracy." J Med Chem **47**(7): 1739-1749.
- Fulda, S., M. U. Kufer, E. Meyer, F. van Valen, B. Dockhorn-Dworniczak and K. M. Debatin (2001). "Sensitization for death receptor- or drug-induced apoptosis by re-expression of caspase-8 through demethylation or gene transfer." Oncogene **20**(41): 5865-5877.
- Furuhashi, M., R. Fucho, C. Z. Gorgun, G. Tuncman, H. Cao and G. S. Hotamisligil (2008). "Adipocyte/macrophage fatty acid-binding proteins contribute to metabolic deterioration through actions in both macrophages and adipocytes in mice." J Clin Invest **118**(7): 2640-2650.
- Furuhashi, M. and G. S. Hotamisligil (2008). "Fatty acid-binding proteins: role in metabolic diseases and potential as drug targets." Nat Rev Drug Discov **7**(6): 489-503.
- Furuhashi, M., S. Ishimura, H. Ota and T. Miura (2011). "Lipid chaperones and metabolic inflammation." Int J Inflamm **2011**: 642612.
- Gallucci, B. B. (1985). "Selected concepts of cancer as a disease: from 1900 to oncogenes." Oncol Nurs Forum **12**(5): 69-78.
- Garaventa, A., R. Luksch, S. Biasotti, G. Severi, M. R. Pizzitola, E. Viscardi, A. Prete, S. Mastrangelo, M. Podda, R. Haupt and B. De Bernardi (2003). "A phase II study of topotecan with vincristine and doxorubicin in children with recurrent/refractory neuroblastoma." Cancer **98**(11): 2488-2494.
- Garaventa, A., R. Luksch, M. S. Lo Piccolo, E. Cavadini, P. G. Montaldo, M. R. Pizzitola, L. Boni, M. Ponzoni, A. Decensi, B. De Bernardi, F. F. Bellani and F. Formelli (2003). "Phase I trial and pharmacokinetics of fenretinide in children with neuroblastoma." Clin Cancer Res **9**(6): 2032-2039.
- Garofalo, C., C. Mancarella, A. Grilli, M. C. Manara, A. Astolfi, M. T. Marino, A. Conte, S. Sigismund, A. Care, A. Belfiore, P. Picci and K. Scotlandi (2012). "Identification of common and distinctive mechanisms of resistance to different anti-IGF-IR agents in Ewing's sarcoma." Mol Endocrinol **26**(9): 1603-1616.
- Gaspar, N., D. S. Hawkins, U. Dirksen, I. J. Lewis, S. Ferrari, M. C. Le Deley, H. Kovar, R. Grimer, J. Whelan, L. Claude, O. Delattre, M. Paulussen, P. Picci, K. Sundby Hall, H. van den Berg, R. Ladenstein, J. Michon, L. Hjorth, I. Judson, R. Luksch, M. L. Bernstein, P. Marec-Berard, B. Brennan, A. W. Craft, R. B. Womer, H. Juergens and O. Oberlin (2015).

- "Ewing Sarcoma: Current Management and Future Approaches Through Collaboration." J Clin Oncol **33**(27): 3036-3046.
- Genheden, S. and U. Ryde (2015). "The MM/PBSA and MM/GBSA methods to estimate ligand-binding affinities." Expert Opin Drug Discov **10**(5): 449-461.
- Gericke, B., J. Raila, J. Sehouli, S. Haebel, D. Kongseng, A. Mustea and F. J. Schweigert (2005). "Microheterogeneity of transthyretin in serum and ascitic fluid of ovarian cancer patients." BMC Cancer **5**: 133.
- Gerster, H. (1997). "Vitamin A-functions, dietary requirements and safety in humans." Int J Vitam Nutr Res **67**(2): 71-90.
- Gettys, S. C., J. E. Anderson and J. E. Davis (2014). "New and emerging therapies for advanced or metastatic soft tissue sarcoma." J Oncol Pharm Pract **20**(4): 288-297.
- Ghyselinck, N. B., C. Bavik, V. Sapin, M. Mark, D. Bonnier, C. Hindelang, A. Dierich, C. B. Nilsson, H. Hakansson, P. Sauvant, V. Azais-Braesco, M. Frasson, S. Picaud and P. Chambon (1999). "Cellular retinol-binding protein I is essential for vitamin A homeostasis." EMBO J **18**(18): 4903-4914.
- Giguere, V. and R. M. Evans (1990). "Identification of receptors for retinoids as members of the steroid and thyroid hormone receptor family." Methods Enzymol **189**: 223-232.
- Goodsell, D. S., G. M. Morris and A. J. Olson (1996). "Automated docking of flexible ligands: applications of AutoDock." J Mol Recognit **9**(1): 1-5.
- Goto, H., H. Takahashi, H. Fujii, K. Ikuta and S. Yokota (2003). "N-(4-Hydroxyphenyl)retinamide (4-HPR) induces leukemia cell death via generation of reactive oxygen species." Int J Hematol **78**(3): 219-225.
- Granowetter, L., R. Womer, M. Devidas, M. Krailo, C. Wang, M. Bernstein, N. Marina, P. Leavey, M. Gebhardt, J. Healey, R. C. Shamberger, A. Goorin, J. Miser, J. Meyer, C. A. Arndt, S. Sailer, K. Marcus, E. Perlman, P. Dickman and H. E. Grier (2009). "Dose-intensified compared with standard chemotherapy for nonmetastatic Ewing sarcoma family of tumors: a Children's Oncology Group Study." J Clin Oncol **27**(15): 2536-2541.
- Graves, R. A., G. A. Ledet, E. Y. Glotser, D. M. Mitchner, L. A. Bostanian and T. K. Mandal (2015). "Formulation and evaluation of biodegradable nanoparticles for the oral delivery of fenretinide." Eur J Pharm Sci **76**: 1-9.
- Gray, H. D., E. S. Gray and C. H. Horne (1985). "Sites of prealbumin production in the human fetus using the indirect immunoperoxidase technique." Virchows Arch A Pathol Anat Histopathol **406**(4): 463-473.
- Grier, H. E. (1997). "The Ewing family of tumors. Ewing's sarcoma and primitive neuroectodermal tumors." Pediatr Clin North Am **44**(4): 991-1004.
- Grier, H. E., M. D. Krailo, N. J. Tarbell, M. P. Link, C. J. Fryer, D. J. Pritchard, M. C. Gebhardt, P. S. Dickman, E. J. Perlman, P. A. Meyers, S. S. Donaldson, S. Moore, A. R. Rausen, T. J. Vietti and J. S. Miser (2003). "Addition of ifosfamide and etoposide to standard chemotherapy for Ewing's sarcoma and primitive neuroectodermal tumor of bone." N Engl J Med **348**(8): 694-701.
- Grossman, A. D., Y. N. Zhou, C. Gross, J. Heilig, G. E. Christie and R. Calendar (1985). "Mutations in the rpoH (htpR) gene of Escherichia coli K-12 phenotypically suppress a temperature-sensitive mutant defective in the sigma 70 subunit of RNA polymerase." J Bacteriol **161**(3): 939-943.
- Grzyb, J., D. Latowski and K. Strzalka (2006). "Lipocalins - a family portrait." J Plant Physiol **163**(9): 895-915.

- Gudas, L. J. (1994). "Retinoids and vertebrate development." J Biol Chem **269**(22): 15399-15402.
- Gudas, L. J. (2012). "Emerging roles for retinoids in regeneration and differentiation in normal and disease states." Biochim Biophys Acta **1821**(1): 213-221.
- Guo, X. (2012). "Surface plasmon resonance based biosensor technique: a review." J Biophotonics **5**(7): 483-501.
- Gygi, S. P., G. L. Corthals, Y. Zhang, Y. Rochon and R. Aebersold (2000). "Evaluation of two-dimensional gel electrophoresis-based proteome analysis technology." Proc Natl Acad Sci U S A **97**(17): 9390-9395.
- Hagen, G. A. and W. J. Elliott (1973). "Transport of thyroid hormones in serum and cerebrospinal fluid." J Clin Endocrinol Metab **37**(3): 415-422.
- Halliday, B. E., D. D. Slagel, T. E. Elsheikh and J. F. Silverman (1998). "Diagnostic utility of MIC-2 immunocytochemical staining in the differential diagnosis of small blue cell tumors." Diagn Cytopathol **19**(6): 410-416.
- Hanahan, D. and R. A. Weinberg (2011). "Hallmarks of cancer: the next generation." Cell **144**(5): 646-674.
- Harada, H., R. Miki, S. Masushige and S. Kato (1995). "Gene expression of retinoic acid receptors, retinoid-X receptors, and cellular retinol-binding protein I in bone and its regulation by vitamin A." Endocrinology **136**(12): 5329-5335.
- Harnish, D. C., H. Jiang, K. J. Soprano, D. M. Kochhar and D. R. Soprano (1992). "Retinoic acid receptor beta 2 mRNA is elevated by retinoic acid in vivo in susceptible regions of mid-gestation mouse embryos." Dev Dyn **194**(3): 239-246.
- Haupt, H. and K. Heide (1966). "[Crystallization of prealbumin from human serum]." Experientia **22**(7): 449-451.
- Heller, J. and J. Horwitz (1973). "Conformational changes following interaction between retinol isomers and human retinol-binding protein and between the retinol-binding protein and prealbumin." J Biol Chem **248**(18): 6308-6316.
- Hertzel, A. V. and D. A. Bernlohr (2000). "The mammalian fatty acid-binding protein multigene family: molecular and genetic insights into function." Trends Endocrinol Metab **11**(5): 175-180.
- Holmes, K., O. L. Roberts, A. M. Thomas and M. J. Cross (2007). "Vascular endothelial growth factor receptor-2: structure, function, intracellular signalling and therapeutic inhibition." Cell Signal **19**(10): 2003-2012.
- Homola, J. (2003). "Present and future of surface plasmon resonance biosensors." Analytical and Bioanalytical Chemistry **377**(3): 528-539.
- Homola, J., S. S. Yee and G. Gauglitz (1999). "Surface plasmon resonance sensors: review." Sensors and Actuators B-Chemical **54**(1-2): 3-15.
- Hosse, R. J., A. Rothe and B. E. Power (2006). "A new generation of protein display scaffolds for molecular recognition." Protein Sci **15**(1): 14-27.
- Hsieh, T. C., C. Ng and J. M. Wu (1995). "The synthetic retinoid N-(4-hydroxyphenyl) retinamide (4-HPR) exerts antiproliferative and apoptosis-inducing effects in the androgen-independent human prostatic JCA-1 cells." Biochem Mol Biol Int **37**(3): 499-506.
- Huang, H. Y., P. B. Illei, Z. Zhao, M. Mazumdar, A. G. Huvos, J. H. Healey, L. H. Wexler, R. Gorlick, P. Meyers and M. Ladanyi (2005). "Ewing sarcomas with p53 mutation or p16/p14ARF homozygous deletion: a highly

lethal subset associated with poor chemoresponse." J Clin Oncol **23**(3): 548-558.

Illingworth, N. A., A. V. Boddy, A. K. Daly and G. J. Veal (2011).

"Characterization of the metabolism of fenretinide by human liver microsomes, cytochrome P450 enzymes and UDP-glucuronosyltransferases." Br J Pharmacol **162**(4): 989-999.

International Human Genome Sequencing, C. (2004). "Finishing the euchromatic sequence of the human genome." Nature **431**(7011): 931-945.

Izumoto, S., D. Younger, A. P. Hays, R. L. Martone, R. T. Smith and J.

Herbert (1992). "Familial amyloidotic polyneuropathy presenting with carpal tunnel syndrome and a new transthyretin mutation, asparagine 70."

Neurology **42**(11): 2094-2102.

Jackson, T. M., M. Bittman and L. Granowetter (2016). "Pediatric Malignant Bone Tumors: A Review and Update on Current Challenges, and Emerging Drug Targets." Curr Probl Pediatr Adolesc Health Care **46**(7): 213-228.

Jenkin, R. D. (1966). "Ewing's sarcoma a study of treatment methods." Clin Radiol **17**(2): 97-106.

Jeong, D. W., Y. M. Choi, S. H. Lee, J. H. Choe, K. C. Hong, H. C. Park and B. C. Kim (2010). "Correlations of trained panel sensory values of cooked pork with fatty acid composition, muscle fiber type, and pork quality characteristics in Berkshire pigs." Meat Sci **86**(3): 607-615.

Jia, D., L. Wei, W. Guo, R. Zha, M. Bao, Z. Chen, Y. Zhao, C. Ge, F. Zhao, T. Chen, M. Yao, J. Li, H. Wang, J. Gu and X. He (2011). "Genome-wide copy number analyses identified novel cancer genes in hepatocellular carcinoma." Hepatology **54**(4): 1227-1236.

Jiang, W. and J. L. Napoli (2013). "The retinol dehydrogenase Rdh10 localizes to lipid droplets during acyl ester biosynthesis." J Biol Chem **288**(1): 589-597.

Jin, B. Y., G. H. Fu, X. Jiang, H. Pan, D. K. Zhou, X. Y. Wei, L. Zhou, L. Chung and S. S. Zheng (2013). "CRABP2 and FABP5 identified by 2D DIGE profiling are upregulated in human bladder cancer." Chin Med J (Engl) **126**(19): 3787-3789.

Jing, C., C. Beesley, C. S. Foster, H. Chen, P. S. Rudland, D. C. West, H. Fujii, P. H. Smith and Y. Ke (2001). "Human cutaneous fatty acid-binding protein induces metastasis by up-regulating the expression of vascular endothelial growth factor gene in rat Rama 37 model cells." Cancer Res **61**(11): 4357-4364.

Jing, C., C. Beesley, C. S. Foster, P. S. Rudland, H. Fujii, T. Ono, H. Chen, P. H. Smith and Y. Ke (2000). "Identification of the messenger RNA for human cutaneous fatty acid-binding protein as a metastasis inducer." Cancer Res **60**(9): 2390-2398.

Jing, Y., J. Zhang, I. J. Bleiweiss, S. Waxman, A. Zelent and Y. L. R. Mira (1996). "Defective expression of cellular retinol binding protein type I and retinoic acid receptors alpha2, beta2, and gamma2 in human breast cancer cells." FASEB J **10**(9): 1064-1070.

Johansen, M., C. W. Redman, T. Wilkins and I. L. Sargent (1999).

"Trophoblast deportation in human pregnancy--its relevance for pre-eclampsia." Placenta **20**(7): 531-539.

Kalemkerian, G. P., R. Slusher, S. Ramalingam, S. Gadgeel and M. Mabry (1995). "Growth inhibition and induction of apoptosis by fenretinide in small-cell lung cancer cell lines." J Natl Cancer Inst **87**(22): 1674-1680.

- Kameko, M., M. Ichikawa, T. Katsuyama, M. Kanai, M. Kato and T. Akamatsu (1986). "Immunohistochemical localization of plasma retinol-binding protein and prealbumin in human pancreatic islets." Histochem J **18**(4): 164-168.
- Kameko, M., H. Ota, K. Ishii, J. Nakayama, T. Katsuyama, M. Kanai and Y. Tsutsumi (1992). "Distribution of retinol-binding protein in the human digestive tract." Virchows Arch B Cell Pathol Incl Mol Pathol **61**(5): 315-322.
- Kanai, M., A. Raz and D. S. Goodman (1968). "Retinol-binding protein: the transport protein for vitamin A in human plasma." J Clin Invest **47**(9): 2025-2044.
- Kane, M. A., F. V. Bright and J. L. Napoli (2011). "Binding affinities of CRBPI and CRBPII for 9-cis-retinoids." Biochimica et biophysica acta **1810**(5): 514-518.
- Kane, M. A., F. V. Bright and J. L. Napoli (2011). "Binding affinities of CRBPI and CRBPII for 9-cis-retinoids." Biochim Biophys Acta **1810**(5): 514-518.
- Kane, M. A., A. E. Folias, A. Pingitore, M. Perri, C. R. Krois, J. Y. Ryu, E. Cione and J. L. Napoli (2011). "Crbpl modulates glucose homeostasis and pancreas 9-cis-retinoic acid concentrations." Mol Cell Biol **31**(16): 3277-3285.
- Kang, Y. (2009). "Analysis of cancer stem cell metastasis in xenograft animal models." Methods Mol Biol **568**: 7-19.
- Kaplan, D. R., B. L. Hempstead, D. Martin-Zanca, M. V. Chao and L. F. Parada (1991). "The trk proto-oncogene product: a signal transducing receptor for nerve growth factor." Science **252**(5005): 554-558.
- Kawaguchi, K., A. Kinameri, S. Suzuki, S. Senga, Y. Ke and H. Fujii (2016). "The cancer-promoting gene fatty acid-binding protein 5 (FABP5) is epigenetically regulated during human prostate carcinogenesis." Biochem J **473**(4): 449-461.
- Kawaguchi, R., J. Yu, M. Ter-Stepanian, M. Zhong, G. Cheng, Q. Yuan, M. Jin, G. H. Travis, D. Ong and H. Sun (2011). "Receptor-mediated cellular uptake mechanism that couples to intracellular storage." ACS Chem Biol **6**(10): 1041-1051.
- Kawatkar, S., H. Wang, R. Czerminski and D. Joseph-McCarthy (2009). "Virtual fragment screening: an exploration of various docking and scoring protocols for fragments using Glide." J Comput Aided Mol Des **23**(8): 527-539.
- Kazmi, S. M., R. K. Plante, V. Visconti and C. Y. Lau (1996). "Comparison of N-(4-hydroxyphenyl)retinamide and all-trans-retinoic acid in the regulation of retinoid receptor-mediated gene expression in human breast cancer cell lines." Cancer Res **56**(5): 1056-1062.
- Kersey, J. H. (1997). "Fifty years of studies of the biology and therapy of childhood leukemia." Blood **90**(11): 4243-4251.
- Kim, H. K., M. Y. Kong, M. J. Jeong, D. C. Han, J. D. Choi, H. Y. Kim, K. S. Yoon, J. M. Kim, K. H. Son and B. M. Kwon (2005). "Investigation of cell cycle arrest effects of actinomycin D at G1 phase using proteomic methods in B104-1-1 cells." Int J Biochem Cell Biol **37**(9): 1921-1929.
- Kimple, M. E., A. L. Brill and R. L. Pasker (2013). "Overview of affinity tags for protein purification." Curr Protoc Protein Sci **73**: Unit 9 9.
- Kimple, M. E. and J. Sonddek (2004). "Overview of affinity tags for protein purification." Curr Protoc Protein Sci **Chapter 9**: Unit 9 9.

- Kishi, S., A. C. Armstrong, S. S. Gidding, L. A. Colangelo, B. A. Venkatesh, D. R. Jacobs, Jr., J. J. Carr, J. G. Terry, K. Liu, D. C. Goff, Jr. and J. A. Lima (2014). "Association of obesity in early adulthood and middle age with incipient left ventricular dysfunction and structural remodeling: the CARDIA study (Coronary Artery Risk Development in Young Adults)." JACC Heart Fail **2**(5): 500-508.
- Kitchen, D. B., H. Decornez, J. R. Furr and J. Bajorath (2004). "Docking and scoring in virtual screening for drug discovery: methods and applications." Nat Rev Drug Discov **3**(11): 935-949.
- Klodos, I., M. Esmann and R. L. Post (2002). "Large-scale preparation of sodium-potassium ATPase from kidney outer medulla." Kidney Int **62**(6): 2097-2100.
- Knudson, A. G., Jr. (1978). "Retinoblastoma: a prototypic hereditary neoplasm." Semin Oncol **5**(1): 57-60.
- Kohler, A., B. Lauritzen and C. J. Van Noorden (2000). "Signal amplification in immunohistochemistry at the light microscopic level using biotinylated tyramide and nanogold-silver staining." J Histochem Cytochem **48**(7): 933-941.
- Koptyra, M., S. Gupta, P. Talati and M. T. Nevalainen (2011). "Signal transducer and activator of transcription 5a/b: biomarker and therapeutic target in prostate and breast cancer." Int J Biochem Cell Biol **43**(10): 1417-1421.
- Kothari, A., W. N. Hittelman and T. C. Chambers (2016). "Cell Cycle-Dependent Mechanisms Underlie Vincristine-Induced Death of Primary Acute Lymphoblastic Leukemia Cells." Cancer Res **76**(12): 3553-3561.
- Kovar, H., A. Auinger, G. Jug, D. Aryee, A. Zoubek, M. Salzer-Kuntschik and H. Gadner (1993). "Narrow spectrum of infrequent p53 mutations and absence of MDM2 amplification in Ewing tumours." Oncogene **8**(10): 2683-2690.
- Krasin, M. J., C. Rodriguez-Galindo, A. M. Davidoff, C. A. Billups, C. E. Fuller, M. D. Neel, L. E. Kun and T. E. Merchant (2004). "Efficacy of combined surgery and irradiation for localized Ewings sarcoma family of tumors." Pediatr Blood Cancer **43**(3): 229-236.
- Kummar, S., M. E. Gutierrez, B. J. Maurer, C. P. Reynolds, M. Kang, H. Singh, S. Crandon, A. J. Murgo and J. H. Doroshow (2011). "Phase I trial of fenretinide lym-x-sorb oral powder in adults with solid tumors and lymphomas." Anticancer Res **31**(3): 961-966.
- Kuppumbatti, Y. S., I. J. Bleiweiss, J. P. Mandeli, S. Waxman and Y. L. R. Mira (2000). "Cellular retinol-binding protein expression and breast cancer." J Natl Cancer Inst **92**(6): 475-480.
- Kuppumbatti, Y. S., B. Rexer, S. Nakajo, K. Nakaya and R. Mira-y-Lopez (2001). "CRBP suppresses breast cancer cell survival and anchorage-independent growth." Oncogene **20**(50): 7413-7419.
- Kwon, J. H., S. T. Park, G. D. Kim, C. R. You, J. D. Kim, H. Y. Woo, J. W. Jang, C. W. Kim, S. H. Bae, J. Y. Choi and S. K. Yoon (2009). "[The value of serum retinol-binding protein 4 levels for determining disease severity in patients with chronic liver disease]." Korean J Hepatol **15**(1): 59-69.
- Kwong, J., K. W. Lo, L. S. Chow, K. F. To, K. W. Choy, F. L. Chan, S. C. Mok and D. P. Huang (2005). "Epigenetic silencing of cellular retinol-binding proteins in nasopharyngeal carcinoma." Neoplasia **7**(1): 67-74.

- Landers, K. A., R. H. Mortimer and K. Richard (2013). "Transthyretin and the human placenta." Placenta **34**(7): 513-517.
- Landry, J. P., Y. Fei and X. D. Zhu (2011). "High Throughput, Label-free Screening Small Molecule Compound Libraries for Protein-Ligands using Combination of Small Molecule Microarrays and a Special Ellipsometry-based Optical Scanner." Int Drug Discov: 8-13.
- Langouche, L., S. Vander Perre, J. Frystyk, A. Flyvbjerg, T. K. Hansen and G. Van den Berghe (2009). "Adiponectin, retinol-binding protein 4, and leptin in protracted critical illness of pulmonary origin." Critical care **13**(4): R112.
- Langouche, L., S. Vander Perre, J. Frystyk, A. Flyvbjerg, T. K. Hansen and G. Van den Berghe (2009). "Adiponectin, retinol-binding protein 4, and leptin in protracted critical illness of pulmonary origin." Crit Care **13**(4): R112.
- Lavelle, D., Y. Sauntharajah and J. Desimone (2008). "DNA methylation and mechanism of action of 5-azacytidine." Blood **111**(4): 2485; author reply 2486.
- Leach, A. R. (1994). "Ligand docking to proteins with discrete side-chain flexibility." J Mol Biol **235**(1): 345-356.
- Lee, D. H. and A. L. Goldberg (1996). "Selective inhibitors of the proteasome-dependent and vacuolar pathways of protein degradation in *Saccharomyces cerevisiae*." J Biol Chem **271**(44): 27280-27284.
- Lehmann, S., C. Paul and H. Torma (2002). "The expression of cellular retinoid binding proteins in non-APL leukemic cells and its association with retinoid sensitivity." Leuk Lymphoma **43**(4): 851-858.
- Lespine, A., B. Periquet, S. Jaconi, M. C. Alexandre, J. Garcia, J. Ghisolfi, J. P. Thouvenot and G. Siegenthaler (1996). "Decreases in retinol and retinol-binding protein during total parenteral nutrition in rats are not due to a vitamin A deficiency." J Lipid Res **37**(12): 2492-2501.
- Levi, L., G. Lobo, M. K. Doud, J. von Lintig, D. Seachrist, G. P. Tochtrop and N. Noy (2013). "Genetic ablation of the fatty acid-binding protein FABP5 suppresses HER2-induced mammary tumorigenesis." Cancer Res **73**(15): 4770-4780.
- Levin, M. S. (1993). "Cellular retinol-binding proteins are determinants of retinol uptake and metabolism in stably transfected Caco-2 cells." J Biol Chem **268**(11): 8267-8276.
- Levin, M. S., E. Li, D. E. Ong and J. I. Gordon (1987). "Comparison of the tissue-specific expression and developmental regulation of two closely linked rodent genes encoding cytosolic retinol-binding proteins." J Biol Chem **262**(15): 7118-7124.
- Lewandowski, K. C., N. Stojanovic, M. Bienkiewicz, B. K. Tan, G. M. Prelevic, M. Press, S. Tuck, P. J. O'Hare and H. S. Randeva (2008). "Elevated concentrations of retinol-binding protein-4 (RBP-4) in gestational diabetes mellitus: negative correlation with soluble vascular cell adhesion molecule-1 (sVCAM-1)." Gynecol Endocrinol **24**(6): 300-305.
- Li, E. and A. W. Norris (1996). "Structure/function of cytoplasmic vitamin A-binding proteins." Annu Rev Nutr **16**: 205-234.
- Li, Z., L. J. Zhang, W. P. Wang, K. Guo, J. Y. Shao and T. H. Rong (2011). "[Correlation between EGFR gene mutation and high copy number and their association with the clinicopathological features in Chinese patients with non-small cell lung cancer]." Zhonghua Zhong Liu Za Zhi **33**(9): 666-670.

- Lin, K. T., R. L. Momparler and G. E. Rivard (1981). "High-performance liquid chromatographic analysis of chemical stability of 5-aza-2'-deoxycytidine." J Pharm Sci **70**(11): 1228-1232.
- Linabery, A. M. and J. A. Ross (2008). "Childhood and adolescent cancer survival in the US by race and ethnicity for the diagnostic period 1975-1999." Cancer **113**(9): 2575-2596.
- Lind, G. E., R. I. Skotheim, M. F. Fraga, V. M. Abeler, M. Esteller and R. A. Lothe (2006). "Novel epigenetically deregulated genes in testicular cancer include homeobox genes and SCGB3A1 (HIN-1)." J Pathol **210**(4): 441-449.
- Liu, R. Z., K. Graham, D. D. Glubrecht, D. R. Germain, J. R. Mackey and R. Godbout (2011). "Association of FABP5 expression with poor survival in triple-negative breast cancer: implication for retinoic acid therapy." Am J Pathol **178**(3): 997-1008.
- Liu, W., N. Chen, H. Jin, J. Huang, J. Wei, J. Bao, C. Li, Y. Liu, X. Li and A. Wang (2007). "Intravenous repeated-dose toxicity study of ZnPcS2P2-based-photodynamic therapy in beagle dogs." Regul Toxicol Pharmacol **47**(3): 221-231.
- Lorkova, L., J. Pospisilova, J. Lacheta, S. Leahomschi, J. Zivny, D. Cibula, J. Zivny and J. Petrak (2012). "Decreased concentrations of retinol-binding protein 4 in sera of epithelial ovarian cancer patients: a potential biomarker identified by proteomics." Oncol Rep **27**(2): 318-324.
- Lovat, P. E., M. Corazzari, B. Goranov, M. Piacentini and C. P. Redfern (2004). "Molecular mechanisms of fenretinide-induced apoptosis of neuroblastoma cells." Ann N Y Acad Sci **1028**: 81-89.
- Lovat, P. E., M. Ranalli, M. Annichiarrico-Petruzzelli, F. Bernassola, M. Piacentini, A. J. Malcolm, A. D. Pearson, G. Melino and C. P. Redfern (2000). "Effector mechanisms of fenretinide-induced apoptosis in neuroblastoma." Exp Cell Res **260**(1): 50-60.
- Lowery, G. H. and J. F. Holt (1951). "Recognition and treatment of vitamin D resistant tickets." J Mich State Med Soc **50**(6): 615-618.
- Lutz, S. Z., A. M. Hennige, S. Feil, A. Peter, A. Gerling, J. Machann, S. M. Krober, M. Rath, A. Schurmann, C. Weigert, H. U. Haring and R. Feil (2011). "Genetic ablation of cGMP-dependent protein kinase type I causes liver inflammation and fasting hyperglycemia." Diabetes **60**(5): 1566-1576.
- Ma, D., D. Baruch, Y. Shu, K. Yuan, Z. Sun, K. Ma, T. Hoang, W. Fu, L. Min, Z. S. Lan, F. Wang, L. Mull and W. W. He (2012). "Using protein microarray technology to screen anti-ERCC1 monoclonal antibodies for specificity and applications in pathology." BMC Biotechnol **12**: 88.
- Maier, T., M. Guell and L. Serrano (2009). "Correlation of mRNA and protein in complex biological samples." FEBS Lett **583**(24): 3966-3973.
- Majumdar, A., A. D. Petrescu, Y. Xiong and N. Noy (2011). "Nuclear translocation of cellular retinoic acid-binding protein II is regulated by retinoic acid-controlled SUMOylation." J Biol Chem **286**(49): 42749-42757.
- Makover, A., D. R. Soprano, M. L. Wyatt and D. S. Goodman (1989). "Localization of retinol-binding protein messenger RNA in the rat kidney and in perinephric fat tissue." J Lipid Res **30**(2): 171-180.
- Makover, A., D. R. Soprano, M. L. Wyatt and D. S. Goodman (1989). "Localization of retinol-binding protein messenger RNA in the rat kidney and in perinephric fat tissue." Journal of lipid research **30**(2): 171-180.

- Malone, W., M. Perloff, J. Crowell, C. Sigman and H. Higley (2003). "Fenretinide: a prototype cancer prevention drug." Expert Opin Investig Drugs **12**(11): 1829-1842.
- Malpeli, G., C. Folli and R. Berni (1996). "Retinoid binding to retinol-binding protein and the interference with the interaction with transthyretin." Biochimica et biophysica acta **1294**(1): 48-54.
- Malpeli, G., M. Stoppini, M. C. Zapponi, C. Folli and R. Berni (1995). "Interactions with retinol and retinoids of bovine cellular retinol-binding protein." Eur J Biochem **229**(2): 486-493.
- Marill, J., T. Cresteil, M. Lanotte and G. G. Chabot (2000). "Identification of human cytochrome P450s involved in the formation of all-trans-retinoic acid principal metabolites." Mol Pharmacol **58**(6): 1341-1348.
- Mariotti, A., E. Marcora, G. Bunone, A. Costa, U. Veronesi, M. A. Pierotti and G. Della Valle (1994). "N-(4-hydroxyphenyl)retinamide: a potent inducer of apoptosis in human neuroblastoma cells." J Natl Cancer Inst **86**(16): 1245-1247.
- Marwarha, G., D. C. Berry, C. M. Croniger and N. Noy (2014). "The retinol esterifying enzyme LRAT supports cell signaling by retinol-binding protein and its receptor STRA6." FASEB J **28**(1): 26-34.
- Mateo-Lozano, S., O. M. Tirado and V. Notario (2003). "Rapamycin induces the fusion-type independent downregulation of the EWS/FLI-1 proteins and inhibits Ewing's sarcoma cell proliferation." Oncogene **22**(58): 9282-9287.
- Matthay, K. K., J. G. Villablanca, R. C. Seeger, D. O. Stram, R. E. Harris, N. K. Ramsay, P. Swift, H. Shimada, C. T. Black, G. M. Brodeur, R. B. Gerbing and C. P. Reynolds (1999). "Treatment of high-risk neuroblastoma with intensive chemotherapy, radiotherapy, autologous bone marrow transplantation, and 13-cis-retinoic acid. Children's Cancer Group." N Engl J Med **341**(16): 1165-1173.
- Mauerer, A., B. Lange, G. H. Welsch, F. Heidenau, W. Adler, R. Forst and R. H. Richter (2014). "Release of Cu²⁺ from a copper-filled TiO₂ coating in a rabbit model for total knee arthroplasty." J Mater Sci Mater Med **25**(3): 813-821.
- Maurer, B. J., O. Kalous, D. W. Yesair, X. Wu, J. Janeba, V. Maldonado, V. Khankaldyyan, T. Frgala, B. C. Sun, R. T. McKee, S. W. Burgess, W. A. Shaw and C. P. Reynolds (2007). "Improved oral delivery of N-(4-hydroxyphenyl)retinamide with a novel LYM-X-SORB organized lipid complex." Clin Cancer Res **13**(10): 3079-3086.
- Maurer, B. J., L. S. Metelitsa, R. C. Seeger, M. C. Cabot and C. P. Reynolds (1999). "Increase of ceramide and induction of mixed apoptosis/necrosis by N-(4-hydroxyphenyl)- retinamide in neuroblastoma cell lines." J Natl Cancer Inst **91**(13): 1138-1146.
- Mazaki-Tovi, S., E. Vaisbuch, R. Romero, J. P. Kusanovic, T. Chaiworapongsa, S. K. Kim, C. L. Nhan-Chang, R. Gomez, Z. Alpay Savasan, I. Madan, B. H. Yoon, L. Yeo, P. Mittal, G. Ogge, J. M. Gonzalez and S. S. Hassan (2010). "Maternal and neonatal circulating visfatin concentrations in patients with pre-eclampsia and a small-for-gestational age neonate." J Matern Fetal Neonatal Med **23**(10): 1119-1128.
- McCormick, D. L. and R. C. Moon (1986). "Antipromotional activity of dietary N-(4-hydroxyphenyl)retinamide in two-stage skin tumorigenesis in CD-1 and SENCAR mice." Cancer Lett **31**(2): 133-138.

- McGuire, S. (2016). "World Cancer Report 2014. Geneva, Switzerland: World Health Organization, International Agency for Research on Cancer, WHO Press, 2015." Adv Nutr **7**(2): 418-419.
- McNally, R. J., K. Blakey, R. C. Parslow, P. W. James, B. G. Pozo, C. Stiller, T. J. Vincent, P. Norman, P. A. McKinney, M. F. Murphy, A. W. Craft and R. G. Feltbower (2012). "Small-area analyses of bone cancer diagnosed in Great Britain provide clues to aetiology." BMC Cancer **12**: 270.
- McSorley, L. C. and A. K. Daly (2000). "Identification of human cytochrome P450 isoforms that contribute to all-trans-retinoic acid 4-hydroxylation." Biochem Pharmacol **60**(4): 517-526.
- Mehta, R. R., M. E. Hawthorne, J. M. Graves and R. G. Mehta (1998). "Metabolism of N-[4-hydroxyphenyl]retinamide (4-HPR) to N-[4-methoxyphenyl]retinamide (4-MPR) may serve as a biomarker for its efficacy against human breast cancer and melanoma cells." Eur J Cancer **34**(6): 902-907.
- Mendoza-Rodriguez, M., H. Arreola, A. Valdivia, R. Peralta, H. Serna, V. Villegas, P. Romero, B. Alvarado-Hernandez, L. Paniagua, D. Marrero-Rodriguez, M. A. Meraz and M. Salcedo (2013). "Cellular retinol binding protein 1 could be a tumor suppressor gene in cervical cancer." Int J Clin Exp Pathol **6**(9): 1817-1825.
- Mershon, S. M., A. L. Anding, J. S. Chapman, M. Clagett-Dame, L. A. Stonerock and R. W. Curley, Jr. (2007). "Solid phase-assisted synthesis and screening of a small library of N-(4-hydroxyphenyl)retinamide (4-HPR) analogs." Bioorg Med Chem Lett **17**(3): 836-840.
- Meyers, P. A., M. D. Krailo, M. Ladanyi, K. W. Chan, S. L. Sailer, P. S. Dickman, D. L. Baker, J. H. Davis, R. B. Gerbing, A. Grovas, C. E. Herzog, K. L. Lindsley, W. Liu-Mares, J. B. Nachman, L. Sieger, J. Wadman and R. G. Gorlick (2001). "High-dose melphalan, etoposide, total-body irradiation, and autologous stem-cell reconstitution as consolidation therapy for high-risk Ewing's sarcoma does not improve prognosis." J Clin Oncol **19**(11): 2812-2820.
- Mills, J. P., H. C. Furr and S. A. Tanumihardjo (2008). "Retinol to retinol-binding protein (RBP) is low in obese adults due to elevated apo-RBP." Exp Biol Med (Maywood) **233**(10): 1255-1261.
- Miser, J. S., R. E. Goldsby, Z. Chen, M. D. Krailo, N. J. Tarbell, M. P. Link, C. J. Fryer, D. J. Pritchard, M. C. Gebhardt, P. S. Dickman, E. J. Perlman, P. A. Meyers, S. S. Donaldson, S. G. Moore, A. R. Rausen, T. J. Vietti and H. E. Grier (2007). "Treatment of metastatic Ewing sarcoma/primitive neuroectodermal tumor of bone: evaluation of increasing the dose intensity of chemotherapy--a report from the Children's Oncology Group." Pediatr Blood Cancer **49**(7): 894-900.
- Mistry, A. R., E. W. Pedersen, E. Solomon and D. Grimwade (2003). "The molecular pathogenesis of acute promyelocytic leukaemia: implications for the clinical management of the disease." Blood Rev **17**(2): 71-97.
- Moal, I. H., R. Moretti, D. Baker and J. Fernandez-Recio (2013). "Scoring functions for protein-protein interactions." Curr Opin Struct Biol **23**(6): 862-867.
- Mody, N. and G. D. McIlroy (2014). "The mechanisms of Fenretinide-mediated anti-cancer activity and prevention of obesity and type-2 diabetes." Biochem Pharmacol **91**(3): 277-286.

- Mohrbacher, A. M., A. S. Yang, S. Groshen, S. Kummar, M. E. Gutierrez, M. H. Kang, D. Tsao-Wei, C. P. Reynolds, E. M. Newman and B. J. Maurer (2017). "Phase I Study of Fenretinide Delivered Intravenously in Patients with Relapsed or Refractory Hematologic Malignancies: A California Cancer Consortium Trial." Clin Cancer Res **23**(16): 4550-4555.
- Monaco, H. L. (2000). "The transthyretin-retinol-binding protein complex." Biochim Biophys Acta **1482**(1-2): 65-72.
- Moody, B. J. (1982). "Changes in the serum concentrations of thyroxine-binding prealbumin and retinol-binding protein following burn injury." Clin Chim Acta **118**(1): 87-92.
- Moon, R. C. (1989). "Comparative aspects of carotenoids and retinoids as chemopreventive agents for cancer." J Nutr **119**(1): 127-134.
- Moon, R. C. and D. L. McCormick (1982). "Inhibition of chemical carcinogenesis by retinoids." J Am Acad Dermatol **6**(4 Pt 2 Suppl): 809-814.
- Moon, R. C., J. F. Pritchard, R. G. Mehta, C. T. Nomides, C. F. Thomas and N. M. Dinger (1989). "Suppression of rat mammary cancer development by N-(4-hydroxyphenyl)retinamide (4-HPR) following surgical removal of first palpable tumor." Carcinogenesis **10**(9): 1645-1649.
- Morales-Espinosa, D., S. Garcia-Roman, C. Teixido, N. Karachaliou and R. Rosell (2015). "Immunotherapy meets targeted therapy: will this team end the war against cancer?" Transl Lung Cancer Res **4**(6): 752-755.
- Morgan, E., P. Kannan-Thulasiraman and N. Noy (2010). "Involvement of Fatty Acid Binding Protein 5 and PPARbeta/delta in Prostate Cancer Cell Growth." PPAR Res **2010**.
- Moriya, H. (2015). "Quantitative nature of overexpression experiments." Mol Biol Cell **26**(22): 3932-3939.
- Morris, D. R. and C. W. Levenson (2013). "Zinc regulation of transcriptional activity during retinoic acid-induced neuronal differentiation." J Nutr Biochem **24**(11): 1940-1944.
- Morris, E. J., J. C. Dreixler, K. Y. Cheng, P. M. Wilson, R. M. Gin and H. M. Geller (1999). "Optimization of single-cell gel electrophoresis (SCGE) for quantitative analysis of neuronal DNA damage." Biotechniques **26**(2): 282-283, 286-289.
- Motani, A., Z. Wang, M. Conn, K. Siegler, Y. Zhang, Q. Liu, S. Johnstone, H. Xu, S. Thibault, Y. Wang, P. Fan, R. Connors, H. Le, G. Xu, N. Walker, B. Shan and P. Coward (2009). "Identification and characterization of a non-retinoid ligand for retinol-binding protein 4 which lowers serum retinol-binding protein 4 levels in vivo." J Biol Chem **284**(12): 7673-7680.
- Murray, P. J. (2007). "The JAK-STAT signaling pathway: input and output integration." J Immunol **178**(5): 2623-2629.
- Myatt, S. S. and S. A. Burchill (2008). "The sensitivity of the Ewing's sarcoma family of tumours to fenretinide-induced cell death is increased by EWS-Fli1-dependent modulation of p38(MAPK) activity." Oncogene **27**(7): 985-996.
- Myatt, S. S., C. P. Redfern and S. A. Burchill (2005). "p38MAPK-Dependent sensitivity of Ewing's sarcoma family of tumors to fenretinide-induced cell death." Clin Cancer Res **11**(8): 3136-3148.
- Myers, J. S., A. K. von Lersner and Q. X. Sang (2016). "Proteomic Upregulation of Fatty Acid Synthase and Fatty Acid Binding Protein 5 and Identification of Cancer- and Race-Specific Pathway Associations in Human Prostate Cancer Tissues." J Cancer **7**(11): 1452-1464.

- Myszka, D. G., X. He, M. Dembo, T. A. Morton and B. Goldstein (1998). "Extending the range of rate constants available from BIACORE: interpreting mass transport-influenced binding data." *Biophys J* **75**(2): 583-594.
- Napoli, J. L. (1993). "Biosynthesis and metabolism of retinoic acid: roles of CRBP and CRABP in retinoic acid: roles of CRBP and CRABP in retinoic acid homeostasis." *J Nutr* **123**(2 Suppl): 362-366.
- Napoli, J. L. (1999). "Interactions of retinoid binding proteins and enzymes in retinoid metabolism." *Biochim Biophys Acta* **1440**(2-3): 139-162.
- Napoli, J. L. (2017). "Cellular retinoid binding-proteins, CRBP, CRABP, FABP5: Effects on retinoid metabolism, function and related diseases." *Pharmacol Ther* **173**: 19-33.
- Navarro-Zorraquino, M., A. Guemes, C. Pastor, J. Soria, R. Sousa, J. C. Salinas, E. Tejero and R. Lozano (2002). "Apoptosis and CD8 and CD54 cell expression in rat small bowel transplantation." *J Surg Res* **103**(1): 37-40.
- Newcomer, M. E., T. A. Jones, J. Aqvist, J. Sundelin, U. Eriksson, L. Rask and P. A. Peterson (1984). "The three-dimensional structure of retinol-binding protein." *The EMBO journal* **3**(7): 1451-1454.
- Newcomer, M. E., T. A. Jones, J. Aqvist, J. Sundelin, U. Eriksson, L. Rask and P. A. Peterson (1984). "The three-dimensional structure of retinol-binding protein." *EMBO J* **3**(7): 1451-1454.
- Newcomer, M. E. and D. E. Ong (2000). "Plasma retinol binding protein: structure and function of the prototypic lipocalin." *Biochim Biophys Acta* **1482**(1-2): 57-64.
- Newcomer, M. E. and D. E. Ong (2000). "Plasma retinol binding protein: structure and function of the prototypic lipocalin." *Biochimica et biophysica acta* **1482**(1-2): 57-64.
- Ng, K. P., G. Potikyan, R. O. Savene, C. T. Denny, V. N. Uversky and K. A. Lee (2007). "Multiple aromatic side chains within a disordered structure are critical for transcription and transforming activity of EWS family oncoproteins." *Proc Natl Acad Sci U S A* **104**(2): 479-484.
- Noy, N. (2000). "Retinoid-binding proteins: mediators of retinoid action." *Biochem J* **348 Pt 3**: 481-495.
- Noy, N., L. Li, M. V. Abola and N. A. Berger (2015). "Is retinol binding protein 4 a link between adiposity and cancer?" *Horm Mol Biol Clin Investig* **23**(2): 39-46.
- O'Byrne, S. M. and W. S. Blaner (2013). "Retinol and retinyl esters: biochemistry and physiology." *J Lipid Res* **54**(7): 1731-1743.
- Oda, A., K. Tsuchida, T. Takakura, N. Yamaotsu and S. Hirono (2006). "Comparison of consensus scoring strategies for evaluating computational models of protein-ligand complexes." *J Chem Inf Model* **46**(1): 380-391.
- Odri, G. A., S. Dumoucel, G. Picarda, S. Battaglia, F. Lamoureux, N. Corradini, J. Rousseau, F. Tirode, K. Laud, O. Delattre, F. Guoin, D. Heymann and F. Redini (2010). "Zoledronic acid as a new adjuvant therapeutic strategy for Ewing's sarcoma patients." *Cancer Res* **70**(19): 7610-7619.
- Ohlmann, C. H., C. Jung and G. Jaques (2002). "Is growth inhibition and induction of apoptosis in lung cancer cell lines by fenretinide [N-(4-hydroxyphenyl)retinamide] sufficient for cancer therapy?" *Int J Cancer* **100**(5): 520-526.
- Okazaki, M., S. Fushida, S. Harada, T. Tsukada, J. Kinoshita, K. Oyama, T. Miyashita, I. Ninomiya and T. Ohta (2017). "Establishing a xenograft mouse

model of peritoneal dissemination of gastric cancer with organ invasion and fibrosis." BMC Cancer **17**(1): 23.

Okuducu, A. F., V. Janzen, Y. Ko, J. C. Hahne, H. Lu, Z. L. Ma, P. Albers, A. Sahin, A. Wellmann, P. Scheinert and N. Wernert (2005). "Cellular retinoic acid-binding protein 2 is down-regulated in prostate cancer." Int J Oncol **27**(5): 1273-1282.

Ong, D. E. (1984). "A novel retinol-binding protein from rat. Purification and partial characterization." J Biol Chem **259**(3): 1476-1482.

Ong, D. E. (1987). "Cellular retinoid-binding proteins." Arch Dermatol **123**(12): 1693-1695a.

Ong, D. E. and D. L. Page (1986). "Quantitation of cellular retinol-binding protein in human organs." Am J Clin Nutr **44**(3): 425-430.

Ong, D. E. and D. L. Page (1987). "Cellular retinol-binding protein (type two) is abundant in human small intestine." J Lipid Res **28**(6): 739-745.

Oridate, N., D. Lotan, M. F. Mitchell, W. K. Hong and R. Lotan (1995).

"Inhibition of proliferation and induction of apoptosis in cervical carcinoma cells by retinoids: implications for chemoprevention." J Cell Biochem Suppl **23**: 80-86.

Orienti, I., G. Zuccari, M. Falconi, G. Teti, N. A. Illingworth and G. J. Veal (2012). "Novel micelles based on amphiphilic branched PEG as carriers for fenretinide." Nanomedicine **8**(6): 880-890.

Orlandi, A., A. Ferlosio, A. Ciucci, F. Sesti, B. Lifschitz-Mercer, G. Gabbiani, L. G. Spagnoli and B. Czernobilsky (2004). "Cellular retinol-binding protein-1 expression in endometrial stromal cells: physiopathological and diagnostic implications." Histopathology **45**(5): 511-517.

Ott, M., J. D. Robertson, V. Gogvadze, B. Zhivotovsky and S. Orrenius (2002). "Cytochrome c release from mitochondria proceeds by a two-step process." Proc Natl Acad Sci U S A **99**(3): 1259-1263.

Ozpolat, B., A. M. Tari, K. Mehta and G. Lopez-Berestein (2004). "Nuclear retinoid receptors are involved in N-(4-hydroxyphenyl) retinamide (Fenretinide)-induced gene expression and growth inhibition in HL-60 acute myeloid leukemia cells." Leuk Lymphoma **45**(5): 979-985.

Paddison, P. J., A. A. Caudy, E. Bernstein, G. J. Hannon and D. S. Conklin (2002). "Short hairpin RNAs (shRNAs) induce sequence-specific silencing in mammalian cells." Genes Dev **16**(8): 948-958.

Paik, J., S. Vogel, R. Piantadosi, A. Sykes, W. S. Blaner and K. Swisshelm (2000). "9-cis-retinoids: biosynthesis of 9-cis-retinoic acid." Biochemistry **39**(27): 8073-8084.

Parkin, D. M., C. A. Stiller, G. J. Draper and C. A. Bieber (1988). "The international incidence of childhood cancer." International journal of cancer. Journal international du cancer **42**(4): 511-520.

Parris, T. Z., L. Aziz, A. Kovacs, S. Hajizadeh, S. Nemes, M. Semaan, C. Y. Chen, P. Karlsson and K. Helou (2014). "Clinical relevance of breast cancer-related genes as potential biomarkers for oral squamous cell carcinoma." BMC Cancer **14**: 324.

Patel, J. B., C. K. Huynh, V. D. Handratta, L. K. Gediya, A. M. Brodie, O. G. Goloubeva, O. O. Clement, I. P. Nanne, D. R. Soprano and V. C. Njar (2004). "Novel retinoic acid metabolism blocking agents endowed with multiple biological activities are efficient growth inhibitors of human breast and prostate cancer cells in vitro and a human breast tumor xenograft in nude mice." J Med Chem **47**(27): 6716-6729.

- Paulussen, M., S. Ahrens, A. W. Craft, J. Dunst, B. Frohlich, S. Jabar, C. Rube, W. Winkelmann, S. Wissing, A. Zoubek and H. Jurgens (1998). "Ewing's tumors with primary lung metastases: survival analysis of 114 (European Intergroup) Cooperative Ewing's Sarcoma Studies patients." J Clin Oncol **16**(9): 3044-3052.
- Paulussen, M., S. Ahrens, J. Dunst, W. Winkelmann, G. U. Exner, R. Kotz, G. Amann, B. Dockhorn-Dworniczak, D. Harms, S. Muller-Weihrich, K. Welte, B. Kornhuber, G. Janka-Schaub, U. Gobel, J. Treuner, P. A. Voute, A. Zoubek, H. Gadner and H. Jurgens (2001). "Localized Ewing tumor of bone: final results of the cooperative Ewing's Sarcoma Study CESS 86." J Clin Oncol **19**(6): 1818-1829.
- Penniston, K. L. and S. A. Tanumihardjo (2006). "The acute and chronic toxic effects of vitamin A." Am J Clin Nutr **83**(2): 191-201.
- Piantedosi, R., N. Ghyselinck, W. S. Blaner and S. Vogel (2005). "Cellular retinol-binding protein type III is needed for retinoid incorporation into milk." J Biol Chem **280**(25): 24286-24292.
- Pignatta, S., I. Orienti, M. Falconi, G. Teti, C. Arienti, L. Medri, M. Zanoni, S. Carloni, W. Zoli, D. Amadori and A. Tesei (2015). "Albumin nanocapsules containing fenretinide: pre-clinical evaluation of cytotoxic activity in experimental models of human non-small cell lung cancer." Nanomedicine **11**(2): 263-273.
- Pishas, K. I. and S. L. Lessnick (2016). "Recent advances in targeted therapy for Ewing sarcoma." F1000Res **5**.
- Plummer, M., C. de Martel, J. Vignat, J. Ferlay, F. Bray and S. Franceschi (2016). "Global burden of cancers attributable to infections in 2012: a synthetic analysis." Lancet Glob Health **4**(9): e609-616.
- Poliakov, E., W. Samuel, T. Duncan, D. B. Gutierrez, N. L. Mata and T. M. Redmond (2017). "Inhibitory effects of fenretinide metabolites N-[4-methoxyphenyl]retinamide (MPR) and 4-oxo-N-(4-hydroxyphenyl)retinamide (3-keto-HPR) on fenretinide molecular targets beta-carotene oxygenase 1, stearoyl-CoA desaturase 1 and dihydroceramide Delta4-desaturase 1." PLoS One **12**(4): e0176487.
- Pollard, M. and P. H. Luckert (1991). "The inhibitory effect of 4-hydroxyphenyl retinamide (4-HPR) on metastasis of prostate adenocarcinoma-III cells in Lobund-Wistar rats." Cancer Lett **59**(2): 159-163.
- Pollard, M., P. H. Luckert and M. B. Sporn (1991). "Prevention of primary prostate cancer in Lobund-Wistar rats by N-(4-hydroxyphenyl)retinamide." Cancer Res **51**(13): 3610-3611.
- Pomorski, A., T. Kochanczyk, A. Miloch and A. Krezel (2013). "Method for accurate determination of dissociation constants of optical ratiometric systems: chemical probes, genetically encoded sensors, and interacting molecules." Anal Chem **85**(23): 11479-11486.
- Ponthan, F., M. Lindskog, N. Karnehed, J. Castro and P. Kogner (2003). "Evaluation of anti-tumour effects of oral fenretinide (4-HPR) in rats with human neuroblastoma xenografts." Oncol Rep **10**(5): 1587-1592.
- Poondru, S., S. Zhou, J. Rake, G. Shackleton, T. H. Corbett, R. E. Parchment and B. R. Jasti (2001). "High-performance liquid chromatographic method for the estimation of the novel investigational anti-cancer agent SR271425 and its metabolites in mouse plasma." J Chromatogr B Biomed Sci Appl **759**(1): 175-178.

- Porter, S. B., L. D. Fraker, F. Chytil and D. E. Ong (1983). "Localization of cellular retinol-binding protein in several rat tissues." Proc Natl Acad Sci U S A **80**(21): 6586-6590.
- Powell, C. A., M. W. Nasser, H. Zhao, J. C. Wochna, X. Zhang, C. Shapiro, K. Shilo and R. K. Ganju (2015). "Fatty acid binding protein 5 promotes metastatic potential of triple negative breast cancer cells through enhancing epidermal growth factor receptor stability." Oncotarget **6**(8): 6373-6385.
- Powles, T., E. McCroskey and A. Paterson (2006). "Oral bisphosphonates as adjuvant therapy for operable breast cancer." Clin Cancer Res **12**(20 Pt 2): 6301s-6304s.
- Preitner, F., N. Mody, T. E. Graham, O. D. Peroni and B. B. Kahn (2009). "Long-term Fenretinide treatment prevents high-fat diet-induced obesity, insulin resistance, and hepatic steatosis." Am J Physiol Endocrinol Metab **297**(6): E1420-1429.
- Puduvalli, V. K., W. K. Yung, K. R. Hess, J. G. Kuhn, M. D. Groves, V. A. Levin, J. Zwiebel, S. M. Chang, T. F. Cloughesy, L. Junck, P. Wen, F. Lieberman, C. A. Conrad, M. R. Gilbert, C. A. Meyers, V. Liu, M. P. Mehta, M. K. Nicholas, M. Prados and C. North American Brain Tumor (2004). "Phase II study of fenretinide (NSC 374551) in adults with recurrent malignant gliomas: A North American Brain Tumor Consortium study." J Clin Oncol **22**(21): 4282-4289.
- Qian, J., J. S. Zhang, X. Q. Wang, J. L. Ji and S. Mei (2009). "Fenretinide stimulates the apoptosis of hepatic stellate cells and ameliorates hepatic fibrosis in mice." Hepatol Res **39**(12): 1229-1247.
- Quadro, L., W. S. Blaner, D. J. Salchow, S. Vogel, R. Piantedosi, P. Gouras, S. Freeman, M. P. Cosma, V. Colantuoni and M. E. Gottesman (1999). "Impaired retinal function and vitamin A availability in mice lacking retinol-binding protein." EMBO J **18**(17): 4633-4644.
- Quesnelle, K. M., A. L. Boehm and J. R. Grandis (2007). "STAT-mediated EGFR signaling in cancer." J Cell Biochem **102**(2): 311-319.
- Raghu, P. and B. Sivakumar (2004). "Interactions amongst plasma retinol-binding protein, transthyretin and their ligands: implications in vitamin A homeostasis and transthyretin amyloidosis." Biochim Biophys Acta **1703**(1): 1-9.
- Rajan, N., W. S. Blaner, D. R. Soprano, A. Suhara and D. S. Goodman (1990). "Cellular retinol-binding protein messenger RNA levels in normal and retinoid-deficient rats." J Lipid Res **31**(5): 821-829.
- Redini, F. and D. Heymann (2015). "Bone Tumor Environment as a Potential Therapeutic Target in Ewing Sarcoma." Front Oncol **5**: 279.
- Reynolds, C. P., Y. Wang, L. J. Melton, P. A. Einhorn, D. J. Slamon and B. J. Maurer (2000). "Retinoic-acid-resistant neuroblastoma cell lines show altered MYC regulation and high sensitivity to fenretinide." Med Pediatr Oncol **35**(6): 597-602.
- Rice, K. L. and H. de The (2014). "The acute promyelocytic leukaemia success story: curing leukaemia through targeted therapies." J Intern Med **276**(1): 61-70.
- Riggi, N., M. L. Suva, C. De Vito, P. Provero, J. C. Stehle, K. Baumer, L. Cironi, M. Janiszewska, T. Petricevic, D. Suva, S. Tercier, J. M. Joseph, L. Guillou and I. Stamenkovic (2010). "EWS-FLI-1 modulates miRNA145 and SOX2 expression to initiate mesenchymal stem cell reprogramming toward Ewing sarcoma cancer stem cells." Genes Dev **24**(9): 916-932.

- Rininsland, F. H., T. Helms, R. J. Asaad, B. O. Boehm and M. Tary-Lehmann (2000). "Granzyme B ELISPOT assay for ex vivo measurements of T cell immunity." *J Immunol Methods* **240**(1-2): 143-155.
- Rodriguez-Galindo, C., C. A. Billups, L. E. Kun, B. N. Rao, C. B. Pratt, T. E. Merchant, V. M. Santana and A. S. Pappo (2002). "Survival after recurrence of Ewing tumors: the St Jude Children's Research Hospital experience, 1979-1999." *Cancer* **94**(2): 561-569.
- Rodriguez-Galindo, C., F. Navid, T. Liu, C. A. Billups, B. N. Rao and M. J. Krasin (2008). "Prognostic factors for local and distant control in Ewing sarcoma family of tumors." *Ann Oncol* **19**(4): 814-820.
- Rondelet, G., L. Fleury, C. Faux, V. Masson, J. Dubois, P. B. Arimondo, L. Willems and J. Wouters (2017). "Inhibition studies of DNA methyltransferases by maleimide derivatives of RG108 as non-nucleoside inhibitors." *Future Med Chem* **9**(13): 1465-1481.
- Rothschild, B. M., B. J. Witzke and I. Hershkovitz (1999). "Metastatic cancer in the Jurassic." *Lancet* **354**(9176): 398.
- Ruberte, E., V. Friederich, G. Morriss-Kay and P. Chambon (1992). "Differential distribution patterns of CRABP I and CRABP II transcripts during mouse embryogenesis." *Development* **115**(4): 973-987.
- Saari, J. C., S. Futterman, G. W. Stubbs, J. T. Heffernan, L. Bredberg, D. Y. Chan and D. M. Albert (1978). "Cellular retinol- and retinoic acid-binding proteins in transformed mammalian cells." *Invest Ophthalmol Vis Sci* **17**(10): 988-992.
- Sabichi, A. L., M. F. Demierre, E. T. Hawk, C. E. Lerman and S. M. Lippman (2003). "Frontiers in cancer prevention research." *Cancer Res* **63**(18): 5649-5655.
- Sabichi, A. L., S. P. Lerner, E. N. Atkinson, H. B. Grossman, N. P. Caraway, C. P. Dinney, D. F. Penson, S. Matin, A. Kamat, L. L. Pisters, D. W. Lin, R. L. Katz, D. E. Brenner, G. P. Hemstreet, 3rd, M. Wargo, A. Bleyer, W. H. Sanders, J. L. Clifford, H. L. Parnes and S. M. Lippman (2008). "Phase III prevention trial of fenretinide in patients with resected non-muscle-invasive bladder cancer." *Clin Cancer Res* **14**(1): 224-229.
- Samuel, W., R. K. Kutty, S. Nagineni, C. Vijayasathy, R. A. Chandraratna and B. Wiggert (2006). "N-(4-hydroxyphenyl)retinamide induces apoptosis in human retinal pigment epithelial cells: retinoic acid receptors regulate apoptosis, reactive oxygen species generation, and the expression of heme oxygenase-1 and Gadd153." *J Cell Physiol* **209**(3): 854-865.
- Sani, B. P., Y. F. Shealy and D. L. Hill (1995). "N-(4-hydroxyphenyl)retinamide: interactions with retinoid-binding proteins/receptors." *Carcinogenesis* **16**(10): 2531-2534.
- Schaefer, W. H., B. Kakkad, J. A. Crow, I. A. Blair and D. E. Ong (1989). "Purification, primary structure characterization, and cellular distribution of two forms of cellular retinol-binding protein, type II from adult rat small intestine." *J Biol Chem* **264**(7): 4212-4221.
- Scharovsky, O. G., L. E. Mainetti and V. R. Rozados (2009). "Metronomic chemotherapy: changing the paradigm that more is better." *Curr Oncol* **16**(2): 7-15.
- Schiavo, R., C. Tullio, M. La Grotteria, I. C. Andreotti, B. Scarpati, L. Romiti, F. Bozzi, P. Pedrazzoli and S. Siena (2007). "Establishment and characterization of a new Ewing's sarcoma cell line from a malignant pleural effusion." *Anticancer Res* **27**(5A): 3273-3278.

- Schleiermacher, G., M. Peter, O. Oberlin, T. Philip, H. Rubie, F. Mechinaud, D. Sommelet-Olive, J. Landman-Parker, D. Bours, J. Michon, O. Delattre and P. Societe Francaise d'Oncologie (2003). "Increased risk of systemic relapses associated with bone marrow micrometastasis and circulating tumor cells in localized ewing tumor." J Clin Oncol **21**(1): 85-91.
- Schlick, T., R. Collepardo-Guevara, L. A. Halvorsen, S. Jung and X. Xiao (2011). "Biomolecular modeling and simulation: a field coming of age." Q Rev Biophys **44**(2): 191-228.
- Schmittel, A., U. Keilholz, E. Thiel and C. Scheibenbogen (2000). "Quantification of tumor-specific T lymphocytes with the ELISPOT assay." J Immunother **23**(3): 289-295.
- Schmittgen, T. D. and K. J. Livak (2008). "Analyzing real-time PCR data by the comparative C(T) method." Nat Protoc **3**(6): 1101-1108.
- Schneider, B. J., F. P. Worden, S. M. Gadgeel, R. E. Parchment, C. M. Hodges, J. Zwiebel, R. L. Dunn, A. J. Wozniak, M. J. Kraut and G. P. Kalemkerian (2009). "Phase II trial of fenretinide (NSC 374551) in patients with recurrent small cell lung cancer." Invest New Drugs **27**(6): 571-578.
- Schuck, A., S. Ahrens, M. Paulussen, M. Kuhlen, S. Konemann, C. Rube, W. Winkelmann, R. Kotz, J. Dunst, N. Willich and H. Jurgens (2003). "Local therapy in localized Ewing tumors: results of 1058 patients treated in the CESS 81, CESS 86, and EICESS 92 trials." Int J Radiat Oncol Biol Phys **55**(1): 168-177.
- Schuck, A., C. Rube, S. Konemann, C. E. Rube, S. Ahrens, M. Paulussen, J. Dunst, H. Jurgens and N. Willich (2002). "Postoperative radiotherapy in the treatment of Ewing tumors: influence of the interval between surgery and radiotherapy." Strahlenther Onkol **178**(1): 25-31.
- Schug, T. T., D. C. Berry, N. S. Shaw, S. N. Travis and N. Noy (2007). "Opposing effects of retinoic acid on cell growth result from alternate activation of two different nuclear receptors." Cell **129**(4): 723-733.
- Schug, T. T., D. C. Berry, I. A. Toshkov, L. Cheng, A. Y. Nikitin and N. Noy (2008). "Overcoming retinoic acid-resistance of mammary carcinomas by diverting retinoic acid from PPARbeta/delta to RAR." Proc Natl Acad Sci U S A **105**(21): 7546-7551.
- Seeliger, D. and B. L. de Groot (2010). "Ligand docking and binding site analysis with PyMOL and Autodock/Vina." J Comput Aided Mol Des **24**(5): 417-422.
- Sell, H. and J. Eckel (2007). "Regulation of retinol binding protein 4 production in primary human adipocytes by adiponectin, troglitazone and TNF-alpha." Diabetologia **50**(10): 2221-2223.
- Selvanathan, S. P., G. T. Graham, H. V. Erkizan, U. Dirksen, T. G. Natarajan, A. Dakic, S. Yu, X. Liu, M. T. Paulsen, M. E. Ljungman, C. H. Wu, E. R. Lawlor, A. Uren and J. A. Toretsky (2015). "Oncogenic fusion protein EWS-FLI1 is a network hub that regulates alternative splicing." Proc Natl Acad Sci U S A **112**(11): E1307-1316.
- Shi, J. H., B. Zheng, S. Chen, G. Y. Ma and J. K. Wen (2012). "Retinoic acid receptor alpha mediates all-trans-retinoic acid-induced Klf4 gene expression by regulating Klf4 promoter activity in vascular smooth muscle cells." J Biol Chem **287**(14): 10799-10811.
- Shingleton, J. L., M. K. Skinner and D. E. Ong (1989). "Characteristics of retinol accumulation from serum retinol-binding protein by cultured Sertoli cells." Biochemistry **28**(25): 9641-9647.

- Shirakami, Y., S. A. Lee, R. D. Clugston and W. S. Blaner (2012). "Hepatic metabolism of retinoids and disease associations." Biochim Biophys Acta **1821**(1): 124-136.
- Shortle, D., K. T. Simons and D. Baker (1998). "Clustering of low-energy conformations near the native structures of small proteins." Proc Natl Acad Sci U S A **95**(19): 11158-11162.
- Shukla, N., J. Schiffman, D. Reed, I. J. Davis, R. B. Womer, S. L. Lessnick, E. R. Lawlor and C. O. G. E. S. B. Committee (2013). "Biomarkers in Ewing Sarcoma: The Promise and Challenge of Personalized Medicine. A Report from the Children's Oncology Group." Front Oncol **3**: 141.
- Shutoh, M., N. Oue, P. P. Aung, T. Noguchi, K. Kuraoka, H. Nakayama, K. Kawahara and W. Yasui (2005). "DNA methylation of genes linked with retinoid signaling in gastric carcinoma: expression of the retinoid acid receptor beta, cellular retinol-binding protein 1, and tazarotene-induced gene 1 genes is associated with DNA methylation." Cancer **104**(8): 1609-1619.
- Siffroi, J. P. and S. Chantot-Bastarud (2004). "[The future of cytogenetics after the sequencing of the human genome]." Morphologie **88**(280): 19-23.
- Silvaroli, J. A., J. M. Arne, S. Chelstowska, P. D. Kiser, S. Banerjee and M. Golczak (2016). "Ligand Binding Induces Conformational Changes in Human Cellular Retinol-binding Protein 1 (CRBP1) Revealed by Atomic Resolution Crystal Structures." J Biol Chem **291**(16): 8528-8540.
- Simkovic, F., S. Ovchinnikov, D. Baker and D. J. Rigden (2017). "Applications of contact predictions to structural biology." IUCrJ **4**(Pt 3): 291-300.
- Simmons, K. J., I. Chopra and C. W. Fishwick (2010). "Structure-based discovery of antibacterial drugs." Nat Rev Microbiol **8**(7): 501-510.
- Singh, P. (2016). "SPR Biosensors: Historical Perspectives and Current Challenges." Sensors and Actuators B-Chemical **229**: 110-130.
- Smathers, R. L. and D. R. Petersen (2011). "The human fatty acid-binding protein family: evolutionary divergences and functions." Hum Genomics **5**(3): 170-191.
- Smith, P. J., S. Soues, T. Gottlieb, S. J. Falk, J. V. Watson, R. J. Osborne and N. M. Bleehen (1994). "Etoposide-induced cell cycle delay and arrest-dependent modulation of DNA topoisomerase II in small-cell lung cancer cells." Br J Cancer **70**(5): 914-921.
- Soerjomataram, I., J. Lortet-Tieulent, D. M. Parkin, J. Ferlay, C. Mathers, D. Forman and F. Bray (2012). "Global burden of cancer in 2008: a systematic analysis of disability-adjusted life-years in 12 world regions." Lancet **380**(9856): 1840-1850.
- Solomon, D. A., T. Kim, L. A. Diaz-Martinez, J. Fair, A. G. Elkahlon, B. T. Harris, J. A. Toretsky, S. A. Rosenberg, N. Shukla, M. Ladanyi, Y. Samuels, C. D. James, H. Yu, J. S. Kim and T. Waldman (2011). "Mutational inactivation of STAG2 causes aneuploidy in human cancer." Science **333**(6045): 1039-1043.
- Song, B., Y. L. Hou, X. Ding, T. Wang, F. Wang, J. C. Zhong, T. Xu, J. Zhong, W. R. Hou and S. R. Shuai (2014). "Comparative analysis and molecular characterization of genomic sequences and proteins of FABP4 and FABP5 from the giant panda (*Ailuropoda melanoleuca*)." Genet Mol Res **13**(1): 992-1004.

- Soni, S., S. Bala, A. Kumar and M. Hanspal (2007). "Changing pattern of the subcellular distribution of erythroblast macrophage protein (Emp) during macrophage differentiation." Blood Cells Mol Dis **38**(1): 25-31.
- Stachurska, E., A. Loboda, J. Niderla-Bielinska, M. Szperl, M. Juszynski, A. Jozkowicz, J. Dulak and A. Ratajska (2011). "Expression of cellular retinoic acid-binding protein I and II (CRABP I and II) in embryonic mouse hearts treated with retinoic acid." Acta Biochim Pol **58**(1): 19-29.
- Stather, D. R., P. MacEachern, A. Chee, E. Dumoulin, C. A. Hergott and A. Tremblay (2012). "Wet laboratory versus computer simulation for learning endobronchial ultrasound: a randomized trial." Can Respir J **19**(5): 325-330.
- Storch, J. and B. Corsico (2008). "The emerging functions and mechanisms of mammalian fatty acid-binding proteins." Annu Rev Nutr **28**: 73-95.
- Subbiah, V., H. H. Chuang, D. Gambhire and K. Kairemo (2017). "Defining Clinical Response Criteria and Early Response Criteria for Precision Oncology: Current State-of-the-Art and Future Perspectives." Diagnostics (Basel) **7**(1).
- Sudhakar, A. (2009). "History of Cancer, Ancient and Modern Treatment Methods." J Cancer Sci Ther **1**(2): 1-4.
- Sunycz, J. A. (2010). "Zoledronic acid infusion for prevention and treatment of osteoporosis." Int J Womens Health **2**: 353-360.
- Sweetman, A. M., S. P. Jarvis, H. Sang, I. Lekkas, P. Rahe, Y. Wang, J. Wang, N. R. Champness, L. Kantorovich and P. Moriarty (2014). "Mapping the force field of a hydrogen-bonded assembly." Nat Commun **5**: 3931.
- Swinney, D. C. and J. Anthony (2011). "How were new medicines discovered?" Nat Rev Drug Discov **10**(7): 507-519.
- Szeto, W., W. Jiang, D. A. Tice, B. Rubinfeld, P. G. Hollingshead, S. E. Fong, D. L. Dugger, T. Pham, D. G. Yansura, T. A. Wong, J. C. Grimaldi, R. T. Corpuz, J. S. Singh, G. D. Frantz, B. Devaux, C. W. Crowley, R. H. Schwall, D. A. Eberhard, L. Rastelli, P. Polakis and D. Pennica (2001). "Overexpression of the retinoic acid-responsive gene Stra6 in human cancers and its synergistic induction by Wnt-1 and retinoic acid." Cancer Res **61**(10): 4197-4205.
- Tacke, F., R. Weiskirchen and C. Trautwein (2008). "Liver function critically determines serum retinol-binding protein 4 (RBP4) levels in patients with chronic liver disease and cirrhosis." Hepatology **48**(5): 1724-1725; author reply 1725-1726.
- Takahashi, N., Y. Watanabe, Y. Maitani, T. Yamauchi, K. Higashiyama and T. Ohba (2008). "p-Dodecylaminophenol derived from the synthetic retinoid, fenretinide: antitumor efficacy in vitro and in vivo against human prostate cancer and mechanism of action." Int J Cancer **122**(3): 689-698.
- Taverner, N. V., J. C. Smith and F. C. Wardle (2004). "Identifying transcriptional targets." Genome Biol **5**(3): 210.
- Tiberio, P., E. Cavadini, G. Abolafio, F. Formelli and V. Appierto (2010). "4-oxo-N-(4-hydroxyphenyl)retinamide: two independent ways to kill cancer cells." PLoS One **5**(10): e13362.
- Todd, R. and D. T. Wong (1999). "Oncogenes." Anticancer Res **19**(6A): 4729-4746.
- Toretsky, J. A., Y. Connell, L. Neckers and N. K. Bhat (1997). "Inhibition of EWS-FLI-1 fusion protein with antisense oligodeoxynucleotides." J Neurooncol **31**(1-2): 9-16.

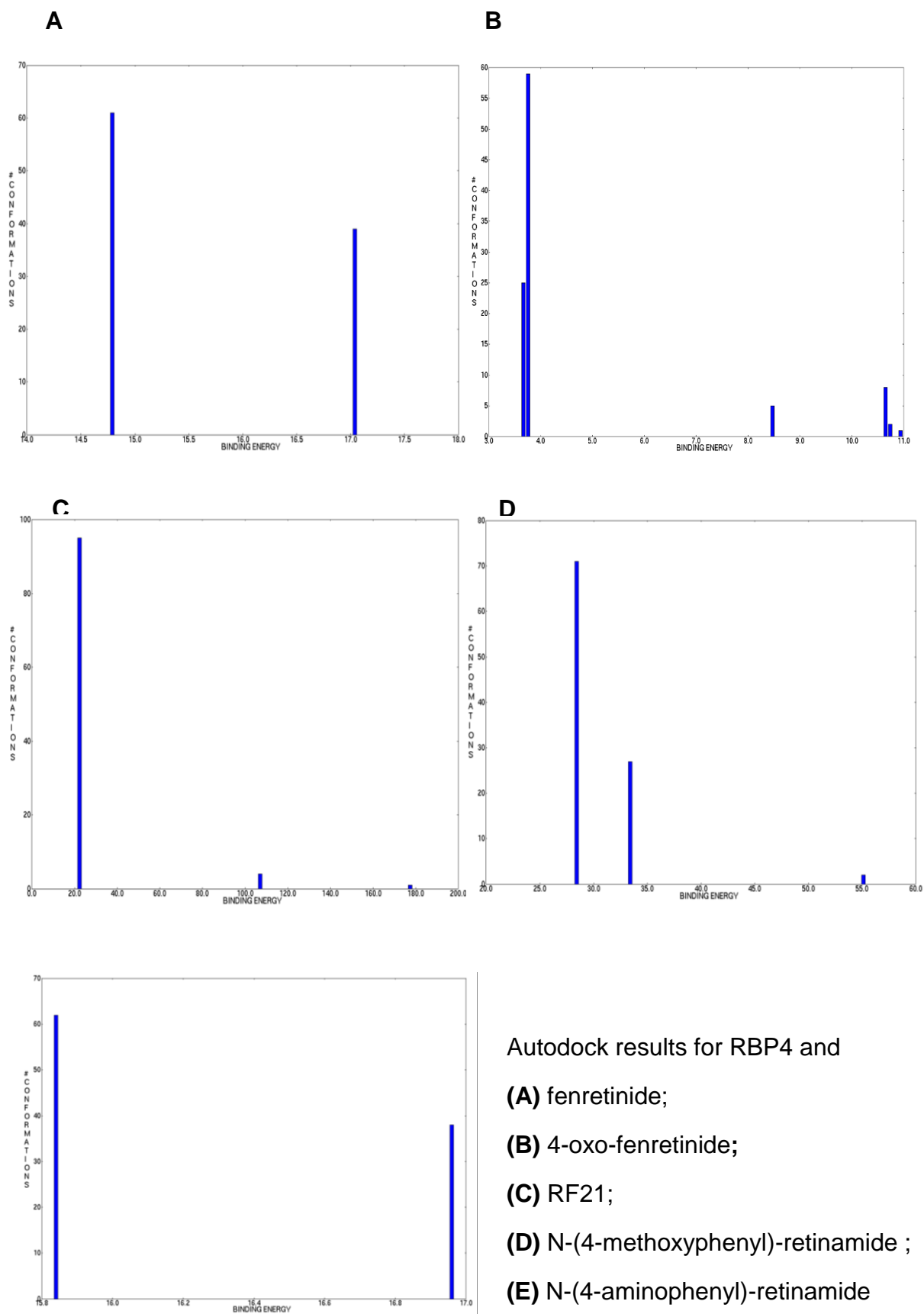
- Trasino, S. E., Y. D. Benoit and L. J. Gudas (2015). "Vitamin A deficiency causes hyperglycemia and loss of pancreatic beta-cell mass." J Biol Chem **290**(3): 1456-1473.
- Trasino, S. E., X. H. Tang, J. Jessurun and L. J. Gudas (2015). "Obesity Leads to Tissue, but not Serum Vitamin A Deficiency." Sci Rep **5**: 15893.
- Uehara, H., T. Takahashi and K. Izumi (2013). "Induction of retinol-binding protein 4 and placenta-specific 8 expression in human prostate cancer cells remaining in bone following osteolytic tumor growth inhibition by osteoprotegerin." Int J Oncol **43**(2): 365-374.
- Ulukaya, E., A. Kurt and E. J. Wood (2001). "4-(N-hydroxyphenyl)retinamide can selectively induce apoptosis in human epidermoid carcinoma cells but not in normal dermal fibroblasts." Cancer Invest **19**(2): 145-154.
- Uren, A., O. Tcherkasskaya and J. A. Toretsky (2004). "Recombinant EWS-FLI1 oncoprotein activates transcription." Biochemistry **43**(42): 13579-13589.
- Vaishampayan, U., L. K. Heilbrun, R. E. Parchment, V. Jain, J. Zwiebel, R. R. Boinpally, P. LoRusso and M. Hussain (2005). "Phase II trial of fenretinide in advanced renal carcinoma." Invest New Drugs **23**(2): 179-185.
- Vallet, J. L. (1994). "Technical note: a radioimmunoassay for porcine retinol binding protein." J Anim Sci **72**(9): 2449-2454.
- van Aalten, D. M., B. L. de Groot, H. J. Berendsen and J. B. Findlay (1996). "Conformational analysis of retinoids and restriction of their dynamics by retinoid-binding proteins." The Biochemical journal **319** (Pt 2): 543-550.
- van Aalten, D. M., J. B. Findlay, A. Amadei and H. J. Berendsen (1995). "Essential dynamics of the cellular retinol-binding protein--evidence for ligand-induced conformational changes." Protein Eng **8**(11): 1129-1135.
- van Jaarsveld, P. P., H. Edelhoch, D. S. Goodman and J. Robbins (1973). "The interaction of human plasma retinol-binding protein and prealbumin." J Biol Chem **248**(13): 4698-4705.
- Vermeulen, J., S. Ballet, O. Oberlin, M. Peter, G. Pierron, E. Longavenne, V. Laurence, J. Kanold, P. Chastagner, O. Lejars, J. Y. Blay, P. Marec-Berard, J. Michon, O. Delattre and G. Schleiermacher (2006). "Incidence and prognostic value of tumour cells detected by RT-PCR in peripheral blood stem cell collections from patients with Ewing tumour." Br J Cancer **95**(10): 1326-1333.
- Veronesi, U., L. Mariani, A. Decensi, F. Formelli, T. Camerini, R. Miceli, M. G. Di Mauro, A. Costa, E. Marubini, M. B. Sporn and G. De Palo (2006). "Fifteen-year results of a randomized phase III trial of fenretinide to prevent second breast cancer." Ann Oncol **17**(7): 1065-1071.
- Villablanca, J. G., W. B. London, A. Naranjo, P. McGrady, M. M. Ames, J. M. Reid, R. M. McGovern, S. A. Buhrow, H. Jackson, E. Stranzinger, B. J. Kitchen, P. M. Sondel, M. T. Parisi, B. Shulkin, G. A. Yanik, S. L. Cohn and C. P. Reynolds (2011). "Phase II study of oral capsular 4-hydroxyphenylretinamide (4-HPR/fenretinide) in pediatric patients with refractory or recurrent neuroblastoma: a report from the Children's Oncology Group." Clin Cancer Res **17**(21): 6858-6866.
- Villani, M. G., V. Appierto, E. Cavadini, A. Bettiga, A. Prinetti, M. Clagett-Dame, R. W. Curley and F. Formelli (2006). "4-oxo-fenretinide, a recently identified fenretinide metabolite, induces marked G2-M cell cycle arrest and apoptosis in fenretinide-sensitive and fenretinide-resistant cell lines." Cancer Res **66**(6): 3238-3247.

- Villani, M. G., V. Appierto, E. Cavadini, M. Valsecchi, S. Sonnino, R. W. Curley and F. Formelli (2004). "Identification of the fenretinide metabolite 4-oxo-fenretinide present in human plasma and formed in human ovarian carcinoma cells through induction of cytochrome P450 26A1." Clin Cancer Res **10**(18 Pt 1): 6265-6275.
- von Levetzow, C., X. Jiang, Y. Gwyne, G. von Levetzow, L. Hung, A. Cooper, J. H. Hsu and E. R. Lawlor (2011). "Modeling initiation of Ewing sarcoma in human neural crest cells." PLoS One **6**(4): e19305.
- Vormoor, J., G. Baersch, S. Decker, M. Hotfilder, K. L. Schafer, L. Pelken, C. Rube, F. Van Valen, H. Jurgens and B. Dockhorn-Dworniczak (2001). "Establishment of an in vivo model for pediatric Ewing tumors by transplantation into NOD/scid mice." Pediatr Res **49**(3): 332-341.
- Vreeland, A. C., L. Levi, W. Zhang, D. C. Berry and N. Noy (2014). "Cellular retinoic acid-binding protein 2 inhibits tumor growth by two distinct mechanisms." J Biol Chem **289**(49): 34065-34073.
- Vreeland, A. C., S. Yu, L. Levi, D. de Barros Rossetto and N. Noy (2014). "Transcript stabilization by the RNA-binding protein HuR is regulated by cellular retinoic acid-binding protein 2." Mol Cell Biol **34**(12): 2135-2146.
- Wang, C., M. A. Kane and J. L. Napoli (2011). "Multiple retinol and retinal dehydrogenases catalyze all-trans-retinoic acid biosynthesis in astrocytes." J Biol Chem **286**(8): 6542-6553.
- Wang, W., H. L. Jia, J. M. Huang, Y. C. Liang, H. Tan, H. Z. Geng, L. Y. Guo and S. Z. Yao (2014). "Identification of biomarkers for lymph node metastasis in early-stage cervical cancer by tissue-based proteomics." Br J Cancer **110**(7): 1748-1758.
- Warrier, R. P., S. Kuvibidila, L. Gordon and J. Humbert (1994). "Transport proteins and acute phase reactant proteins in children with sickle cell anemia." J Natl Med Assoc **86**(1): 33-39.
- Wei, J. S., Y. K. Song, S. Durinck, Q. R. Chen, A. T. Cheuk, P. Tsang, Q. Zhang, C. J. Thiele, A. Slack, J. Shohet and J. Khan (2008). "The MYCN oncogene is a direct target of miR-34a." Oncogene **27**(39): 5204-5213.
- Weijnen, C. F., S. S. Rich, J. B. Meigs, A. S. Krolewski and J. H. Warram (2002). "Risk of diabetes in siblings of index cases with Type 2 diabetes: implications for genetic studies." Diabet Med **19**(1): 41-50.
- Weiss, K. L., G. Alshafie, J. S. Chapman, S. M. Mershon, H. Abou-Issa, M. Clagett-Dame and R. W. Curley, Jr. (2001). "An unhydrolyzable analogue of N-(4-hydroxyphenyl)retinamide. synthesis and preliminary biological studies." Bioorg Med Chem Lett **11**(12): 1583-1586.
- White, D. E. and S. A. Burchill (2010). "Fenretinide-dependent upregulation of death receptors through ASK1 and p38alpha enhances death receptor ligand-induced cell death in Ewing's sarcoma family of tumours." Br J Cancer **103**(9): 1380-1390.
- Williams, C., K. Edvardsson, S. A. Lewandowski, A. Strom and J. A. Gustafsson (2008). "A genome-wide study of the repressive effects of estrogen receptor beta on estrogen receptor alpha signaling in breast cancer cells." Oncogene **27**(7): 1019-1032.
- Williams, L., A. Somasekar, D. J. Davies, J. Cronin, S. H. Doak, R. Alcolado, J. G. Williams, A. P. Griffiths, J. N. Baxter and G. J. Jenkins (2009). "Aneuploidy involving chromosome 1 may be an early predictive marker of intestinal type gastric cancer." Mutat Res **669**(1-2): 104-111.

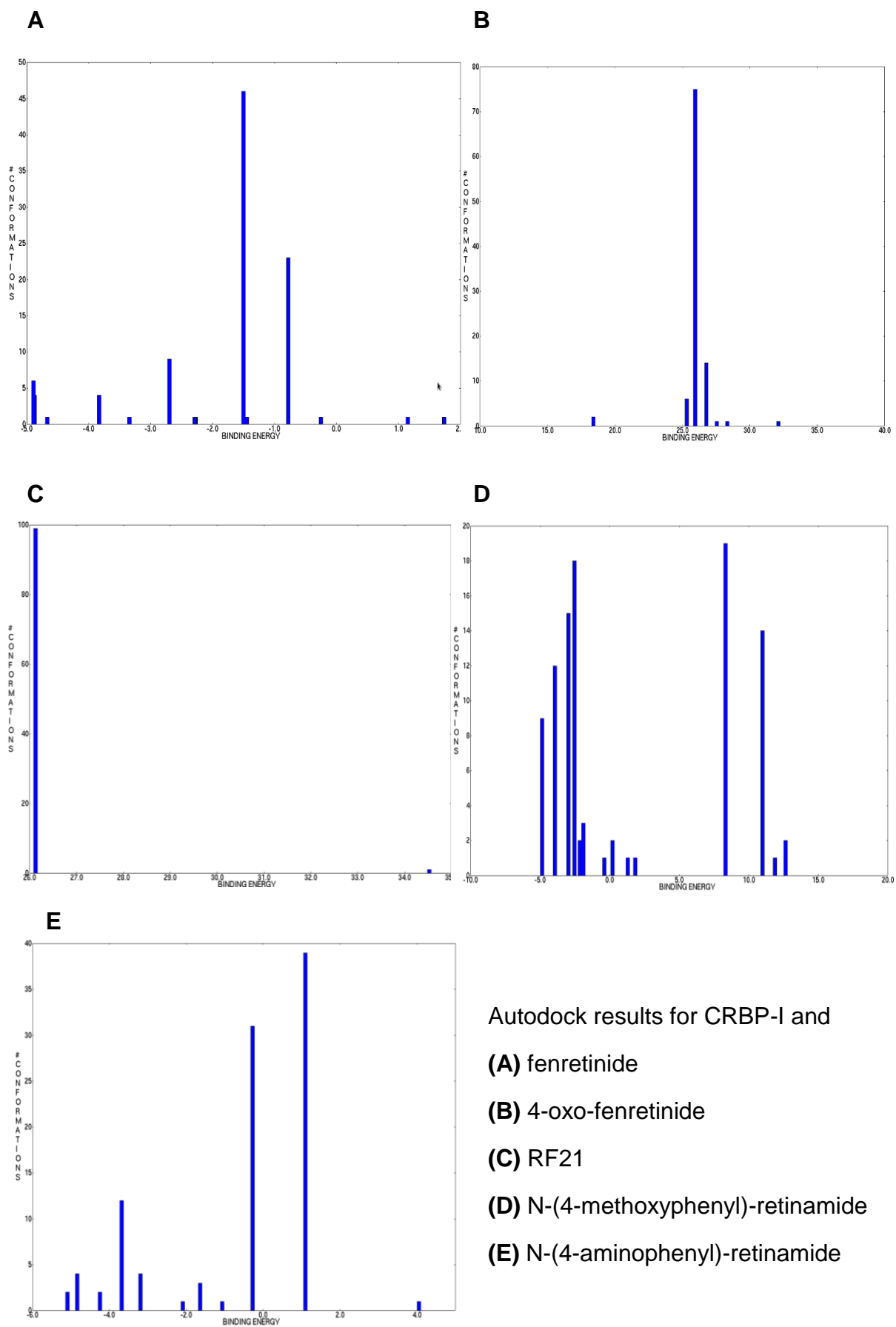
- Williams, S. J., D. Cvetkovic and T. C. Hamilton (2009). "Vitamin A metabolism is impaired in human ovarian cancer." Gynecol Oncol **112**(3): 637-645.
- Winkler, S., M. Hempel, S. Bruckner, H. M. Tautenhahn, R. Kaufmann and B. Christ (2016). "Identification of Pathways in Liver Repair Potentially Targeted by Secretory Proteins from Human Mesenchymal Stem Cells." Int J Mol Sci **17**(7).
- Wu, Y., H. Li, R. J. Loos, Q. Qi, F. B. Hu, Y. Liu and X. Lin (2009). "RBP4 variants are significantly associated with plasma RBP4 levels and hypertriglyceridemia risk in Chinese Hans." J Lipid Res **50**(7): 1479-1486.
- Wysocka-Kapcinska, M., J. A. Campos-Sandoval, A. Pal and J. B. Findlay (2010). "Expression and characterization of recombinant human retinol-binding protein in *Pichia pastoris*." Protein Expr Purif **71**(1): 28-32.
- Xu, L., C. Song, M. Ni, F. Meng, H. Xie and G. Li (2012). "Cellular retinol-binding protein 1 (CRBP-1) regulates osteogenesis and adipogenesis of mesenchymal stem cells through inhibiting RXRalpha-induced beta-catenin degradation." Int J Biochem Cell Biol **44**(4): 612-619.
- Yanase, H., H. Shimizu, T. Kanda, H. Fujii and T. Iwanaga (2001). "Cellular localization of the diazepam binding inhibitor (DBI) in the gastrointestinal tract of mice and its coexistence with the fatty acid binding protein (FABP)." Arch Histol Cytol **64**(4): 449-460.
- Yang, Q., T. E. Graham, N. Mody, F. Preitner, O. D. Peroni, J. M. Zabolotny, K. Kotani, L. Quadro and B. B. Kahn (2005). "Serum retinol binding protein 4 contributes to insulin resistance in obesity and type 2 diabetes." Nature **436**(7049): 356-362.
- Yang, Q., R. Wang, W. Xiao, F. Sun, H. Yuan and Q. Pan (2016). "Cellular Retinoic Acid Binding Protein 2 Is Strikingly Downregulated in Human Esophageal Squamous Cell Carcinoma and Functions as a Tumor Suppressor." PLoS One **11**(2): e0148381.
- Yao-Borengasser, A., V. Varma, A. M. Bodles, N. Rasouli, B. Phanavanh, M. J. Lee, T. Starks, L. M. Kern, H. J. Spencer, 3rd, A. A. Rashidi, R. E. McGehee, Jr., S. K. Fried and P. A. Kern (2007). "Retinol binding protein 4 expression in humans: relationship to insulin resistance, inflammation, and response to pioglitazone." The Journal of clinical endocrinology and metabolism **92**(7): 2590-2597.
- Yao, P. L., J. L. Morales, B. Zhu, B. H. Kang, F. J. Gonzalez and J. M. Peters (2014). "Activation of peroxisome proliferator-activated receptor-beta/delta (PPAR-beta/delta) inhibits human breast cancer cell line tumorigenicity." Mol Cancer Ther **13**(4): 1008-1017.
- Yu, S., L. Levi, G. Casadesus, G. Kunos and N. Noy (2014). "Fatty acid-binding protein 5 (FABP5) regulates cognitive function both by decreasing anandamide levels and by activating the nuclear receptor peroxisome proliferator-activated receptor beta/delta (PPARbeta/delta) in the brain." J Biol Chem **289**(18): 12748-12758.
- Zanotti, G., M. Marcello, G. Malpeli, C. Folli, G. Sartori and R. Berni (1994). "Crystallographic studies on complexes between retinoids and plasma retinol-binding protein." J Biol Chem **269**(47): 29613-29620.
- Zhang, J., Z. Pan and A. Sheppard (2017). "Both canonical and noncanonical Wnt signalling may be required for detoxification following ETP class mycotoxin exposure." Toxicol Lett **271**: 12-19.

- Zhang, W., A. C. Vreeland and N. Noy (2016). "RNA-binding protein HuR regulates nuclear import of protein." *J Cell Sci* **129**(21): 4025-4033.
- Zhang, X. and M. Oglesbee (2003). "Use of surface plasmon resonance for the measurement of low affinity binding interactions between HSP72 and measles virus nucleocapsid protein." *Biol Proced Online* **5**: 170-181.
- Zhang, Y. R., Y. Q. Zhao and J. F. Huang (2012). "Retinoid-binding proteins: similar protein architectures bind similar ligands via completely different ways." *PLoS One* **7**(5): e36772.
- Zheng, W. L. and D. E. Ong (1998). "Spatial and temporal patterns of expression of cellular retinol-binding protein and cellular retinoic acid-binding proteins in rat uterus during early pregnancy." *Biol Reprod* **58**(4): 963-970.
- Zhou, L., X. Cheng, B. A. Connolly, M. J. Dickman, P. J. Hurd and D. P. Hornby (2002). "Zebularine: a novel DNA methylation inhibitor that forms a covalent complex with DNA methyltransferases." *J Mol Biol* **321**(4): 591-599.
- Ziv, Y., M. K. Gupta, J. W. Milsom, A. Vladislavjevic, M. Brand and V. W. Fazio (1994). "The effect of tamoxifen and fenretinimide on human colorectal cancer cell lines in vitro." *Anticancer Res* **14**(5A): 2005-2009.
- Zizola, C. F., S. K. Frey, S. Jitngarmkusol, B. Kadereit, N. Yan and S. Vogel (2010). "Cellular retinol-binding protein type I (CRBP-I) regulates adipogenesis." *Mol Cell Biol* **30**(14): 3412-3420.
- Zsoldos, Z., D. Reid, A. Simon, B. S. Sadjad and A. P. Johnson (2006). "eHiTS: an innovative approach to the docking and scoring function problems." *Curr Protein Pept Sci* **7**(5): 421-435.
- Zsoldos, Z., D. Reid, A. Simon, S. B. Sadjad and A. P. Johnson (2007). "eHiTS: a new fast, exhaustive flexible ligand docking system." *J Mol Graph Model* **26**(1): 198-212.
- Zusterzeel, P. L., W. H. Peters, G. J. Burton, W. Visser, H. M. Roelofs and E. A. Steegers (2007). "Susceptibility to pre-eclampsia is associated with multiple genetic polymorphisms in maternal biotransformation enzymes." *Gynecol Obstet Invest* **63**(4): 209-213.

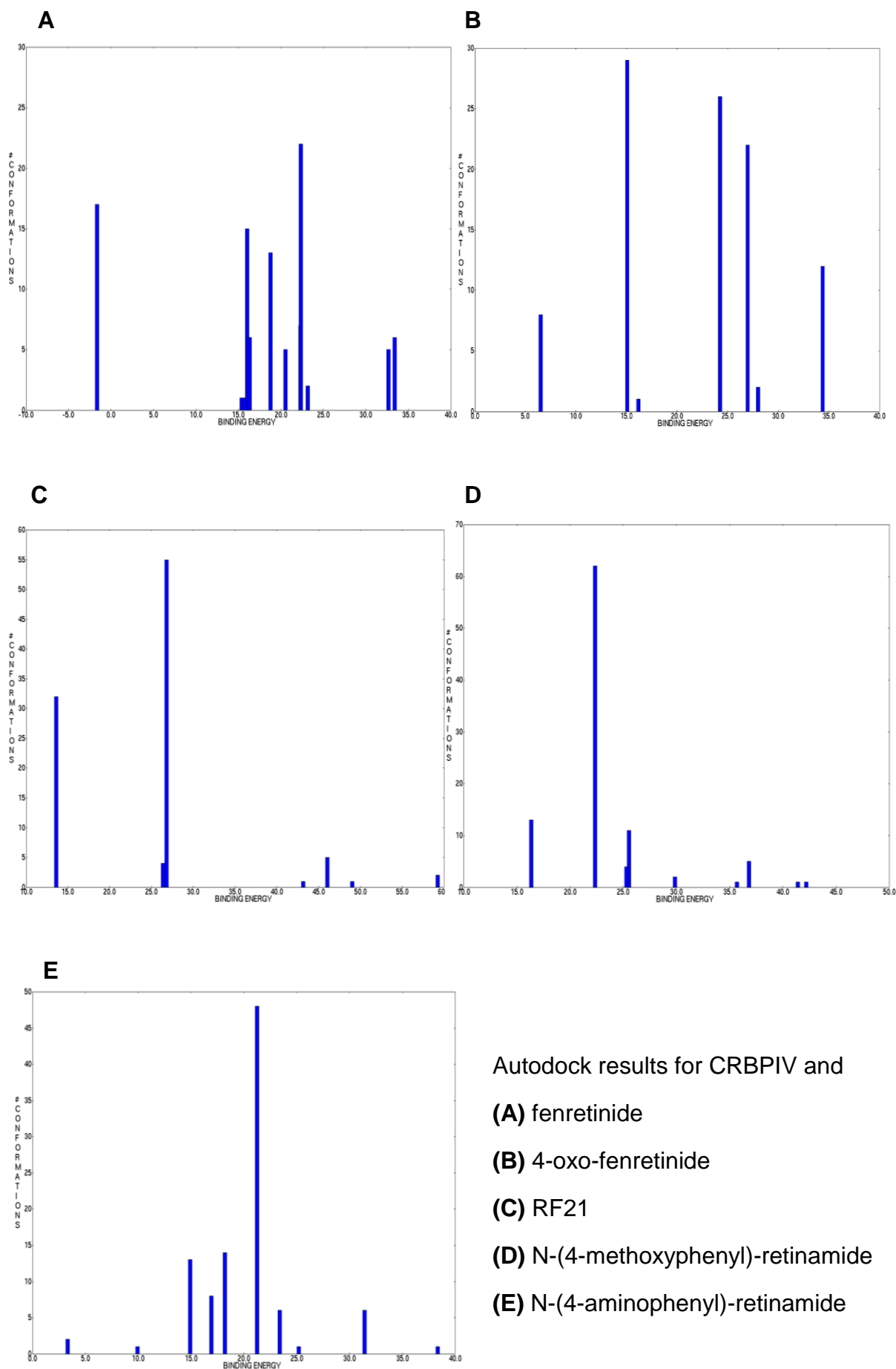
APPENDIX 1



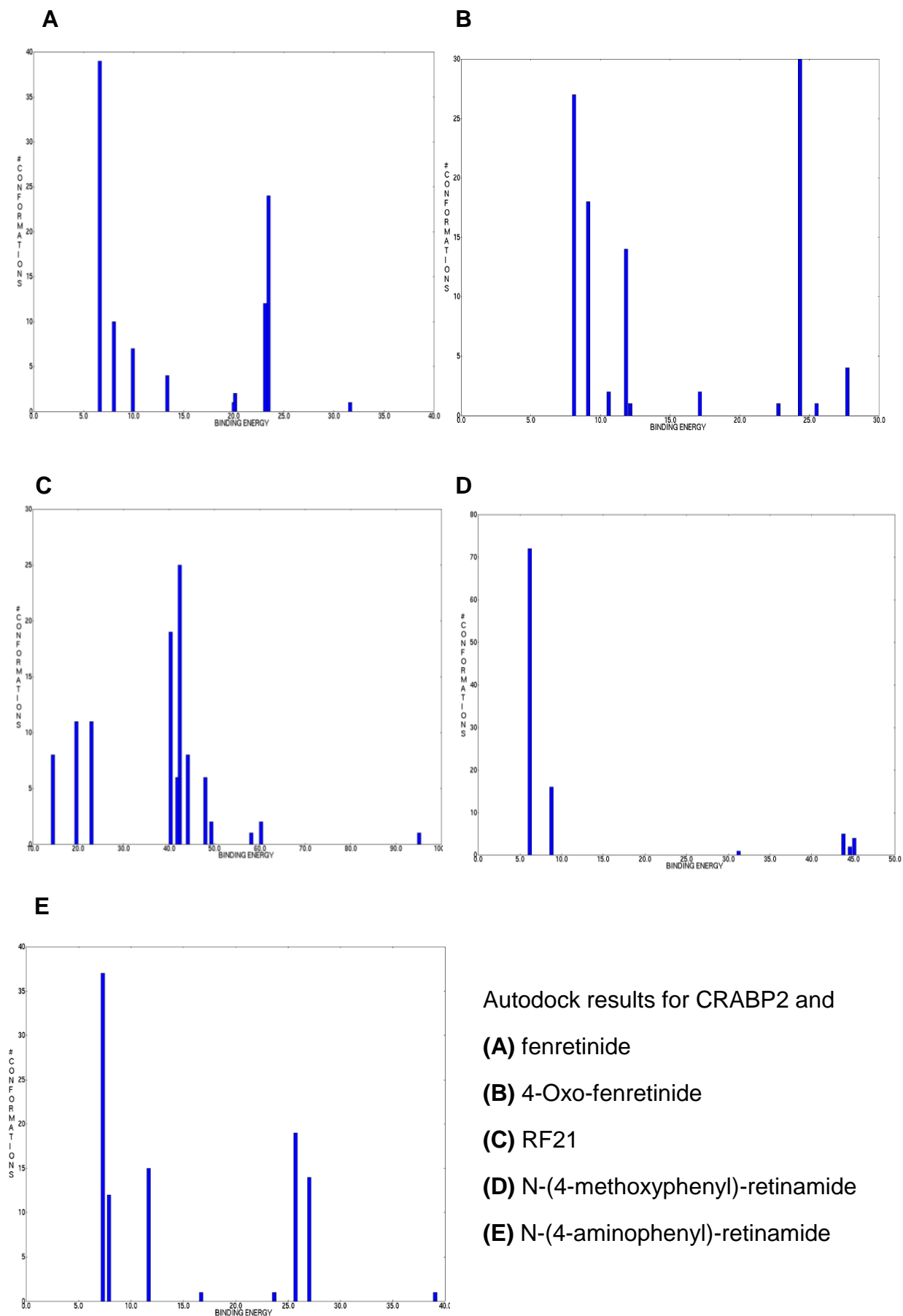
APPENDIX 2



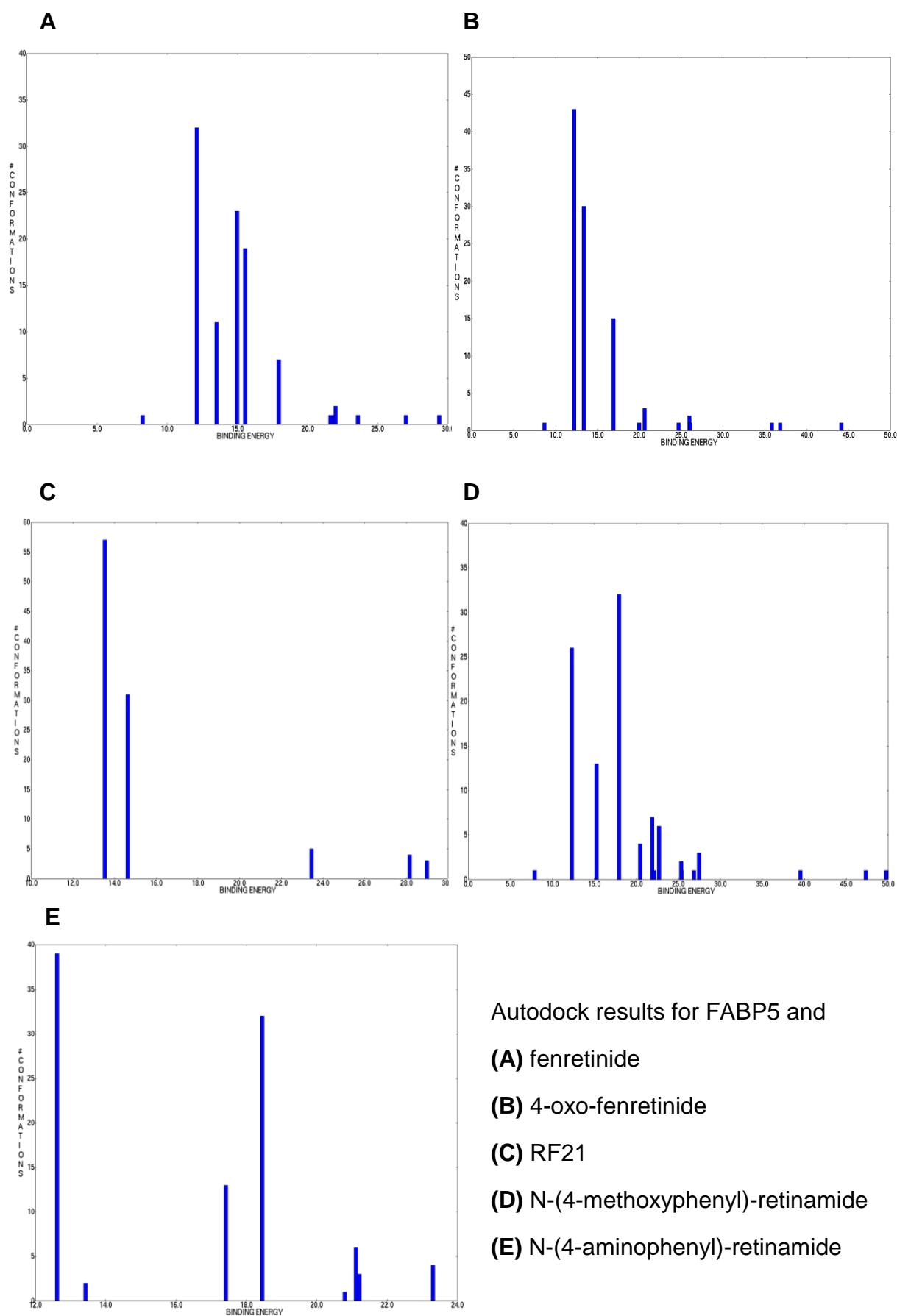
APPENDIX 3



APPENDIX 4



APPENDIX 5



—

—